RHEOLOGY AND PROCESSABILITY OF TEFLON® FEP RESINS FOR WIRE COATING

by

EVGUENI E. ROZENBAOUM

Candidate of Technical Science, Moscow University of Chemical Technology, 1993
Dip. Chem. Eng., Moscow University of Chemical Technology, 1988

A THESIS SUBMITTED IN PARTIAL FULFILLMENT OF THE REQUIREMENTS FOR THE
DEGREE OF DOCTOR OF PHILOSOPHY

in

the Faculty of Graduate Studies
Department of Chemical and Bio-Resource Engineering

We accept this thesis as conforming to the required standard

THE UNIVERSITY OF BRITISH COLUMBIA
July 1998

© 1998 Evgueni E. Rozenbaoum

Department of _Chemical Engineering_

The University of British Columbia
Vancouver, Canada

Date _Oct. 14, 1998_

Abstract

Experiments were carried out in both parallel plate and capillary rheometers for a variety of tetrafluoroethylene/hexafluoropropylene (TFE/HFP) copolymers and TFE/HFP/per-fluoro(alkyl vinyl ether) (TFE/HFP/PAVE) terpolymers, also known as Teflon® FEP polymers, having different molecular weights and compositions (HFP and PAVE content). The critical conditions for the onset of melt fracture and the influence of temperature, molecular weight, and composition of the resins are determined. The critical molecular weight for the onset of entanglements was found to be about 100,000, a value much higher than those previously reported. The relationships between the processability of the wire coating Teflon® FEP resins and their composition, viscosity, ability to crystallize, and melt elasticity were established. The experimental data were used for a thorough rheological modeling of the behavior of these resins. The latter includes calculation of their linear relaxation time spectra and nonlinear parameters using a multi-mode Phan-Thien and Tanner (PTT) constitutive equation.

A new data analysis procedure based on a mathematical model for the nonisothermal capillary flow of polymer melts coupled with heat transfer is developed. The computer simulations proposed can be used to provide detailed velocity, temperature, and pressure distributions and to recover the parameters of the employed slip velocity model corrected for the effect of viscous heating. Finally, the effect of various processing aids on the processability of fluoropolymers and polyolefins during extrusion and wire coating was studied. It was found that polyethylene works as a processing aid in the extrusion of Teflon® FEP resins in the same way as fluoropolymers do in the extrusion of polyolefins. Finally, the processing additive based on a boron nitride (BN) composition was found to eliminate sharkskin melt fracture and postpone gross melt fracture to significantly higher shear rates for a variety of polymers.

Table of Contents

List of Figures

List of Tables

Acknowledgements

1 Introduction

Fluoropolymers are among the oldest high-performance polymers, dating from the discovery of polytetrafluoroethylene (PTFE) in 1938. Since their commercial introduction, annual worldwide production has grown to about 125 mln lbs. (Feiring *et al.*, 1994). Although their production is small compared to other commodity thermoplastics such as polyethylene and polypropylene, fluoropolymers are of great commercial and scientific interest due to their unique combination of properties. These include excellent chemical stability and dielectric properties, anti-stick characteristics, mechanical strength, and low flammability. Their most important uses are in electronics and electrical applications, especially for wiring insulation, chemical processing equipment, laboratory ware and tubing, material for roofing and houseware.

PTFE, the homopolymer of tetrafluoroethylene (TFE), was introduced commercially by DuPont as Teflon® in 1950. It is insoluble in any known solvent, has a high melting point (about 327°C) and a very high melt viscosity. Therefore, its processing requires unusual methods such as cold pressing or sintering and paste extrusion. To provide similar product features with conventional processing, the Teflon® FEP (copolymers of TFE and hexafluoropropylene (HFP)) and Teflon® PFA (copolymers of TFE and perfluoropropylvinylether (PPVE)) fluoropolymers were developed by DuPont. These resins combine many of the best properties of Teflon® PTFE with the possibility of conventional melt processing due to their lower melting point. They are widely used as linings for pipe and chemical processing equipment, roll covers, and wire and cable

coating, including aircraft hookup wire, plenum cable, fire alarm cable, flat cable and others.

The wire-coating process is one of the most important applications of Teflon® FEP resins. This process involves a continuous extrusion for primary insulation of conducting wires with molten polymers for mechanical strength and environmental protection purposes. There are two basic types of coating dies used at present: pressure-coating and tube-coating dies. In the pressure-coating die, the wire is coated under pressure in the die. This technique is used usually for the application of the primary coating where good adhesion is important. In the case of the tube-coating die, the polymer coating is applied outside the die in the melt cone controlled by vacuum. Only the latter case is studied in this work.

The design problems encountered in wire coating are related to melt flow under stable flow conditions at the highest possible extrusion rate and to production of a coating of specified thickness and uniformity. At some critical condition, polymers undergo flow instabilities which lead to a nonuniform coating. Similar problems are encountered in other types of extrusion processes even though the die geometry is different.

It is well known that in many commercially important polymer processing operations, including wire coating, flow instabilities occur (Petrie and Denn, 1976). In these processes, a polymeric melt emerging from a slit or die often shows surface distortions at throughput rates above a critical value. As a result of these instabilities, the final product becomes unattractive and commercially unacceptable.

Most of the previous studies on extrusion instabilities known collectively as *melt fracture* have examined the behavior of various types of polyethylenes (Ramamurthy,

1986; Kalika and Denn, 1987; Hatzikiriakos and Dealy, 1992a,b), polyisoprenes and polybutadienes (Vinogradov *et al.*, 1972a; Lim and Schowalter, 1989), polydimethylsiloxanes (El Kissi and Piau, 1990), but very few studies have reported on the processing of Teflon® fluoropolymer resins (Tordella, 1969).

Flow instabilities in viscoelastic liquids have been the subject of several major reviews over the past decades (Petrie and Denn, 1976; Boudreaux and Cuculo, 1977; Tanner, 1985; Denn, 1990; Larson, 1992). Although melt fracture was first observed decades ago (Nason, 1945), there is still disagreement about the mechanisms causing these instabilities. The considerable complexity of the physical mechanisms, including the volume rheological properties and interaction with the solid boundaries governing polymer melt flow is the reason for the difficulties and controversies that still exist today. In many cases, the understanding of instabilities in polymer flow is speculative. However, it is evident that melt fracture is a complex phenomenon which may involve several independent mechanisms and much remains to be done in understanding its origins.

It is obvious that the rate of production is limited by the onset of the above discussed flow instabilities. To increase the process output, one must eliminate melt fracture or postpone it to higher rates. The most common approach to achieve this objective is the use of *processing aids*. These are usually fluoroelastomers that can be added to the resin at concentrations of a few hundred ppm, e.g. at the time of processing or introduced as a masterbatch. These processing aids reduce the pressure required to extrude the resin at a particular flow rate and eliminate or postpone melt fracture to higher extrusion rates.

The objective of this thesis is to perform a thorough rheological characterization of a number of Teflon® resins, study melt fracture in extrusion of these resins, and provide possible ways to eliminate or delay melt fracture in extrusion and wire coating by use of processing aids. Several aspects of numerical simulation and modeling of the flow of molten polymers in extrusion dies are also studied in this thesis.

2   Literature Review

2.1   Chemical Structure and Physical Properties of Fluoroplastics

Fluoroplastics are a class of paraffinic polymers that have some or all of the hydrogen replaced by fluorine. They include polytetrafluoroethylene (PTFE), copolymer of tetrafluoroethylene and hexafluoropropylene (FEP), perfluoroalkoxy resin (PFA), amorphous perfluoroplastics (AF), and some others not examined in this thesis.

PTFE is a completely fluorinated polymer manufactured by free radical polymerization of tetrafluoroethylene. PTFE is a linear crystalline polymer with a melting point of about 327°C. Its density falls in the range

$$-\!\!\!-\ CF_2 -\!\!\!-\ CF_2-\!\!\!-$$

between 2,130 and 2,190 kg/m³. PTFE has exceptional resistance to chemicals. Its dielectric constant (2.1) and loss factor are low and stable across a wide temperature and frequency range.

FEP is produced by copolymerization of tetrafluoroethylene (TFE) and hexafluoropropylene (HFP). It has predominantly linear chains. FEP has a crystalline melting point of about 265°C

$$-CF_2-\!\!-CF_2-\!\!-CF_2-\!\!-\underset{\displaystyle CF_3}{\overset{\displaystyle |}{CF}}-$$

determined by differential scanning calorimetry (DSC) and density of 2,150 kg/m³. It is a soft plastic with tensile strength, wear resistance, and creep resistance lower than those of many other engineering plastics. It is chemically inert with a low dielectric constant (2.1) over a wide range of frequencies and temperature.
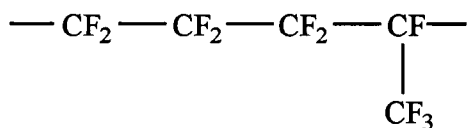
PFA resins are a relatively new commercially available class of melt-processable fluoroplastics. They have a melting point of about 290°C and density in the range of 2,130 to 2,160 kg/m^3. PFA is similar to PTFE and FEP, although it has somewhat better mechanical properties than FEP at elevated

$$-CF_2-CF_2-\underset{\underset{C_nF_{2n+1}}{\overset{|}{\underset{|}{O}}}}{CF}-CF_2-CF_2-$$

temperatures. It is about equivalent to PTFE as far as chemical resistance is concerned. Recently, terpolymers of TFE, HFP, and PAVE became commercially available. They combine the mechanical properties of FEP and PFA resins.
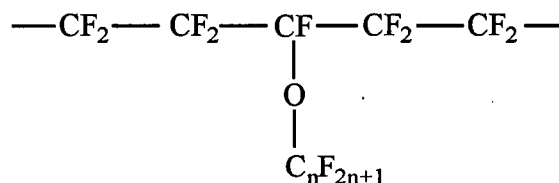
AF is produced by random copolymerization of the cyclic monomer, perfluoro-2,2-dimethyldioxole, with TFE. It combines the outstanding chemical, thermal, and electrical properties of the crystalline perfluoropolymers with high optical clarity, better mechanical properties, and solubility in selected fluorocarbon solvents.
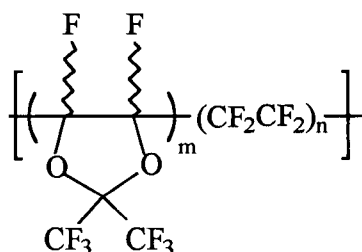
$$\left[\underset{\underset{\underset{CF_3 \quad CF_3}{O \diagdown \diagup O}}{\underset{}{}}}{\left(\underset{}{\overset{F \quad F}{\diagup \quad \diagup}}\right)_m}(CF_2CF_2)_n\right]$$

2.2 Rheological Measurements

Rheology is the science that deals with the way materials deform when forces are applied to them. The key words in this definition of rheology are *deformation* and *force*. To learn anything about the rheological properties of a material, one must either measure the deformation resulting from a given force or measure the force required to produce a given deformation. As a measure of force, one can use the stress, which is defined as the

ratio of the applied force to the area it acts on. Deformation can be described in terms of strain or rate of strain.

There are two basic flows used to characterize polymers: shear and shear-free flows. For these two types of flow, the components of the stress and rate of deformation tensors take on a distinct form.

The laboratory procedure that most closely approximates simple shear is to place a thin layer of fluid between two flat plates, clamp one of the plates in place, and move the second plate at a constant velocity, u, as shown
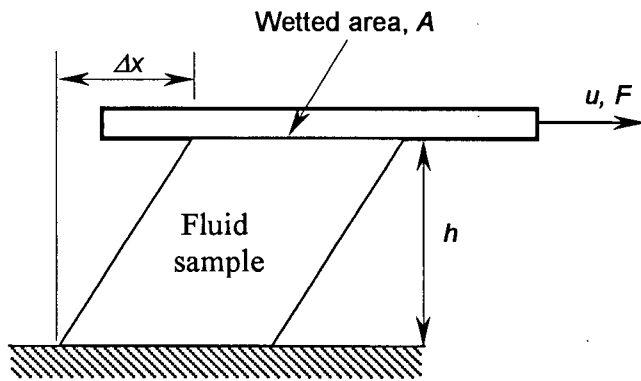
Figure 2-1 Simple shear flow

in Figure 2-1. Under no-slip conditions, the shear strain and shear rate can be written as follows:

$$\gamma(t) = \frac{\Delta x}{h} \tag{2-1}$$

$$\dot{\gamma}(t) = \frac{u}{h} \tag{2-2}$$

The velocity field is given as:

$$v_x = \dot{\gamma}(t)y \quad v_y = v_z = 0 \tag{2-3}$$

The components of the rate of deformation tensor are:

$$\dot{\gamma}_{ij} = \dot{\gamma}(t)\begin{pmatrix} 0 & 1 & 0 \\ 1 & 0 & 0 \\ 0 & 0 & 0 \end{pmatrix} \tag{2-4}$$

and the stress tensor components are of the form:

$$\begin{pmatrix} \tau_{xx} & \tau_{xy} & 0 \\ \tau_{xy} & \tau_{yy} & 0 \\ 0 & 0 & \tau_{zz} \end{pmatrix} \qquad (2\text{-}5)$$

When slip is present, the true shear rate is less than the nominal shear rate, as illustrated in Figure 2-2.

$$\dot{\gamma} = \dot{\gamma}_n = u/h \qquad\qquad \dot{\gamma}_n = \dot{\gamma} + 2u_s/h$$
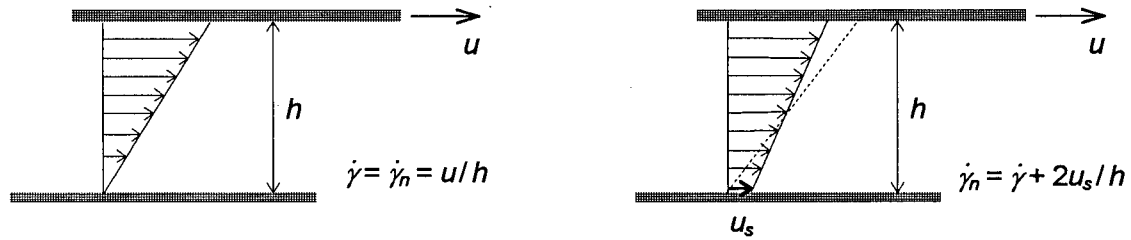
Figure 2-2. Velocity profiles in simple shear under no-slip (left) and slip conditions (right).

For simple (uniaxial) extension (see Figure 2-3), the measure of deformation is the Hencky strain defined as:

$$\varepsilon = \ln\left(\frac{\delta X_1(t)}{\delta X_1(t_0)}\right) \qquad (2\text{-}6)$$
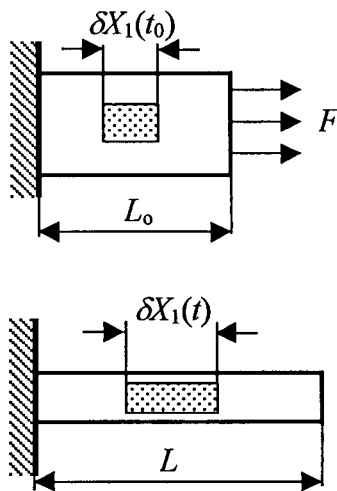
where $\delta X_1(t_0)$ and $\delta X_1(t)$ are the initial length at time t_0 of a material element measured in the direction of stretching and at a later time, t, after deformation has occurred, respectively. For a sample with initial length L_0, this becomes:

$$\varepsilon = \ln\left(\frac{L}{L_0}\right) \qquad (2\text{-}7)$$

Figure 2-3. Simple extension

The Hencky strain rate is defined as:

$$\dot{\varepsilon} = \frac{d \ln L}{dt} \qquad (2\text{-}8)$$

The velocity field in uniaxial extension becomes:

$$v_1 = \dot{\varepsilon}x \quad v_2 = -\frac{1}{2}\dot{\varepsilon}y \quad v_3 = -\frac{1}{2}\dot{\varepsilon}z \qquad (2\text{-}9)$$

The components of the rate of deformation tensor are:

$$\dot{\gamma}_{ij} = \begin{pmatrix} 2\dot{\varepsilon} & 0 & 0 \\ 0 & -\dot{\varepsilon} & 0 \\ 0 & 0 & -\dot{\varepsilon} \end{pmatrix} \qquad (2\text{-}10)$$

and the stress tensor has only diagonal components:

$$\tau_{ij} = \begin{pmatrix} \tau_{xx} & 0 & 0 \\ 0 & \tau_{yy} & 0 \\ 0 & 0 & \tau_{zz} \end{pmatrix} \qquad (2\text{-}11)$$

Polymer melts are non-Newtonian fluids. This means that they do not obey Newton's law of viscosity, that is

$$\tau = \eta\dot{\gamma} \qquad (2\text{-}12)$$

where η is the constant viscosity. The complexity of the structure of these liquids makes it possible for the structure to vary with the shear rate, and this change in structure results in a change in the viscosity. The complex rheological behavior of polymers has two important practical consequences. First, no single rheological property gives a complete rheological characterization of the material, and, second, the measurement of a rheological property requires careful control. Below, a very short review of the rheological instruments and techniques used for rheological measurements in this thesis is presented. Detailed description of the rheological measurements and equipment can be found in Dealy (1982) and Dealy and Wissbrun (1990).

2.2.1 Sliding Plate Rheometer

For this work, an Interlaken sliding plate rheometer with a flush-mounted shear stress transducer was used. The basic features of a sliding plate rheometer are shown in Figure 2-4 (Giacomin *et al.*, 1989). An end plate is acted on by the shear stress generated by the fluid and transmits the resulting moment to the cantilever beam. To avoid melt penetration into the gap around the end plate, the deflection of the latter must be limited to very small levels.
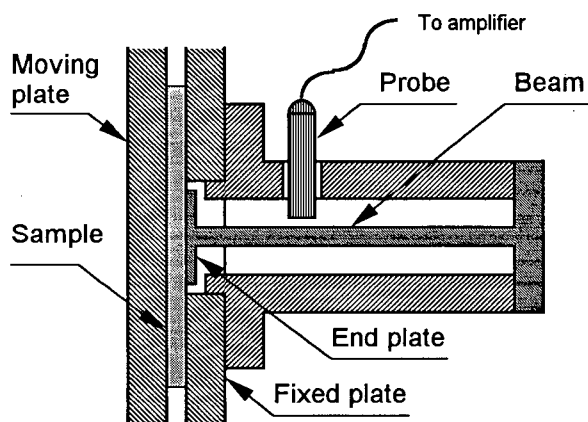
Figure 2-4. Schematic diagram of the shear stress transducer.

That is why a capacitance system was used, where a capacitor is formed by the probe acting as one of the plates, and the beam as the second plate.

The advantages of the sliding plate are that there are no effects of pressure on measurements, and that the edge effects can be eliminated by measuring the shear stress locally (using flush-mounted shear stress transducer). The equations for simple shear presented in previous section are fully applicable to the analysis of the data obtained by means of this instrument.

2.2.2 Parallel Plate Rheometer

Measurements of rheological properties at low shear rates and deformations are usually carried out in rotational rheometers such as the cone-and-plate or parallel-plate rheometers (Figure 2-5). In this work, a Rheometrics System IV parallel-plate rheometer
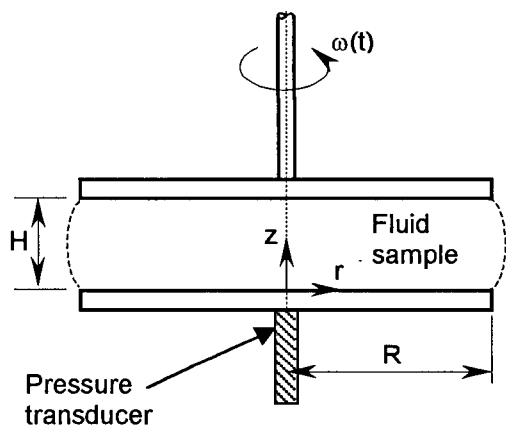
Figure 2-5 Parallel plate rheometer

was used. The two plates are mounted on a common axis of symmetry, and the sample is inserted in the space between them, The upper plate is rotated at a specified angular velocity $\omega(t)$ and as a result the sample is subjected to shear. The motion of the upper plate is programmed, and the resulting torque, M, is measured (so called constant strain rheometers). Reproducibility of such a device lies within ±2%. Another mode of operation is fixing the torque and measuring the displacement (constant-stress rheometers).

The most widely used experiments to determine the linear viscoelastic properties of polymers are small amplitude oscillatory shear tests. In this experiment, a sample of material is subjected to a simple shear ring deformation such that the shear strain is a function of time given by:

$$\gamma(t) = \gamma_0 \sin(\omega t) \tag{2-13}$$

where γ_0 is the strain amplitude and ω is the frequency. The stress is then measured as a function of time. It can be shown that the shear stress is sinusoidal in time and independent of strain (small linear viscoelastic limit):

$$\sigma(t) = \sigma_0 \sin(\omega t + \delta) \tag{2-14}$$

where σ_0 is the stress amplitude and δ is a phase shift, or the mechanical loss angle. Using a trigonometric identity, one can rewrite Equation (2-14) in the following form:

$$\sigma(t) = \gamma_0 \left[G'(\omega)\sin(\omega t) + G''(\omega)\cos(\omega t) \right] \tag{2-15}$$

where $G'(\omega)$ is the storage modulus and $G''(\omega)$ is the loss modulus. These two quantities can be calculated from the amplitude ratio, $G_d = \sigma_0 / \gamma_0$, and the phase shift, δ, as follows:

$$G' = G_d \cos(\delta) \tag{2-16}$$

$$G'' = G_d \sin(\delta) \tag{2-17}$$

This allows defining a complex modulus, $G^*(\omega)$, as follows:

$$G^*(\omega) = G'(\omega) + iG''(\omega) \tag{2-18}$$

Alternatively, the stress can be expressed in terms of two material functions, η' and η'', having units of viscosity as follows:

$$\sigma(t) = \dot{\gamma}_0 \left[\eta'(\omega)\cos(\omega t) + \eta''(\omega)\sin(\omega t) \right] \tag{2-19}$$

thus defining the complex viscosity:

$$\eta^*(\omega) = \eta'(\omega) - i\eta''(\omega) \tag{2-20}$$

2.2.3 Capillary Rheometer

The most widely used type of melt rheometer is the capillary rheometer. This device (Figure 2-6) consists of a melt reservoir, or barrel, for melting the polymer and a plunger or piston that causes the melt to flow through the capillary die of known diameter, D, and length, L. The quantities normally measured are the flow rate, Q, (related to the piston speed) and the driving pressure, ΔP, (related to force on the piston that is measured by means of a load cell). Reproducibility of capillary rheometers is $\pm 5\%$.
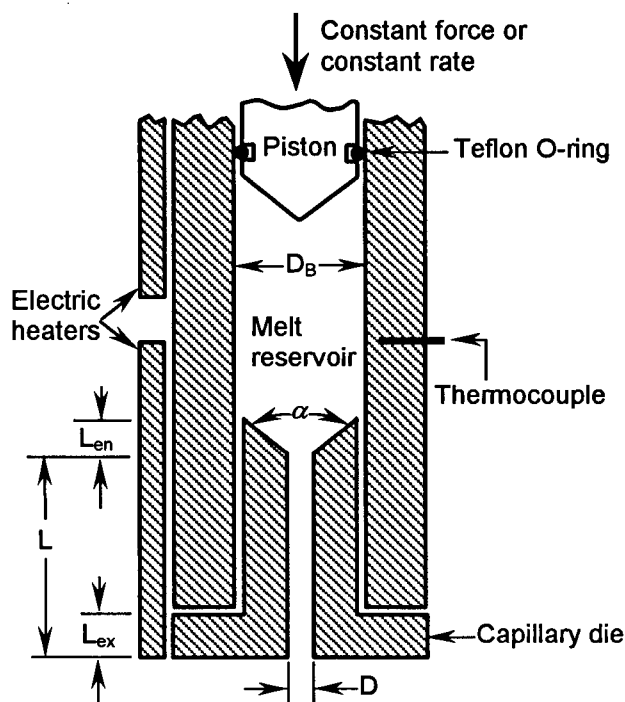
Figure 2-6 Capillary rheometer

Capillary rheometers are used primarily to determine the viscosity in the shear rate range of 5 to 1,000 s^{-1}. To calculate the viscosity, one must know the wall shear stress and the wall shear rate. For steady-state, fully-developed flow of an incompressible Newtonian fluid, the wall shear stress, σ_w, can be calculated as:

$$\sigma_w = \frac{\Delta P D}{4L}$$

(2-21)

The magnitude of the wall shear rate, $\dot{\gamma}_w$, for a Newtonian fluid can be calculated as:

$$\dot{\gamma}_w = \frac{32Q}{\pi D^3}$$

(2-22)

For the case of a non-Newtonian fluid, this quantity is called the apparent wall shear rate, $\dot{\gamma}_A$, that is the rate that a Newtonian fluid would have at the same volumetric flow rate Q:

$$\dot{\gamma}_A = \frac{32Q}{\pi D^3}$$

(2-23)

Capillary flow of a Newtonian fluid is a controlable flow which means that the flow kinematics does not depend on on the nature of the fluid. Capillary flow of molten polymers, however, is only a partially controllable flow. This means that the velocity distribution in this flow is governed not only by the boundary conditions but also depends

on the nature of the fluid. To account for this, at least two corrections should be applied to the experimental data. First, the velocity profile in the flow of a polymeric fluid is nonparabolic, and one must correct the wall shear rate, $\dot{\gamma}_w$, defined by Equation (2-22). This correction, generally known as the Rabinowitch correction, can be calculated as (Dealy and Wissbrun, 1990):

$$b = \frac{d(\log \dot{\gamma}_A)}{d(\log \sigma_w)} \qquad (2\text{-}24)$$

It is noted that the correction factor b is a local quantity depending on $\dot{\gamma}_A$. It can be shown that the true wall shear rate then can be obtained by use of the following equation (Dealy and Wissbrun, 1990):

$$\dot{\gamma}_w = \left(\frac{3+b}{4}\right)\dot{\gamma}_A \qquad (2\text{-}25)$$

For a power-law fluid, the shear stress is given by

$$\sigma = K\dot{\gamma}^n \qquad (2\text{-}26)$$

where σ is the shear stress, $\dot{\gamma}$ is the shear rate, K is the consistency index, and n is the power law exponent. It can be shown that the wall shear rate for a power law fluid can be expressed as:

$$\dot{\gamma}_w = \left(\frac{3+1/n}{4}\right)\dot{\gamma}_A \qquad (2\text{-}27)$$

Thus, it can be seen from Equations (2-25) and (2-27) that the Rabinowitch correction is equal to $1/n$ for a power law fluid and 1 for a Newtonian fluid. It mainly represents deviation from Newtonian behavior.
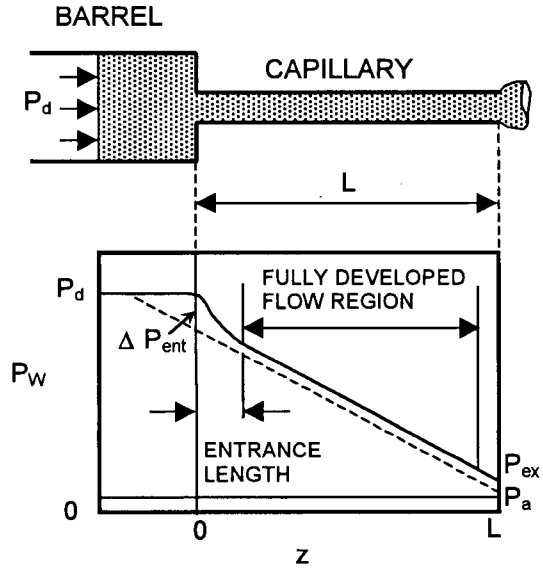
Figure 2-7. Wall pressure distribution for capillary flow (from Dealy, 1982)

Second, the pressure drop must be corrected for the additional pressure required for the melt to pass through the contraction between the barrel and the capillary. The wall pressure distribution actually observed for capillary flow of molten polymers is sketched in Figure 2-7. One can see that the pressure drop, $\Delta P = P_d - P_a \approx P_d$ is clearly not the wall pressure drop that one would observe for fully developed flow in a capillary of a length L. There is a significant pressure drop near the entrance of the die, ΔP_{ent}. There may also be residual pressure at the die exit, called the exit pressure, ΔP_{ex}, but it is quite small compared to ΔP_{ent}. The total pressure correction for exit and entrance regions is called the end pressure, ΔP_{end}, that is,

$$\Delta P_{end} = \Delta P_{ex} + \Delta P_{ent}$$
(2-28)

The true wall shear stress is then obtained as:

$$\sigma_w = \frac{(\Delta P - \Delta P_{end})}{4(L/D)}$$
(2-29)

The pressure correction, ΔP_{end}, or the Bagley end correction can be determined by use of a scheme proposed by Bagley (1957). He suggested to measure the driving pressure, P_d, at various values of the flow rate, Q, using a variety of capillaries having different lengths. For each value of the apparent wall shear rate (Equation (2-23)) he then plotted
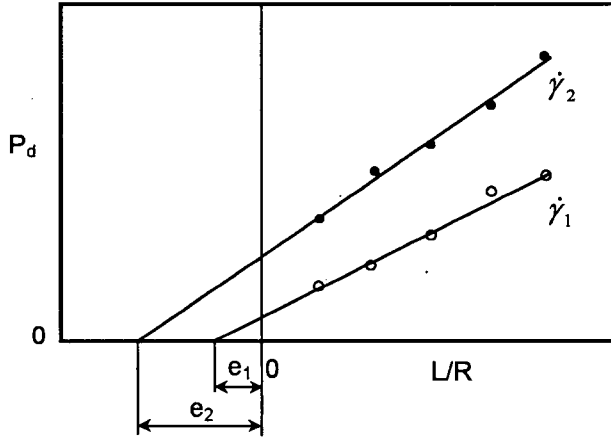
Figure 2-8. Bagley plot for determining the end correction.

driving pressure versus L/D and drew a straight line through the points as shown in Figure 2-8. Extrapolating the lines to the $P_d=0$ axis, he then obtained an end correction, e. Thus, the true wall shear stress can then be calculated as follows:

$$\sigma_W = \frac{P_d}{4(L/D + e)} \tag{2-30}$$

An alternative way to determine the end correction is to use orifice capillaries with $L/D=0$.

The measurements of the entrance pressure drop, ΔP_{ent}, are often used for estimating the extensional viscosity, η_E. According to Cogswell (1978), this pressure drop has two components, one due to shear and one to extension. The extensional rate, $\dot{\varepsilon}$, for a power law fluid is then:

$$\dot{\varepsilon} = \frac{4\dot{\gamma}_A \eta_A}{3(n+1)\Delta P_{ent}} \tag{2-31}$$

where n is the power-law index and η_A is the apparent viscosity $(\eta_A = \sigma_w/\dot{\gamma}_A)$. The principal stretching stress, $\sigma_E = \sigma_{11} - \sigma_{22}$, is defined as:

$$\sigma_E = \frac{3}{8}(n+1)\Delta P_{ent} \tag{2-32}$$

and hence the extensional viscosity, $\eta_E = \sigma_E/\dot{\varepsilon}$, can be written as follows:

$$\eta_E = \frac{9(n+1)^2 (\Delta P_{ent})^2}{32\eta_A \dot{\gamma}_A^2}$$ (2-33)

More details on capillary rheometry including a discussion of viscous heating, pressure effects, wall slip, and polymer degradation can be found in Dealy (1982) and Dealy and Wissbrun (1990).

2.3 Flow Curve

Various flow instabilities observed in the flow of polymeric liquids through capillary dies, generally known as melt fracture, are reflected in the apparent flow curve, determined by means of a capillary rheometer. This is essentially a log-log plot of the wall shear stress, σ_w, as a function of the apparent shear rate, $\dot{\gamma}_A$.

A typical apparent flow curve for a linear polymer is shown in Figure 2-9. One may identify five different flow regions. Initially there is a *stable* region where the extrudate appears smooth and glossy (region 1). In this region, the viscosity can be represented by a power-law expression (Equation (2-26)).

Beyond some critical wall shear stress, σ_{c1}, the first visual
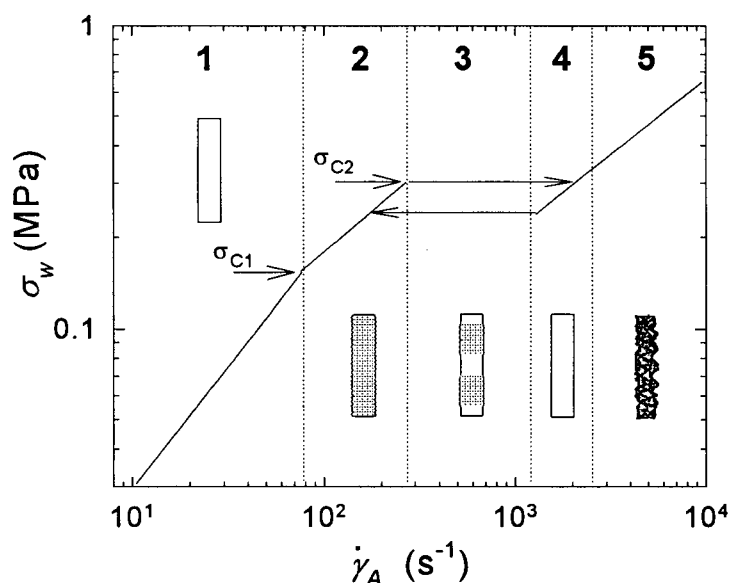
Figure 2-9 A typical apparent flow curve of a linear polymer

manifestation of an extrusion instability appears as a high-frequency, small-amplitude distortion of the extrudate known as *sharkskin* (region 2). The onset of sharkskin appears to coincide with a change in the slope of the apparent flow curve. At a second critical value σ_{c2} and within a certain range of apparent shear rates, the flow ceases to be stable (region 3). It is the region of *oscillating,* or *stick-slip,* melt fracture where the extrudate has the appearance of alternating smooth and distorted portions . In this region, pressure drop sometimes oscillates between two extreme values. The periodic variations of the pressure and apparent shear rate define a hysteresis loop that connects the two branches of the apparent flow curve. At higher throughputs there is sometimes a transition to a second stable flow regime in which the extrudate again becomes smooth. This is a *superextrusion* region (region 4). Finally, at still higher shear rates, there is a transition to a wavy chaotic distortion (*gross melt fracture*) which gradually becomes more severe with increase in $\dot{\gamma}_A$ (region 5). This typical behavior has been observed in the capillary extrusion of many linear polymers such as high density and linear low density polyethylene (Kalika and Denn, 1987), polytetrafluoroethylene (Tordella, 1969), polybutadiene (Vinogradov *et al.*, 1972b), and others.

2.4 Melt Fracture

Melt fracture is an instability which occurs beyond a critical shear rate or stress in a capillary die. The term melt fracture was introduced by Tordella (1956) because of the audible tearing noises which accompanied the distortion of the extrudate. Another term *elastic turbulence,* which is sometimes used to describe the same phenomenon (Vinogradov and Ivanova, 1968), has now largely disappeared.

Melt fracture is most easily observed during extrusion at high throughputs through a long die. Below some critical throughput the surface of the extrudate is smooth and glossy. At a critical throughput value and higher the surface becomes distorted. The nature of the surface distortions is dependent on the type of a polymer. The most complete set of phenomena is observed in the extrusion of linear polyethylenes (Kalika and Denn, 1987). At a first critical stress, which is typically of the order of 0.1-0.2 MPa, the extrudate surface exhibits a small-amplitude, high-frequency periodic distortion. This is generally known as surface melt fracture or sharkskin. As the name implies, sharkskin is a roughness that usually modulates the extrudate diameter by no more than 1% and consists of semiregular cracks or grooves that run mainly perpendicular to the flow (Piau et al., 1990; Benbow and Lamb, 1963). However, Piau and El Kissi (1992) using a photographic technique pointed out that in the case of highly entangled polymers, the size and spacing of these cracks may be of the same order of magnitude as the diameter of the extrudate. They stated that in this case, it is impossible to define sharkskin as a small-amplitude, high-frequency roughness, and that this definition concerns only a secondary phenomenon, based on observations carried out well downstream of the outflow section and hence after relaxation of the stresses and cracks. Surface melt fracture often manifests itself as a change in the slope of the apparent flow curve (Ramamurthy, 1986) as discussed in the previous section.

There is a second critical stress at which periodic pressure pulsations are frequently observed. The extrudate surface alternately shows relatively smooth and sharkskin regions. This is known as *stick-slip*, or *spurt* flow. The average stress remains approximately constant in the stick-slip region. Note that oscillations in pressure drop are

not always observed. Pudjijanto and Denn (1994) as well as Waddon and Keller (1990, 1992) found a stable "island" in the stick-slip region of polyethylene, where pressure oscillations stopped, extrusion pressure significantly dropped, and the extrudate became reasonably smooth. This island exists only in a narrow temperature window and a small variation of temperature, e.g. of the order of 1 °C, can interchange oscillations with a stable response. If the shear rate is increased further, a second stable flow regime may be encountered in which the emerging extrudate is smooth again (Tordella, 1969). This region is generally known as the superextrusion region. Finally at even higher shear rates the extrudate becomes grossly distorted and is characterized by a wavy, chaotic, and non-periodic appearance; this is so called gross melt fracture.

While the origins of extrudate distortions are still in dispute, there is agreement that sharkskin and gross melt fracture are distinguished not only by the appearance of the extrudate, but also by the critical conditions for their onset and by the character of the accompanying flow inside the die. Gross melt fracture occurs when the wall shear stress reaches a critical condition that seems to depend only on the polymeric fluid and little or not at all on the characteristics of the die (diameter, length, and the material of construction) (Kalika and Denn, 1987; Piau et al., 1990). Sharkskin, on the other hand, does not occur for all polymers (Denn, 1990), and for those for which it does occur, the onset condition has been found to depend on the shape of the outlet region of the die (Piau et al., 1990), the length of the die (Moynihan et al., 1990) and in some cases on the material of construction of the die or the presence of lubricants or sticking agents at the die surface (Ramamurthy, 1986; Hatzikiriakos and Dealy, 1991b). Finally, it is generally accepted that sharkskin originates at the die exit (Howells and Benbow, 1962), while the

flow within the die is unsteady only when gross melt fracture occurs (Benbow and Lamb, 1963).

2.5 Mechanisms to Explain Melt Fracture

The mechanisms or explanations of melt fracture which have been proposed involve one or more of the following features: die entry and exit effects, thermal effects, and slip at the die wall. These will now be discussed to some detail.

2.5.1 Mechanisms to explain sharkskin phenomenon

It is commonly accepted that sharkskin is developed at the die exit. The first theory about surface melt fracture (sharkskin) was proposed by Howells and Benbow (1962) and later by Cogswell (1977). They hypothesized that the polymer fractures due to high stretching rates and to high stresses as a result of the abrupt change (shear to free surface flow) in the boundary condition at the exit of the die. Bergem (1976) carried out capillary experiments for different polymers, using a tracer technique. He found that sharkskin arose from a tearing of the melt at the exit of the capillary. Piau *et al.* (1988) showed that cracks on the surface of extrudate always originate at the exit of the die. It should be noted that the existence of localized stresses at the die exit is confirmed by birefringence photographs (Vinogradov and Malkin, 1980). Tremblay (1991) simulated the flow of a linear polydimethylsiloxane melt. He showed that high stresses at the die exit produce negative hydrostatic pressure. He suggested that cavitation should occur very close to the die lip, thus leading to surface effects. Why there should be a critical condition for this phenomenon is not explained.

Kurtz (1992) suggested that two critical conditions are required for sharkskin. First, a critical value of the wall shear stress must be exceeded and, second, the extrudate must be stretched for a sufficient period of time as it leaves the die. Moynihan *et al.* (1990) added to this conclusion that the melt should be first "pre-stressed" critically at the entry region of the die.

Ramamurthy (1986) suggested that the onset of sharkskin was attended by the occurrence of wall slip in the capillary. This suggestion is supported by a noticeable slope change in the flow curve at the onset of sharkskin (Kurtz, 1984) which can be interpreted as slip. However, Piau and El Kissi (1992) argued that slip in the die cannot explain the origin of the sharkskin. Hatzikiriakos (1994) carried out numerical simulations of the flow of high density and linear low density polyethylenes under slip conditions and showed that slip is not a necessary condition for the occurrence of the sharkskin phenomenon, although it may affect it. Instead, a critical extension rate at the capillary exit and a critical pre-stress of the polymer at the land region of the die provide the necessary conditions for its occurrence.

Wang *et al.* (1996) speculated that the slope change in the flow curve arises from a combination of interfacial slip and cohesive failure due to chain disentanglement initiated on the die wall in the exit region. Since the disentanglement state is unstable for the adsorbed chains, it is followed by a consequent re-entanglement, thus producing entanglement-disentanglement fluctuations that cause the sharkskin phenomenon. They found that the sharkskin dynamics (detailed characterization of distortions) is in good correlation with chain relaxation processes.

2.5.2 Die entry effects

Observations of the flow into the die at extrusion rates above and below that at which gross melt fracture occurs show that in some circumstances there is a clear interaction between the converging flow at the die entry and flow instabilities in the die. Most researches suggest that the region upstream of the contraction is the site of initiation of the gross melt fracture type of instability. They base their opinion on experimental observations using essentially two methods: observation of flow tracers in the fluid, and flow birefringence. This latter technique for observing and investigating polymer flow through capillaries was intensively studied by Vinogradov and Malkin (1980), and the appearance of melt fracture was characterized by the observation of birefringence patterns before and after the critical regime. However, the precise instability mechanism is not completely clear yet, and it seems to be affected by various properties, such as fluid rheology, capillary die entrance geometry, and thermal effects. One explanation, given by Bagley and Schreiber (1961), is that the liquid polymer is fractured by elongational stresses in the entry region of the die. They gave a critical capillary wall recoverable shear strain criterion for the onset of gross melt fracture. White (1973) gave a different explanation based on experimental observations of the flow of a viscoelastic fluid through a contraction. He argued that a hydrodynamic instability was initiated in the form of a spiral flow when a critical Weissenberg number ($We=\lambda v/\delta$, where λ is the characteristic relaxation time, δ is the spacing, and v is the relative velocity) was reached. In his opinion, this instability is the initial mechanism of polymer melt extrudate distortions.

Most authors agree in claiming that, above a certain extrusion rate, the flow upstream of the contraction becomes unstable. These instabilities occur in the form of sudden pulsations, which were confirmed by visualization (Piau *et al.*, 1990) and birefringence measurements (Tordella, 1969). They showed that such instabilities started along the upstream flow axis owing to the high elongation stresses that develop in this area. These instabilities trigger the phenomenon of gross melt fracture, which is often seen in the form of a regular helix oscillating at the same frequency as that of the pulsations of the upstream elongational flow (Piau *et al.*, 1990).

2.5.3 Wall slip

At this point, it is appropriate to refer to wall slip as a possible explanation of flow instabilities. It is convenient to use the word *slip* to describe events which are incompatible with the usual *no-slip* boundary condition of continuum mechanics. This phenomenon has been fully reviewed by several authors in the past (Petrie and Denn, 1977; Schowalter, 1988; Denn, 1992).

It has long been recognized that polymer melts may violate the classical no-slip boundary condition of Newtonian fluid mechanics at solid surfaces. The classical experimental example of the effect of slip on the stability of the polymer shear flow is the spurt phenomenon (Vinogradov *et al.*, 1972b). Deviations from the no-slip boundary condition were observed by many other investigators (Laun, 1982; Lin, 1985). Lim and Schowalter (1989) reported observations of slip for a polybutadiene melt using a heat transfer technique to record deviations from fully-developed flow. Kurtz (1984), Ramamurthy (1986) and Kalika and Denn (1987) showed that the flow curves obtained

for various polyethylenes were discontinuous and exhibited a change in slope corresponding to the occurrence of surface melt fracture. Ramamurthy (1986) therefore associated the appearance of this phenomenon with a loss of adherence at the interface between the polymer and wall material. He also observed that the onset of surface distortion was dependent on the material of construction of the die, and it could be delayed or eliminated by changing the material of the die, although this is in contrast to observations for poly(vinyl alcohol)-borax solutions (Kraynik and Schowalter, 1981). This is a clear manifestation that the nature of the interface plays a crucial role in this phenomenon.

The addition of fluoropolymers to the resin eliminates surface defects in spite of the fact that it promotes wall slip (Rudin *et al.*, 1985). Thus, it is clear that the wall slip itself is not the primary cause of sharkskin. The same conclusion was drawn by Hatzikiriakos and Dealy (1991a,b) who carried out experiments in a sliding plate rheometer and later (1992a) in a capillary rheometer to determine the effect of the presence of two fluoropolymers on the slip velocity of a HDPE. They found that in one case slip increased while in the second case it decreased, although both fluoropolymers eliminated surface defects.

The mechanism of wall slip is not yet clear. One hypothesis involves the well known theory of Vinogradov (Vinogradov *et al.*, 1972b). He argued for a transition at some critical wall stress from a melt state to a so called "forced high elastic state" in which the polymer melt could be treated as a rubbery solid, and thus adhesive failure could be understood. Another mechanism is based on the ability of polymer molecules to entangle and form a physical network. According to Brochard and de Gennes (1992),

there exists a monolayer of a polymer next to a wall where molecules are attached to the wall through several sites along their backbone. These chains are connected with the bulk of the material through entanglements. Under flow, the polymer molecules in the bulk are stretched, and in turn, they apply forces to the molecules at the interface through the entanglements. At some critical shear stress, some of the chains detach from the interface, and as a result, a weak slip boundary condition is obtained. This process depends on the interfacial conditions, e.g. the presence of fluoropolymer coatings which reduce polymer adsorption. If the shear stress is increased further, sudden disentanglement occurs, and a strong slip close to plug flow is obtained. Consequently, the polymer chains relax and entangle again, and this alternating transition between a weak and strong slip keeps on in a continuous fashion resulting in pressure drop oscillations in capillary flow. This flow mainly depends on the molecular characteristics of the polymer, e.g. the number of entanglements.
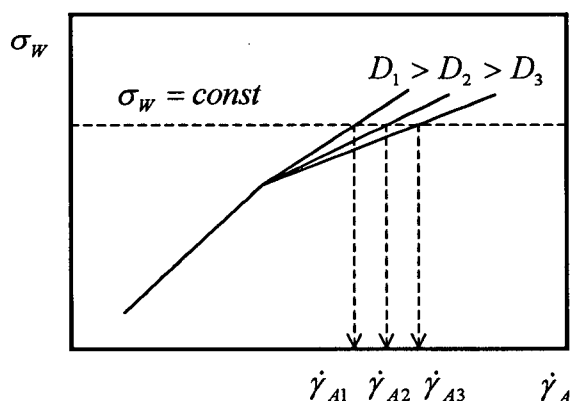
Figure 2-10. Flow curves under slip condition

The traditional way of inferring wall slip is the so called Mooney method (Mooney, 1931) based on an apparent die diameter dependence of the rheological measurements. According to this technique, the flow curves determined with a series of capillaries having the same length-to-diameter ratio (to eliminate the pressure effect) and different diameters diverge at the critical shear stress for the onset of slip as is shown in Figure 2-10. Then the apparent shear rate, $\dot{\gamma}_A$, in a cylindrical die is given by the following formula:

$$\dot{\gamma}_A = \dot{\gamma}_{A,s} + 8\frac{u_s}{D} \qquad (2\text{-}34)$$

where $\dot{\gamma}_{A,s}$ is the real wall shear rate corrected for slip and u_S is the slip velocity. For a given shear stress, $\dot{\gamma}_A$ is linearly dependent on $1/D$ with slope equal to $8u_S$. Therefore, by using dies of different radii, the slip velocity can be determined. Obviously, this technique is indirect and it does not take into account possible temperature effects on the apparent flow curve. It should also be noted that there is discrepancy in the values of slip velocity calculated by various authors. Thus the slip velocity measured by Atwood and Schowalter (1989) for HDPE using a hot-film probe is very high compared to that reported by Ramamurthy (1986). This variation in the reported values seems to be due to differences in experimental methods and poor control of conditions at the interface.

The most reliable data on the slip velocities could be obtained by direct measurements of velocity profiles near the die wall by using laser velocimetry or a radioactive tracer technique (Binnington *et al.*, 1983). However, there is a lack of such experimental studies for polymer melt flows. Galt and Maxwell (1964) performed direct measurements of velocity profiles in capillary flows of molten branched polyethylenes using a particle tracer technique. Migler *et al.* (1993) used a fluorescent optical technique to measure slip velocities directly. Both studies were carried out at shear stresses, which were to small to be of much interest to polymer processing.

Several attempts have been made to model the slip velocity. For this purpose, power-law expressions relating the slip velocity to the wall shear stress have been proposed by several investigators. Hill *et al.* (1990) developed a framework based on the theory of elastomer adhesion. Agreement between the theory and the slip velocity data reported by Kalika and Denn (1987) is remarkably good. Hatzikiriakos and Dealy

(1992a) formulated a theory of wall slip based on an extension of a kinetic adsorption/desorption analysis first proposed by Lau and Schowalter (1986). The theory fits their data from both capillary and plate rheometers quite well. Stewart (1993), using a rate-activation energy theory, derived an expression for the slip velocity which includes a hyperbolic sine term in place of the "σ_W^m" term. It also includes a geometric-mean approximation for the work of adhesion that incorporates the surface energetics of the polymer and presumed coating layers explicitly into the model. Agreement with the data of both Kalika and Denn (1987) and Hatzikiriakos and Dealy (1992a) is quite good. Hatzikiriakos (1993) derived a theoretical slip velocity model by using a rate activation theory similar to that used by Stewart. Leonov (1990) and later Adewale and Leonov (1997) proposed the non-monotonic wall slip model based on a statistical theory of the adhesive friction of elastomers. Their model takes into account the delay in breaking polymeric chains off the wall due to Brownian oscillations of the chain segments attached to the wall. This results in the appearance of an S-shaped dependence in the curve relating wall stress to slip velocity, and may be used to provide qualitative description of the spurt effect.

It should be noted that all these proposed models are "static" models, where the slip velocity depends on the instantaneous value of the wall stress. However, Hatzikiriakos and Dealy (1991a) suggested that the slip velocity may depend on the past states of the local wall shear and normal stresses. This is similar to the concept of the fluid memory in viscoelasticity, where the local state of stress depends on the past deformation history to which the fluid particles were subjected. To incorporate such a relaxation process, the usual no-slip boundary condition is replaced by a memory function relating the slip

velocity to the history of the wall stress. Such a model can be used to describe the slip behavior of melts under transient conditions. A dynamic slip velocity model was recently developed by Hatzikiriakos and Kalogerakis (1994) and later by Hatzikiriakos (1995). The behavior of a polymer/metal interface was simulated by using a network kinetic theory. The model predictions were found to adequately represent the experimental data for HDPE. Finally, it should be noted that all proposed models require fitting of certain model parameters to experimental data.

2.6 Pressure Driven Flow of Molten Polymers

2.6.1 Viscous Heating

In polymer processing, *pressure driven flow* of molten polymers occurs in a large variety of flow geometries. The polymer is forced through a channel by a pressure gradient (flow in an extruder die) or it is dragged along a moving wall (rotating screw in a stationary barrel). Very often the channel flow is followed by a *free surface flow* (film blowing, coating, etc.). These flows take place at relatively high rates of deformation, temperatures, and often at high temperature gradients. Velocity and temperature fields influence each other: the temperature field affects the flow through the temperature dependence of the rheological properties, and the velocity field influences the temperature field through the mechanisms of convection heat transfer and thermal energy production by viscous dissipation. The latter represents the conversion of mechanical energy (work of deformation) into thermal energy (Winter, 1977; Cox and Macosko, 1974). This phenomenon, generally known as *viscous heating*, is significant in the processing of molten polymers. Most polymers have high viscosities and low thermal

conductivities, which in combination with large process shear rates can lead to significant local increases in temperature.

Thermal effects can contribute to the stability or instability of the flow of molten polymers. Lupton and Regester (1965) studied a possible effect of viscous heating and wall slip on flow instabilities in HDPE. They concluded that temperature increases were too small to cause the instability in the polymer flow, i.e., the discontinuity could not arise through viscous heating. Sukanek *et al.* (1973) concentrated on the effect of viscous heating for a Newtonian fluid with a temperature dependent viscosity. Their analysis for plane Couette flow showed a variety of modes of instability, but no clear interpretation was offered in the context of melt flow instability. Pearson and Shah (1973) studied the development of the temperature field due to an imposed temperature gradient between the flow and the wall and the resultant changes in the velocity field for Newtonian and power-law fluids. By using a linearized stability analysis, they concluded that an instability might arise with temperature differences of the order of 100°C. This is unlikely to be relevant in normal extrusion, and the conclusion here, in agreement with the remarks of Pearson *et al.* (1973), is that this mechanism for instability is not relevant to melt fracture. However, Cox and Macosco (1974) observed large temperature rises in capillary extrusion of acrylonitrile butadiene styrene which could be as high as 70°C.

Reher *et al.* (1988) have used a specially constructed capillary die with flush-mounted thermocouples and have reported a significant rise in the temperature for the capillary flow of PVC. They concluded that this increase in temperature could be explained as a consequence of the wall slip phenomenon (local friction). Hence, it would

be wrong to ignore the thermal effects in polymer flow analysis if viscous heating is relevant or if there is evidence of wall slip.

2.6.2 System of Equations

Heat transfer during the capillary extrusion of polymer melts has been the subject of several reviews and studies over the past decades (Winter, 1977; Warren, 1988). The problem is governed by the following equations (Bird $et\ al.$, 1962), namely the equation of conservation of mass

$$\partial\rho/\partial t + \underline{\nabla}\cdot(\rho\underline{v}) = 0 \qquad (2\text{-}35)$$

the equation of motion

$$\rho\,D\underline{v}/Dt = \underline{\nabla}\cdot\underline{\underline{\tau}} + \rho\underline{g} \qquad (2\text{-}36)$$

and the conservation of energy equation

$$\rho\,De/Dt = \underline{\nabla}\cdot(k\underline{\nabla}T) + \underline{\underline{\tau}}:\underline{\nabla v} \qquad (2\text{-}37)$$

where $\partial/\partial t$ denotes partial and D/Dt the substantial derivative, ρ and k are the fluid density and thermal conductivity, respectively, $\underline{v}$ is the velocity vector, e is the internal energy, T is the temperature, and $\underline{\underline{\tau}}$ is the stress tensor. Equations (2-35)-(2-37) are usually supplemented by the constitutive equation (see below) and appropriate boundary conditions.

2.6.3 Constitutive Equation and Relaxation Time Spectrum

Constitutive equations are mathematical relationships that allow one to calculate the stress in liquid, given the deformation history. In general, the constitutive equation can be written as follows:

$$\tau = \tau(\mathbf{C}^{-1})$$ (2-38)

where $\mathbf{C}^{-1}(t',t)$ is the Finger tensor which describes the change in shape of a small material element between times t' and t (deformation history). Constitutive equations are often derived from constitutive models. A constitutive model is a set of assumptions about the molecular forces and motions that produce stress. A comprehensive review of constitutive equations and models for polymer melts and solutions can be found in Larson (1988).

The classical framework of linear viscoelasticity (Ferry, 1980) describes the stress in polymers with a universal equation. All the material properties coalesce into a single material function, the relaxation modulus, $G(t)$:

$$G(t) = \int_0^\infty \frac{d\lambda}{\lambda} H(\lambda) \exp(-t/\lambda)$$ (2-39)

where λ is the relaxation time, and $H(\lambda)$ is the relaxation time spectrum. The time dependence of rheology for majority of polymeric melts is completely described by $H(\lambda)$, even at large strains or high strain rates. The shape of $H(\lambda)$ is often correlated with specific molecular architectures.

The relaxation modulus, $G(t)$, can also be expressed in terms of the Maxwell element analogy, that is the assembly consisting of a spring in series with a dashpot. If one takes the spring constant to be analogous to the initial shear modulus, g_0, of the polymeric liquid, and the time constant, that is a ratio of the dashpot and spring constants, to be analogous to the relaxation time of the liquid, λ, then the shear relaxation modulus is:

$$G(t) = g_0 [\exp(-t/\lambda)]$$ (2-40)

and the constitutive equation is

$$\tau_{ij}(t) = \int_{-\infty}^{t} g_0 \left\{ \exp[-(t-t')/\lambda] \right\} \dot{\gamma}_{ij}(t') dt' \qquad (2\text{-}41)$$

This is called the integral form of the Maxwell model.

Actual relaxation processes cannot be described by a single exponential function. Greater flexibility can be obtained by use of the "generalized Maxwell model", which is the rheological constitutive equation analogous to the mechanical assembly shown in Figure 2-11. The forces in the various elements are additive, and the relaxation modulus is:

$$G(t) = \sum_{i=1}^{N} g_i \left[\exp(-t/\lambda_i) \right] \qquad (2\text{-}42)$$

where g_i and λ_i are the initial modulus and relaxation time corresponding to each Maxwell element. Then the generalized (multi-mode) Maxwell model can be written as follows:
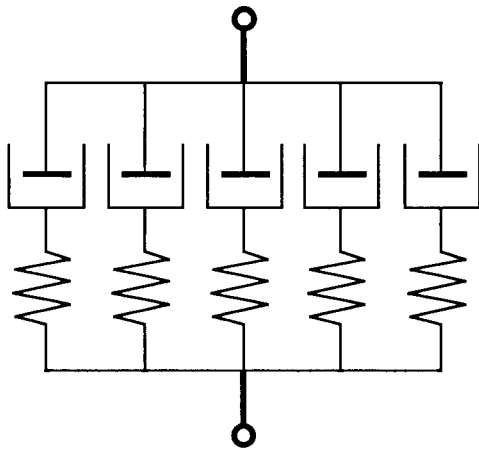
Figure 2-11 Mechanical analog of the generalized Maxwell model

$$\tau_{ij}(t) = \int_{-\infty}^{t} \sum_{k=1}^{N} g_k \left\{ \exp[-(t-t')/\lambda_k] \right\} \dot{\gamma}_{ij}(t') dt' \qquad (2\text{-}43)$$

By use of sufficient number of elements, this equation can be made to describe almost any experimental behavior within the linear viscoelastic regime. The set of (g_i, λ_i) pairs is called the discrete relaxation time spectrum of the material. The discrete relaxation spectrum is a discrete analogue of the continuous relaxation spectrum.

The relaxation spectrum, $H(\lambda)$, cannot be measured directly in an experiment. Instead, linear viscoelastic data such as the dynamic moduli $G'(\omega)$ and $G''(\omega)$ are used to calculate the discrete relaxation spectrum, that is the Maxwell model parameters (g_i, λ_i), by means of a suitable fitting procedure. Such fitting methods include least-square approximations (Baumgaertel and Winter, 1989; Laun, 1978), regularization methods (Honerkamp and Weese, 1989), the maximum entropy method (Elster and Honerkamp, 1991), and some others (Tschoegl and Emri, 1993). Some of the methods have been compared by Orbey and Dealy (1991). Baumgaertel and Winter (1989) proposed a method for representing the relaxation spectrum of a material with the fewest possible Maxwell modes while remaining within the experimental scatter of the available dynamic data. Such a representation is called a *parsimonious* model (PM-spectrum). Details of the method can be found elsewhere (Winter, 1997).

3 Objectives

*T*he primary objective of this work is a comprehensive and thorough study of the rheology of Teflon® FEP resins. The processability of Teflon® FEP resins in the extrusion through channels of different shapes is also studied. In more detail, the objectives of the thesis can be summarized as follows:

1. To conduct a thorough rheological characterization of a number of Teflon® FEP resins by means of a parallel-plate and capillary rheometers. To study their rheological properties as a function of:

    - Temperature

    - Pressure

    - Molecular weight

    - Composition

    - Crystallinity

2. To determine the critical conditions (wall shear stress and shear rate) for the onset of melt fracture and wall slip as functions of:

    - Temperature

    - Pressure

    - Molecular weight

    - Composition

    - Interface conditions

3   To develop numerical codes for solving the following problems:

    - Determination of relaxation time spectra from dynamic mechanical data

- Determination of parameters of a constitutive equation from suitable experimental data

- Numerical simulation of the flow of molten polymers in a capillary die accounting for thermal and wall slip effects

- Calculation of wall slip velocities in capillary flow subject to thermal effects from experimental data.

4. To study the processability of a number of polymers including of Teflon® FEP resins and polyolefins in extrusion with a wire coating die as a function of:

- Temperature

- Interface conditions

- Presence of additives

5. To study the effect of processing aids on the processability of Teflon® FEP polymers and polyolefins. To propose possible explanations of elimination of melt fracture.

Thesis organization. The essential results of this thesis have been published or submitted as publications (see Rosenbaum and Hatzikiriakos, 1997; Rosenbaum *et al.*, 1995, 1996, 1998a,b). However, additional work and results not included in these papers are presented here.

Chapter 4 is based on the paper *Rheological Characterization of Well-Defined Tetrafluoroethylene/Hexafluoropropylene Copolymers* to be published *in Rheologica Acta*. It includes results obtained using linear oscillatory shear experiments in a parallel-plate rheometer with a variety of Teflon® FEP resins having different molecular weights and compositions.

Chapter 5 is based on the paper *Flow Implications in the Processing of DuPont Tetrafluoroethylene/Hexafluoropropylene Copolymers* published in *International Polymer Processing*, volume X (1995) and the presentation at ANTEC'95 (Rosenbaum *et al.*, 1995). It includes the results obtained in the capillary rheometer study of a variety of Teflon® FEP resins. Also, a few results not included in this paper, but presented at ANTEC'96 (Kazatchkov *et al.*, 1996), are discussed in this chapter.

The results of the experimental study were used for the rheological characterization of the Teflon® FEP resins presented in Chapter 6. The latter contains the portion of the paper to be published in *Rheologica Acta* concerned with calculation of the relaxation time spectra and estimation of the critical molecular weight based on the relaxation spectra. It also includes results on the modeling of the rheological behavior of Teflon® FEP resins by means of the Phan-Tien and Tanner constitutive equation.
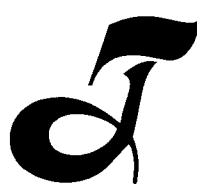
Chapter 7 is a comprehensive analysis of the flow of molten polymers in a capillary channel. It includes the entire paper *Wall Slip in the Capillary Flow of Molten Polymers Subject to Viscous Heating* published in *AIChE Journal*, volume 43 (1997) and the paper presented at ANTEC'96 (Rosenbaum and Hatzikiriakos, 1996). In this chapter, several aspects of the numerical simulation of nonisothermal capillary flows with a slip boundary condition are considered in detail. Specifically, a new numerical technique to calculate the slip velocity is proposed, and the results for a number of commercial resins including polyethylene, polypropylene, and Teflon® FEP are presented.

In Chapter 8, the effect of various processing aids on the processability of fluoropolymers and polyolefins is studied. It is based partially on the paper published in

International Polymer Processing and the paper presented at ANTEC'98 (Rosenbaum *et al.*, 1998a).

Finally, in Chapter 9, a few conclusions are drawn, recommendations for future work are given, and the contributions made to general knowledge in this field are discussed.

4   Oscillatory Flow Measurements on Teflon® FEP Resins

he rheology of tetrafluoroethylene/hexafluoropropylene (TFE/HFP) copolymers and tetrafluoroethylene/hexafluoropropylene/perfluoro(alkyl vinyl ether) (TFE/HFP/ PAVE) terpolymers, also known as Teflon® FEP polymers, having different molecular weight and composition (HFP and PAVE content) was studied by means of a parallel-plate rheometer. Three groups of polymers having different molecular weights and composition with nearly constant polydispersity (around 2.5) were considered; namely, Group A having a relatively low melting temperature (amorphous with a high content of HFP), Group B having a higher melting point (semi-crystalline with a lower content of HFP), and Group C with high melting point resins having a different content of PAVE. The zero-shear viscosity of the resins was found to scale with the molecular weight with the well-established scaling factor of 3.4. The critical molecular weight for the onset of entanglements, M_c, was found to be about 100,000, a value much higher than those previously reported in the literature for other polymers. The rheology of resins in the second and third groups (higher melting point) was found to exhibit a strong dependence on thermal history during oscillatory-shear measurements. The data obtained in experiments at different temperatures without a preheating to a certain value (330°C) exhibited a violation of the time-temperature superposition principle and no well-defined values of the zero-shear viscosity. This is attributed to residual crystallinity even at temperatures well above their melting point (260°C). However, the same experiments with preheating and subsequent cooling to the desired temperature resulted in a very good time-temperature scaling. The resins of the

third group were tested in an attempt to derive correlations between the rheological properties and their processing behavior in wire coating. The incorporation of PAVE in the molecules of the resin did not substantially change its rheology. However, the rheological measurements with controlled cooling revealed that the terpolymers, which are better processing resins, crystallize at higher temperatures.

4.1 Introduction

Teflon® FEP resins, which are copolymers of tetrafluoroethylene (TFE) and hexafluoropropylene (HFP), are of great commercial importance. The first member of this family of Teflon® resins was Teflon® FEP 100, a commercial resin having 92 mole % TFE and 8 mole % HFP. It has a fairly high molecular weight, so its melt processing is difficult. In wire coating operations, the maximum speed at which FEP 100 can be drawn onto the wire is about 500 ft/min. In order to be able to coat wire at a higher speed, a new resin, FEP 3100, was developed. It has a slightly higher level of HFP and lower molecular weight, and it can be run at about 1300 ft/min. Recently, FEP 3100 was replaced with a new resin, FEP 4100. It has a superior stress crack resistance and can be coated onto a wire at 2000 ft/min. The outstanding performance of FEP 4100 is due to the fact that a portion of the HFP is replaced with perfluoro(alkyl vinyl ether) (PAVE).

Despite their increasing commercial interest, very few studies have been published on the rheological characterization of Teflon® FEP resins. This can be partly attributed to the fact that TFE/HFP copolymers are, in general, insoluble in any known solvents. This greatly complicates determination of their molecular weights (MW) and molecular weight distributions (MWD). The few reported methods that have been used to determine

MW and MWD of Teflon® polymers include end-group analysis in combination with dynamic melt rheometery (Wu, 1985, Tuminello, 1989), laser light scattering (Chu *et al.*, 1987), and viscosity measurements (Chu and Linliu, 1995). Nevertheless, none of these methods can safely provide accurate results on the determination of the molecular characteristics of Teflon® polymers.

With the introduction of the amorphous perfluoroplastics, which are soluble in selected fluorocarbon solvents, it became possible to accurately determine the MW of these resins and thus perform more reliable and systematic rheological measurements. One of the objectives of this chapter is to report results on dynamic mechanical measurements of a series of well-characterized (in terms of MW and MWD) amorphous TFE/HFP (Teflon®) copolymers. More specifically, the effect of MW on the zero-shear viscosity and relaxation spectra of these resins is studied. The latter are determined by two methods: the so-called BSW relaxation spectrum method (Baumgaertel *et al.*, 1990) and the parsimonious method that calculates the discrete relaxation spectrum with a minimum number of Maxwell modes (Baumgaertel and Winter, 1989). This modeling study will be presented in Chapter 6 (Rheological Characterization of Teflon® FEP Resins).

Another objective of the present chapter is to show some of the difficulties that may arise during rheological testing of commercial semi-crystalline Teflon® FEP polymers. It is known that crystalline polymers exhibit some unusual flow properties that can be influenced by thermal and mechanical pretreatment such as pre-heating and pre-shear (Lagasse and Maxwell, 1976). Unfortunately, many experiments carried out on FEP resins at temperatures much higher than their melting point, where one might assume the

absence of any crystals in the melt, prove that residual crystals play a significant role in determining important aspects of their rheology. Unless residual crystallinity is taken into account, it can lead to some confusion and complications in the rheological data analysis.

Finally, oscillatory shear measurements were used to compare different Teflon® FEP wire coating resins in an attempt to identify correlations with their processing behavior. Specifically, the effect of the third component, PAVE, on the rheological properties of TFE/HFP/PAVE terpolymers and their ability to crystallize was analyzed. The latter was thought to potentially affect processability in the draw-down region of the wire coating process where temperatures drop rapidly, and the elongational flow would favor crystallization.

4.2 Experimental

4.2.1 Materials and Characterization

Three groups of well-characterized TFE/HFP copolymers of different molecular weights and TFE/HFP/PAVE terpolymers of a different composition (courtesy of Du Pont Fluoroproducts, Wilmington, DE) were studied. The first group of resins had a high content of HFP and a relatively low melting temperature (hereinafter referred to as TFE/HFP resins of Group A, listed in Table 4-1). The second group of resins had a lower content of HFP and therefore a higher melting temperature, around 260°C (hereinafter referred to as resins FEP of Group B, listed in Table 4-2). The resins of the third group (hereinafter referred to as resins TFE/HFP/PAVE of Group C, listed in Table 4-3) were similar to those of Group B but contained a small amount of PAVE. The composition of the resins of Group A is approximately 50±5 wt. % HFP and 50±5 wt. % TFE. The

composition of the Group B resins is approximately 15 wt. % HFP and 85 wt. % TFE. The composition of the resins of Group C is approximately 11 wt. % HFP, 88 wt. % TFE, and below 1 wt. % PAVE except for the control resin (FEP-2 of Group B) which has a slightly different ratio of TFE/HFP and no PAVE. Compositions were determined by fluorine NMR in the melt state at 300-340°C. DSC analysis showed that the crystalline melting point of Groups B and C resins is about 270°C and the crystallization temperature upon cooling from the melt-state is about 249°C. The molecular weights of the Group A resins were in the range of 76,000 to 400,000 kg/kmol, Group B in the range of 165,000 to 262,000 kg/kmol, and those of Group C from 208,000 to 220,000 kg/kmol. Most resins had similar polydispersity (M_w/M_n) of about 2.5 except for the resin TFE/HFP-1 (Group A) that had polydispersity of more than 3. The molecular weight and polydispersity were determined by GPC using Fluorinert® FC-75 (3M Corporation) solutions versus linear polyhexafluoropropylene oxide standards, one with M_n=20,000 and the other with M_n=70,000. The molecular weight, polydispersity, melt index, and composition of all resins are listed in Tables 4-1, 4-2, and 4-3.

Table 4-1. Molecular parameters of TFE/HFP resins with lower melting temperature (Group A)

Sample	Composition wt.% HFP/TFE	M_w kg/kmol	M_w/M_n	Melt index 200 °C, 15 kg
TFE/HFP 1	45.5/54.5	76,000	3.27	-
TFE/HFP 2	55.0/45.0	124,000	2.38	4 (5 kg)
TFE/HFP 3	45.5/54.5	199,000	2.14	-
TFE/HFP 4	51.3/48.7	327,000	2.56	0.67
TFE/HFP 5	48.0/52.0	350,000	-	0.17
TFE/HFP 6	48.0/52.0	400,000	-	0.33

Table 4-2. Molecular parameters of TFE/HFP (FEP) resins with higher melting temperature (Group B).

Sample	Composition wt.% HFP/TFE	Melt index	M_w/M_n	M_w kg/kmol
FEP-1	15.0/85.0	44	2.5	165,000
FEP-2	15.0/85.0	18	2.5	220,000
FEP-3	15.0/85.0	9	2.5	262,000

Table 4-3. Molecular parameters of TFE/HFP/PAVE resins (Group C).

Sample	Composition wt.% HFP/TFE/PAVE	Melt index	M_w/M_n	M_w kg/kmol
Control (FEP-2)	15.0/85.0/0.00	18	2.5	220,000
TFE/HFP/PAVE-1	11.05/88.26/0.69	20-24	2.5	208,000
TFE/HFP/PAVE-2	11.09/88.17/0.74	20-24	2.5	208,000
TFE/HFP/PAVE-3	10.85/88.21/0.94	20-24	2.5	208,000

4.2.2 Rheological Measurements

Linear viscoelastic measurements were performed in a Rheometrics System 4 mechanical spectrometer having a parallel plate geometry (plates of diameter equal to 25 mm). Frequency sweep experiments were performed in a frequency range from 0.01 to 500 rad/s after ensuring that operation was within the linear viscoelastic region (sufficiently small shear strain). The gap between the plates was adjusted to about 1 mm. To remove residual monomers prior to testing, the Group A resins were vacuum stripped at 140°C for 24-72 hours, depending on the amount of residual monomers. The stripping duration was controlled both visually (cessation of bubble formation) and rheologically (viscosity measurements). The sample was assumed to be free of monomers when the viscosity remained essentially unchanged for at least three consecutive measurements at the same frequency. After this stripping period, the polymers were molded into disks 25 mm in diameter and 1.5 mm high and cooled quiescently to room temperature. Since

degradation is not a factor for these stable polymers within the experimental range of temperature, no nitrogen environment was used for the rheological measurements.

Measurements of the dynamic moduli of the Group A polymers were performed at 200°C and those of Groups B and C in the range from 290 to 350°C. The lower temperature limit was chosen to avoid residual crystallization, while the upper limit was secected to prevent thermal decomposition. For the polymers of Group B, two different measurement techniques were used in order to study the importance of pre-heating and residual crystals on their rheology. In the first case, after the rheometer was equilibrated at the desired experimental temperature for 10 min, the sample was placed between the plates, melted, and equilibrated again at the same temperature. Then the gap between the plates was adjusted, the edges of the sample were trimmed, and the measurements proceeded at that temperature. In the second case, all the above steps are repeated except that before starting the test, the sample was pre-heated to the higher temperature of 330°C. This temperature was maintained for at least 1 min, long enough to melt all residual crystals, and then the sample was cooled to the desired experimental temperature. The polymer was then allowed to equilibrate for 5 min prior to testing. The preheating technique was also used in characterizing the Group C resins.

4.3 Results

4.3.1 Low Melting Point TFE/HFP Resins (Group A)

Figure 4-1 plots the dynamic modulus curves (G' and G'' respectively) of the six TFE/HFP copolymers of Group A as a function of frequency, ω, at 200°C. The data indicate that the distinct region for flow at low frequencies, the so-called terminal zone,
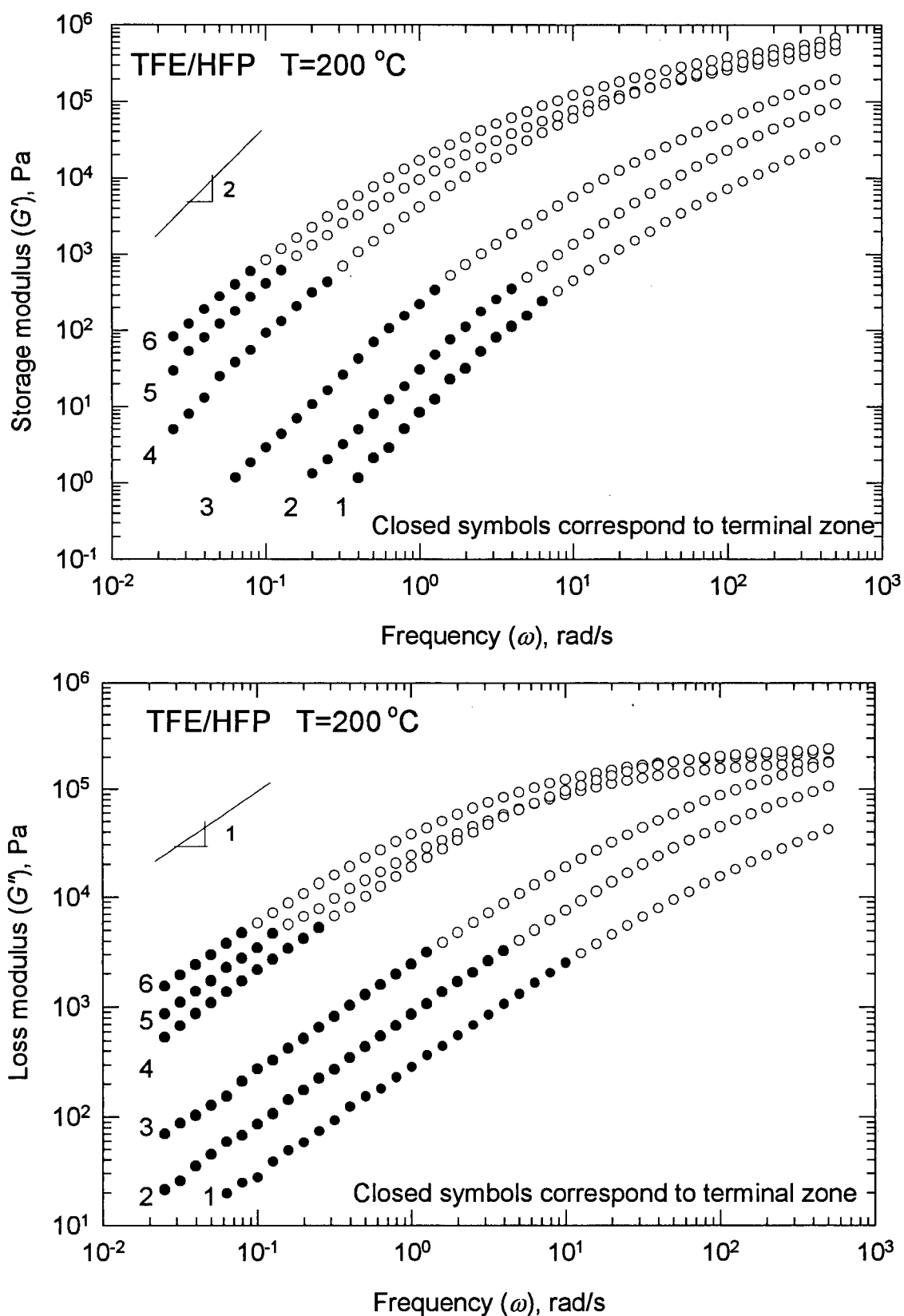
Figure 4-1. The storage and loss moduli, $G'(\omega)$ and $G''(\omega)$, of the TFE/HFP copolymers of Group A (Table 4-1) at 200°C.

has been reached ($G' \propto \omega^2$ and $G'' \propto \omega$ in Figure 4-1). However, the entanglement region

is not well pronounced as in the case of monodisperse polymers (a clear plateau for G'

and a clear maximum followed by a minimum for G''). Instead, it overlaps with a

transition to the glass regime at high frequencies.

Figure 4-2 depicts the complex viscosity data, $|\eta^*| = \sqrt{(G')^2 + (G'')^2}/\omega$, for the

same resins calculated from the data of Figure 4-1. The viscosity curves clearly show a
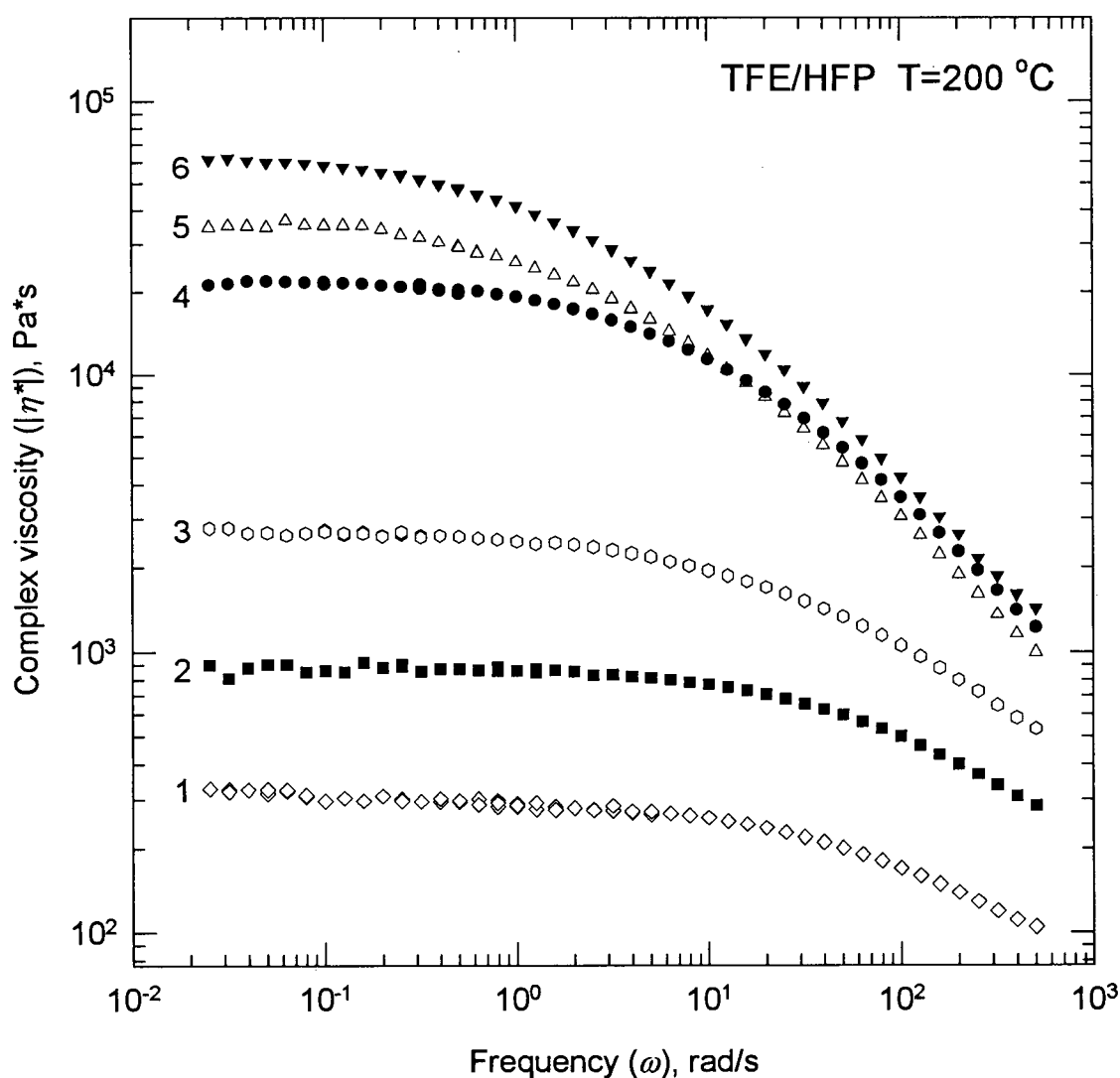
Figure 4-2. The complex viscosity $|\eta^*(\omega)|$ of the TFE/HFP copolymers of Group A
(Table 4-1) at 200°C. The zero-shear viscosity is clearly obtained for all
resins of this group

Newtonian region of essentially constant viscosity at low frequencies as well as a well-defined power law region at higher ones. Figure 4-3 plots the normalized complex viscosity (dividing by the corresponding zero-shear viscosity, η_o) as a function of frequency. It can be seen that the degree of shear-thinning increases with increase in the molecular weight, and that the onset of shear thinning shifts to smaller frequencies (rates) with increase in the molecular weight. This expected behavior has also been reported for a number of other polymers (Dealy and Wissbrun, 1990).
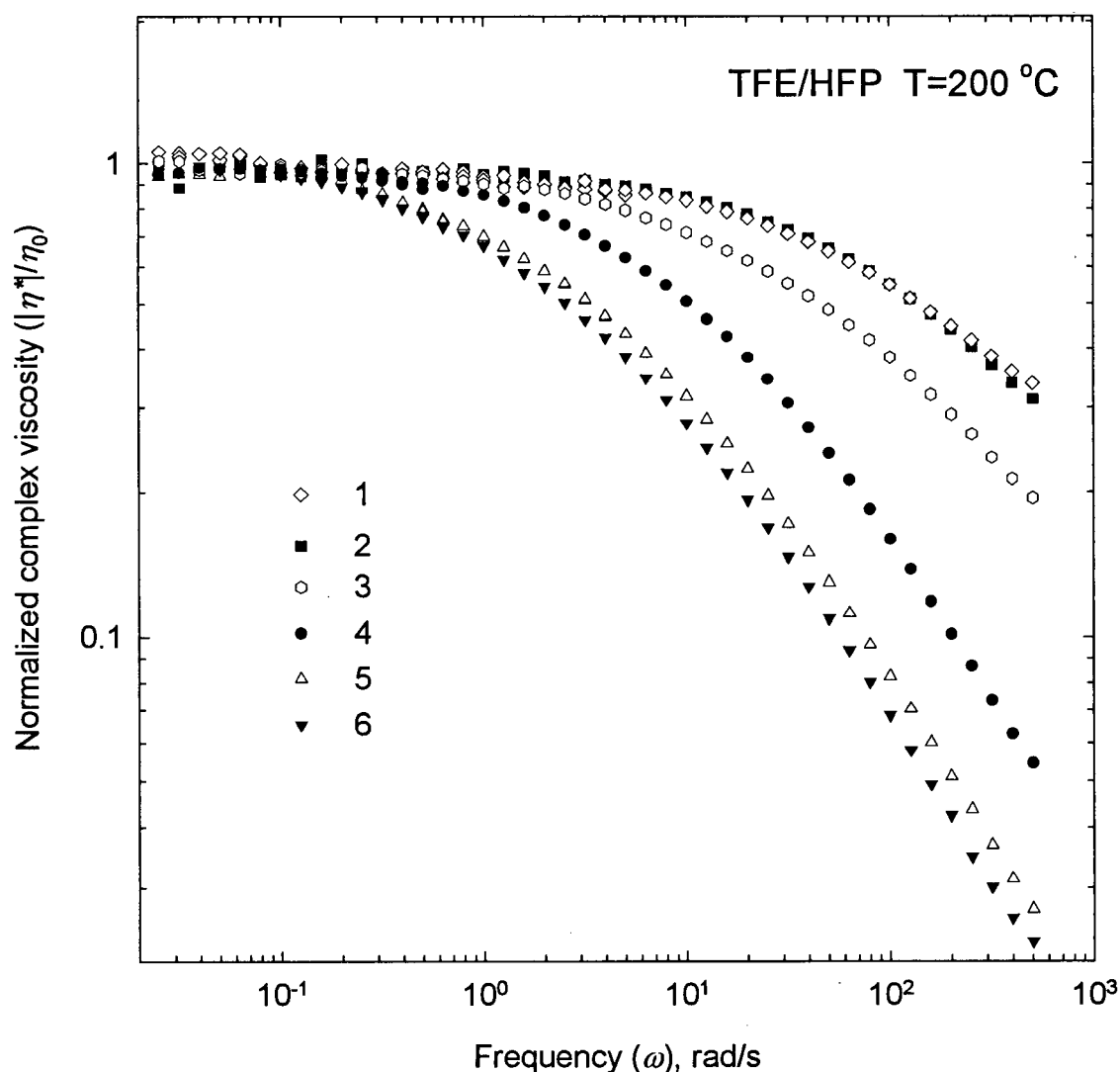
Figure 4-3. The normalized complex viscosity $|\eta^*(\omega)|/\eta_0$ of the TFE/HFP copolymers of Group A at 200°C

Figure 4-4 plots the zero-shear viscosity of TFE/HFP resins as a function of molecular weight. For the data points corresponding to 200°C, one can clearly identify a smooth transition from an about linear dependence of η_0 on M_w to a power-law
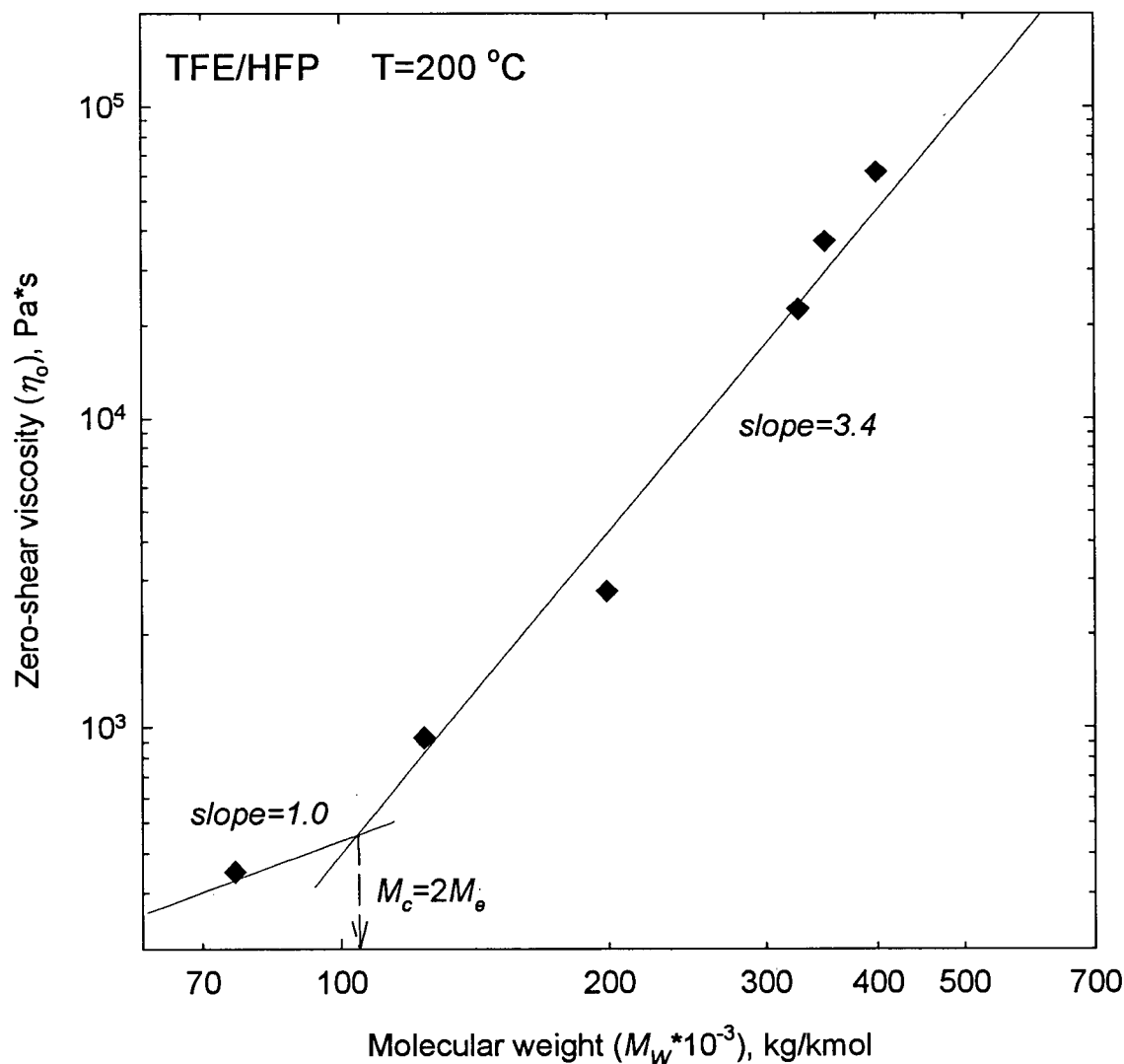
Figure 4-4. The molecular weight dependence of the zero-shear viscosity η_0 of TFE/HFP copolymers (Group A) at 200°C

dependence ($\eta_0 \propto M_w^n$) with $n \approx 3.4$. The small scatter in the graph can be attributed to variations in the polydispersity and the content of HFP in these samples. These findings are in agreement with previous studies on the dependence of the zero shear viscosity of

nearly monodisperse linear polymers on the molecular weight. A transition at M_c from linear to a power-law behavior with exponent of about 3.4 has been repeatedly reported (Van Krevelen, 1991). Note that the critical molecular weight, M_c that can be estimated from this set of data, lies in the range between 80,000 and 110,000 kg/kmol. This value is somewhat high compared to those previously reported in the literature. For example Wu (1985) calculated the value of M_c to be close to 12,500 kg/kmol for high melting point FEPs, while Tuminello (1989) estimated this value to be about 14,000 kg/kmol. This point of disagreement will be discussed in more detail later, in Chapter 6. It is noted that the clear deviation of the lowest molecular weight η_0 from the 3.4 power low behavior was also reported by Kazatchkov *et al.* (1996). There, a series of similar TFE/HFP polymer melts were studied by means of a sliding-plate rheometer. The resins were not thermally treated before experimentation as in the present study. Nevertheless, a very similar relationship between η_0 and M_w was observed that resulted in about the same high M_C value. This observation leads me to believe that crosslinking, which might have taken place during vacuum stripping, is not present in the current study.

4.3.2 High Melting Point FEP Resins (Group B)

Figure 4-5 depicts the master curves of the storage and loss moduli as well as that of the complex viscosity of the FEP-2 polymer (Table 2) at the reference temperature of 300°C. These experiments were performed without any preheating at a higher temperature. For a "thermorheologically simple" material (Dealy and Wissbrun, 1990), it is often found that data taken at several temperatures can be brought together on a single master curve by means of "time-temperature superposition" (TTS). According to this

principle, the data for different temperatures can be superposed by introducing a shift

factor, a_T, determined empirically. Thus, if one makes a plot of a rheological property

versus time, a_T is obtained from the horizontal shift necessary to bring the data for any

temperature T onto the same curve as data for temperature T_{ref}. For example, flow curves

(shear stress vs. shear rate) would be plotted as shear stress versus $\dot{\gamma}\, a_T$.

In Figure 4-5, the time-temperature superposition principle on frequency sweep
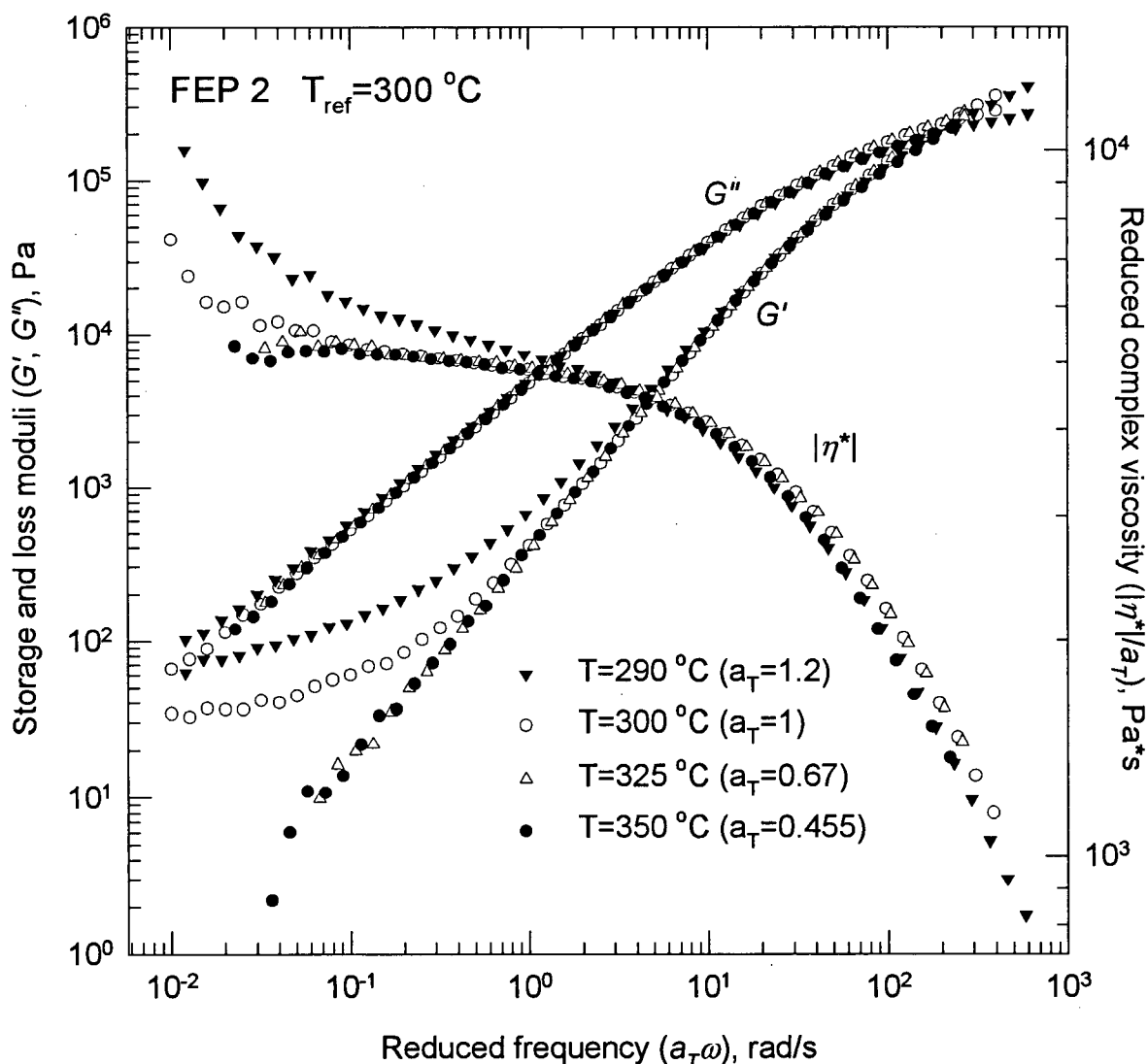
Figure 4-5. Master curves of the storage modulus $G'(\omega)$, loss modulus $G'(\omega)$, and complex
viscosity $|\eta^*(\omega)|$ of Teflon® FEP-2 copolymer at the reference temperature of
300°C. The dynamic linear viscoelastic experiments were performed without any
preheating.

data obtained at temperatures varying from 290 to 350 °C was applied. It can be seen from Figure 4-5 that the superposition of the data is very good for temperatures higher than 325 °C. However, for lower temperatures, it clearly fails for the range of reduced frequencies below 10 s^{-1}. This failure is more pronounced for G' data, where a distinctive "shoulder" appears in the low frequency region instead of approaching the typical slope of 2 in the terminal zone. The height of this "shoulder" apparently scales with temperature. Based on these data, no zero-shear viscosity can be found at least for temperatures lower than 325°C. Similar behavior was also observed for the other polymers of Group B (not shown here).

Behavior such as that depicted in Figure 4-5 was previously observed for other semi-crystalline polymers (Guskey and Winter, 1991; Plazek, 1996). Such behavior normally indicates some degree of molecular association, possibly due to formation of a crystalline structure that leads to solid-like elasticity. It is believed that some residual crystallinity still exists at temperatures well above the crystalline melting point. Moreover, these residual crystals can grow with time as a result of the induced shear (shear-induced crystallization). This is clearly demonstrated in Figure 4-6. Two time sweep experiments for FEP-2 at the same temperature of 290°C were performed. The first was carried out without any pre-heating and the second with pre-heating at 330°C before switching back to 290°C (see experimental section for details). This temperature of 330°C seems to be high enough for residual crystals to completely melt since no failure of TTS was observed above 325 °C. One can see from Figure 4-6 that without preheating the storage modulus increases with time by a significant factor due to shear-induced crystallization. On the other hand, if the sample is initially pre-heated, the magnitude of

G' remains within experimental error (±3%) throughout the test. This means that, by preheating the sample, the centers of possible crystal nucleation have been completely eliminated, thus preventing growth of crystalline structure.

The experimental results plotted in Figure 4-5 were repeated for the same temperatures but this time with preheating at 330°C. The results are plotted in Figure 4-7. Clearly, the time-temperature superposition principle now applies over the whole range of temperature (290-350°C) and frequency examined in this work. For the sake of
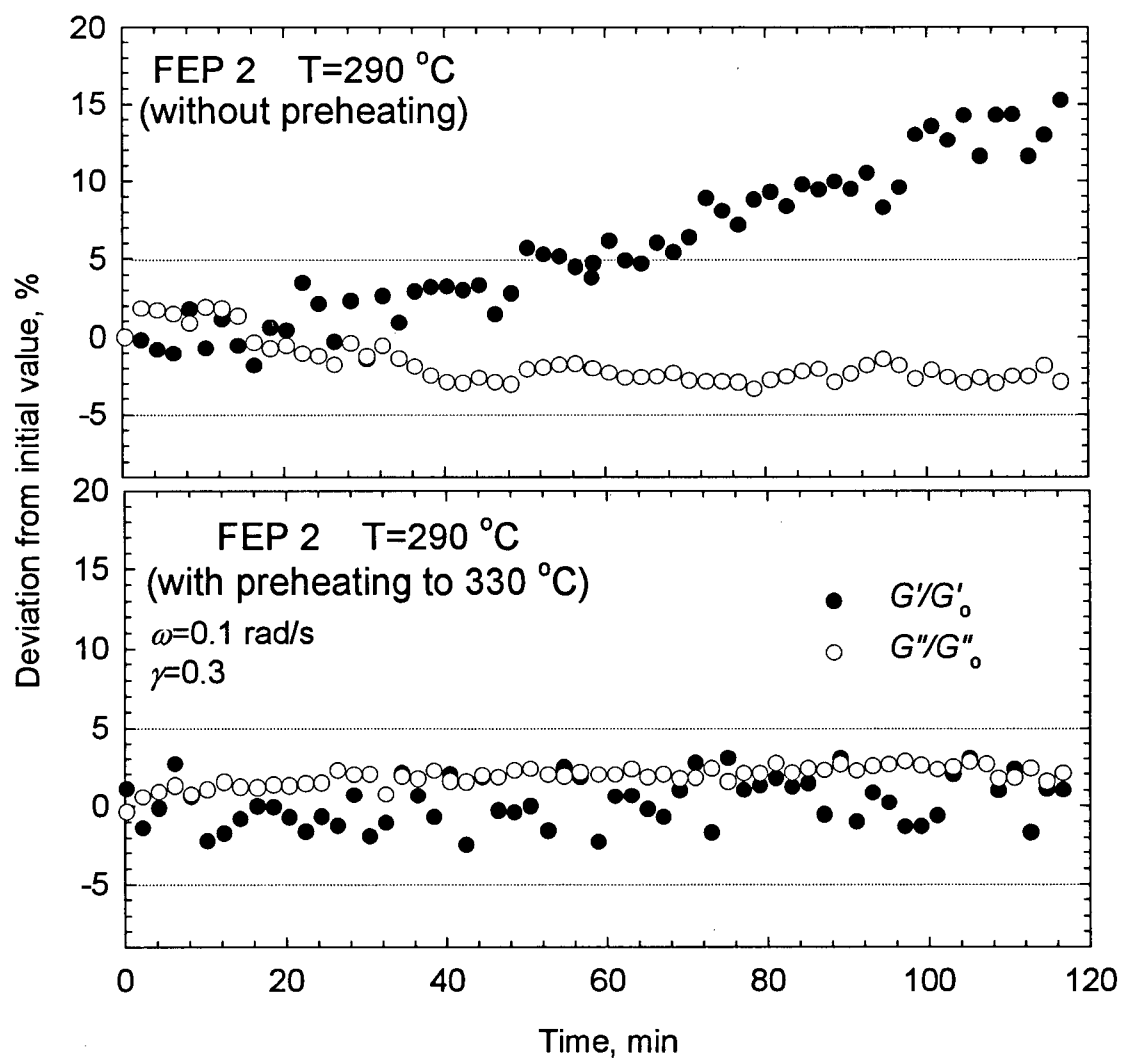
Figure 4-6. The effect of preheating on the dynamic moduli of Teflon® FEP-2 copolymer during time sweep experiments at 290 °C

comparison, the data points for 275°C, i.e. the temperature close to the melting point, are

also shown in the plot. One can see that these points (275°C) do not fall on the master

curve. This means that even after pre-heating and subsequent cooling to this low

temperature, there is enough time for new crystals to form and grow upon shearing.

Figure 4-8 represents the horizontal shift factor, a_T, as a function of temperature
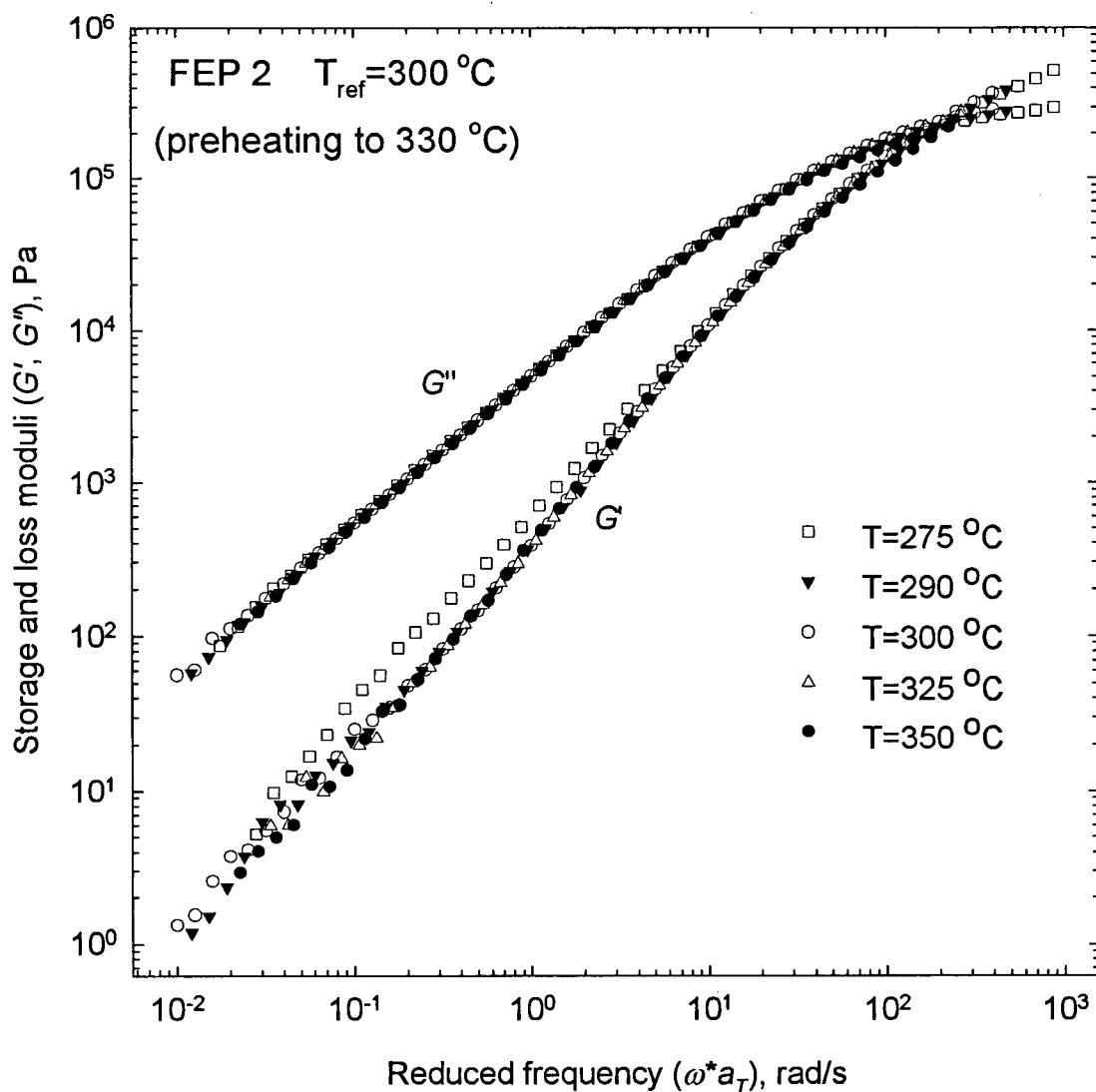
Figure 4-7. Master curves of the storage, $G'(\omega)$, and loss modulus, $G'(\omega)$, of Teflon®
FEP-2 copolymer at the reference temperature of 300°C with preheating at
330°C

for the FEP-2. The Arrhenius type equation was found to adequately describe the available data:

$$a_T = \exp\left[\frac{E_a}{R}\left(\frac{1}{T} - \frac{1}{T_{ref}}\right)\right]$$

(4-1)

where E_a is the flow activation energy, R is the universal gas constant, and T_{ref} is the reference temperature (300°C). This equation is often found to be valid as long as the temperature is at least 100 K above the glass transition temperature, T_g, which is 200 K for Teflon®. Closer to T_g, the WLF equation has been found useful (see Dealy and Wissbrun, 1990). However, at these high temperatures, either equation can be used to fit
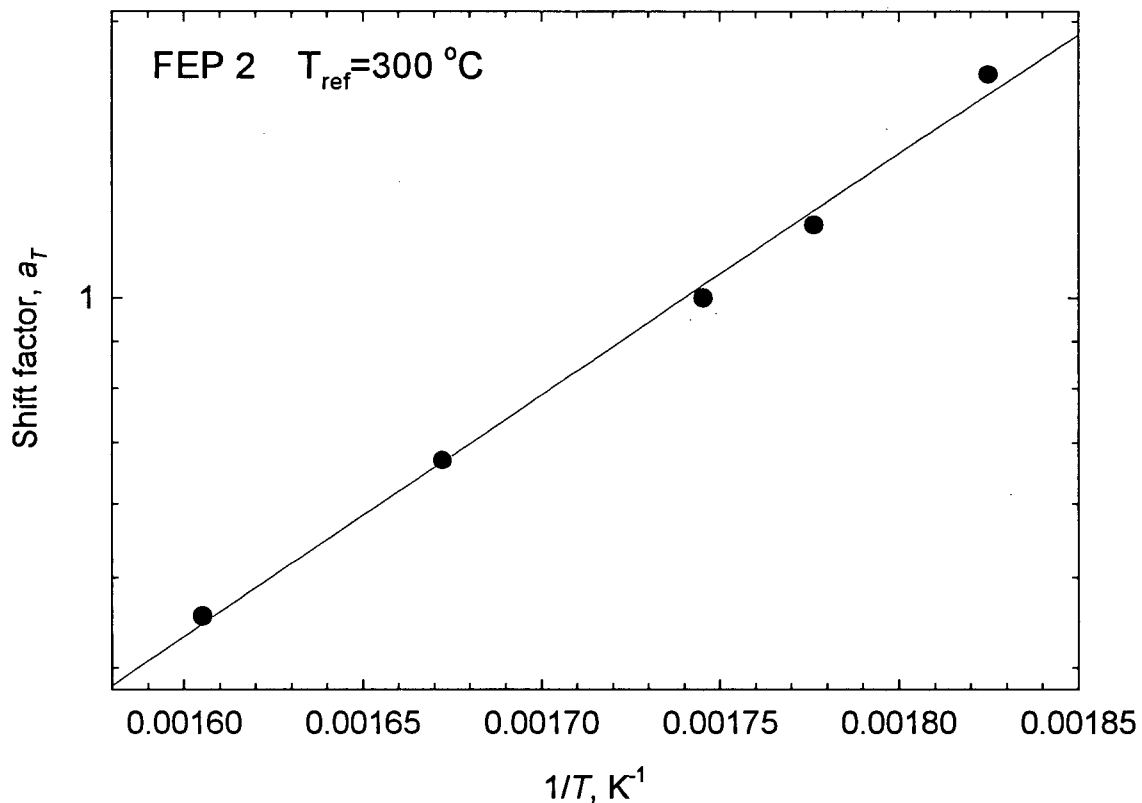
Figure 4-8. The horizontal shift factor, a_T, resulted from the application of the time-temperature superposition of dynamic linear viscoelastic experimental data for Teflon® FEP-2 copolymer

experimental values of a_T. The flow activation energy was found to be equal to 50,000

kJ/kmol and essentially independent of molecular weight. This is much lower than the

value of E_a=84,000 kJ/kmol reported by Wu (1985) for his series of FEP resins. This can

be attributed to differences in the composition of the resins used by Wu (1985) and those

in the present work.

Figure 4-9 depicts the dependence of the zero-shear viscosity on the molecular
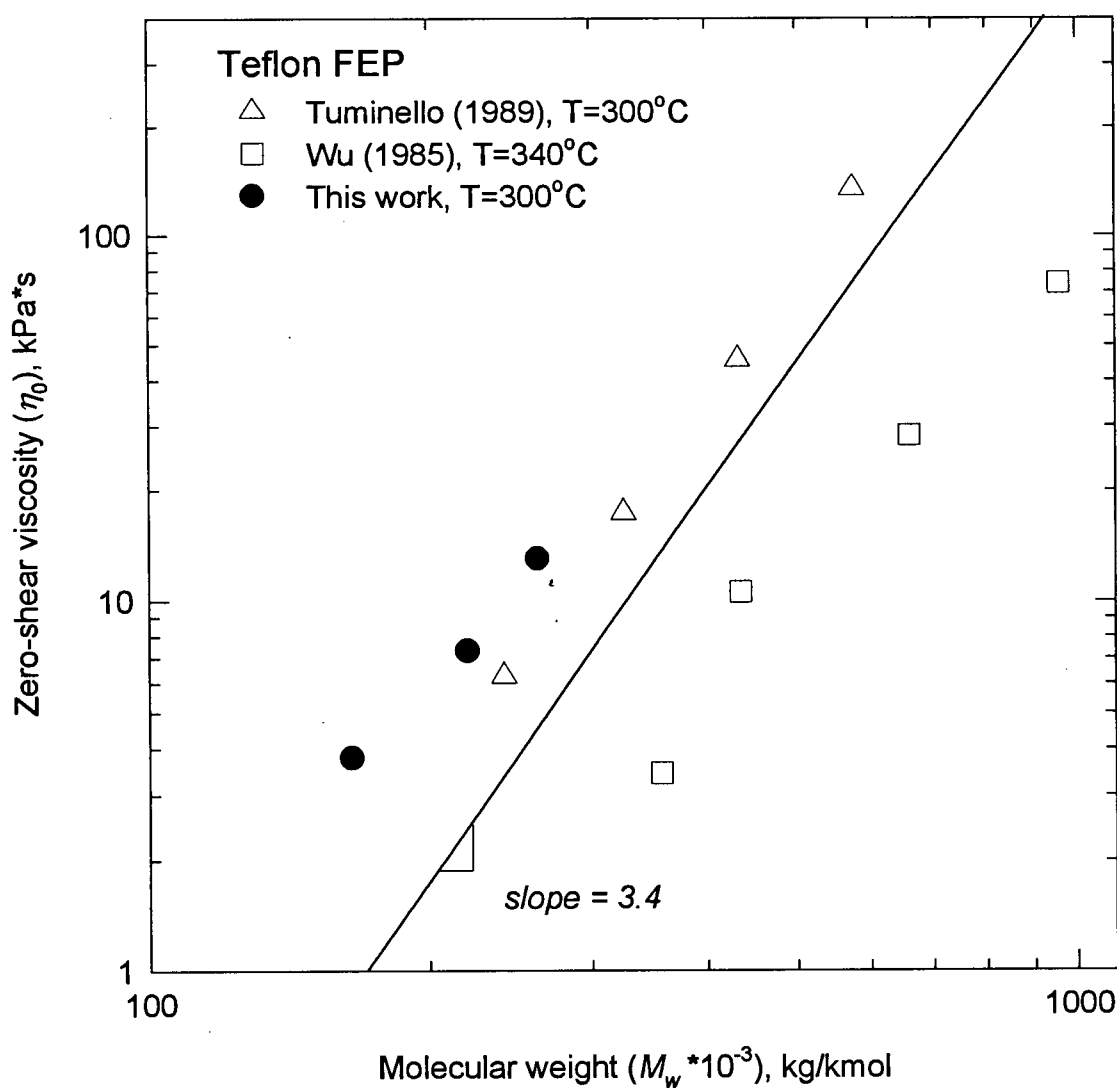
Figure 4-9. The dependence of the zero-shear viscosity of the TFE/HFP copolymers of
Group B on M_w at 300°C (present work; Tuminello, 1989) and 340°C (Wu,
1985)

weight for the Group B resins, along with the data points reported by Tuminello (1989) and Wu (1985). A straight line having a slope equal to 3.4 also appears on the graph for reference purposes. The available data show clearly that a power-law relationship exists between η_0 and M_w. The slope turns out to be close to the value of 3.4 reported previously for many other linear polymers when the M_w is greater than a critical value, M_c (Van Krevelen, 1991).

4.3.3 Terpolymers TFE/HFP/PAVE (Group C)

The viscoelastic properties of the Group C resins were measured at 300°C with preheating at 330°C as described above. Figure 4-10 plots the storage and loss moduli as well as the complex viscosity for all the resins of this group including the control resin, FEP-2. All the resins have similar viscosities except for the control whose viscosity is higher due to higher molecular weight. A slight difference in the viscosity of the terpolymers can be attributed to minor variations in the PAVE content. In general, the resins with lower viscosity process better since they are more extendable in the melt state. This is true when one compares the control resin with the other terpolymers.

A comparison of the dynamic moduli revealed differences between the co- and terpolymers. Looking at the modulus curves, one can see that the G'' curve and high-frequency part of the G' curve of the control resin lie above those for the three terpolymers whose dynamic moduli are virtually identical. This can be explained by a higher molecular weight of the control. However, the G' curve clearly shows that at low frequencies (below 0.2 rad/s) the storage modulus of the terpolymers is higher than that of the control resin. This means that an addition of PAVE makes a terpolymer more

elastic than a copolymer. The higher elasticity of the terpolymers may be a reason for their better processability.

Another reason for the better processability of the terploymers may be its enhanced ability to crystallize compared to the control copolymer. For this purpose, a series of rheological tests with controlled cooling was done to study crystallization of the resins of this group. The procedure was as follows. After preheating at 330 °C, the sample was
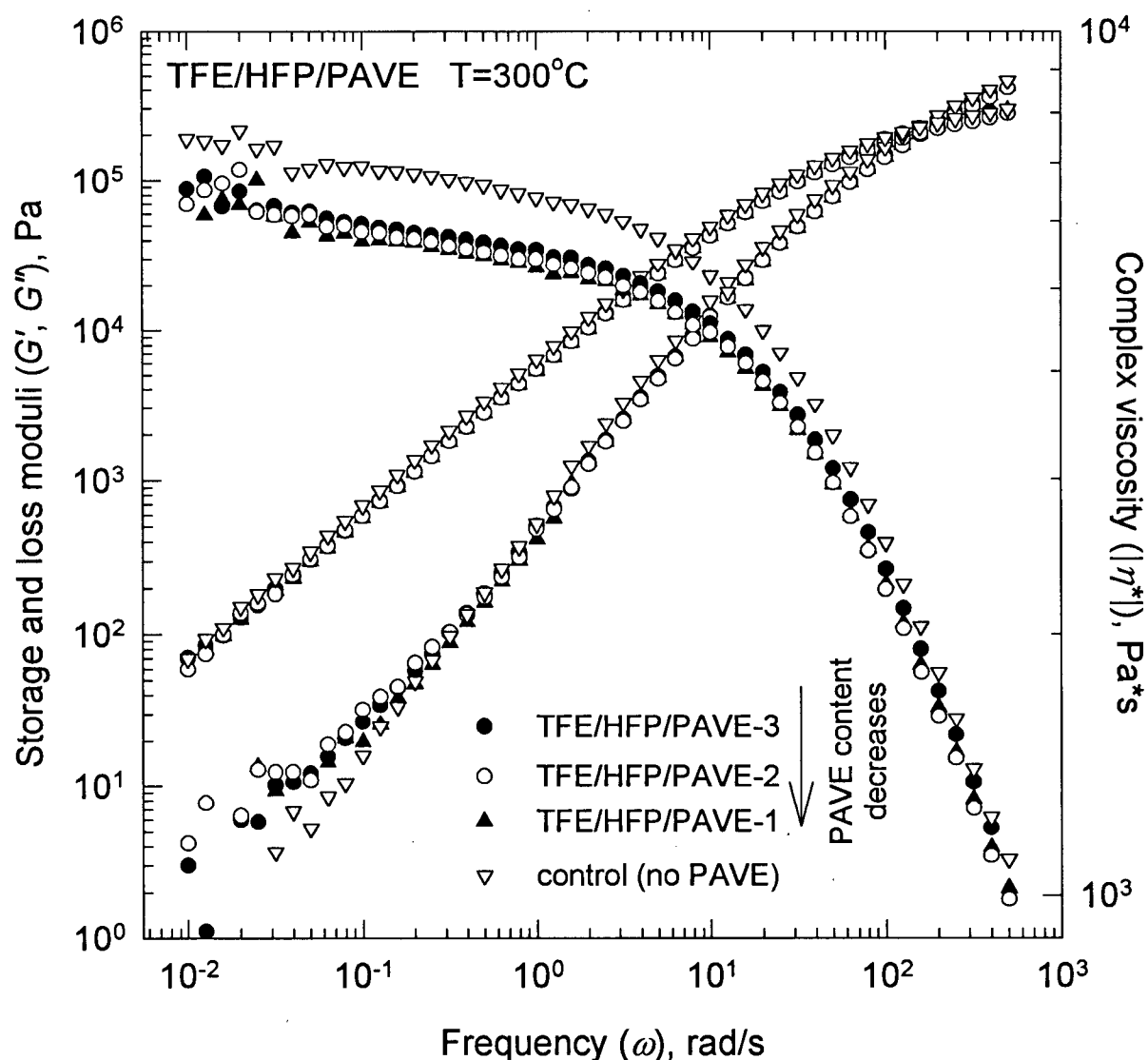
Figure 4-10. The storage modulus, $G'(\omega)$, loss modulus, $G'(\omega)$, and complex viscosity, $|\eta^*|$, of Teflon® FEP terpolymers (Group C) at 300°C with preheating at 330°C

cooled to 280 °C, equilibrated for five minutes, then rheologically tested at frequencies in

the range from 0.1 to 1 rad/s. The cooling interval between two consecutive

measurements varied from 2 to 5 °C. The cooling rate was about 1 °C/min. Both the gel

point, T_{gel}, and the breadth of crystallization, ΔT_{cryst}, were determined. The gel point, was

defined as the temperature at which G' at every frequency becomes higher than G'', i.e.

the transition from liquid to solid state. The breadth of crystallization, ΔT_{cryst}, was defined

as the temperature difference at which the viscosity increases from 10^4 to 10^6 Pa·s.
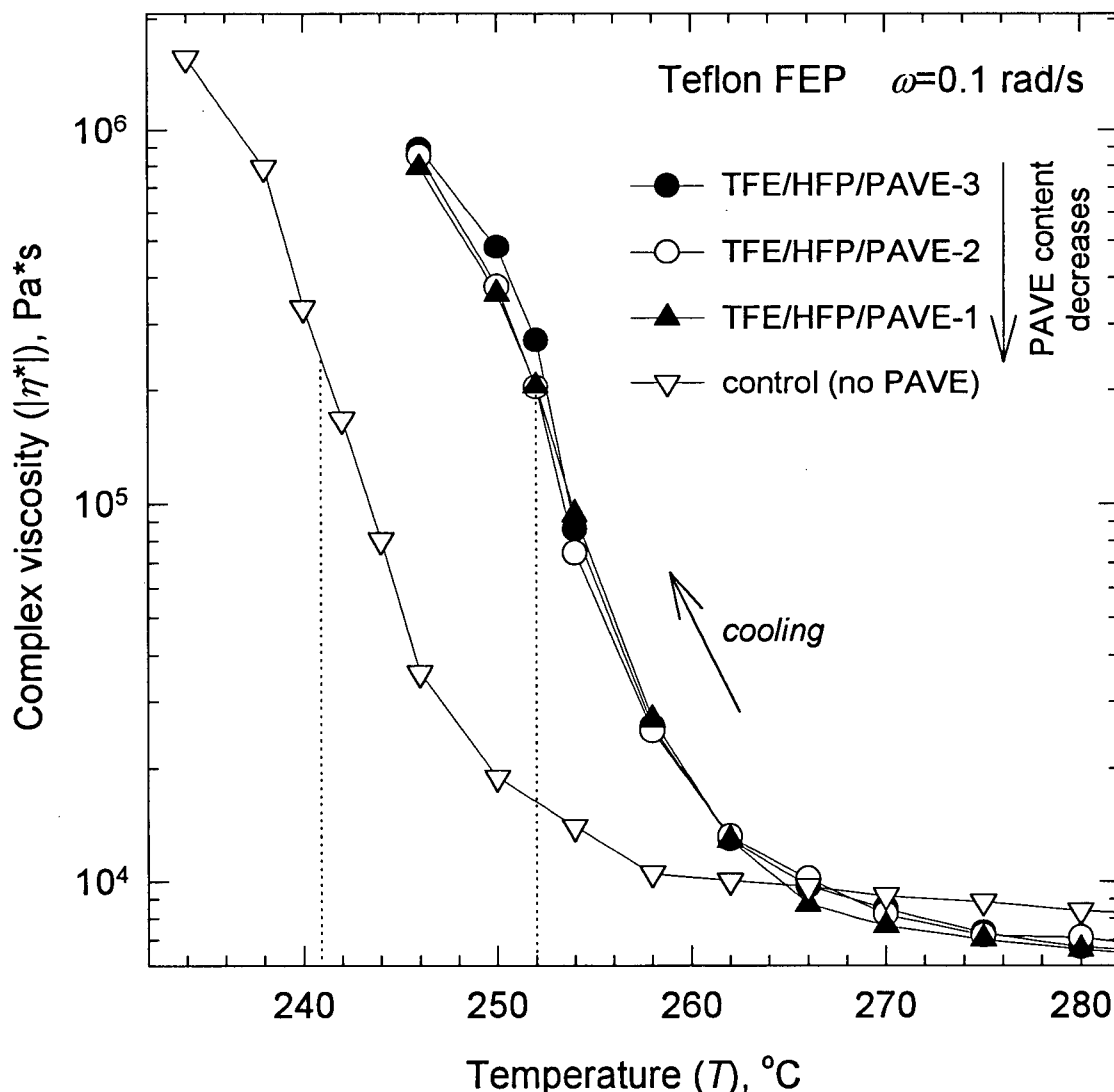
Figure 4-11. Viscosity of Teflon FEP resins (Group C) measured during programmed cooling at 0.1 rad/s

The viscosity curves at 0.1 rad/s for all four resins measured during this programmed cooling are plotted in Figure 4-11. Upon cooling, the viscosity dramatically increases at the onset of crystallization. All the terpolymers behaved in a similar manner. This behavior is compared to the control copolymer in the same plot. The gel point was always higher for the terpolymers than the copolymer. For the terpolymers it was close to 252 °C, while for the copolymer it was about 241 °C. The breadth of crystallization of the copolymer (27 °C) was higher than that of the terpolymers (20 °C). This clearly shows that the better processable terpolymers crystallize faster and at higher temperature than the copolymer (control resin).

In general, one can say that parameters such as lower viscosity, higher onset of crystallization, and higher melt elasticity at low frequency (shear rate) are consistent with better processability of Teflon® FEP resins.

5   Capillary Flow Measurements on Teflon® FEP Resins

*T*he melt fracture behavior of several Teflon® FEP resins was studied in capillary extrusion in order to identify the critical conditions for the onset of melt fracture and wall slip. These resins were copolymers of tetrafluoroethylene (TFE) and hexafluoropropylene (HFP) and terpolymers of TFE, HFP, and perfluoro(alkyl vinyl ether) (PAVE) of different molecular weight and content of PAVE. The incorporation of the third monomer in the molecules of the resin was found to improve the processability of polymer without substantially changing its rheology. Surface melt fracture (sharkskin) appeared at wall shear stresses greater than about 0.18 MPa, practically independent of temperature in the range of 300 to 350^0C. At higher apparent shear rates, oscillating melt fracture was observed due to the presence of wall slip and compressibility of the melt. Furthermore, a superextrusion region was identified at apparent rates greater than about 700 s^{-1}, beyond those where oscillating melt fracture was obtained. In this region, the extrudate appears smooth again.

5.1   Introduction

Despite their great industrial importance, very few works have been published on the processing of Teflon® FEP fluoropolymers. Tordella (1969) studied the melt fracture behavior of Teflon® FEP. He found that, above some critical shear stress (or shear rate), the flow of molten polymers through capillaries is accompanied by the onset of surface melt fracture ("ripple" according to his terminology) followed by a second critical stress at which a discontinuity in the flow curve occurs (oscillating melt fracture). The onset of

the discontinuity in the flow curve was associated with the appearance of wall slip. He also reported that the critical wall shear stress for the onset of oscillations increases slightly with temperature, but is independent of capillary radius for fixed length-to-diameter ratios. He has also pointed out the similar behavior of linear polyethylenes which were investigated to a greater extent by others (Lin, 1985; Ramamurthy, 1986; Kalika and Denn, 1987; Hatzikiriakos and Dealy, 1992a,b,c).

In the capillary extrusion of linear polymers, four distinct flow regions may be identified (Kalika and Denn, 1987) (see Figure 2-9). At increasing apparent shear rates, these are the following: the first region is a stable flow region, where the extrudate has a smooth surface; at higher apparent shear rates, small amplitude periodic distortions appear on the extrudate surface and this flow region is referred to as the sharkskin region; the third flow region is the stick-slip region, where the shear stress becomes a double-valued function of the apparent shear rate, and the extrudate appearance alternates periodically between zones of roughness (stick) and smoothness (slip); finally, the fourth region is beyond the stick-slip regime where the extrudate appears to be grossly distorted. It is noted that a similar behavior was also observed in the capillary extrusion of polybutadienes (Lim and Schowalter, 1989), polyisoprenes (Vinogradov *et al.*, 1972a), and polydimethylosiloxanes (Piau *et al.*, 1990; El-Kissi and Piau, 1990).

In this chapter, the results from experiments carried out in a capillary rheometer for several Teflon® FEP resins are reported. The rheology and processing characteristics of these fluoropolymers are studied in order to determine the critical conditions for the onset of wall slip, sharkskin and gross melt fracture.

5.2 Experimental

The rheology and processability of several Teflon® FEP resins were studied by carrying out capillary experiments. These resins were: a tetrafluoroethylene (TFE) - hexafluoropropylene (HFP) - perfluoro(alkyl vinyl ether) (PAVE) terpolymer (commercial FEP 4100), its 3 modifications with different contents of PAVE (the resins 1-3 of Group C in Chapter 4), and 3 FEP resins of different molecular weight (Group B in Chapter 4) including FEP-2 (commercial FEP 3100). The commercial resin FEP 4100 had a molecular weight of about 208,000 and a polydispersity of about 2. The melting points of these resins were found to be around 260 °C, determined using differential scanning calorimetry (DSC) analysis. The experiments were carried out on an Instron constant-speed piston-driven capillary rheometer. Circular dies of various diameters, D, and length-to-diameter ratios, L/D, were used (Table 5-1). All the circular dies had a 90° entrance angle. Orifice dies were also used to determine the Bagley correction in order to get an accurate determination of the flow curve. The experiments were carried out at three different temperatures, namely 300°C, 325°C and 350°C.

Table 5-1. Circular dies used

Diameter, mm	L/D ratios
0.254 (0.01")	0, 20, 40
0.508 (0.02")	0, 20, 40, 100
0.762 (0.03")	0, 10, 20, 40, 70, 100
1.270 (0.05")	0, 20,40, 70

5.3 The Bagley End Correction

To determine the pressure drop associated with changes in the velocity distribution near the entrance and exit of the capillary, a series of orifice dies having different diameters were used (see Table 5-1). Figure 5-1 shows the Bagley end correction, ΔP_{end}, as a function of apparent shear rate, $\dot{\gamma}_A \equiv 4Q/\pi R^3$, where Q is the
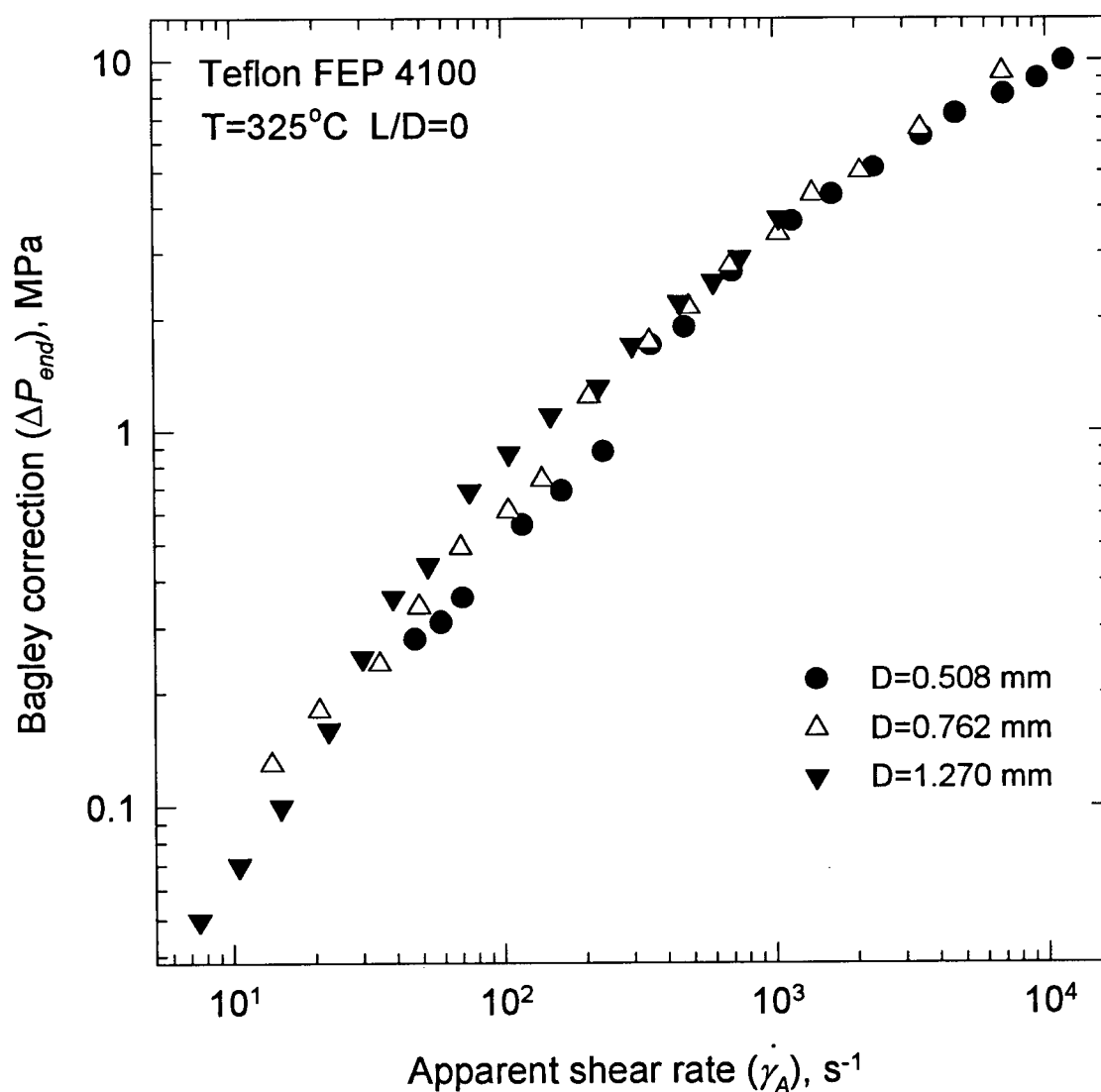
Figure 5-1. The Bagley end correction of resin FEP 4100 at 325 °C as a function of the apparent shear rate

volumetric flow rate and R is the capillary radius. It can be seen that the Bagley correction is slightly dependent on the orifice radius particularly at the smaller values of the apparent shear rate. Specifically, the Bagley correction increases with increase in the orifice diameter. Similar behavior was also obtained at the other two temperatures, namely 300 and 350 °C, for this polymer. Meissner (1975) has also reported such a diameter dependence of the Bagley correction.

Figure 5-2. The Bagley end correction of resin FEP 4100 at 325°C as a function of the wall shear stress
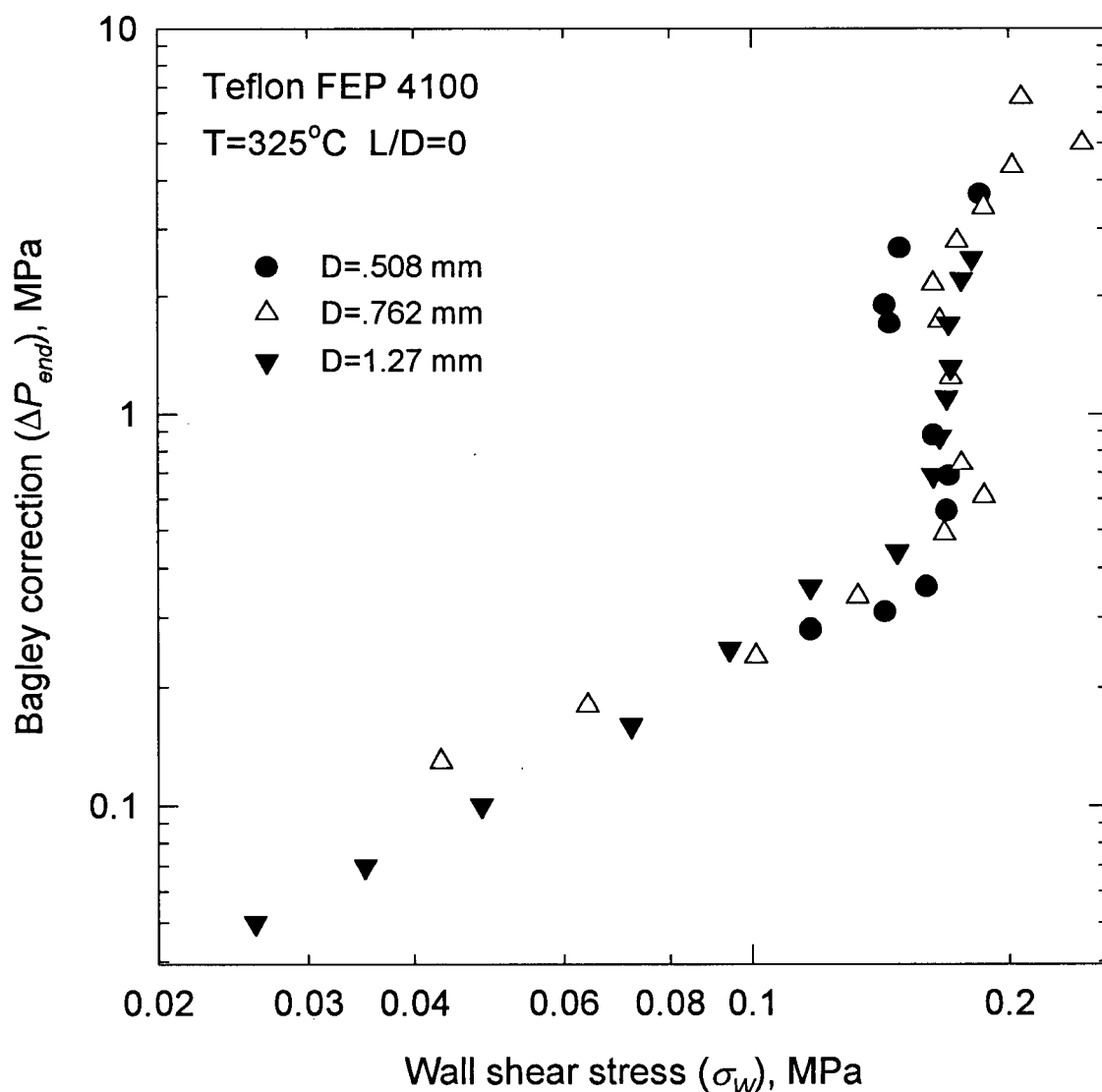
For the same resin, Figure 5-2 plots the Bagley end correction as a function of the wall shear stress, σ_W. It can be seen that, at a critical value of the wall shear stress, the Bagley correction increases discontinuously. This is due to the fact that at this critical shear stress an oscillating melt fracture phenomenon occurs as discussed below. Similar behavior was also obtained at the other two temperatures, as well as for the other resins .

5.4 Viscosity

In determining the viscosity, only data in the prefractured region were considered. At higher apparent shear rates where melt fracture is obtained, wall slip is present. Thus,
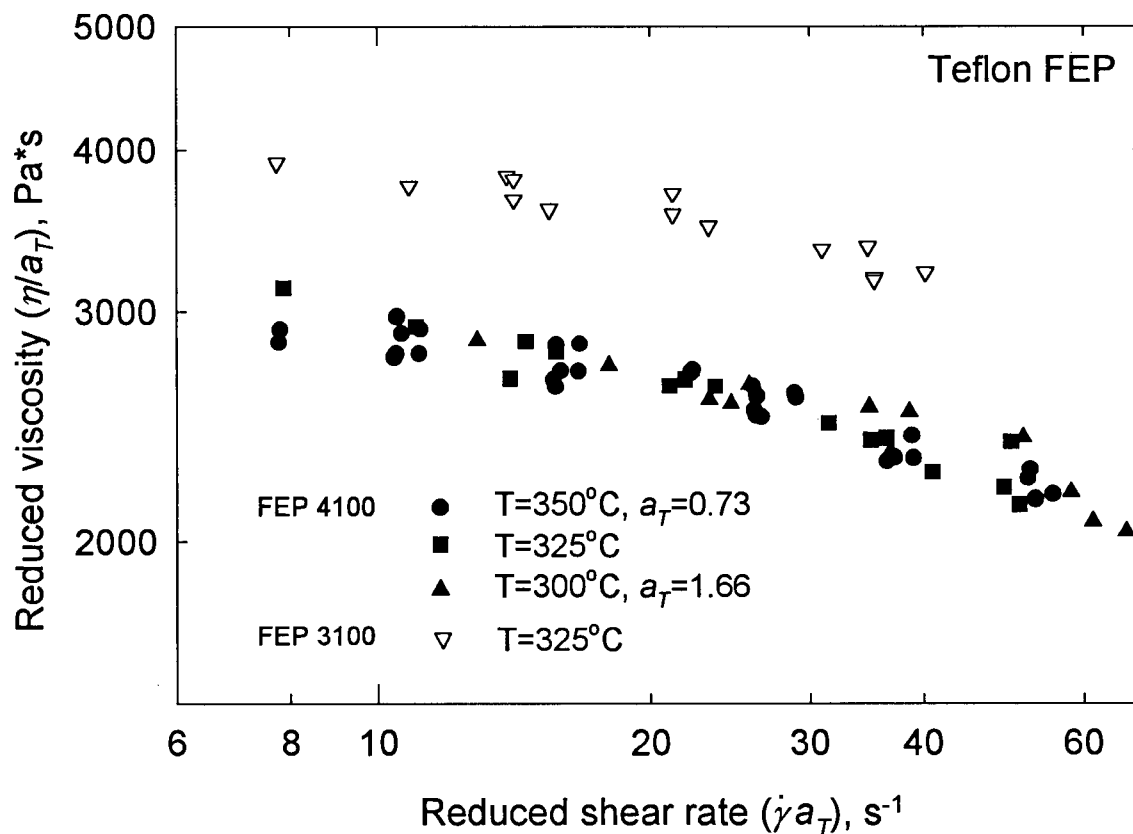
Figure 5-3. The reduced viscosity of resins FEP 3100 and 4100 at 325 °C and ambient pressure

to determine the true deformation imposed on the melt, one should apply a correction in order to account for the effects of slip. The Rabinowitch correction was also applied to the experimental data.

The resulting viscosity curves for fluoropolymers FEP 4100 and 3100 are plotted in Figure 5-3 for all three temperatures. Note that the data for FEP 4100 have been reduced to the temperature of 325 °C, in order to compare its viscosity with that of resin FEP 3100 (experiments for FEP 3100 were performed only at 325 °C). The shift factors according to the time-temperature superposition principle for the other temperatures are 0.73 for 350°C and 1.66 for 300°C. Note also that all the data refer to ambient pressure (a pressure correction was applied, see below). In spite of the apparent scatter in the data for FEP 4100, the deviation of the data from the mean value is within ±4%. Also the shear thinning behavior of both materials is very weak. Essentially, the melts have a Newtonian viscosity for shear rates less than about 10 s^{-1} and a power law one for higher shear rates with a power law exponent equal to 0.85. Finally, one may observe that the viscosity of FEP 3100 resin is higher than that of FEP 4100 by about 25%, which shows the effect of the higher molecular weight of FEP 3100.

5.5 The Flow Curve

Using the Bagley corrections determined previously, one can now determine the apparent flow curves for capillaries having different diameters and L/D ratios (wall shear stress vs. apparent shear rate). The wall shear stress, σ_W, is assumed to be uniform along the capillary and is defined as:

$$\sigma_W = (P_d - P_{end})/(4L/D) \tag{5-1}$$

where P_d is the driving pressure and P_{end} is the end correction pressure or Bagley correction.

A typical apparent flow curve for the temperature of 350°C is shown in Figure 5-4. One may identify five different flow regions. Initially there is a stable region (roughly for apparent shear rates less than 70 s^{-1}) where the extrudate appears smooth and glossy (representative photographs for all flow regimes are presented in a subsequent section).
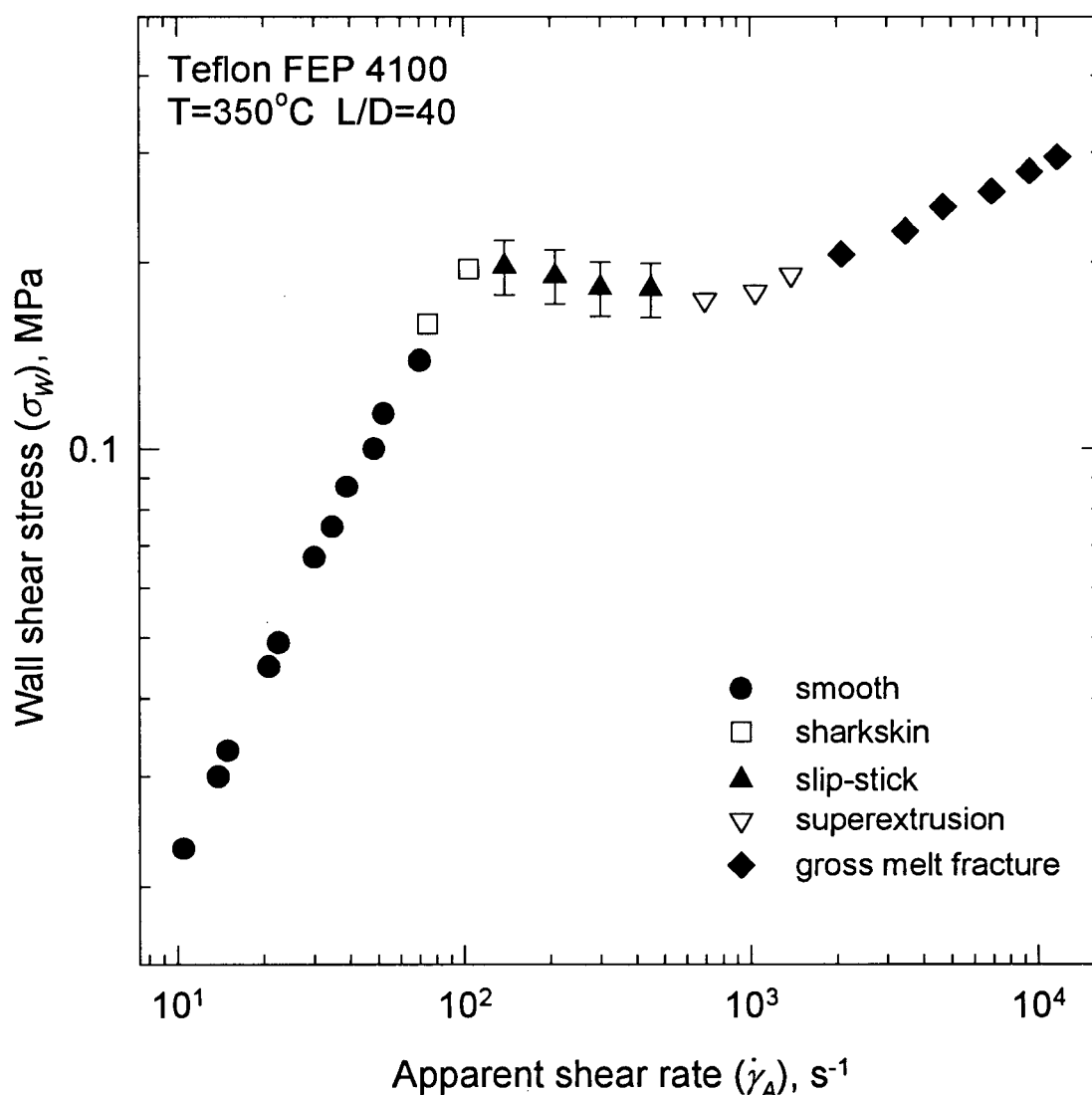
Figure 5-4. A typical flow curve of resin FEP 4100 at 350 °C using a capillary die having a diameter of 0.762 mm and a length-to-diameter ratio of 40. The various flow regions are also illustrated

This stable regime is nearly Newtonian where the viscosity of the material appears to be slightly dependent on the apparent shear rate (see Figure 5-3). At wall shear stress of about 0.18 MPa small amplitude periodic distortions on the surface of extrudate appear (surface or sharkskin melt fracture region).

A sharp change in the slope of the apparent flow curve defines the onset of the oscillating (or "stick-slip") melt fracture region, where the pressure oscillates between two extreme values and the extrudate has the appearance of alternating smooth and distorted portions. This region is obtained for apparent shear rates falling between about 100 and 700 s^{-1}. What is plotted on Figure 5-4 for this region is the average shear stress of these two extreme values. The maximum and minimum values of stress obtained during oscillations are indicated by error bars. For shorter capillaries the slope of the flow curve in this region is distinctly negative while for longer capillaries an almost plateau-like region is obtained. It also has to be mentioned that oscillations are not always obtained within this region. For certain apparent shear rates and capillary dies, the flow becomes apparently stable but the extrudate still exhibits a stick-slip appearance. This behavior was more pronounced in the extrusion of FEP 3100.

For apparent shear rates greater than about 700 s^{-1} and up to 2000 s^{-1} the pressure drop becomes stable but, most importantly, the extrudate is also smooth. This is referred to as the superextrusion flow region. It is noted that slip is present in this region, and this is discussed in a subsequent section. Finally, beyond this superextrusion region the flow is again stable but the extrudate appears grossly distorted. Note that the transition from the superextrusion region to the gross melt fracture region is fairly smooth, and the extrudate distortion gradually becomes more severe with increasing shear rate.

5.6 The Effect of Pressure on the Flow Curve

Figure 5-5 shows apparent flow curves for resin FEP 4100 obtained with dies having a constant diameter and various L/D ratios. It can be seen that the data for apparent shear rates less than about 80 s^{-1} (stable region where the extrudate appears
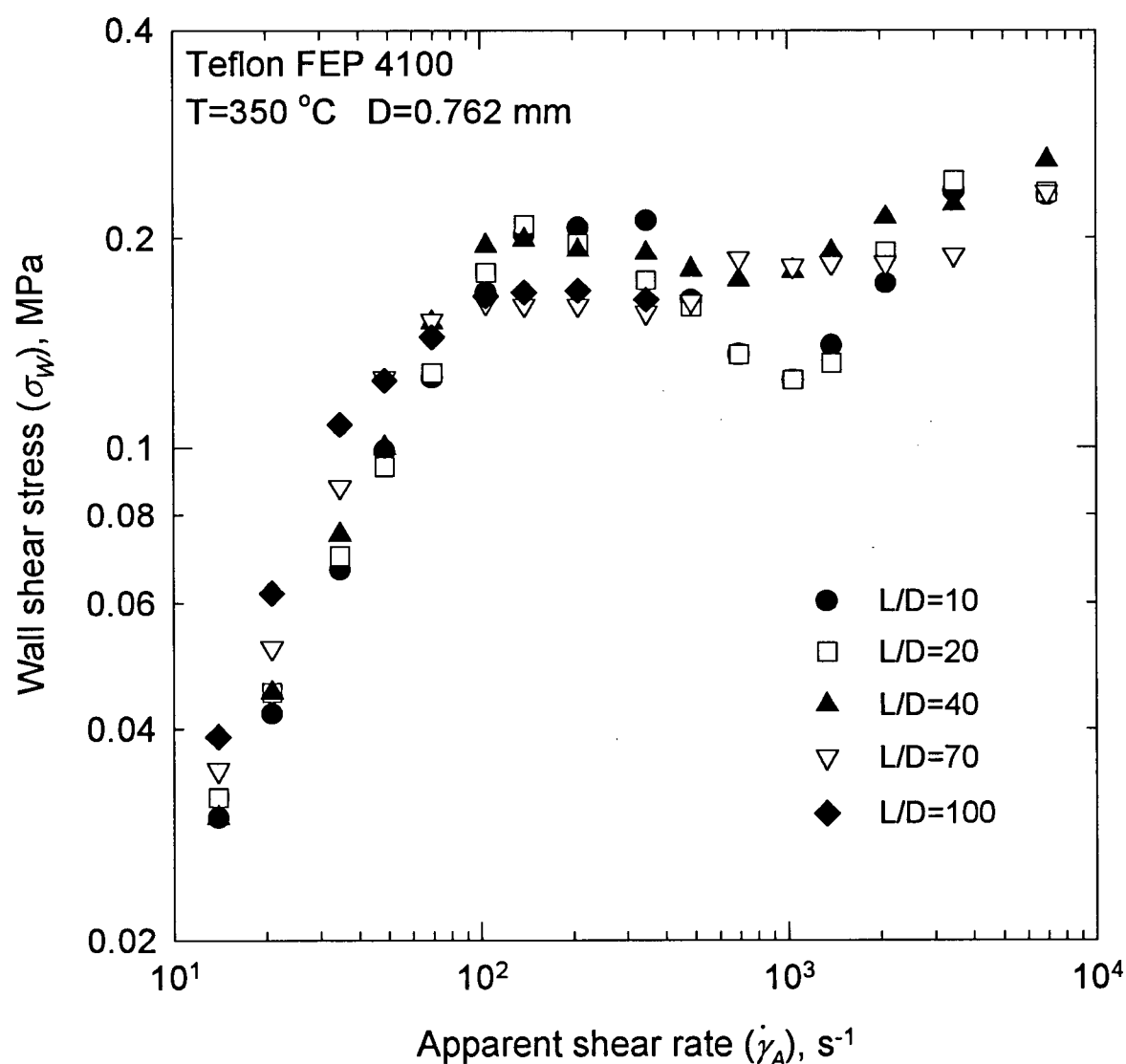
Figure 5-5. The effect of pressure on the flow curves of resin FEP 4100 at 350 °C using capillary dies having a diameter of 0.762 mm and various length-to-diameter ratios

smooth) do not fall on a single curve. Instead, the apparent flow curves shift to higher

values of the wall shear stress with increasing L/D ratio, thus pressure. This implies that

the viscosity of FEP 4100 is a function of pressure.

The pressure dependence of viscosity is typically represented by an exponential

function (first order approximation) which for a given temperature can be written as:

$$\eta = \eta^0 \exp(\alpha P) \tag{5-2}$$

where η^0 is the viscosity at ambient pressure, α is the pressure coefficient of viscosity

and P is the absolute pressure. To obtain the pressure coefficient of viscosity, α, the data

points corresponding to various values of L/D ratio in the smooth region were brought

together on a single curve by varying α. Note that, at very low shear rates and for small

L/D ratio, the wall shear stress is insensitive to the pressure coefficient, so caution should

be exercised in selecting the data points. The value of α required to superpose the data

reasonably well was found to be $(2.25 \pm 0.87) \cdot 10^{-8}$ Pa^{-1} (for the 95% confidence interval

and a sample of 14 points). This value is consistent with measurements reported for other

polymer melts. A value of 2.9×10^{-8} Pa^{-1} was reported for polystyrenes by Penwell *et al.*

(1971), but it is higher than those reported in the literature for polyethylenes: e.g., Kalika

and Denn (1987) reported the pressure coefficient of viscosity for a LLDPE to be $5 \cdot 10^{-9}$

Pa^{-1}, while for HDPE α is believed to be less than $0.52 \cdot 10^{-9}$ Pa^{-1} (Rauwendaal and

Fernandez, 1985).

The resulting pressure-corrected flow curves are shown in Figure 5-6. It can be

observed that in the smooth region a relatively good superposition of the data results. On

the other hand, the pressure correction introduces a greater separation of the data than

before, particularly in the stick-slip region and beyond. However, in defining the critical

shear stress for the onset of melt flow instability, one should use the actual and not the pressure-corrected shear stress. Furthermore, due to the relatively strong effect of pressure on viscosity in this case, it may be more appropriate to define the critical shear stress for the onset of melt fracture as the shear stress at the inlet to the capillary. This is significantly higher than that at the exit for long capillaries. Thus, while it is apparent from Figure 5-5 that the critical shear stress for the onset of oscillations increases with decreasing L/D ratio, when the shear stress at the inlet is determined, oscillations occur at
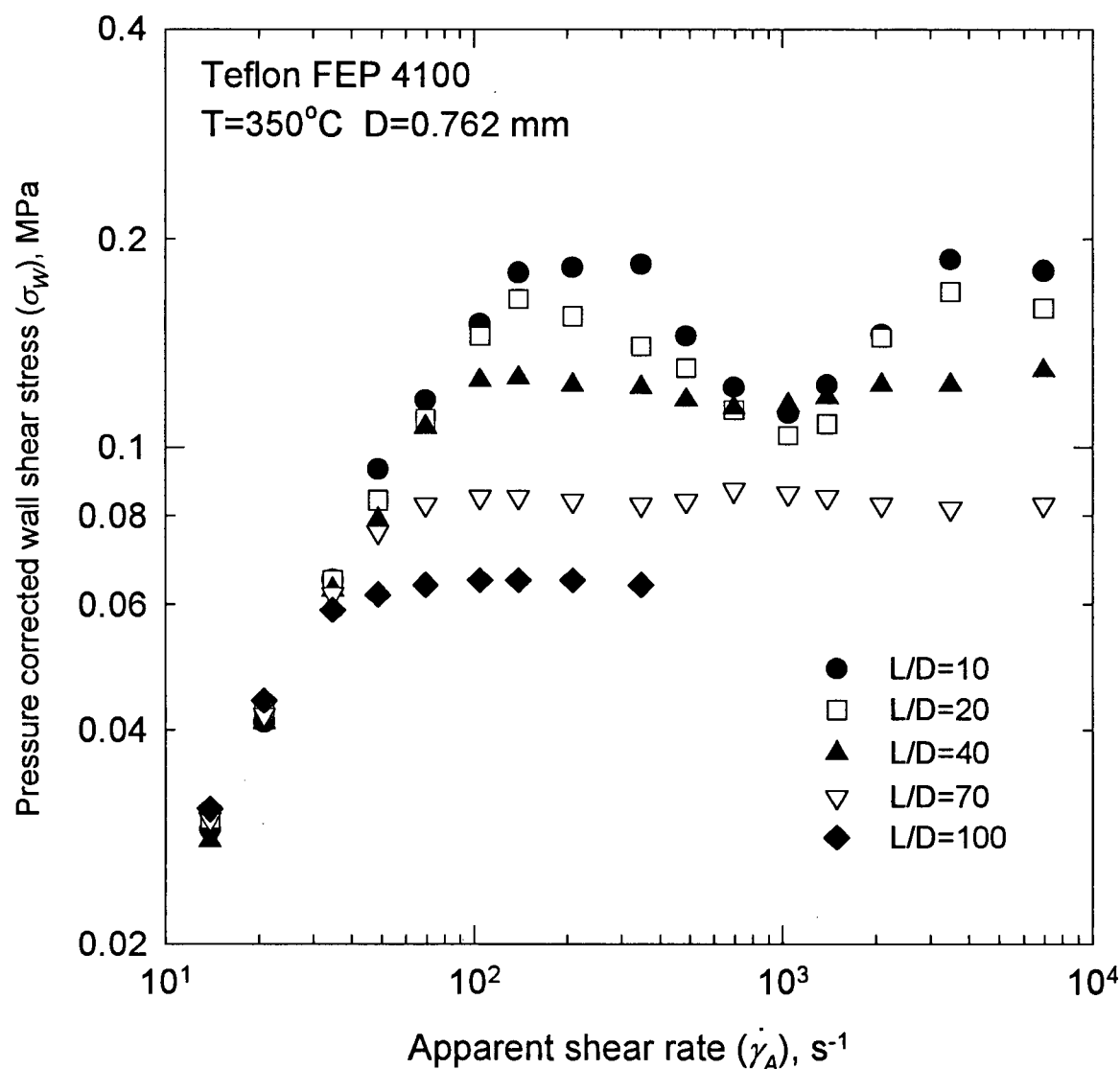
Figure 5-6. Pressure-corrected flow curves of resin FEP 4100 at 350 °C

about the same critical shear stress value, that is about 0.20 MPa (Penwell *et al.*, 1971).

As discussed before, one may see in Figure 5-5 that the absolute value of the slope in the stick slip region increases with decreasing L/D ratio and, for long enough capillaries, an almost perfect plateau region is obtained. This is somewhat surprising and in contrast to what has been reported by Hatzikiriakos and Dealy (1992a) for the oscillating melt fracture of linear polyethylenes, where the difference between the two extreme shear stress values in the oscillating flow regime scales linearly with the L/D ratio of the capillary, and thus pressure.

5.7 Wall Slip

To detect the presence of slip, one may use the Mooney technique. According to this technique the flow curves determined with a series of capillaries having different diameters diverge if slip is present. In addition, to eliminate the effects of pressure on viscosity and slip velocity one should keep constant the L/D ratio of the capillary die. This technique was used in the past for a series of HDPE's and it was found that these polymers slip at critical shear stresses in the range of 0.1-0.18 MPa depending on the molecular weight and polydispersity of the resin (Hatzikiriakos and Dealy, 1992a). Ramamurthy (1986) also determined critical shear stresses in the same range for LLDPE's.

Figure 5-7 shows the apparent flow curves of FEP 4100 determined with dies having different diameters but constant L/D ratio. It can be seen that these flow curves show diameter dependence for wall shear stresses beyond the oscillating flow region. This implies the presence of slip in this high shear rate branch of the flow curve. The

same behavior was obtained at the other two temperatures and also with capillaries

having other L/D ratios. It can also be seen that, at very high apparent shear rates, the

curves seem to converge. This may be due to the effect of viscous heating which is

significant at high shear rates. The effect of viscous heating is more pronounced for

capillaries having a larger diameter provided that the L/D ratio is kept constant (Ybarra

and Eckert, 1980; Cox and Macosko, 1974). Shidara and Denn (1993) have discussed the

effect of viscous heating for a molten polystyrene in slit extrusion. To explain their re-
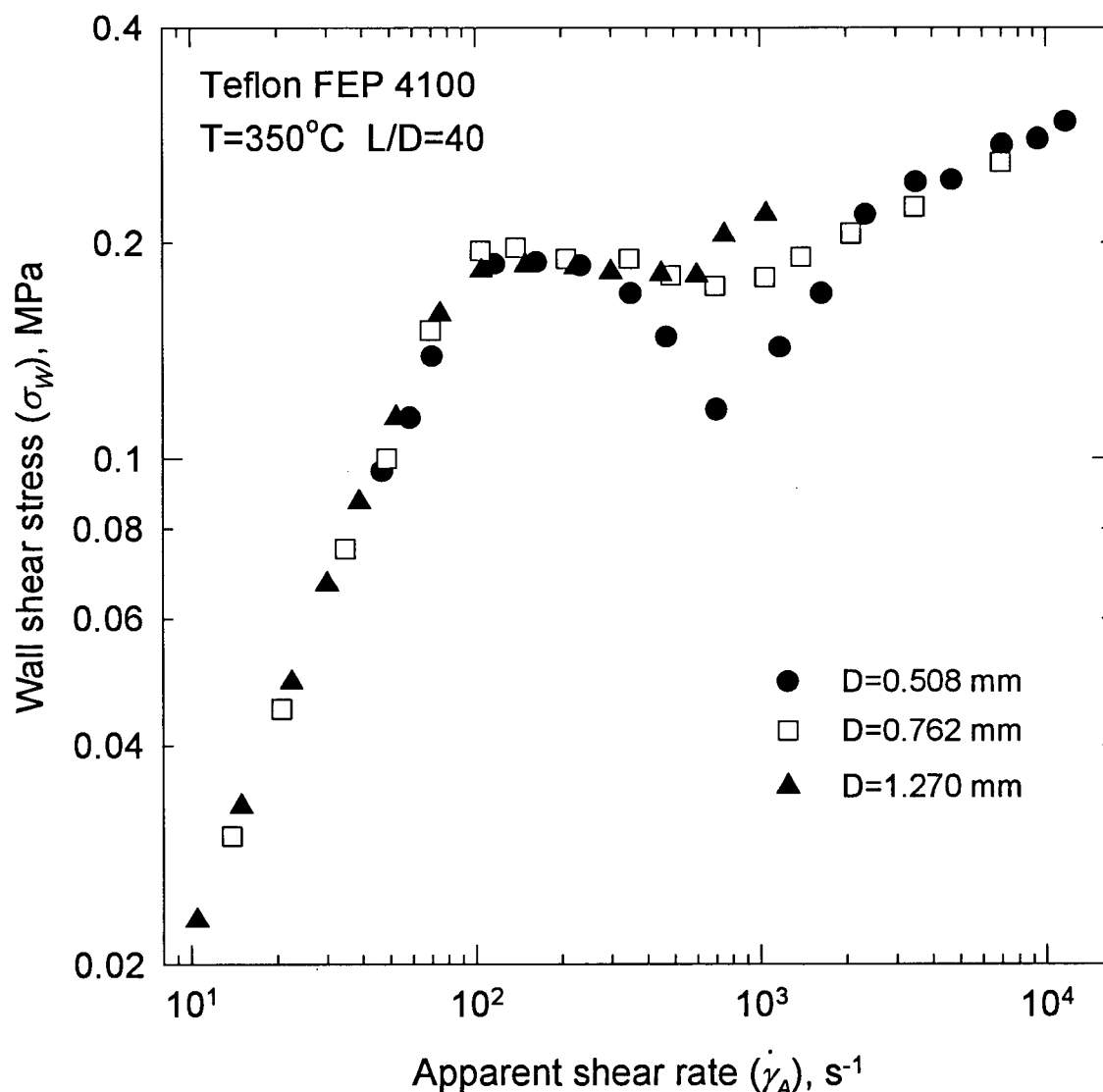
Figure 5-7. The effect of the capillary diameter on the flow curve of resin FEP 4100 at
350 °C. Wall slip is present in the regions where the flow curve becomes
diameter dependent

sults, they assessed this effect to be significant. Because the effect of pressure on the viscosity of polystyrenes and FEP resins is similar, one expects that the effect of viscous heating should also be of similar significance. Shidara and Denn (1993) also pointed out that a numerical solution of the full field in capillary/slit flow incorporating pressure and temperature effects is needed. This solution is also needed in order to calculate the slip velocity as a function of the wall shear stress in the present case. The numerical simula-
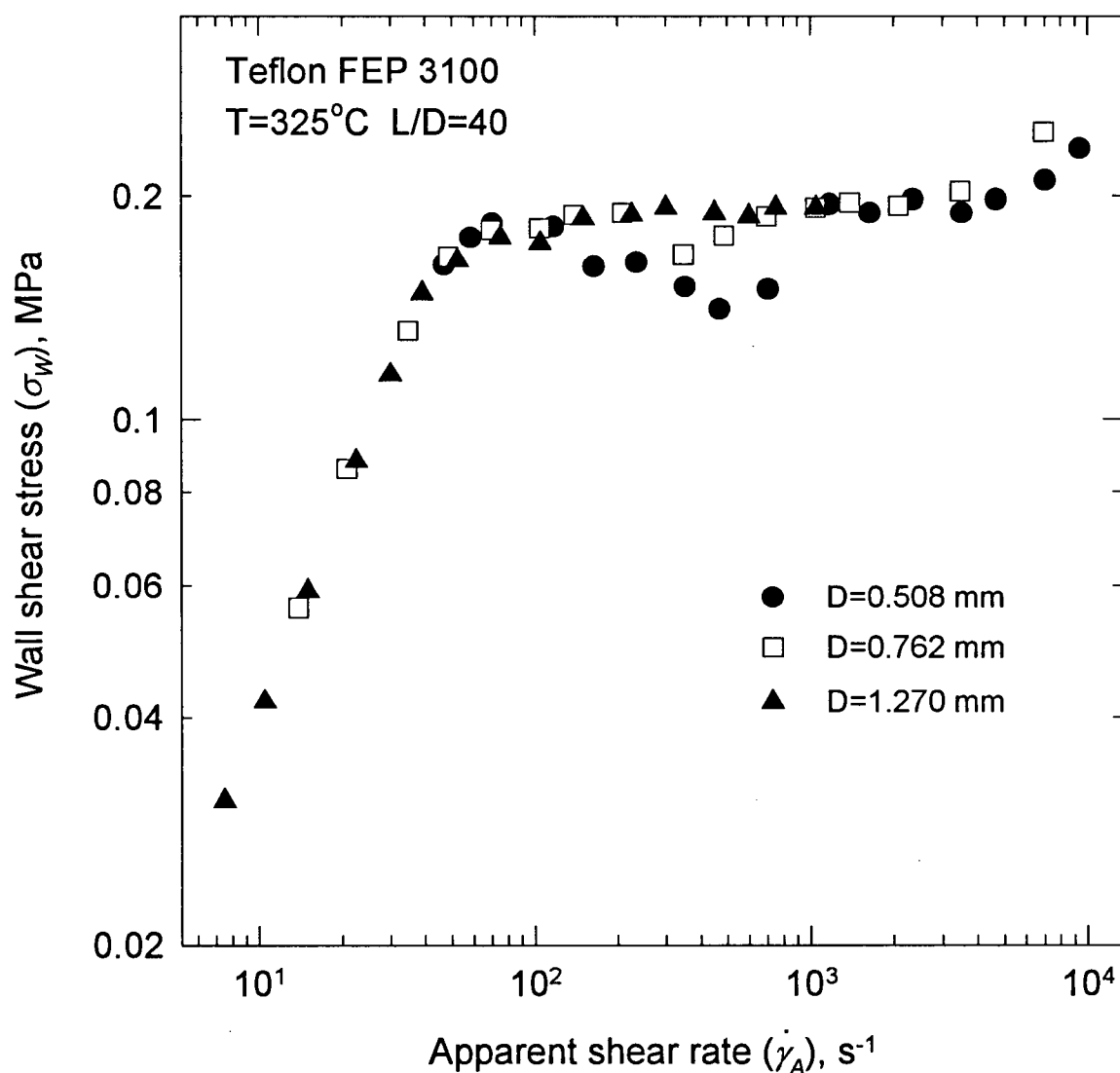
Figure 5-8. The effect of the capillary diameter on the flow curve of resin FEP 3100 at 325 °C. Wall slip is present in the regions where the flow curve becomes diameter dependent

tion of the capillary flow subject to viscous heating will be discussed in Chapter 7.

It should be mentioned that the diameter dependence of the apparent flow curves was also observed for FEP 3100 as can be seen in Figure 5-8. There, the apparent flow curves obtained by using capillaries having a fixed *L/D* ratio and different diameters are plotted. The diameter dependence is clear in the oscillating flow region but less evident at higher shear stresses, which may be attributed to the effect of viscous heating as discussed above.

5.8 Extrudate Distortions

Samples of FEP 4100 extrudates produced at various shear rates using a capillary having a length-to-diameter ratio of 40 and diameter of 0.762 mm are shown in Figure 5-9a-e. Five extrudate samples are shown, each one corresponding to the five different flow regions discussed previously. At low rates the extrudate appears smooth (Figure 5-9a). At higher shear rates, small amplitude periodic distortions appear on the surface of extrudates (sharkskin or surface melt fracture, Figure 5-9b) and this behavior is obtained over a short range of apparent shear rates. The extrudate obtained in the unstable flow region (oscillating melt fracture) consists of two distinct zones (Figure 5-9c): a smooth section, corresponding to slip with decreasing pressure (superextrusion region), and a rough one, corresponding to stick with increasing pressure (sharkskin region). The onset of oscillating melt fracture is characterized by a sharp decrease in the slope of the flow curve (Figure 5-4). As one may see from Figures 5-5, 5-7, and 5-8, the critical shear stress for the onset of sharkskin is independent of the diameter and length-to-diameter ratio of the capillary die. At higher apparent rates in the superextrusion region, the

a   b   c   d   e
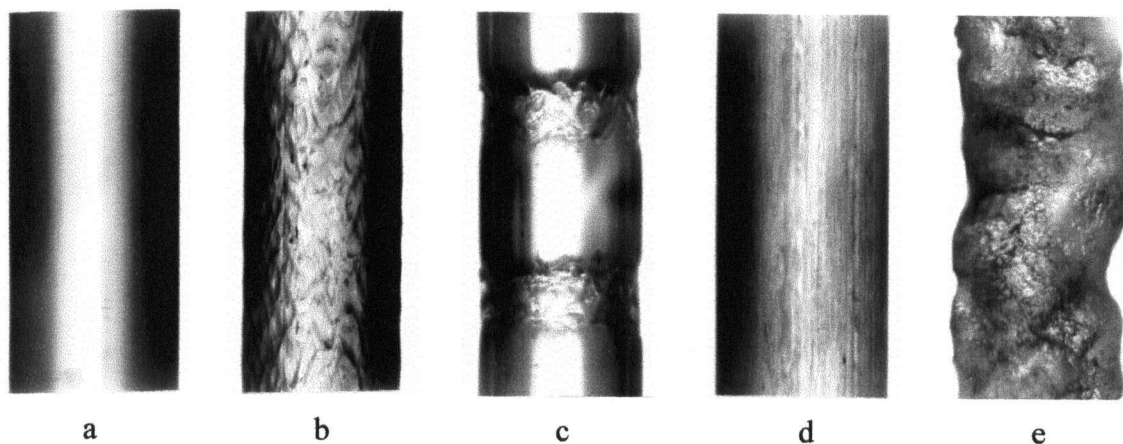
Figure 5-9. Representative photographs to illustrate the extrudate appearance of FEP 4100 extrudates in the five flow regions

extrudates seem to be smooth (Figure 5-9d) but not as glossy as in the prefractured region. Finally, the gross melt fracture region is characterized by severe irregularities where the distortion depth is of the order of the extrudate diameter (Figure 5-9e). The severity of distortions increases with the shear rate. The onset of gross melt fracture was detected to occur at a critical shear stress of about 0.22 MPa for capillary dies having L/D ratios from 10 to 100.

The effect of temperature on the various flow regimes in the capillary extrusion of FEP 4100 is illustrated in Figure 5-10. There, the FEP4100 flow curves, obtained with a capillary die having a diameter of 0.508 mm and an L/D ratio of 40 are plotted for three different temperatures. It can be seen that in the stable region, as the temperature is increased, the flow curves shift to higher values of the wall shear stress as expected (higher viscosity). However, the onset of oscillating melt fracture occurs at smaller apparent shear rates and wall shear stresses as the temperature is decreased. As a result, the flow curves at different temperatures cross each other and, at high enough apparent shear rates, almost coincide. The superextrusion region (smooth extrudate at conditions
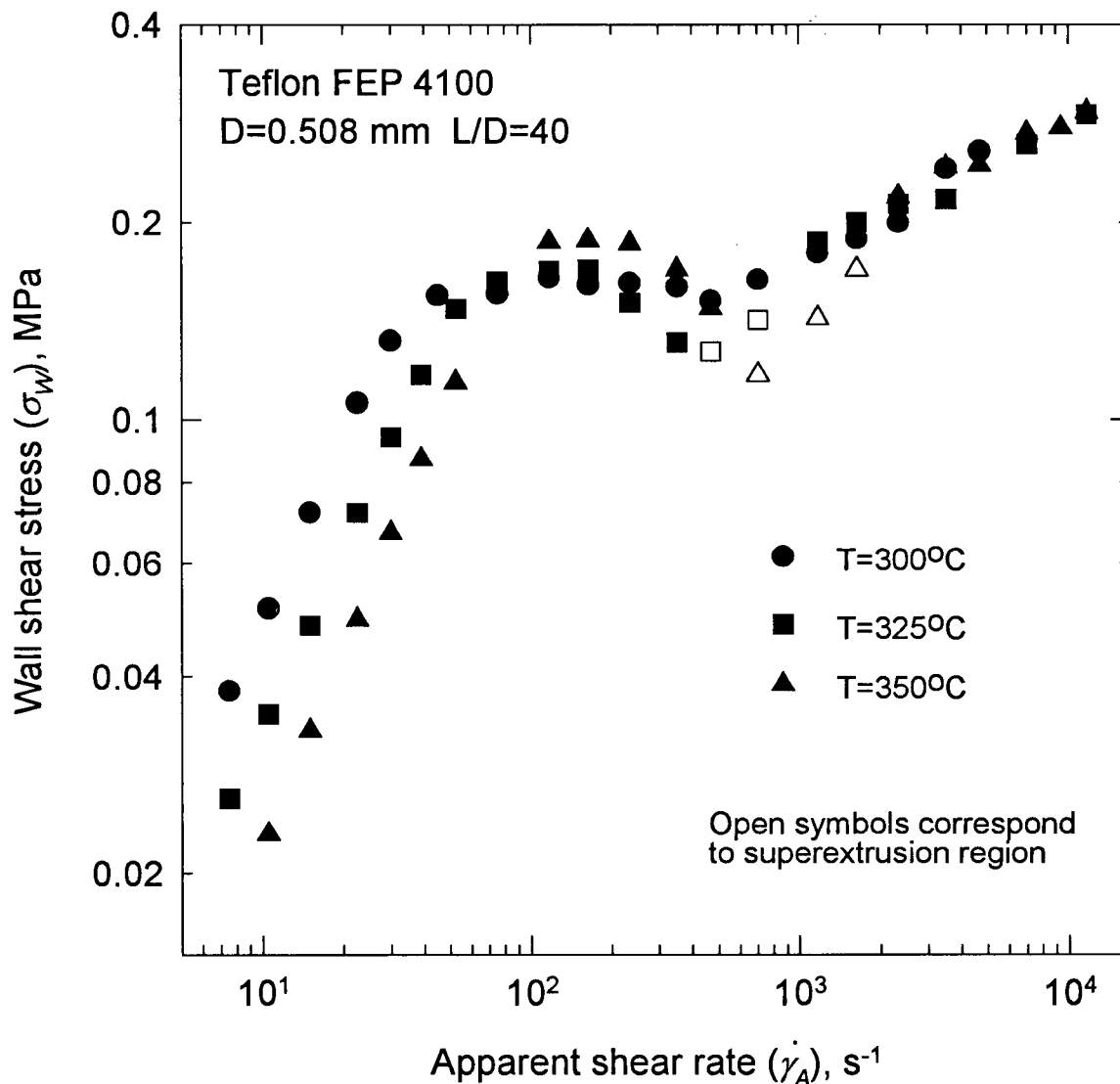
Figure 5-10. The effect of temperature on the flow curve of resin FEP 4100. Note the strong effect of T on the superextrusion flow region

beyond the oscillating melt fracture region) is also affected by temperature. It can be seen from Figure 5-10 (open symbols) that at 350°C the superextrusion region expands over a range of apparent shear rates between 700 and 2000 s⁻¹, at 325°C this range becomes shorter, between 470 and 700 s⁻¹, while for 300°C there is no clearly defined superextrusion region at all.

5.9 The Oscillating Melt Fracture

Figure 5-11 shows the pressure drop as a function of time during a typical run in the oscillating melt fracture region. It can be seen that the pressure always oscillates between two extreme values, with the frequency of the oscillations increasing as the amount of material in the rheometer reservoir declines. Also, near the end of the run, the pressure drop amplitude decreases gradually. The oscillations are mainly due to the combined effect of the wall slip and of the compressibility of the material resin (Hatzikiriakos and Dealy, 1992a; Pearson, 1965).

The effect of compressibility can be seen better in Figure 5-12, where the period
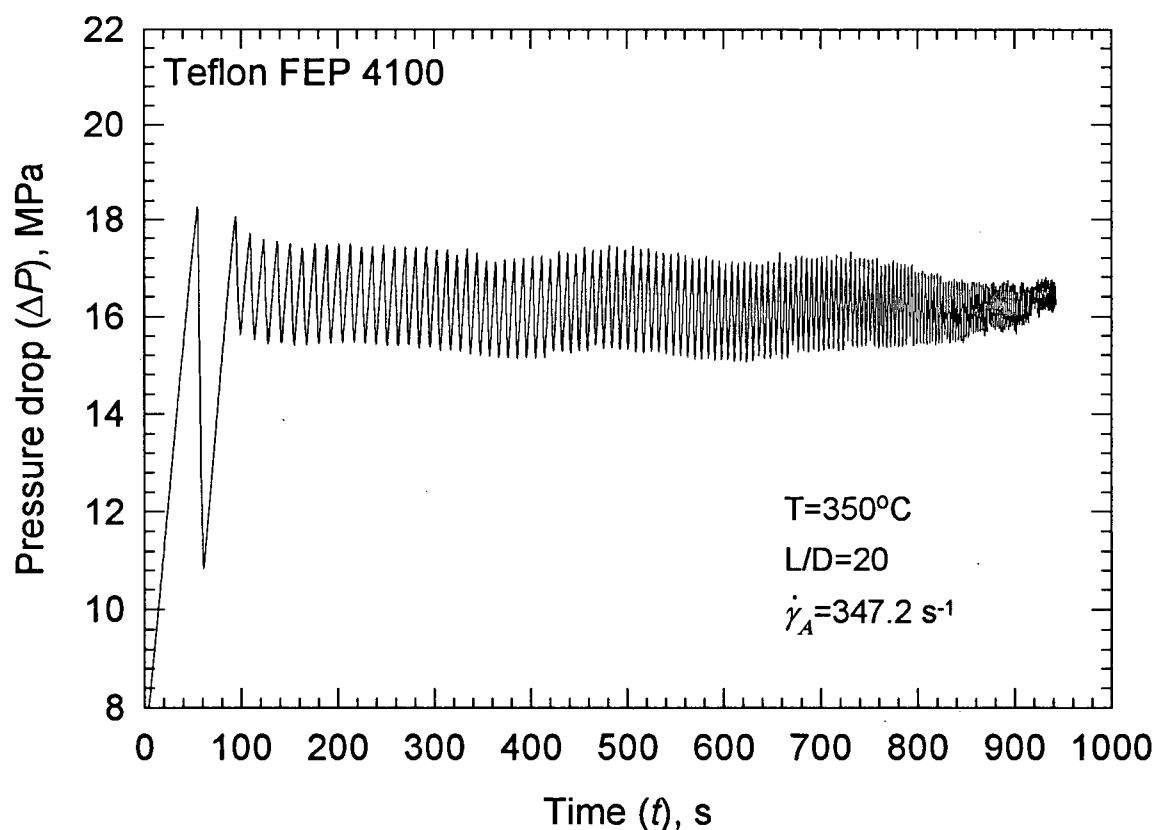
Figure 5-11. Pressure drop oscillations during capillary extrusion of resin Teflon FEP 4100 at 350 °C. Note that the frequency of pressure drop oscillations increases with decrease of the material in the barrel

of oscillations is plotted as a function of the length of the reservoir occupied by polymer.

In general, an essentially linear relationship is obtained for all three cases between these

two variables, which clearly shows the effect of the compressibility of the material. In

other words the period of oscillations scales linearly with the amount of polymer in the

rheometer reservoir as it is pointed out by Hatzikiriakos and Dealy (1994) .
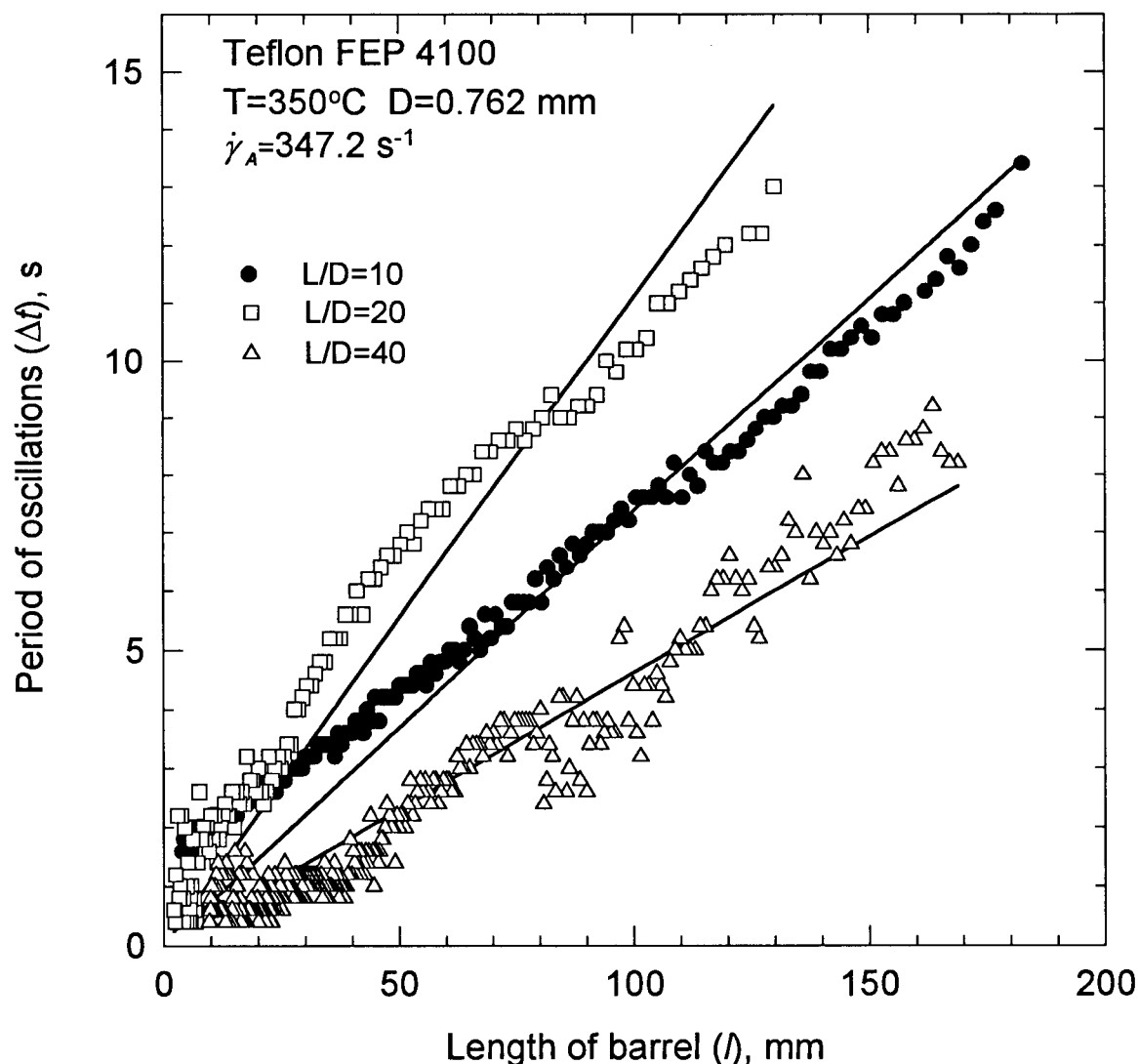
Figure 5-12. The period of oscillations as a function of the volume of polymer (FEP
4100) in the rheometer reservoir for three capillary dies having different
L/D ratios and a constant diameter at 350 °C

However, it was expected that for a fixed length of the barrel occupied by polymer, the period of oscillations should scale with the L/D ratio (Hatzikiriakos and Dealy, 1992a). This does not seem to be the case as may be inferred from Figure 5-12, i.e. the period of oscillations increases from L/D=10 to L/D=20 but decreases from L/D=20 to L/D=40. In addition, as previously discussed, the difference between the two extreme shear stress values does not also scale with the L/D ratio as in the case of the oscillating melt fracture of HDPE's (Hatzikiriakos and Dealy, 1992a). Moreover, within this flow region, multiple "windows" of apparent shear rates were identified where the pressure drop instead of oscillating assumes a steady-state value. For example, Figure 5 -
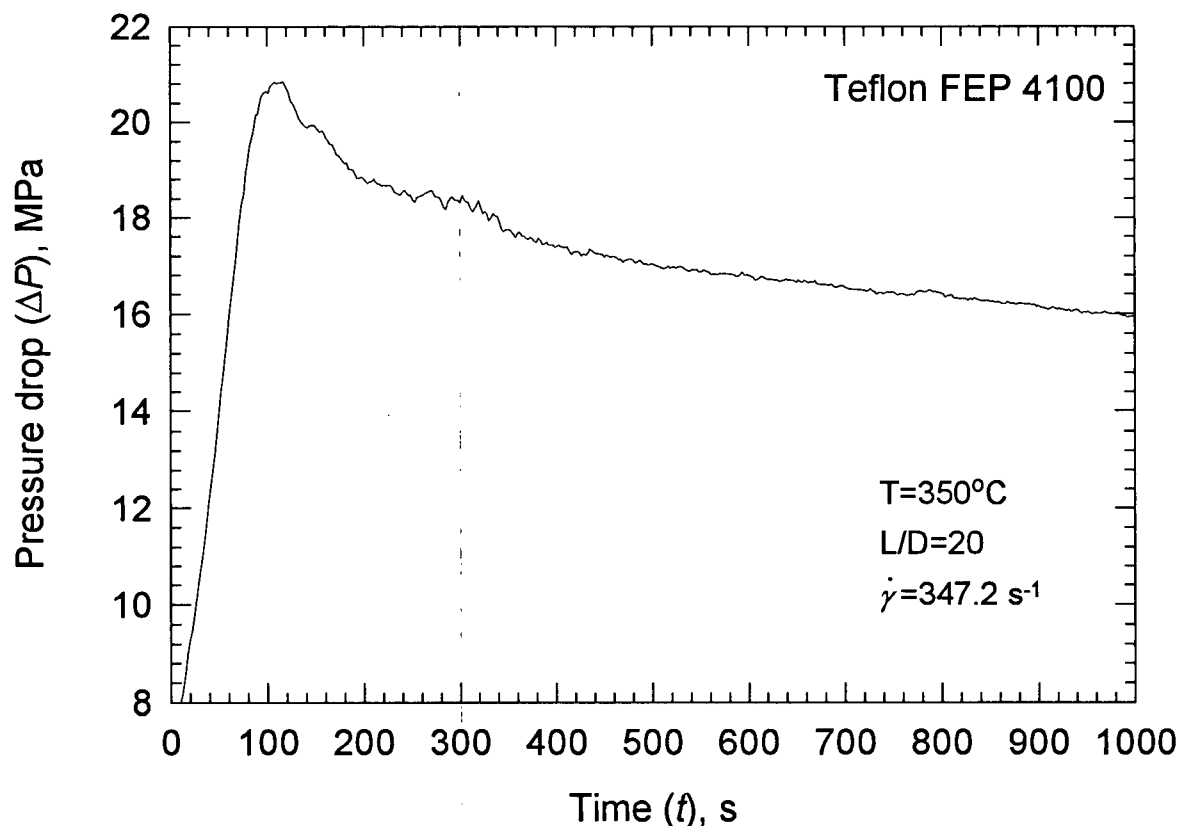
Figure 5-13. A repeat of the experiment plotted in Figure 5-11. Instead of persisting oscillations, a stable response is obtained

13 shows one repeat of the experiment plotted in Figure 5-11. Instead of obtaining oscillations, the pressure drop tends to assume a steady-state value. This same experiment has been repeated several times and it was found that in some cases oscillations persist throughout the experiment (Figure 5-11), while in the other cases the pressure after overshooting tends to assume a steady-state value (Figure 5-13). It is noted, however, that the steady-state value of the pressure in Figure 5-13 is about equal to the average of the two extreme pressure values of the oscillations plotted in Figure 5-11. It seems that the pressure response is sensitive to the initial conditions which could be different in the two experiments, i.e., small fluctuations in temperature of ± 1 °C. Even such a small variation in the initial temperature can give a much different response. Recently, Pudjijanto and Denn (1994) discovered a stable "island" in the slip-stick region of a linear low-density polyethylene. This island exists only in a narrow temperature window and a small variation of temperature, i.e., of the order of 1 °C, can interchange oscillatory and stable responses.

5.10 A Comparison of the Processability of the two FEP Resins

As noted above, experiments for FEP 3100 were also carried out to identify differences in the processing between the two FEP resins. While these two resins have close molecular weight and polydispersity, a small amount of PAVE has been incorporated in the molecules of FEP 4100 (about 0.8 wt.%). As noted before, the viscosity of FEP 4100 is about 25% lower than that of FEP 3100 which can be attributed to a difference in the molecular weight (see Figure 5-8). Figure 5-14 shows the apparent flow curves of the two resins obtained at the temperature of 325°C using a capillary

having an L/D ratio of 40 and D equal to 0.508 mm. In general, FEP 3100 exhibits the

same behavior as FEP 4100, and one could distinguish the same flow regions as those

identified for FEP 4100. However, some of the differences observed can be summarized

as follows:

- The critical apparent shear rate for the onset of sharkskin melt fracture of FEP 3100
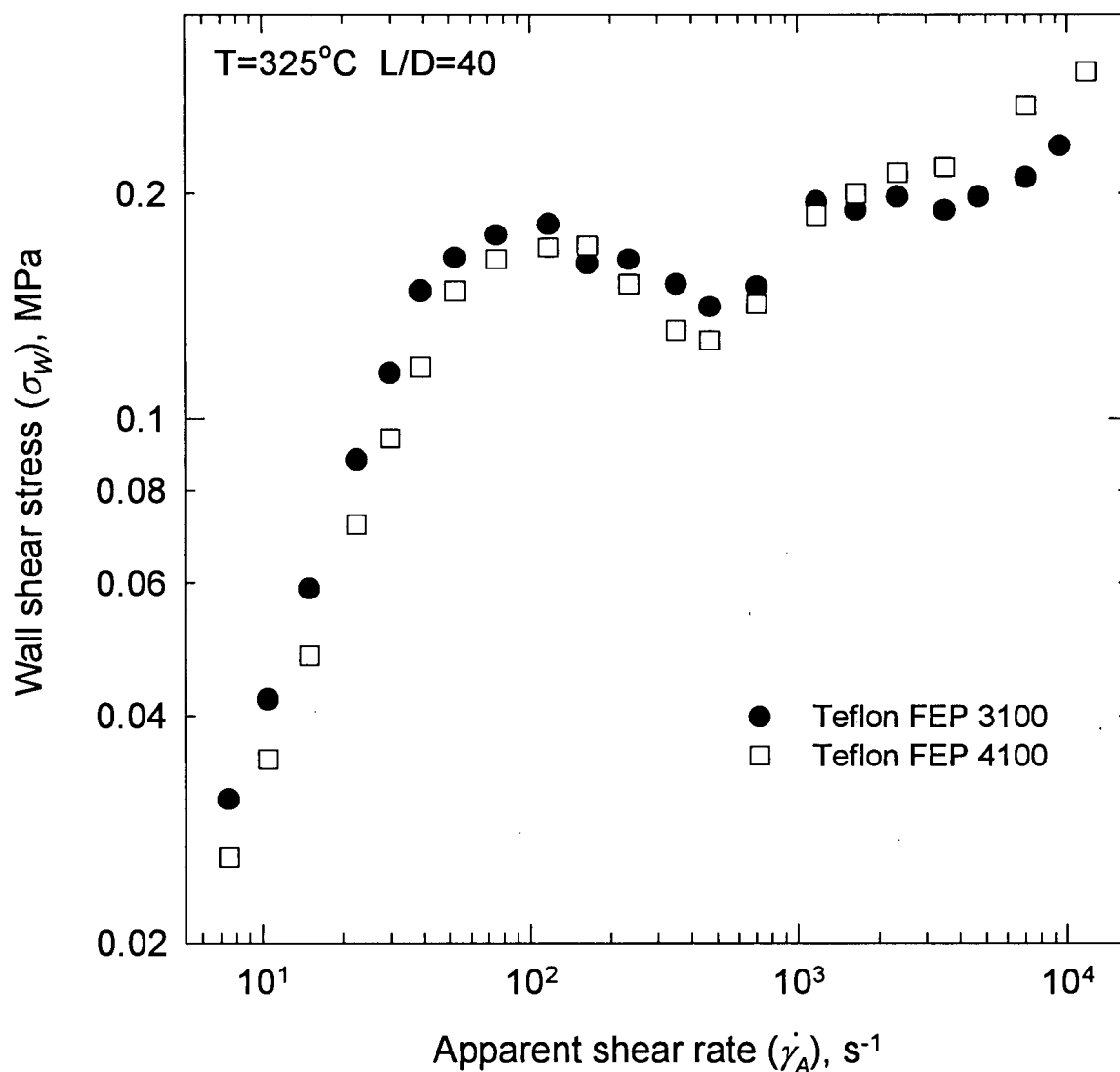
Figure 5-14. A comparison of the flow curves for two FEP resins (FEP 3100 and FEP 4100) at 325 °C

was found to be about 40 s^{-1} while that for FEP 4100 is about 70 s^{-1}. Thus, the presence of PAVE in FEP 4100 greatly extends the range of the stable region.

- The oscillations of the pressure drop for FEP 3100 have a much smaller amplitude than for FEP 4100. In spite of this, the extrudates of both resins still exhibited the stick-slip melt fracture appearance.

- The range of the superextrusion region for FEP 3100 is wider; it ranges from 250 s^{-1} to 700 s^{-1}. However, the critical conditions for the onset of gross melt fracture are practically the same in both resins.

- Finally, the addition of PAVE makes the molecules more flexible. This increases the melt strength, improves the stress crack resistance, and, as a result, allows higher speeds in wire coating (Stewart, 1994).

5.11 Effect of the Molecular Weight

Capillary rheometer experiments were carried out with a series of TFE/HFP copolymers (Group B in Table 4-2) in order to assess their processability and its relationship with molecular weight and structure. Figure 5-15 shows the flow curves for three FEP resins having different molecular weights. It can be seen that all resins have an almost Newtonian viscosity in the prefractured region at fairly high shear rates. The onset of the sharkskin melt fracture occurs at the same value of the wall shear stress, but due to different viscosities it appears to occur at lower critical values of the apparent shear rate for resins with higher molecular weights. The superextrusion region starts approximately at the same value of the apparent shear rate for all resins. Beyond this region, the curves seem to coincide. At these high shear rates, where the flow virtually becomes plug-like,
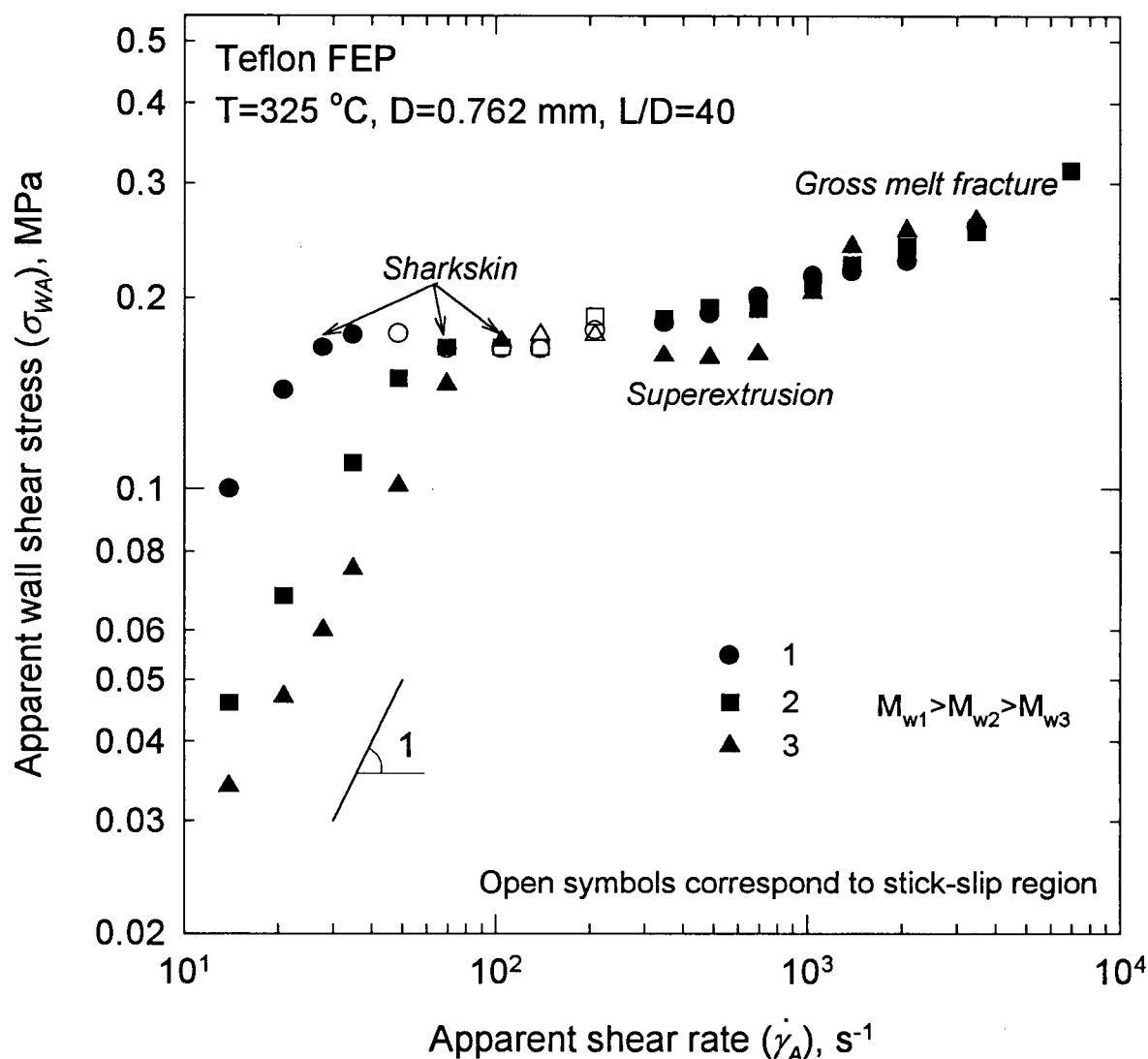
Figure 5-15. The effect of molecular weight on the flow curve of TFE/HFP copolymer resins (FEP-1, 2, and 3 of Group B in Table 4-2)

the pressure drop is mainly governed by the friction between individual monomers and the wall (strong slip), and apparently the polymer properties become independent of molecular weight. Also, at these high rates, viscous heating and energy dissipation at the polymer-wall interface are high enough to also affect the shape of the flow curves.
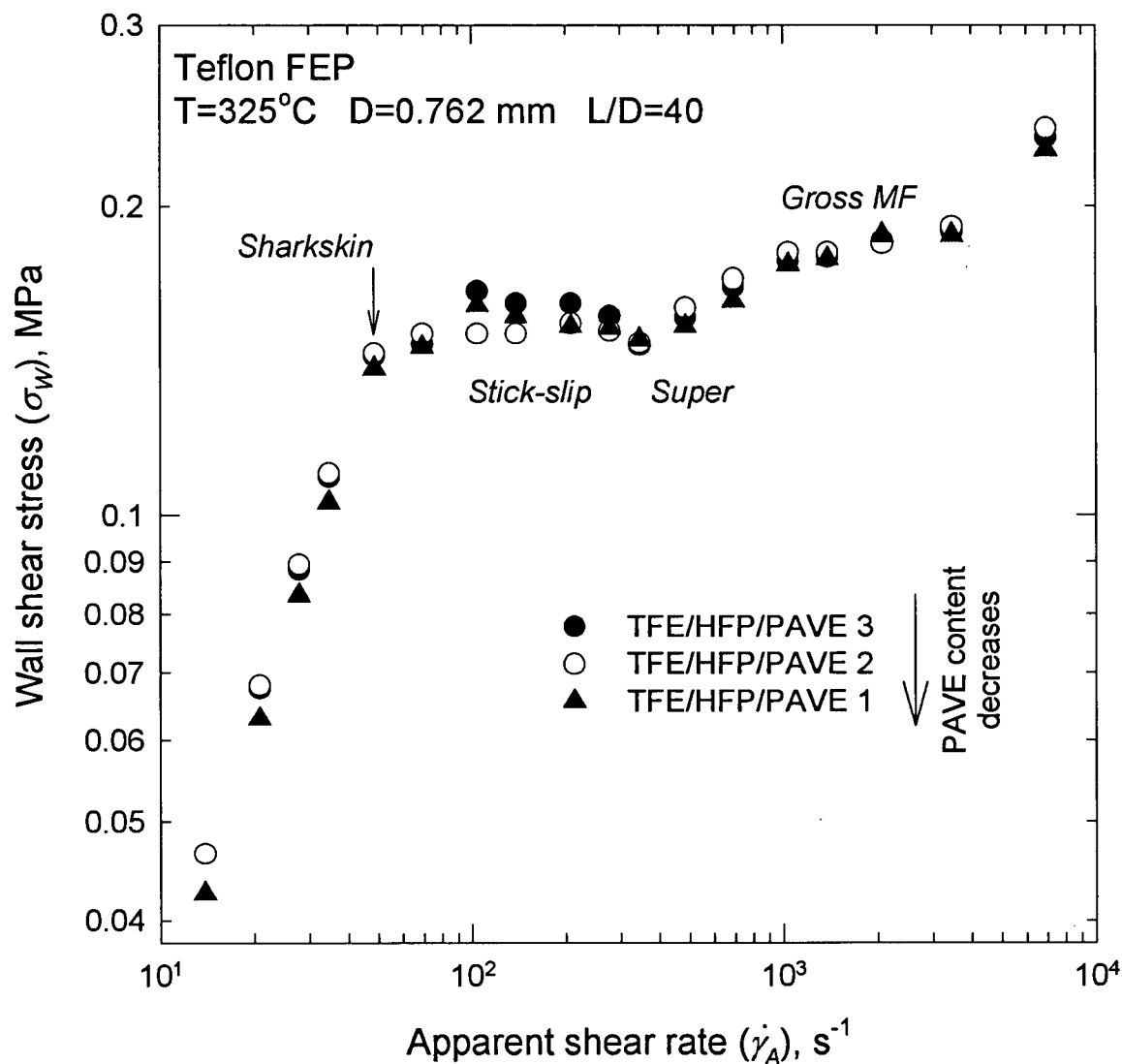
Figure 5-16. The effect of PAVE content on the flow curve of TFE/HFP/PAVE terpolymer resins (TFE/HFP/PAVE-1, 2, and 3 of Group C in Table 4-3)

5.12 Effect of the PAVE Content

The effect of the incorporation of PAVE into molecules of the copolymer was discussed in some previous sections. In this section, an attempt to assess the effect of the PAVE content on the processability of the terpolymer was made.

Figure 5-16 plots the flow curves for three FEP terpolymers having different contents of PAVE (the resins of Group C, Table 4-3). Unfortunately, because of the small variations in the PAVE content in the resins, it was impossible to identify significant differences in their processability as it can be assessed by means of a capillary rheometer. One can see that rheology does not change much with increase in the PAVE content. A small difference in the viscosity of the resins in the prefractured region (within 10%) is consistent with the results obtained in a parallel-plate rheometer (see Chapter 4). The critical shear stress corresponding to the onset of melt fracture as well as the breadth of each flow region are about the same for all the resins and close to those of FEP 4100. However, from practical tests on wire coating, where elongational flow is dominant, it is noticed that, in general, the resins with the higher content of PAVE are processed better (Stewart, 1994).

6 Rheological Characterization of Teflon® FEP Resins

$\mathcal{T}$he rheological data for a number of Teflon® FEP polymers, obtained by means of both a parallel-plate and capillary rheometers, were used for a thorough rheological modeling of the behavior of these resins. The latter includes calculation of their linear relaxation time spectra and nonlinear parameters using a multi-mode Phan-Thien and Tanner (PTT) constitutive equation. The relaxation time spectrum, $H(\lambda)$, calculated by use of the BSW model (developed for monodisperse linear polymers) followed a scaling relationship in the terminal zone with a scaling exponent of 0.13. However, at higher frequencies the model fails to predict adequately the experimental data. The longest relaxation time calculated from both the BSW model and the discrete relaxation spectra (λ_i, g_i), which was determined by use of a parsimonious fitting software, depends on the molecular weight in a similar way as the zero-shear viscosity does with the well-established scaling factor of 3.4. It was found that the PTT model can represent rheological data for Teflon® FEP resins very well and may be used in relevant processing flow simulations, e.g. in wire coating.

6.1 Introduction

The molecular mobility of polymeric liquids expresses itself in a relaxation time spectrum. It can be written as a continuous function, $H(\lambda)$, or as a sum of discrete terms, each of them having a characteristic time constant, λ_i, and a so called relaxation strength, g_i (see Equation (2-42)). Modeling of polymer processing and analysis of processing

experiments require knowledge of the relaxation time spectrum. It allows prediction of linear stress responses, e.g. in start-up of shear followed by relaxation, step strain, etc. Moreover, at large strains or strain rates, where some additional strain dependent perturbations of the constitutive equation are needed, the time dependent part of the rheological behavior is completely described by $H(\lambda)$. Therefore, it is significant to have available the means of converting dynamic mechanical data (dynamic moduli G' and G'') into the relaxation time spectrum.

The determination of the relaxation time spectrum has been recognized as an ill-posed problem with degree of ill-posedness increasing as the number of relaxation times increases (Tschoegl and Emri, 1993; Honerkamp and Weese, 1989). The ill-posedness means that infinitely many parameter sets can be found that are equally satisfactory from the point of view of fitting the data. Baumgaertel and Winter (1989) showed that this problem can be avoided by simply keeping the number of relaxation modes small. They developed an algorithm for recovering the discrete relaxation spectrum from linear viscoelastic data known as *parsimonious spectrum* (PS) (Baumgaertel and Winter, 1992). The corresponding numerical code is commercially available and known as IRIS. The basic idea of this method is to find the spectrum with the smallest number of Maxwell modes that still represents the data within the experimental error margin. This can be obtained by a simultaneous adjustment of λ_i and g_i, which are treated as freely adjustable material parameters during the fitting procedure. The right choice of the number of relaxation modes, N, is essential for the success of the algorithm. For small values of N, the spectrum is too coarse, and model calculations using the spectrum appear wavy. As more and more modes are considered, the waviness and the deviation between the fitted

spectrum and the data decrease. This can be shown in Figure 6-1 where the minimized

standard deviation, SD, is plotted. It is defined as

$$SD^2 = \frac{1}{M}\sum_{i=1}^{M}\left[1 - \frac{1}{G'(\omega_k)}\sum_{i=1}^{N}\frac{g_i(\omega_k\lambda_i)^2}{1+(\omega_k\lambda_i)^2}\right]^2 + \left[1 - \frac{1}{G''(\omega_k)}\sum_{i=1}^{N}\frac{g_i\omega_k\lambda_i}{1+(\omega_k\lambda_i)^2}\right]^2 \qquad (6\text{-}1)$$

where M is the number of data points. The noise in the data set yields a natural limit to

this improvement since the fit cannot be better than the standard deviation due to the

noise. Taking more modes is meaningless because the fitting does not improve

significantly with the extra modes and the values of g_i fluctuate erratically. The resulting

spectrum is claimed to be unique since various very differently looking discrete spectra

recovered by this procedure reduce to the same continuous spectrum $H(\lambda)$. Details of the
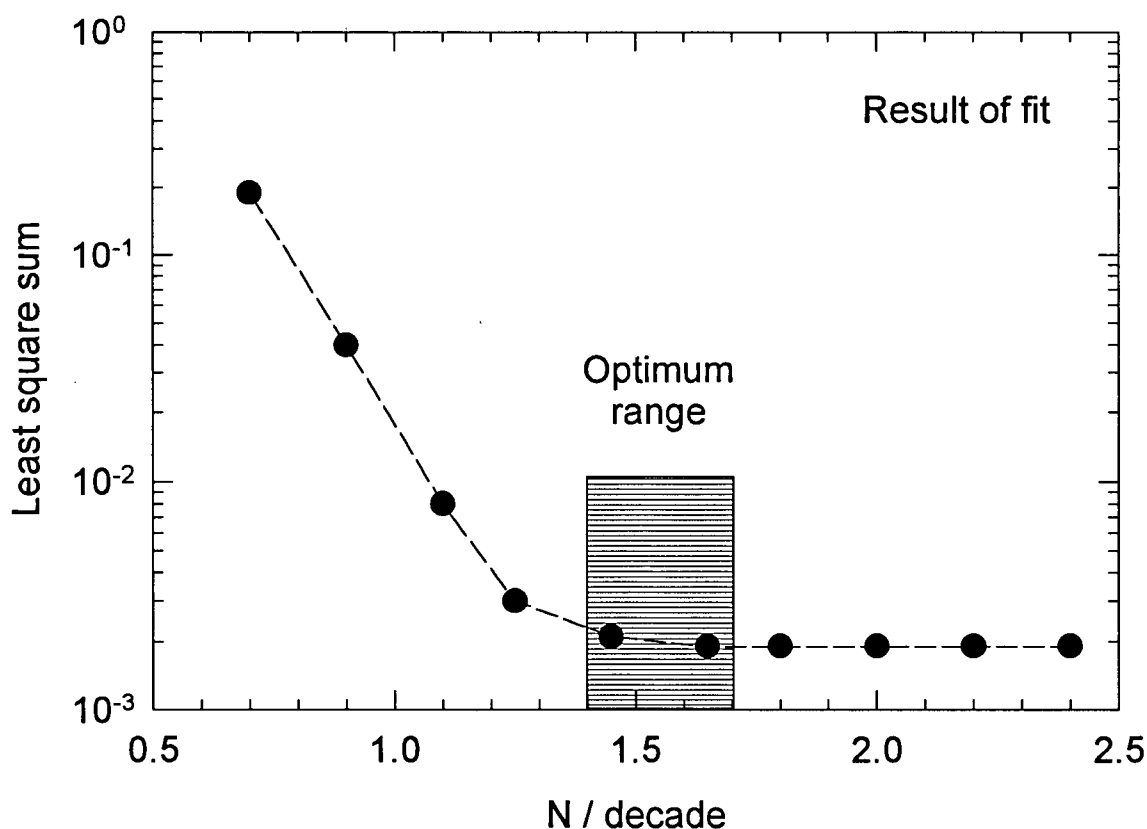
Figure 6-1. The standard deviation between the best possible fit and data. The fit improves when the number of Maxwell modes increases. Above a certain number of modes, the fit does not improve much further and the problem becomes ill-posed (from Winter et al., 1993)

method can be found elsewhere (Winter et al., 1993; Winter, 1997).

An alternative way to describe the relaxation time spectrum is to define correlations between the molecular parameters and macroscopic properties such as the longest relaxation time, plateau modulus, etc. Unfortunately, this can be done only for limiting cases. Baumgaertel *et al.* (1990) found that the relaxation spectrum of linear flexible polymers with molecules of (nearly) uniform length can be very well represented as

$$H(\lambda) = \begin{cases} n_e G_N^0 \left[\left(\dfrac{\lambda}{\lambda_c} \right)^{-n_g} + \left(\dfrac{\lambda}{\lambda_{max}} \right)^{n_e} \right], & \text{for } \lambda \leq \lambda_{max} \\ 0, & \text{for } \lambda > \lambda_{max} \end{cases} \tag{6-2}$$

where G_N^0 is the plateau modulus, λ_{max} is the longest relaxation time, n_e and n_g are the slopes of the spectrum in the entanglement and glass transition zones, respectively, and λ_c is the crossover time to the glass transition. The first term in the brackets represents the high frequency glass transition region, while the second term describes the entanglement and flow region. Equation (6-2) was tested using data for narrowly distributed polybutadienes and polysterenes and gave excellent results. Later, Baumgaertel and Winter (1992) modified this spectrum to suit broadly distributed polymers by replacing the abrupt cut-off at the longest relaxation time with a stretched exponential cut-off, as follows:

$$H(\lambda) = \left[H_g \left(\dfrac{\lambda}{\lambda_c} \right)^{-n_g} + n_e G_N^0 \left(\dfrac{\lambda}{\lambda_c} \right)^{n_e} \right] \exp(-\lambda/\lambda_{max})^{\beta} \qquad \text{for } M_W \gg M_c \tag{6-3}$$

where H_g is the glass-transition constant, M_W and M_c are the molecular weight and critical molecular weight, respectively, and β is the cut-off exponent.

In this chapter, the effect of MW on the relaxation spectra of Teflon® FEP resins was studied. The spectra are determined by use of both the method employing the BSW relaxation spectrum and the parsimonious method. For this purpose, a numerical code capable of recovering the discrete relaxation spectra from dynamic mechanical data was developed. The Phan-Thien and Tanner (PTT) constitutive model (Phan-Thien and Tanner, 1977) was also used to fit the experimental data from both capillary and parallel-plate rheometers to identify the additional nonlinear parameters that are necessary to carry out numerical simulation of complex viscoelastic flows.

6.2 Method of Evaluating Relaxation Time Spectrum

The method of calculating the relaxation time spectrum is similar to that described in Winter (1997). The discrete relaxation spectrum corresponds to a discrete relaxation modulus with a sum of exponential decays (Maxwell modes):

$$G(t) = \sum_{i=1}^{N} g_i \left[\exp(-t/\lambda_i) \right] \qquad (2\text{-}42)$$

where $g_i = H_i \Delta_i (\ln \lambda)$. A finite number of Maxwell modes, N, has to be determined: (g_i, λ_i) with $i=1,2,...,N$. To calculate g_i, one must know the step size $\Delta_i(\ln \lambda)$. A variable size is used in this work since this allows a closer fit of the data with fewer parameters. Both g_i and λ_i are variable in the spectrum calculation. The range of frequencies of the small amplitude oscillatory shear tests, $\omega_{min} < \omega < \omega_{max}$, determines the relaxation time window, $1/\omega_{max} < \lambda < 1/\omega_{min}$.

The discrete spectrum expresses itself in discrete moduli:

$$G'(\omega) = \sum_{i=1}^{N} g_i \frac{(\omega\lambda_i)^2}{1+(\omega\lambda_i)^2} \tag{6-4}$$

$$G''(\omega) = \sum_{i=1}^{N} g_i \frac{\omega\lambda_i}{1+(\omega\lambda_i)^2} \tag{6-5}$$

which can fit any G', G" data with a suitable choice of parameters (g_i, λ_i). The parameters are determined by minimization of the standard deviation, SD, (Equation 6-1). The minimization technique is the limited memory BFGS method (Zhu *et al.*, 1997). The above algorithm was implemented in the numerical code called UBCFIT. The code works as follows. Required are input data *G'*, *G"* within a finite frequency window. The minimization procedure simultaneously adjusts parameters (g_i, λ_i) to obtain the best fit of the experimental data. The number of relaxation modes, *N*, is also freely adjustable. The algorithm starts with some small value of *N* and keeps increasing it until the standard deviation stops to significantly decrease or becomes equal to the standard deviation in the data due to noise.

The code was tested on two sets of data for LLDPE Dowlex-2049 and model polybutadiene star polymer, and the results were compared with those obtained by the commercial software IRIS.

Comparative test 1: LLDPE Dowlex 2049. The data were obtained from McGill University and presented in Figure 6-2 together with the fit obtained by means of UBCFIT software. One can see that the fit is very good. Figure 6-3 shows the dependence of the standard deviation, SD, on the number of relaxation modes, *N*. The best fit is obtained with 8 relaxation modes. Further increase in the number of the modes does not improve the fit significantly. For the same data set, the control run of IRIS software resulted in 6 relaxation modes. However, if one compares the UBCFIT results

for 6 modes with those of IRIS (see Table 6-1), one can see that they are almost identical. Obviously, 8 modes give even better fit without unnecessary overfitting. The resulting relaxation spectrum is plotted in Figure 6-4.
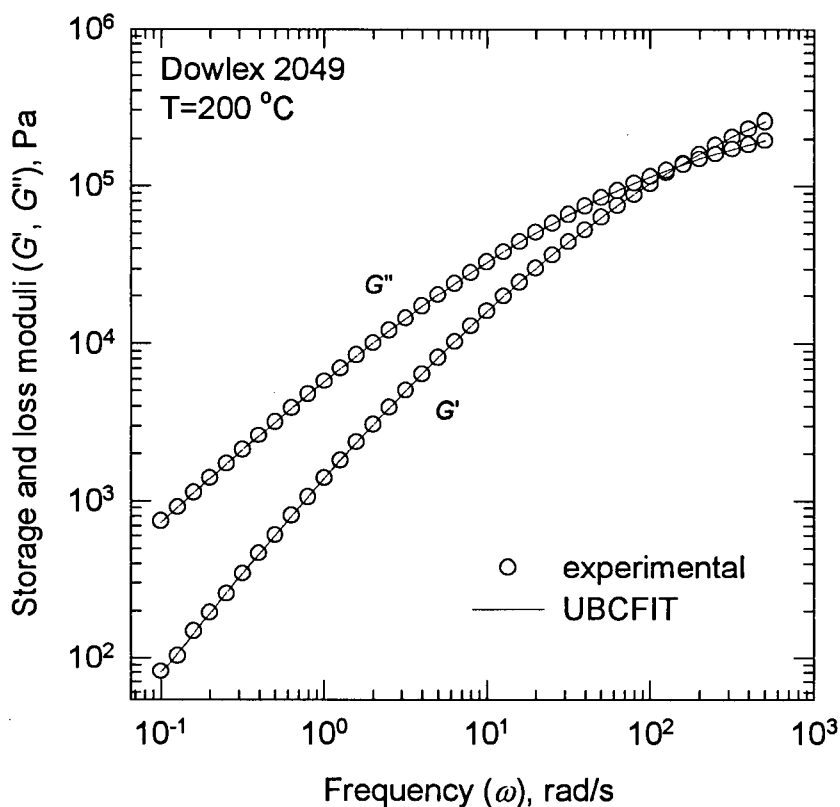
Figure 6-2. Storage and loss moduli for Dowlex 2049 at 200°C. Solid lines correspond to fitting obtained by means of UBCFIT software

Table 6-1. Discrete relaxation spectrum for Dowlex 2049 at 200°C (6 modes only). Comparison with results obtained by IRIS software

	UBCFIT		IRIS	
i	λ_i	g_i	λ_i	g_i
1	9.276E-04	4.228E+05	9.295E-04	4.228E+05
2	6.953E-03	1.377E+05	6.973E-03	1.376E+05
3	3.700E-02	4.688E+04	3.713E-02	4.678E+04
4	1.979E-01	1.021E+04	1.992E-01	1.016E+04
5	1.116E+00	1.453E+03	1.127E+00	1.439E+03
6	7.394E+00	1.580E+02	7.527E+00	1.554E+02
SD	1.80328E-2		1.80877E-2	
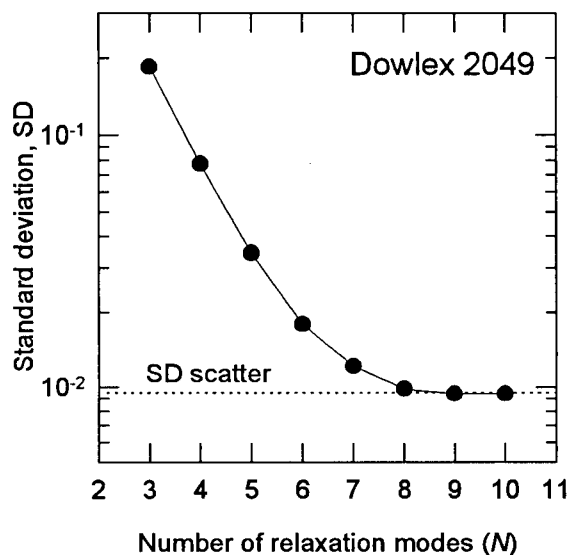
Figure 6-3. Dependence of the standard deviation on the number of relaxation mode
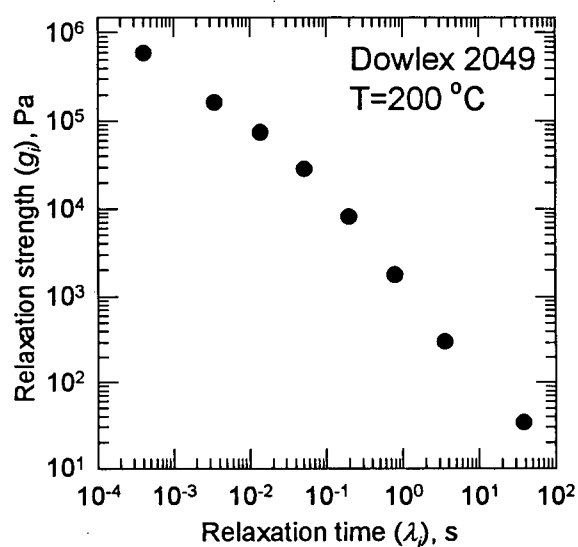
Figure 6-4. Relaxation time spectrum for Dowlex 2049 at 200°C (8 modes)

Comparative test 2: model polybutadiene star polymer. The data for the second test is taken from Vlassopoulos *et al.* (1997). In this case, the shape of the mastercurves for the loss and storage moduli is significantly more complex than that in the previous case (see Figure 6-5). Nevertheless, the fit obtained by the UBCFIT software is still very good (plotted in the same figure). Figure 6-6 plots the dependence of the standard error on the number of relaxation modes. One can see that acceptable accuracy is achieved with 14 relaxation modes. The fit does not improve significantly for $N>14$. The IRIS software resulted in 16 relaxation modes with a standard deviation higher than that obtained by UBCFIT with 14 modes (see Figure 6-6). Figure 6-7 depicts the resulting relaxation spectrum.

Overall, the developed software for evaluating relaxation time spectra produces results *not worse* than those obtained by commercial software such as IRIS.
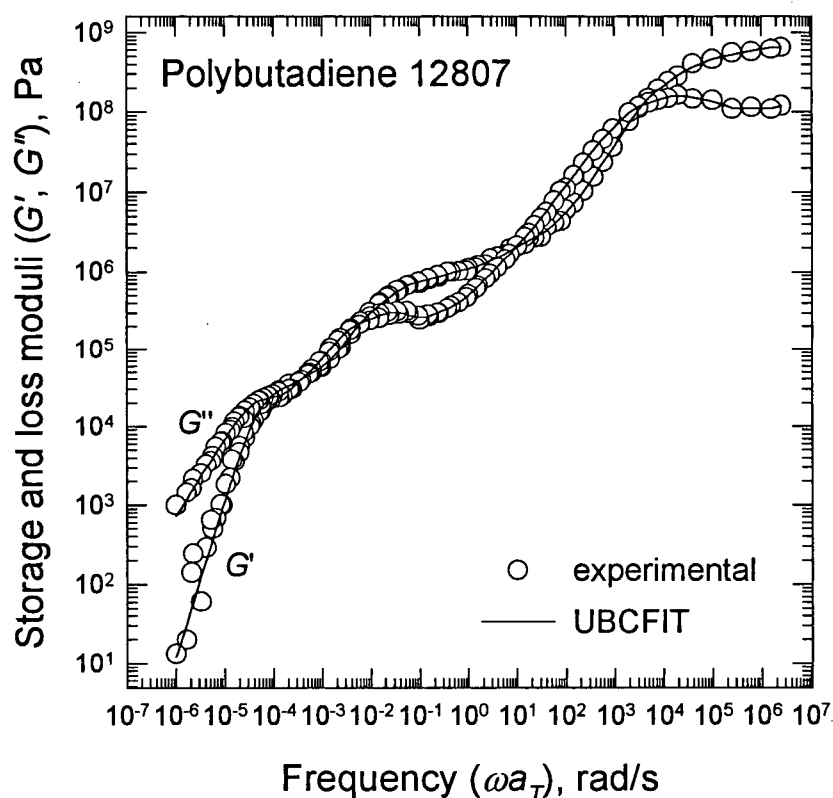
Figure 6-5. Storage and loss moduli for star polymer polybutadiene 12807 (Vlassopoulos *et al.*, 1997). Solid lines represent the fit obtained by means of UBCFIT software.
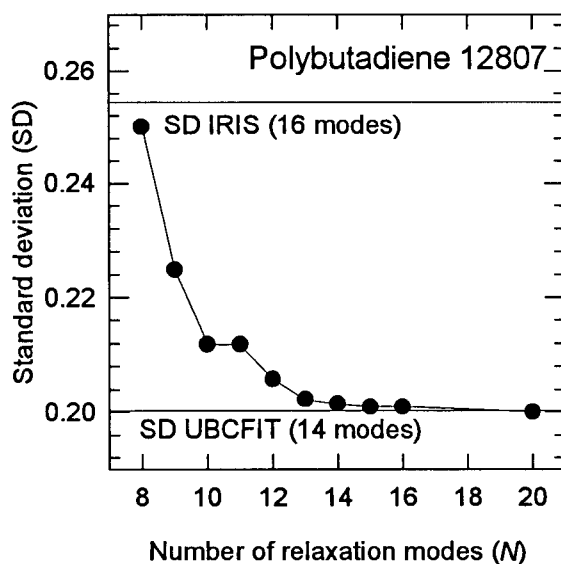
Figure 6-6. Dependence of the standard deviation on the number of relaxation mode for star polymer PB 12807
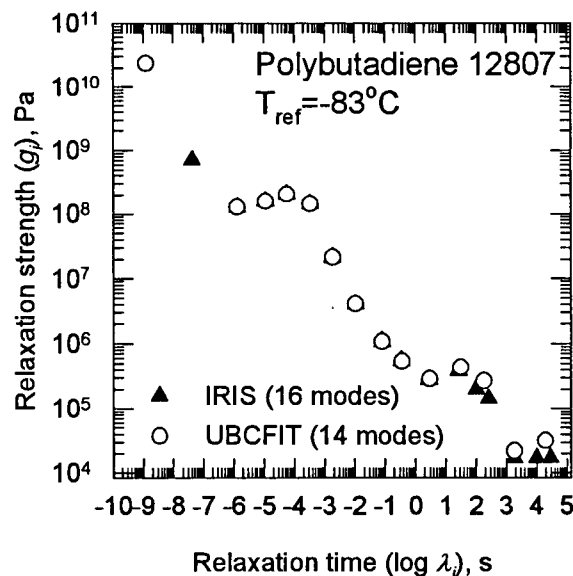
Figure 6-7. Relaxation time spectrum for PB 12807 at -83°C. Comparison of the UBCFIT and IRIS spectra

6.3 Rheological Characterization Using Relaxation Spectra

6.3.1 A Method to Estimate the Critical Molecular Weight

In Chapter 4, the value of the critical molecular weight, M_e, for TFE/HFP copolymers was experimentally obtained that seems to be quite high compared to those previously reported in literature. Below, a method to calculate M_e, which seems to support the conclusion drawn in that chapter is presented.

For linear flexible polymers, the entanglement molecular weight, M_e, can be calculated from (Van Krevelen, 1991; Larson, 1988)

$$M_e = g_N \frac{\rho R T}{G_N^0} \tag{6-6}$$

where g_N is a numerical factor (close to 1 for flexible polymers), ρ is the polymer density, and G_N^0 is the plateau modulus. In general, the plateau modulus is independent of the molecular weight and its distribution, for polymers with MW greater than M_e. Knowing G_N^0, it is possible to calculate the critical molecular weight as $M_c \approx 2M_e$, where M_e can be calculated from Equation (6-6). Unfortunately, the plateau modulus is a difficult, sometimes impossible quantity to measure. Usually, it is calculated from dynamic mechanical data for monodisperse polymers where a well-defined plateau in the G' plot or a maximum in G'' appears (Ferry, 1980). Using this approach, Wu (1985) found the value of G_N^0 for a series of FEP resins to be equal to 1.2×10^6 Pa. Similarly, Tuminello (1989) reported a value of 1.1×10^6 Pa. However, in most cases, this approach is not applicable, because the dynamic moduli curves do not exhibit a plateau or a maximum. For example Figure 4-1 shows neither a plateau nor a maximum in the G', G'' curves, thus making calculation of G_N^0 problematic. Moreover, when the dynamic moduli do

exhibit such behavior, it does not assure the accuracy in the $G_N{}^0$ determination. This is due to the fact that the relevant experimental data points for the $G_N{}^0$ determination are in the high frequency range where spectrometers exhibit the highest experimental error.

As an alternative way to calculate $G_N{}^0$, one can make use of the empirical BSW relaxation time spectrum. Referring back to Figures 4-1 and 4-2, one can see the well-defined terminal zone in both dynamic moduli curves. The terminal zone can be clearly identified by the characteristic slope of the moduli in the low frequency region. Thus, neglecting the contribution of the glassy region in the BSW spectrum (Equation (6-3)), one can calculate its parameters (including $G_N{}^0$) by fitting the contribution of the flow region to experimental points in the terminal zone by means of the following formulae:

$$G'(\omega) = \int_0^{\lambda_{max}} H(\lambda) \frac{\omega^2 \lambda^2}{1 + \omega^2 \lambda^2} \frac{d\lambda}{\lambda} \tag{6-7}$$

$$G''(\omega) = \int_0^{\lambda_{max}} H(\lambda) \frac{\omega \lambda}{1 + \omega^2 \lambda^2} \frac{d\lambda}{\lambda} \tag{6-8}$$

The fitting procedure is similar to that described by Jackson *et al.* (1994). The BSW fitting for the terminal zone is shown in Figures 6-8 and 6-9. The value of $G_N{}^0$ found from this analysis turned out to be equal to 1.41×10^5 Pa. Using Equation (6-6), the critical molecular weight recovered from $G_N{}^0$ is equal to 101,000 kg/kmol. This result is found to be much higher than the values reported by Wu (1985) and Tuminello (1989). However, the value of $G_N{}^0$ calculated in this work results in a value for the critical molecular weight that is remarkably close to that determined from the experimental data plotted in Figure 4-4 (a value for M_c between 80,000 and 110,000 kg/mol).

As mentioned above, this result for M_c seems to be quite high compared to those for other polymers. Indeed, for most polymers, the critical molecular weight lies in the

range between 3,000 for polyethylene and 35,000 for polystyrene (Porter, 1995) with a

few exceptions that can have a much higher M_c. The same source reports a value of about

12,000 for the M_c of PTFE. This seems to be reasonable only if one compares the

molecular weights of the repeating units in the molecules of PE and PTFE. However, for

FEP, M_c should be at least about 1.5 times higher if the number of carbon atoms per
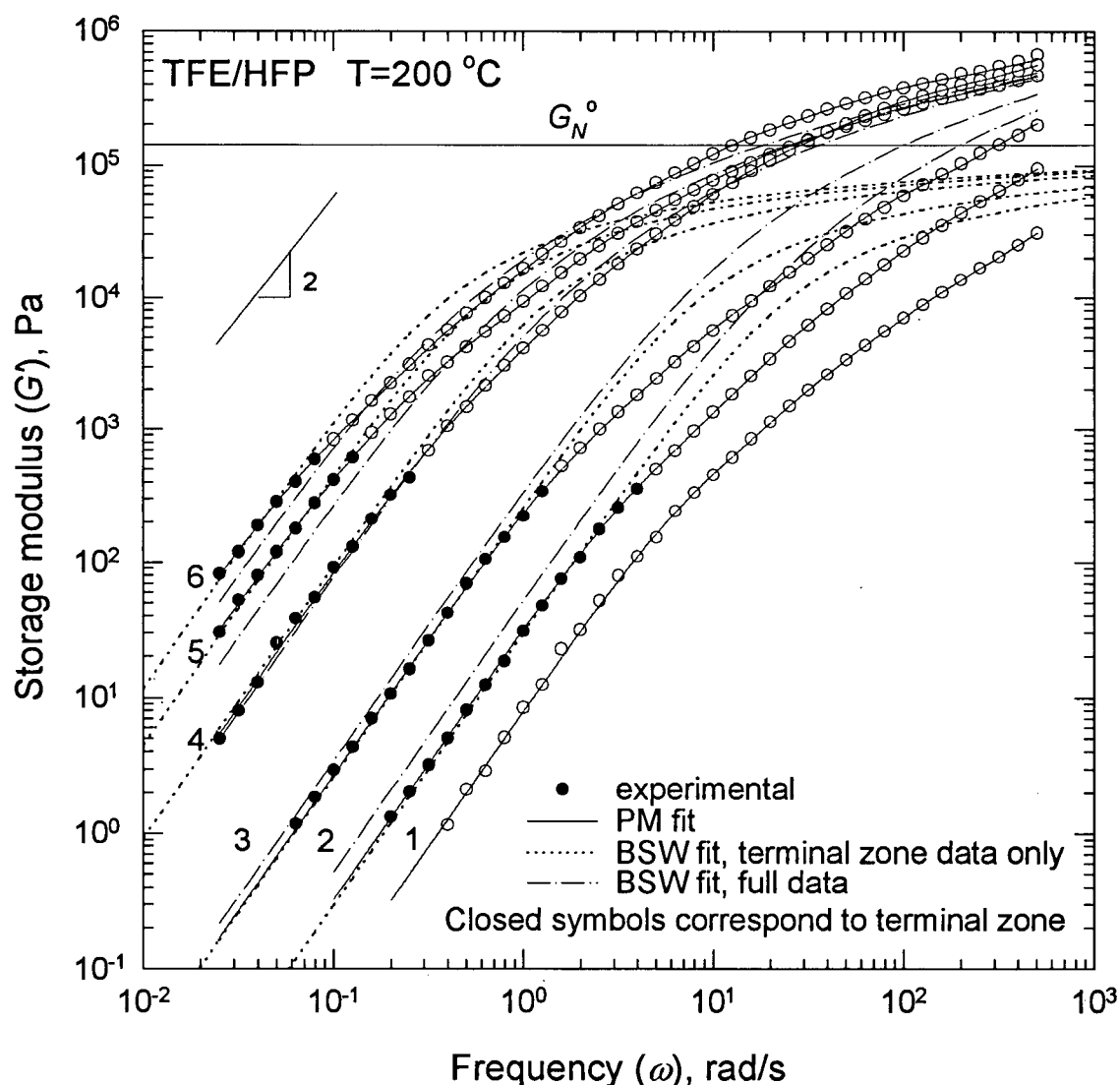
Figure 6-8. The storage modulus $G'(\omega)$ of the TFE/HFP copolymers of Group A at 200°C. The solid lines represent the fit with the parsimonious (PM) spectrum. The dash-dotted lines are the fit with the BSW spectrum with stretched exponential cut-off calculated from the full set of experimental data. Finally, the dotted lines are the fit with the BSW spectrum to the terminal zone data points (closed symbols). The plateau modulus determined from the data analysis is also drawn as reference

entanglement is the same because of the incorporated HFP copolymer, whose molecular

weight is twice that of TFE (content of HFP in the copolymer is about 50 wt. %).

Moreover, Teflon® or FEP molecules cannot exhibit the planar zigzag formation of the

crystalline regions as PE macromolecules do. The large fluorine atoms restrict the
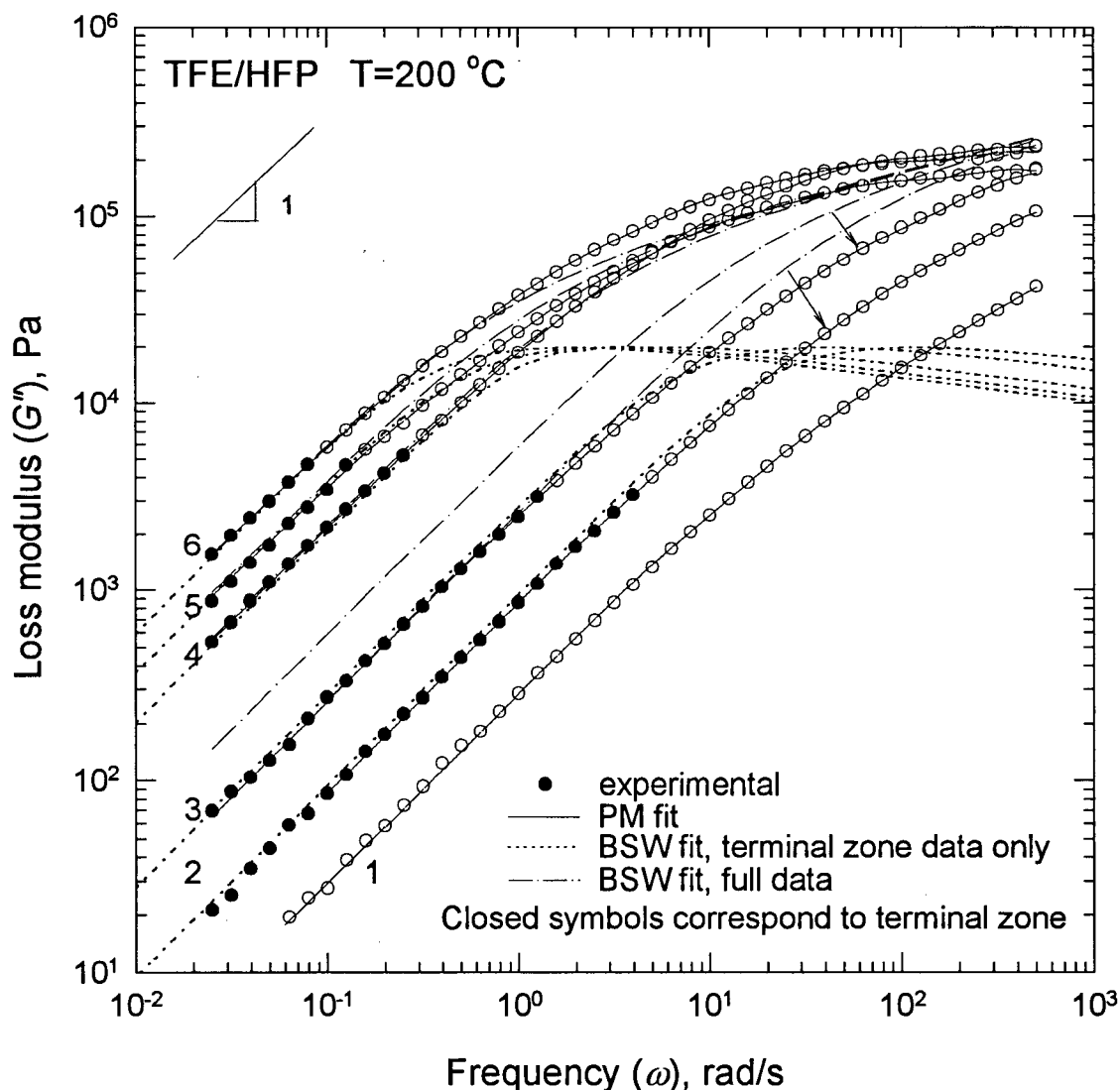
Figure 6-9. The loss modulus $G''(\omega)$ of the TFE/HFP copolymers of Group A at 200°C. The solid lines represent the fit with the parsimonious (PM) spectrum. The dash-dotted lines are the fit with the BSW spectrum with stretched exponential cut-off calculated from the full set of experimental data. Finally, the dotted lines are the fit with the BSW spectrum to the terminal zone data points (closed symbols)

flexibility of the molecule due to the nature of C-F bond and the repulsion between the negative fluorine atoms. As a result, the FEP molecule is a very stiff one, thus requiring a much higher molecular weight to be able to form entanglements. Therefore based on the experimental results that were also explained in terms of relevant modeling, it is believed that the critical molecular weight, M_c, for FEP resin should be several times higher than 12,000 (Wu, 1985) or 14,000 (Tuminello, 1989) and equal to about 100,000 kg/mol. An attempt to fit Equation (6-3) to the entire set of experimental data for the whole range of frequencies was also made. The results from this procedure are plotted in Figures 6-8 and 6-9. One can see that the fit was satisfactory only for the high molecular weight resins (M_W>300,000). On the other hand, it clearly fails for the resins with M_W<200,000. This provides additional support to the conclusion that M_c should be very high as was observed experimentally. It is noted that Equation (6-3) is valid only for M_W>>M_c (Baumgaertel and Winter, 1992). The value of M_c recovered by this fitting procedure turned out to be even higher, namely 136,000 kg/kmol.

6.3.2 The Relaxation Spectrum of TFE/HFP Copolymers

The experimental data were also analyzed by means of a discrete relaxation spectrum (parsimonious model). The results of the parsimonius (PM) fit are also plotted in Figures 6-8 and 6-9. It can be seen that it describes all the available experimental data well.

Figure 6-10 shows the calculated parsimonius (PM) relaxation spectra for the TFE/HFP resins (Group A in Chapter 4) together with the continuous BSW spectra. One can see that the discrete g_i-values do not fall on the continuous curves. However, the
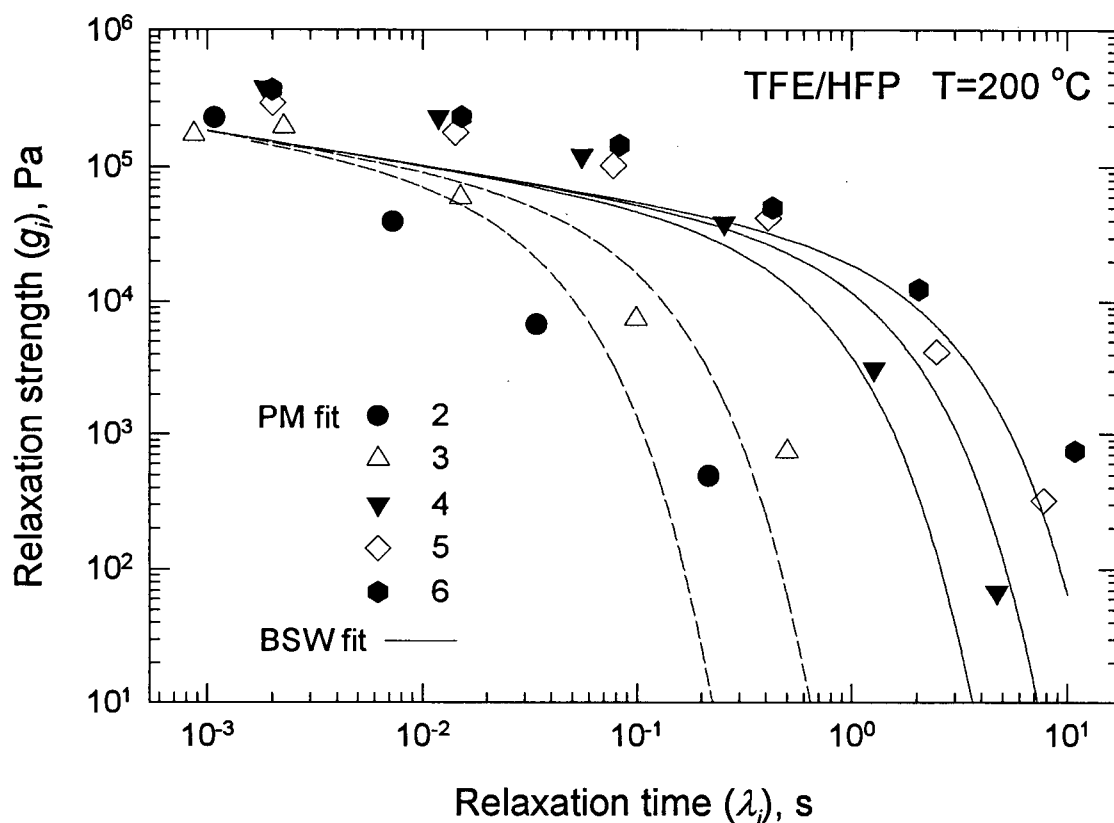
Figure 6-10. Comparison of the continuous BSW (continuous lines) and the discrete parsimonious (PM) spectra of the TFE/HFP copolymers of Group A
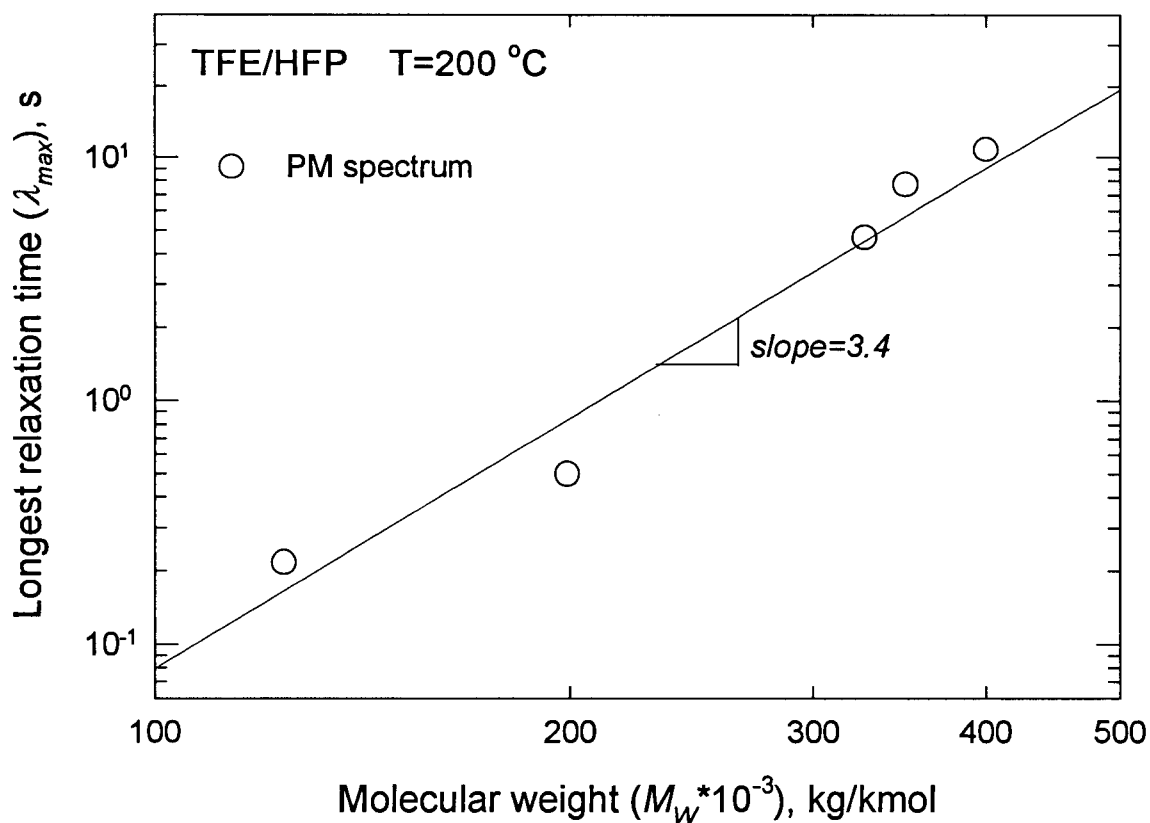
Figure 6-11. The molecular weight dependence of the longest relaxation time of the TFE/HFP copolymers of Group A calculated from the parsimonious (PM) model
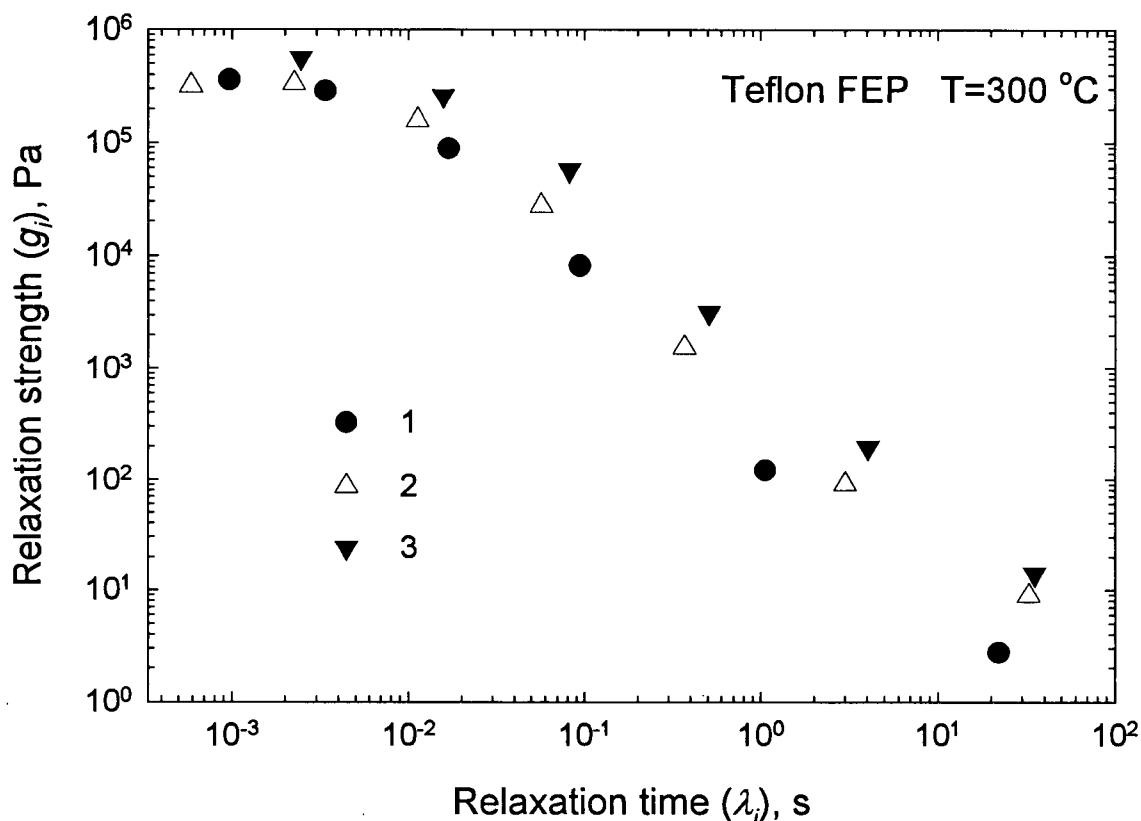
Figure 6-12. The discrete parsimonious (PM) spectra of the TFE/HFP copolymers of Group B (FEP resins)

shape of the discrete spectra corresponding to the high molecular weight TFE/HFP is about the same as that of the continuous. The regular shift between the two types of spectra can be explained by discretization (Baumgaertel and Winter, 1992) and does not violate their equivalency. On the contrary, the shape of the spectra calculated by both methods for the low molecular weight resins is very different, thus supporting presented results for M_c.

Figure 6-11 depicts the values of the maximal relaxation time λ_{max} determined from the PM model as a function of the molecular weight M_W. One can see that the values of λ_{max} obtained in this way follow the expected power-law relation with a slope of 3.4.

Figure 6-12 represents the PM relaxation spectra obtained for the series of high

melting point FEP resins (Group B in Chapter 4). The PM fit, together with the BSW fit,

is shown in Figures 6-13 and 6-14. Note that the BSW fit is not as accurate as the PM.

This is due to the much more complicated morphology of these melts that can not be

described by this particular empirical spectrum which requires the existence of a terminal

zone. While it can be seen from Figure 6-14 that the terminal zone seems to be reached

(slope equal to 1), the G' curves in Figure 6-13 extend to lower frequencies without
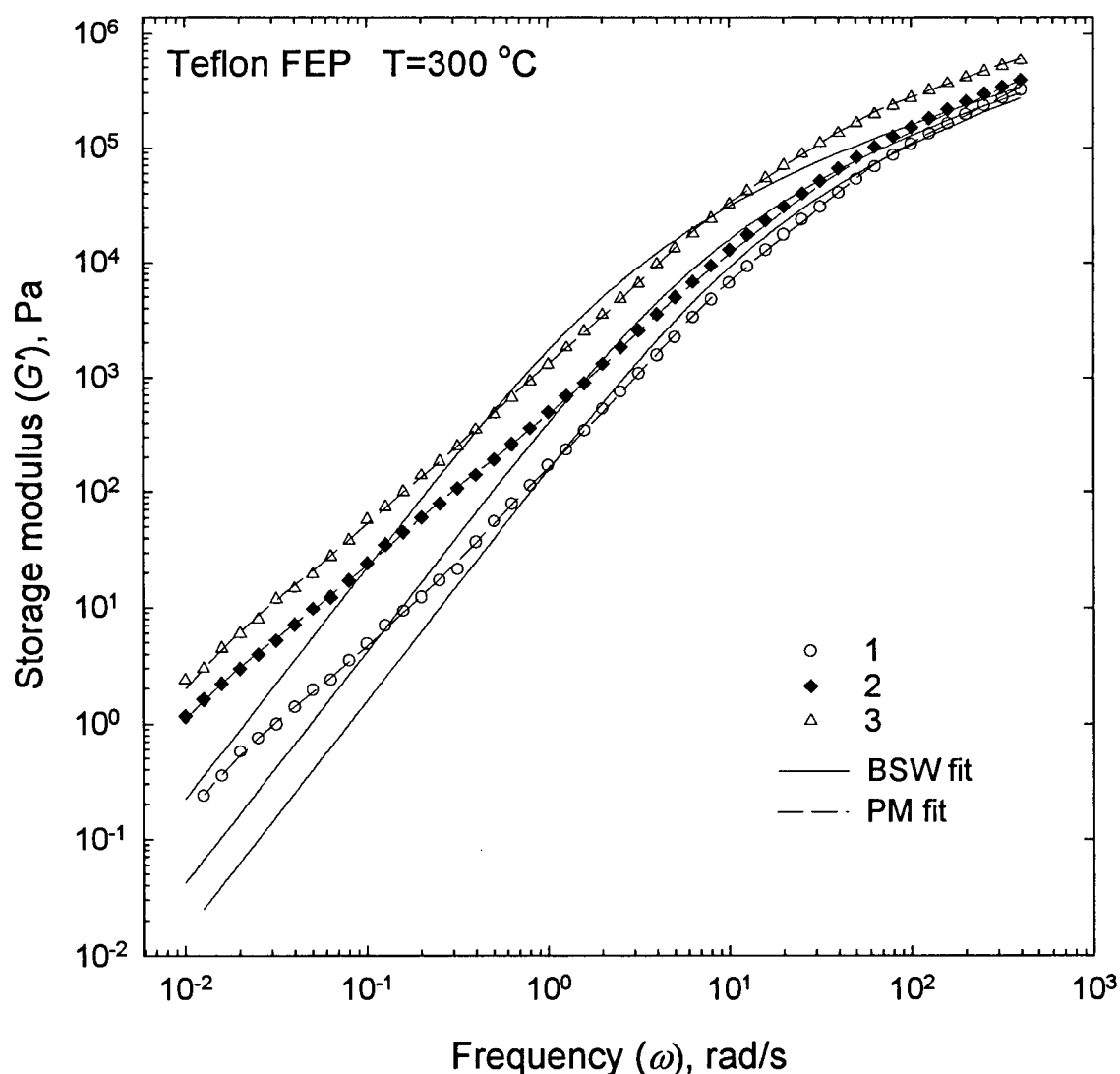
Figure 6-13. The storage modulus, $G'(\omega)$, of the TFE/HFP copolymers of Group B at 300°C. The dashed lines represent the fit with the parsimonious (PM) spectrum, while the solid lines are the fit with the BSW spectrum using stretched exponential cut-off

attaining the limiting slope of 2. This suggests that either the terminal zone is not reached yet or crystallinity still plays a role in spite of the fact that pre-heating has been used.
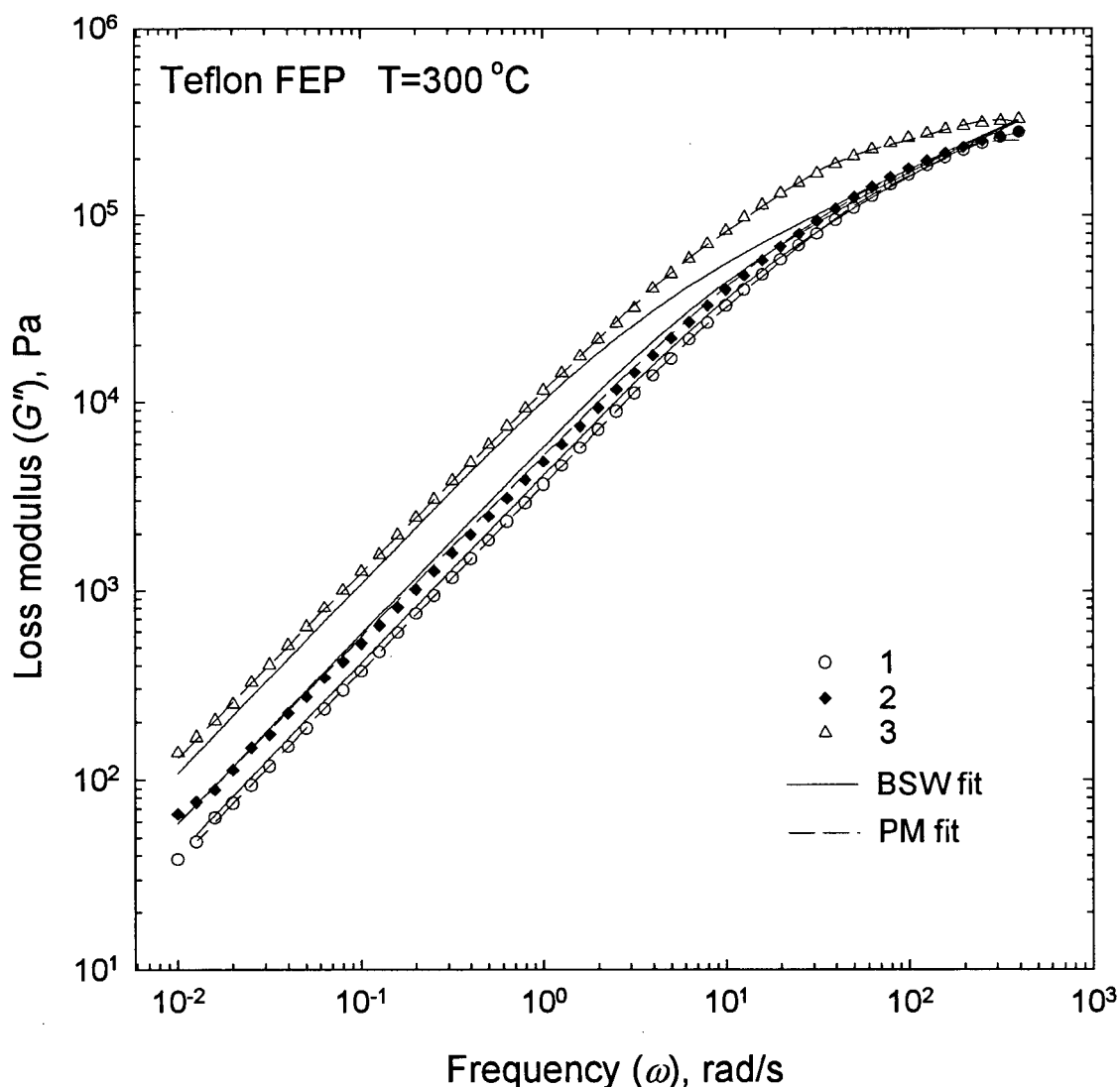
Figure 6-14. The loss modulus, $G''(\omega)$, of the TFE/HFP copolymers of Group B (FEP resins) at 300°C. The dashed lines represent the fit with the parsimonious (PM) spectrum, while the solid lines are the fit with the BSW spectrum using a stretched exponential cut-off

6.4 Constitutive Modeling

The Phan-Thien and Tanner model is a constitutive equation based on the network theory of concentrated polymer solutions and melts. In general, it can be written as follows:

$$\underline{\underline{\tau}}^{p} = \sum_{i=1}^{N} \underline{\underline{\tau}}_{i} \qquad (6\text{-}9)$$

$$Z(tr\underline{\underline{\tau}}_{i})\underline{\underline{\tau}}_{i} + \lambda_{i}\hat{\underline{\underline{\tau}}}_{i} + \frac{\xi_{i}}{2}\lambda_{i}(\underline{\underline{\dot{\gamma}}} \cdot \underline{\underline{\tau}}_{i} + \underline{\underline{\tau}}_{i} \cdot \underline{\underline{\dot{\gamma}}}) = -\eta_{i}\underline{\underline{\dot{\gamma}}} \qquad (6\text{-}10)$$

where $Z = \exp\left(-\dfrac{\varepsilon_{i}}{g_{i}}tr\underline{\underline{\tau}}_{i}\right), \underline{\underline{\tau}}^{p}$ is the stress tensor, $\underline{\underline{\tau}}_{i}$ is the contribution of the i-th relaxation mode to the total stress, λ_{i} and g_{i} are the relaxation time and relaxation strength of the i-th mode, respectively (relaxation spectrum), $\eta_{i}=\lambda_{i}\cdot g_{i}$ is the viscosity of the i-th mode, and $\underline{\underline{\dot{\gamma}}}$ is the rate-of-deformation tensor. The particular form of Z was chosen because the exponential term results in a maximum in the steady-state extensional viscosity in accordance with experimental data on polymer melts (Hatzikiriakos et al., 1997a). In addition to the constants defining the relaxation time spectrum, this model involves two non-linear parameters per mode, ε_{i} and ξ_{i}. The former characterizes the rate of destruction of polymer segments in the network model and the latter, the rate of "slip" (non-affine) deformation. The term involving ξ_{i} is most important in shear flows, and the parameter ε_{i} is dominant in shear-free (e.g. elongational) flows. The caret in Equation (6-10) denotes the upper convected derivative of τ_{i}, and is defined by:

$$\hat{\underline{\underline{\tau}}}_{i} = \frac{\partial \underline{\underline{\tau}}_{i}}{\partial t} + \underline{v} \cdot \underline{\nabla}\underline{\underline{\tau}}_{i} - \left(\underline{\underline{\dot{\gamma}}} \cdot \underline{\underline{\tau}}_{i} + \underline{\underline{\tau}}_{i} \cdot \underline{\underline{\dot{\gamma}}}\right) \qquad (6\text{-}11)$$

Fitting data by means of the PTT model requires knowledge of both the shear and extensional viscosities. The shear viscosity is readily obtained using a parallel-plate (low shear rates) and capillary (high shear rates) rheometers. The extensional viscosity can be estimated from capillary rheometry data by means of the Cogswell analysis (see Equations (2-31)-(2-33)).

Using Equations (2-3)-(2-5) and (2-9)-(2-11), the components of the matrix Equations (6-9)-(6-11) can be rewritten for each mode as follows (Bird et al., 1987):

- Simple shear:

$$\tau_{xx} : \qquad \exp\left[-\frac{\varepsilon}{g}(\tau_{xx}+\tau_{yy})\right]\tau_{xx} + \xi\lambda\dot{\gamma}\tau_{xy} - 2\lambda\dot{\gamma}\tau_{xy} = 0 \qquad (6\text{-}12)$$

$$\tau_{xy} : \qquad \exp\left[-\frac{\varepsilon}{g}(\tau_{xx}+\tau_{yy})\right]\tau_{xy} + \frac{\xi}{2}\lambda\dot{\gamma}(\tau_{xx}+\tau_{yy}) - \lambda\dot{\gamma}\tau_{yy} = -\eta\dot{\gamma} \qquad (6\text{-}13)$$

$$\tau_{yy} : \qquad \exp\left[-\frac{\varepsilon}{g}(\tau_{xx}+\tau_{yy})\right]\tau_{yy} + \xi\lambda\dot{\gamma}\tau_{xy} = 0 \qquad (6\text{-}14)$$

- Simple extension

$$\tau_{xx} : \qquad \exp\left[-\frac{\varepsilon}{g}(\tau_{xx}+\tau_{yy}+\tau_{zz})\right]\tau_{xx} + \lambda\dot{\varepsilon}\tau_{xx} - \xi\lambda\dot{\varepsilon}\tau_{xx} = \eta\dot{\varepsilon} \qquad (6\text{-}15)$$

$$\tau_{yy} : \qquad \exp\left[-\frac{\varepsilon}{g}(\tau_{xx}+\tau_{yy}+\tau_{zz})\right]\tau_{yy} + \lambda\dot{\varepsilon}\tau_{yy} - \xi\lambda\dot{\varepsilon}\tau_{yy} = \eta\dot{\varepsilon} \qquad (6\text{-}16)$$

$$\tau_{zz} : \qquad \exp\left[-\frac{\varepsilon}{g}(\tau_{xx}+\tau_{yy}+\tau_{zz})\right]\tau_{zz} - 2\lambda\dot{\varepsilon}\tau_{zz} + 2\xi\lambda\dot{\varepsilon}\tau_{zz} = -2\eta\dot{\varepsilon} \qquad (6\text{-}17)$$

Equations (6-12)-(6-17) define 6×N coupled algebraic equations for the stress tensor components in shear and shear-free flows, where N is the number of relaxation modes. They are solved with respect to the stress components in order to obtain the

values of the shear and extensional viscosities, $\eta = \sum_{i=1}^{N} \tau_{xy_i} / \dot{\gamma}$ and $\eta_E = \sum_{i=1}^{N} (\tau_{xx} - \tau_{yy})_i / \dot{\varepsilon}$,

respectively. In turn, these calculated values are fitted to experimental data. The fitting

algorithm works as follows. The linear parameters of the relaxation spectrum (λ_i, g_i) are

first estimated by means of the UBCFIT software. They are used as an initial guess for

the PTT fitting code. Then all the parameters are fitted simultaneously by means of an

iterative minimization procedure in order to minimize the squared deviation between the
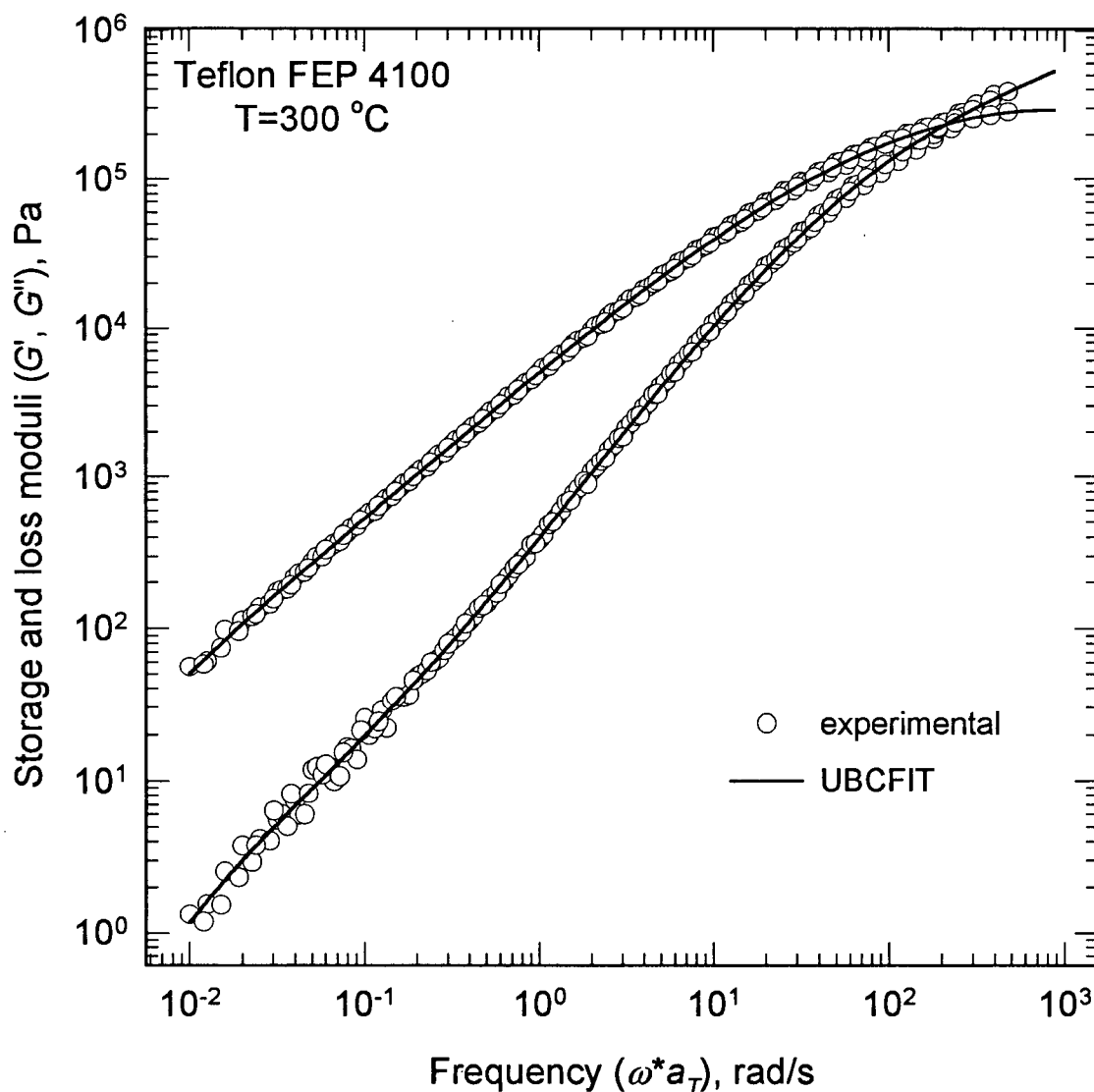
Figure 6-15. The dynamic moduli mastercurves for Teflon® FEP 4100 at T_{ref}=300°C. Solid lines represent the relaxation spectrum fit

calculations and the experimental data. The minimization method used for this purpose is the constrained BFGS method (Zhu *et al.*, 1997). The PTT model parameters are subject to the following constraints: $\varepsilon_i \geq 0$ and $0 \leq \xi_i \leq 1$ (Phan-Thien and Tanner, 1977).

As an example, let us consider Teflon® FEP 4100. The relaxation spectrum was recovered by means of the UBCFIT software and resulted in 7 relaxation modes (Table 6-2). The experimental data points for the dynamic moduli of FEP are plotted in Figure 6-15 along with the model predictions (solid lines) obtained using the calculated spectrum. Figure 6-16 shows the complex, shear, and extensional viscosity of FEP 4100 as a function of frequency, shear, and extensional rate respectively. All the data are reduced to 300°C. It can be seen that the complex viscosity (parallel plate rheometer) agrees very well with the shear viscosity (capillary rheometer) up to the point corresponding to the onset of melt fracture. Only the data from the prefractured region only were taken into account in this fitting procedure. The solid lines in Figure 6-16 represent the predictions of the PTT model with 7 modes for the rheological properties of this polymer. The parameters of the model are listed in Table 6-2. This example shows that the multi-mode PTT model can represent the rheological behavior of Teflon FEP resins quite well, and therefore such a model can be used effectively in process simulation such as wire coating.

Table 6-2. Parameters in the PTT constitutive equation for Teflon® FEP 4100

i	λ_i (s)	g_i (Pa)	η_i (Pa·s)	ξ_i	ε_i
1	1.1470E-03	4.9050E+05	5.6260E+02	2.2040E-02	7.5680E-01
2	6.0390E-03	2.2702E+05	1.3710E+03	1.4960E-01	4.0030E-01
3	2.9410E-02	6.6202E+04	1.9470E+03	2.2730E-01	8.1920E-01
4	1.9110E-01	4.8231E+03	9.2170E+02	2.0270E-01	8.2170E-02
5	1.6600E+00	1.7241E+02	2.8620E+02	5.6530E-02	1.9230E-03
6	1.0130E+01	1.8628E+01	1.8870E+02	6.8470E-02	8.2600E-02
7	5.6520E+01	3.6235E+00	2.0480E+02	5.0100E-02	1.6320E+00
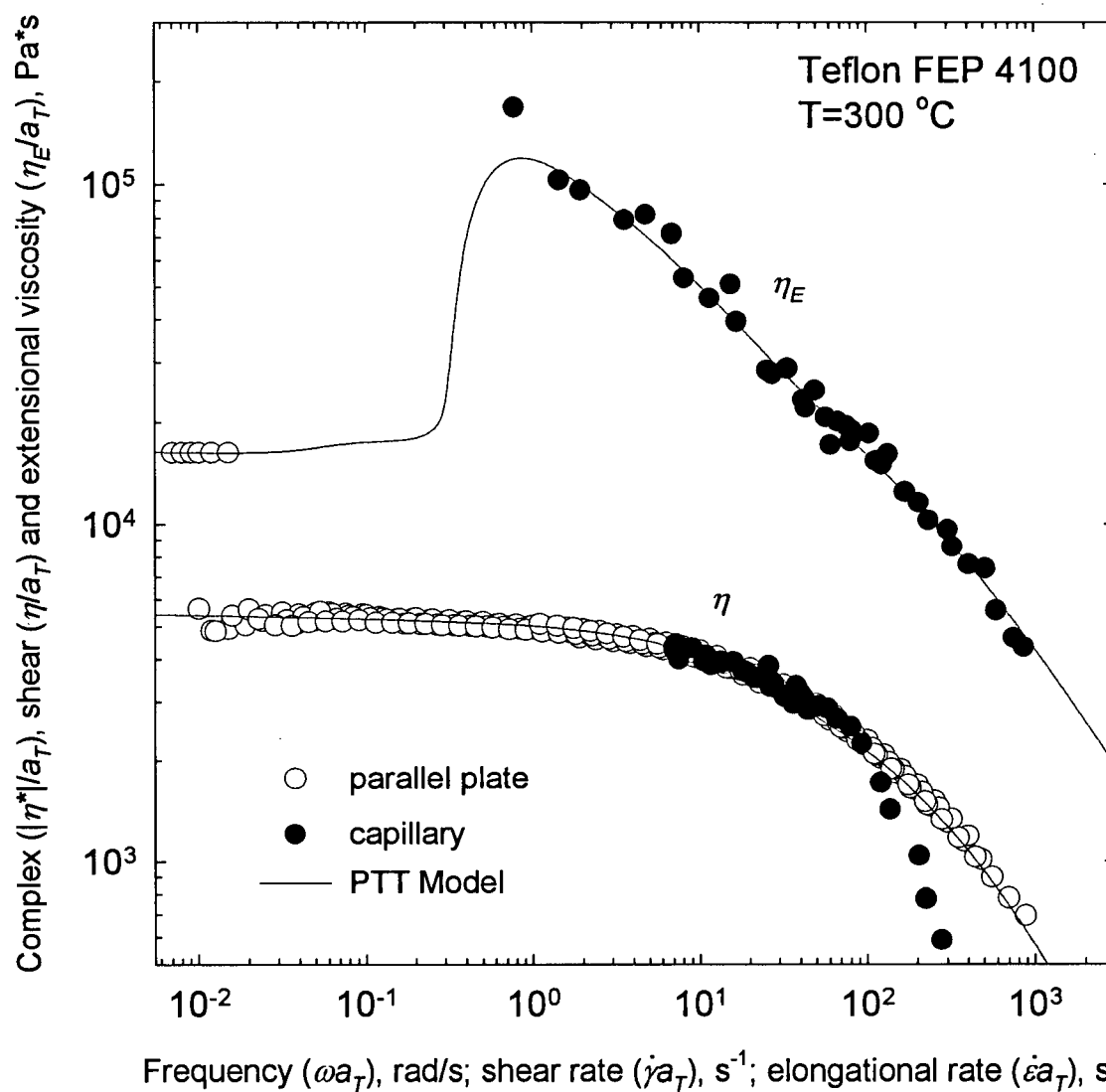
Figure 6-16. The complex, shear, and extensional viscosity of Teflon® FEP 4100. The solid lines represent the fit obtained by means of a 7-mode PTT constitutive equation.

7   Modeling of Capillary Flow of Molten Polymers

*T*he traditional way of determining the slip velocity of molten polymers is the classical Mooney technique which utilizes experimental data obtained from a capillary rheometer. However, measurements of the rheological properties of polymer melts in capillary flow at high shear rates are often complicated by viscous heating which is not taken into account by this method. A data analysis procedure based on a mathematical model for nonisothermal capillary flow of molten polymers is developed. Conduction, convection, and viscous heating are included, together with the effect of wall slip. The technique provides detailed velocity and temperature fields in the die and can be used to determine the slip velocity at high shear rates corrected for the effect of viscous heating. It is tested for the capillary flow of several polymers including polystyrene, polypropylene, high density and linear low density polyethylenes, and Teflon® FEP.

7.1   Introduction

It is generally accepted that polymer melts, unlike Newtonian fluids, may violate the classical no-slip boundary condition of Newtonian fluid mechanics and slip over solid surfaces when the wall shear stress exceeds a critical value (Ramamurthy, 1986; Kalika and Denn, 1987; Hatzikiriakos and Dealy, 1991a). In several polymer processes, the melts are subject to very large shear stresses which often exceed this critical value (usually about 0.1 MPa). To simulate these processes realistically, a reliable slip velocity model is needed that adequately describes the interfacial behaviour of polymer melts.

It is also well known that whenever a viscous material is deformed in a flow field, some of the work of deformation is converted into thermal energy by means of viscous dissipation (Winter, 1977; Cox and Macosko, 1974). This phenomenon, generally known as viscous heating, is typical in the processing of molten polymers. Most polymers have high viscosities and low thermal conductivities, which in combination with large process shear rates can lead to significant temperature increases.

One of the common tools used to study the rheological behaviour of molten polymers as well as the wall slip phenomenon is a capillary rheometer. The traditional way to detect the presence of wall slip and quantify it, is by using experimental data from a capillary rheometer and the classical Mooney method (Mooney, 1931). This technique requires the performance of capillary experiments with a series of dies having the same length-to-diameter ratio, L/D, in order to keep constant the effect of pressure and different diameters, D. If slip occurs, the flow curves (wall shear stress versus apparent shear rate) start diverging (become diameter dependent) at a certain value of wall shear stress. This value is taken to be the critical shear stress for the onset of slip. The Mooney method has been used for a variety of polymers by several authors in the past to determine their slip velocity as a function of the wall shear stress (Lupton and Regester, 1965; Blyler and Hart, 1970; Ramamurthy, 1986; Hatzikiriakos and Dealy, 1992a).

One of the basic assumptions of the Mooney method is that the temperature and pressure effects (see Section 2.3.3) can be neglected. However, it is reasonable to expect that the effect of viscous heating can be quite significant at sufficiently high shear rates at least for some types of polymers. Thus, one would expect that the Mooney method cannot be applied in all cases. Indeed, many researchers have pointed out that

experimental data points on the Mooney plot (apparent shear rate versus inverse of capillary diameter) often do not fall on a straight line as this technique presumes (Lupton and Regester, 1965; Shih, 1979; Hatzikiriakos *et al.*, 1995). Instead, the data define curves exhibiting a tendency to bend towards the higher apparent shear rates with increase in the die diameter (convex downwards). Usually such anomalies are ignored by researchers in the field, which may lead to inaccurate slip velocity calculations.

Viscous heating in the capillary extrusion of polymer melts has been the subject of several reviews and studies over the past decades (Winter, 1977; Warren, 1988). Essentially, most of the previous investigators solved the mass, momentum, and energy equations which describe laminar flow in a capillary or slit under conditions where viscous heating is important (Ybarra and Eckert, 1980; Dinh and Armstrong, 1982; Milthorpe and Tanner, 1987; Ko and Lodge, 1991). However, very few of them considered the combined effects of viscous heating and wall slip in their numerical analyses. An attempt to do this was made by Lupton and Regester (1965). They carried out an analysis of the combined effects of slip velocity and viscous heating by using a simplified mathematical model for the flow of a power law fluid, in an attempt to explain the origin of melt fracture.

In this chapter, the results of a numerical simulation of the capillary flow for polymer melts are presented in order to assess the effect of viscous heating on the slip velocity measurements. Moreover, using the mathematical model, a new data analysis procedure is proposed which is found to be suitable for slip velocity calculations corrected for the effect of viscous heating. The method is applied successfully to

experimental data for several polymers, including polypropylene, high density and linear low density polyethylenes, and Teflon® FEP.

7.2 Mathematical Model

Consider flow of a non-Newtonian fluid in a capillary of radius R and length L where r and z are the coordinates in the radial and axial directions respectively. The relevant nonzero velocity components are v_r and v_z, and the relevant physical properties of the fluid under consideration are its density, ρ, heat capacity, C_p, and thermal conductivity, k. For the mathematical model one can make the following assumptions:

- Steady laminar axisymmetric flow prevails.

- Flow is assumed to be fully-developed at $z=0$. This assumption is based on laser velocimetry measurements showing that the velocity profile approaches its fully developed form within a distance of about $0.1D$ (Dealy and Wissbrun, 1990).

- The radial velocity is sufficiently small to be neglected in the momentum and energy equations, and is included only in the continuity equation.

- Pressure variations in the radial direction are small compared to those in the axial direction.

- The effects of inertia and gravity are negligible.

- Axial heat conduction is negligible compared to axial convection.

- The heat capacity and thermal conductivity are considered to be temperature dependent and the fluid density is pressure and temperature dependent. The relevant

equations to calculate these properties are taken from Van Krevelen (1991) and given later in this chapter.

- Fluid viscosity is a function of temperature and pressure and the fluid follows a "power-law" model. The rz-component of the stress tensor may be written as follows:

$$\tau_{rz} = K \exp[\alpha P + A(T_{ref} - T)]\left|\frac{\partial v_z}{\partial r}\right|^{n-1}\left(\frac{\partial v_z}{\partial r}\right) \tag{7-1}$$

where τ_{rz} is the rz component of the stress tensor, P is the absolute pressure, T is the temperature, T_{ref} is a reference temperature, K and n are the consistency index and the power law exponent of the power-law model, respectively, and α and A, are the pressure and temperature dependence coefficients of the viscosity respectively.

- There is a finite slip velocity at the wall u_s.

With these assumptions the equations of continuity, momentum and energy reduce to:

$$\frac{1}{r}\frac{\partial(r\rho v_r)}{\partial r} + \frac{\partial(\rho v_z)}{\partial z} = 0 \tag{7-2}$$

$$\frac{\partial P}{\partial z} - \frac{1}{r}\frac{\partial(r\tau_{rz})}{\partial r} = 0 \tag{7-3}$$

$$\rho C_p v_z \frac{\partial T}{\partial z} = \frac{1}{r}\frac{\partial}{\partial r}\left(rk\frac{\partial T}{\partial r}\right) + \tau_{rz}\left(\frac{\partial v_z}{\partial r}\right) + T\varepsilon v_z \frac{dP}{dz} \tag{7-4}$$

The mass flow rate constancy equation is: $\quad 2\pi \int_0^R \rho v_z r\,dr = \dot{m} \tag{7-5}$

Boundary conditions: $\tag{7-6}$

$z=0: \quad T=T_0$

$z=L: \quad P=P_a$

$r=0: \quad \partial T/\partial r=0 \quad \partial v_z/\partial r=0 \quad v_r=0$

$$r=R: \quad v_z=u_s \qquad v_r=0 \qquad -\frac{\partial T}{\partial r} = \frac{k_w}{kR} \frac{1}{\ln(1+t/R)}(T-T_0)$$

where k_W and t are the thermal conductivity and thickness of the wall respectively, T_0=const is the temperature of the surroundings (at the outer surface of the die) taken to be equal to that of the polymer at the die inlet.

The second term on the right side of Equation (7-4) is the viscous heating term while the last term allows for the effect of expansion cooling due to fluid compressibility. The parameter ε is the coefficient of thermal expansion defined as $\varepsilon = -\frac{1}{\rho}\left(\frac{\partial \rho}{\partial T}\right)_P$. Note that Equation (7-4) is valid for both purely viscous and viscoelastic materials and independent of the choice of the constitutive equation (Astarita and Sarti, 1974).

The thermal boundary condition at the wall is not known in general, and one has to guess this condition. Most of the studies prescribe idealized conditions (without heat generation due to slip) such as:

- constant wall temperature (T_W=const)

- adiabatic wall ($\partial T/\partial r = 0$)

- constant heat flux at the wall ($\partial T/\partial r = $ const)

The latter condition was successfully used in previous studies (e.g. Winter, 1977) and is believed to be the most realistic one. Only this thermal boundary condition will be used in numerical calculations.

For the sake of simplicity, the local slip velocity is modeled at this point by a modified power-law expression (no pressure and temperature dependence):

$$u_s = \frac{a}{1+(\sigma_c/\sigma_W)^{10}} \sigma_W^m \qquad (7\text{-}7)$$

where σ_W is the wall shear stress. The factor $1/[1+(\sigma_c/\sigma_W)^{10}]$ basically zeroes the slip velocity for stresses less than σ_c and becomes about equal to one for shear stresses slightly greater than σ_c. It is noted that this model is only used to illustrate the proposed method. A more general and accurate form of a slip velocity model will be presented and used below. Equations (7-1)-(7-7) were solved utilizing an implicit finite-difference technique similar to that described by Warren (1988). The temperature distribution is calculated from the energy equation (7-4), but since the velocity and pressure are not known a priori they must be calculated as part of the iterative process for solving the energy equation. Combining Equations (7-1), (7-3), and (7-5), one can obtain the following expression for a new estimate of v_z:

$$v_z(r,z) = \frac{\dot{m}}{2\pi \int\limits_{0}^{R}\int\limits_{R}^{r}\left(\frac{r}{\eta}\right)^{1/n} \rho dr \cdot r dr} \int\limits_{R}^{r}\left(\frac{r}{\eta}\right)^{1/n} dr$$

The iterative process is started by assuming a constant temperature in the die and a velocity profile at the die inlet corresponding to isothermal fully developed flow. The integrals in the above equation are performed stepwise down the die to give the velocity distribution in the die. Equation (7-4) is then solved to give the temperature distribution, which in turn is used to modify the viscosity. The new viscosity is substituted into the integrals, and the process is repeated until convergence is obtained.

One comment concerning the thermal properties of the polymers is as follows. It is known that viscoelastic fluids are anisotropic and their physical and thermal properties can exhibit a dependence on the history of the kinematics. Cocci and Picot (1973) reported a slight dependence of the effective thermal conductivity of polymers on the

shear rate (up to 10% in the range of shear rates from 0 to 200 s^{-1}). The same effect can be expected for the heat capacity. However, there are no reliable expressions to take into consideration these effects in this study. Nevertheless, several test runs were performed to estimate their influence in the calculations. It was found that simultaneous increases of both thermal conductivity and heat capacity by 10% results in less than a 1% change in the wall shear stress over a wide range of shear rates. Based on this, the effect of deformation history on the thermal properties of polymers was excluded from this study.

7.3 Physical Properties of the Polymers Studied

All correlations, relationships and physical properties are taken from Van Krevelen (1991). The density of polymers is assumed to be a function of temperature and pressure, that is $\rho = \rho(T, P)$. It is modeled by using the Spencer-Gilmore equation (modified Van der Waals equation) which has the following form:

$$(1/\rho - \omega)(P + \pi) = RT/M \tag{7-8}$$

where ρ is density (g/cm^3), P is applied pressure (bar), T is temperature (K), ω is specific volume at $P=0$ and $T=0$ (cm^3/g), π is internal pressure (bar), and M is molecular weight of the interacting unit, usually taken to be the structural unit of the polymer (g/mol). From Equation (7-8) one can calculate the density as:

$$\rho = \left(\frac{RT}{M(p+\pi)} + \omega \right)^{-1} \tag{7-9}$$

The coefficient of thermal expansion is defined as: $\varepsilon \equiv -\frac{1}{\rho}\left(\frac{\partial \rho}{\partial T}\right)_p$

The term εT in the energy equation (7-4) can be obtained by differentiating (7-9) with

respect to T, i.e. $\qquad\qquad\qquad \varepsilon T = 1 - \rho\omega \qquad\qquad\qquad\qquad$ (7-10)

The heat capacity is assumed to be a function of temperature and given by:

$$C_p(T) = C_p(298\,\text{K}) \cdot (1 + 1.2 \cdot 10^{-3} \cdot T) \qquad\qquad (7\text{-}11)$$

where C_p is in J/(mol·K), T in °C.

The thermal conductivity is assumed to be a function of temperature. From a generalized

curve for the thermal conductivity of polymers, one can find for $T{>}T_g$:

$$k(T) = k(T_g) \cdot (1.2 - 0.2 \cdot T/T_g) \qquad\qquad (7\text{-}12)$$

where T_g is the glass transition temperature (K), and $k(T)$ is in W/(m·K).

All constants for the four resins studied (polyethylene, polypropylene, polystyrene,

and Teflon® FEP) are tabulated in Table 7-1.

Table 7-1. Physical properties of the studied polymers

Type of polymer	π, bar	ω, cm³/g	M, g/mol	C_p^{298}, J/(mol·K)	T_g, K	$k(T_g)$, W/(m·K)
Polypropylene	2470	0.83	42.1	91	260	0.144
Polyethylene	3290	0.88	28.1	63	195	0.326
Polystyrene	1870	0.82	104.1	178	373	0.172
Teflon® FEP	1680	0.495	100	96	200	0.100

7.4 Numerical Analysis and Results

To study the combined effect of viscous heating and wall slip, numerical

simulations for the flow of a hypothetical polymer melt having physical properties similar

to those of a typical polystyrene melt, were performed. These constants were found in

Van Krevelen (1991) and are listed in Table 7-2. Three cases were analyzed numerically

in order to understand the relative significance of the viscous heating and slip flow effects

on the flow curve (wall shear stress

versus apparent shear rate):

- No viscous heating with slip

- Viscous heating with no slip

- Viscous heating with slip

For the sake of simplicity, no

Table 7-2. Constants in Equations (7-1)-(7-7) for a hypothetical polystyrene fluid		
Equation (7-1)	A, K^{-1}	0.02
	K, Pa·s^n	35000
	T_{ref}, °C	190
	α, Pa	$3.5 \cdot 10^{-9}$
	n	0.4
Equation (7-7)	a	1.2
	σ_c, MPa	0.12
	m	3

expansion cooling was taken into account in this case study.

First consider the case of *no viscous heating with slip*. Figure 7-1 plots the flow

curves calculated for three capillary dies having different diameters, namely 0.508, 0.762,

and 1.27 mm and a constant L/D ratio equal to 40. The quantities plotted in Figure 7-1 are

defined by Equations (2-23) and (2-29) and can be rewritten as follows:

$$\dot{\gamma}_A = \frac{4Q}{\pi R^3} \tag{7-13}$$

$$\sigma_W = \frac{\Delta PR}{2L} \tag{7-14}$$

where, $\dot{\gamma}_A$ is the apparent shear rate, ΔP is the total pressure drop along the capillary, and

Q is the volumetric flow rate. It is noted that in the presence of viscous heating or for a

pressure-dependent slip boundary condition, the wall shear stress is not constant along

the capillary. Therefore, the above defined wall shear stress represents only an average

quantity.

It can be seen from Figure 7-1 that at some critical wall shear stress the curves start

diverging, clearly indicating the diameter dependence of the flow curves. It can also be

seen that the flow curve which corresponds to the capillary having the smaller diameter,

Figure 7-1. Calculated flow curves for a hypothetical material having physical properties listed in Table 7-2 under the influence of a slip boundary condition (slip with no viscous heating case).

deviates more from the no-slip flow curve. These observations are consistent with the assumption of a wall slip boundary condition and the applicability of the Mooney technique.

Now consider the second case, that is *viscous heating with no slip*. Figure 7-2 depicts flow curves for the same hypothetical polymer, capillary dies and conditions as in the previous case (Figure 7-1). It can be seen that at relatively low values of the apparent

shear rate all curves coincide due to the fact that the effect of viscous heating is

insignificant at these small rates. However, as the apparent shear rate increases, the

temperature increase becomes significant, and the flow curves start diverging and become

diameter dependent. The degree of divergence depends primarily on the physical

properties of the polymer and particularly on the temperature dependence coefficient of

the viscosity. However, the trend in the diameter dependence of the flow curves is

opposite to that obtained in the first case (no viscous heating with slip). As can be seen
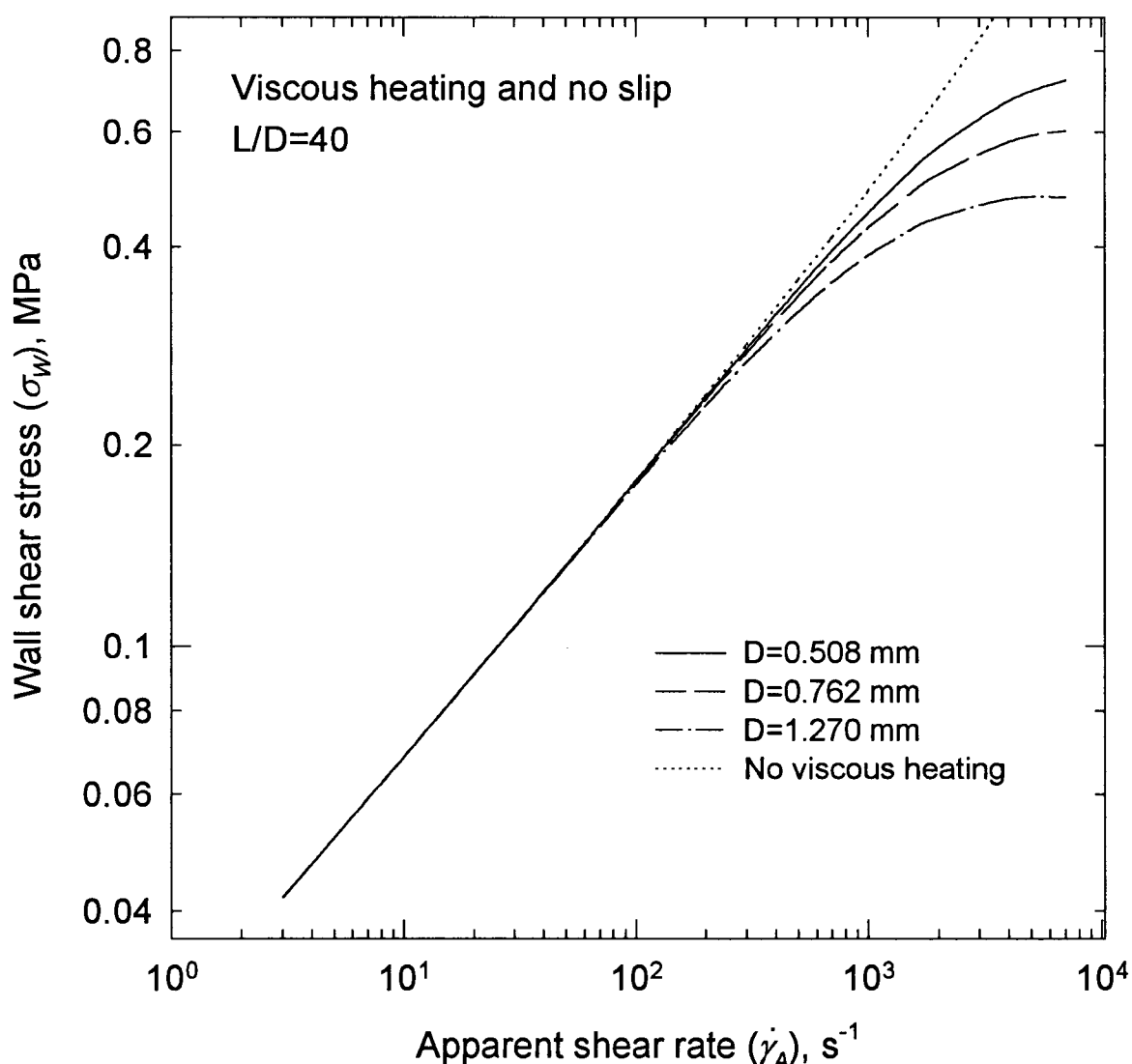
Figure 7-2. Calculated flow curves for a hypothetical material having physical properties
listed in Table 7-2 under the influence of viscous heating effects (no slip with
viscous heating case).

from Figure 7-2, the viscous heating effect is more pronounced for capillary dies having a larger diameter. This is obvious since radial heat conduction is less efficient in large dies. In addition, the die with the larger diameter is in fact longer since the ratio L/D is kept constant. Thus due to increased length the viscous heating is more significant for a capillary die of a larger diameter.

Obviously, it is reasonable to expect that, in the presence of the two above described competing effects, namely those of slip and viscous heating on the flow curves, significant deviation from the assumptions of the Mooney method may result. Indeed, this case of *viscous heating with slip* is presented in Figure 7-3. The flow curves were calculated for the combined effect of wall slip and viscous heating for the same hypothetical material, capillary dies and conditions. At the onset of slip flow, the curves start diverging which indicates that slip occurs. At these relatively small apparent shear rates the viscous heating effects are negligible and slip effects dominate. However, as the apparent shear rate increases, the effect of viscous heating becomes more significant, especially for capillary dies having a larger diameter. This effect causes significant deviation from the case of "no viscous heating with slip", and as a result the flow curves begin to converge, and eventually cross each other at relatively higher apparent shear rates where the viscous heating effects become more dominant. Needless to say, the Mooney technique does not apply to such cases. It is also possible in some cases for the effect of viscous heating to mask the detection of wall slip by suppressing the diameter dependence of the flow curves. Such a case is discussed later.
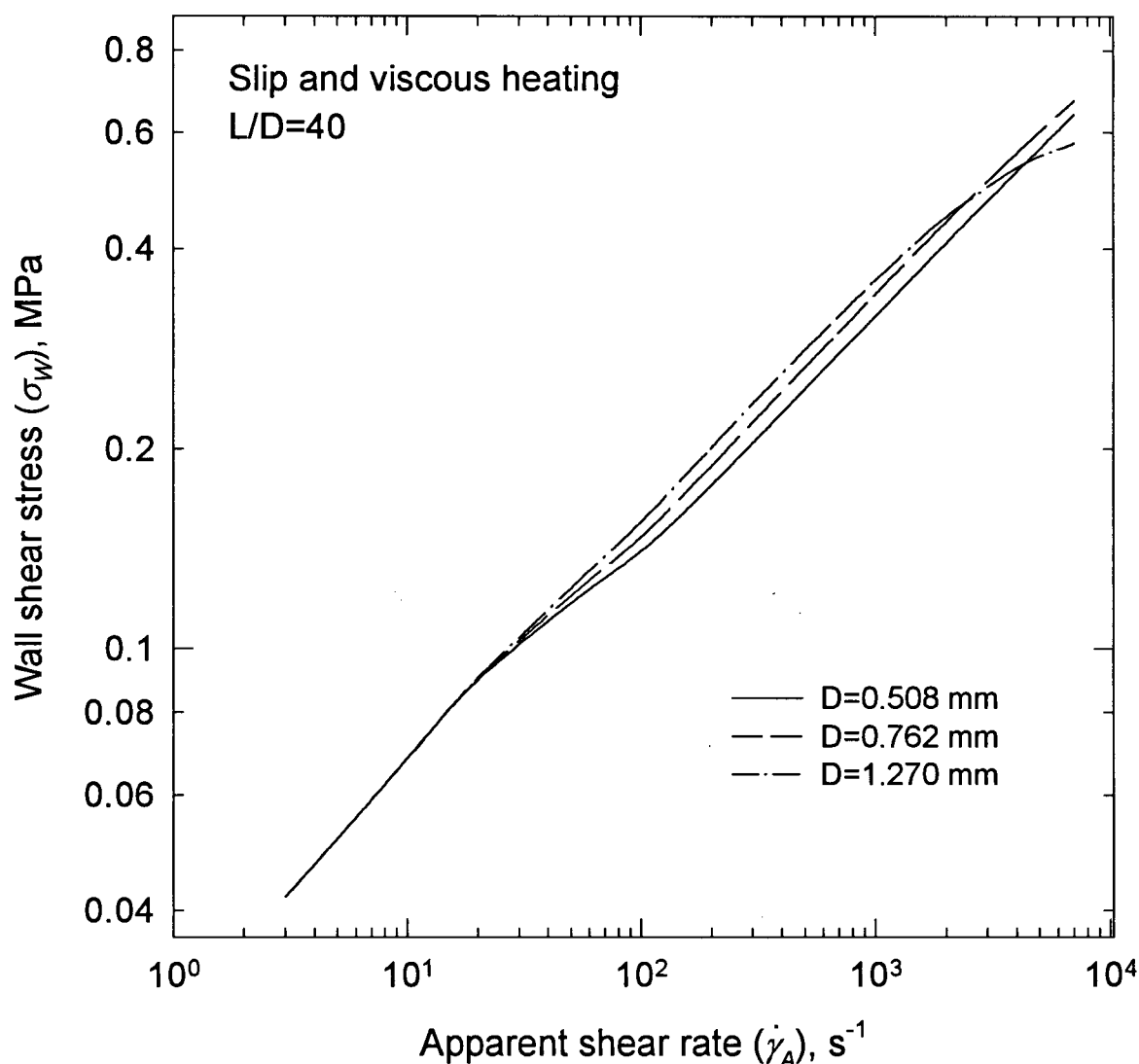
Figure 7-3. Calculated flow curves for a hypothetical material having physical properties listed in Table 7-2 under the influence of slip and viscous heating effects (slip with viscous heating case)

To demonstrate the failure of the Mooney method in the presence of viscous heating effects, consider the Mooney plot shown in Figure 7-4, that is the relationship between the apparent shear rate and the reciprocal capillary diameter at fixed values of the wall shear stress. Two cases have been plotted; one with and one without viscous heating. One can see that the inclusion of viscous heating causes significant curvature in the Mooney plot particularly at higher shear stress values. Such curvature has been

confirmed by many experimental studies (Lupton and Regester, 1965; Shih, 1979;

Hatzikiriakos *et al.*,1995). This implies that some error in the calculation of the slip

velocities using the Mooney technique is inevitable, especially in the case of significant

viscous heating. Moreover, for capillary dies having a relatively large diameter, the

thermal effects become quite substantial, especially at high wall shear stresses. As a

result the curves pass through a minimum and turn upward sharply as can be seen in

Figure 7-4. These results are consistent with the experimental data obtained by Vassalo
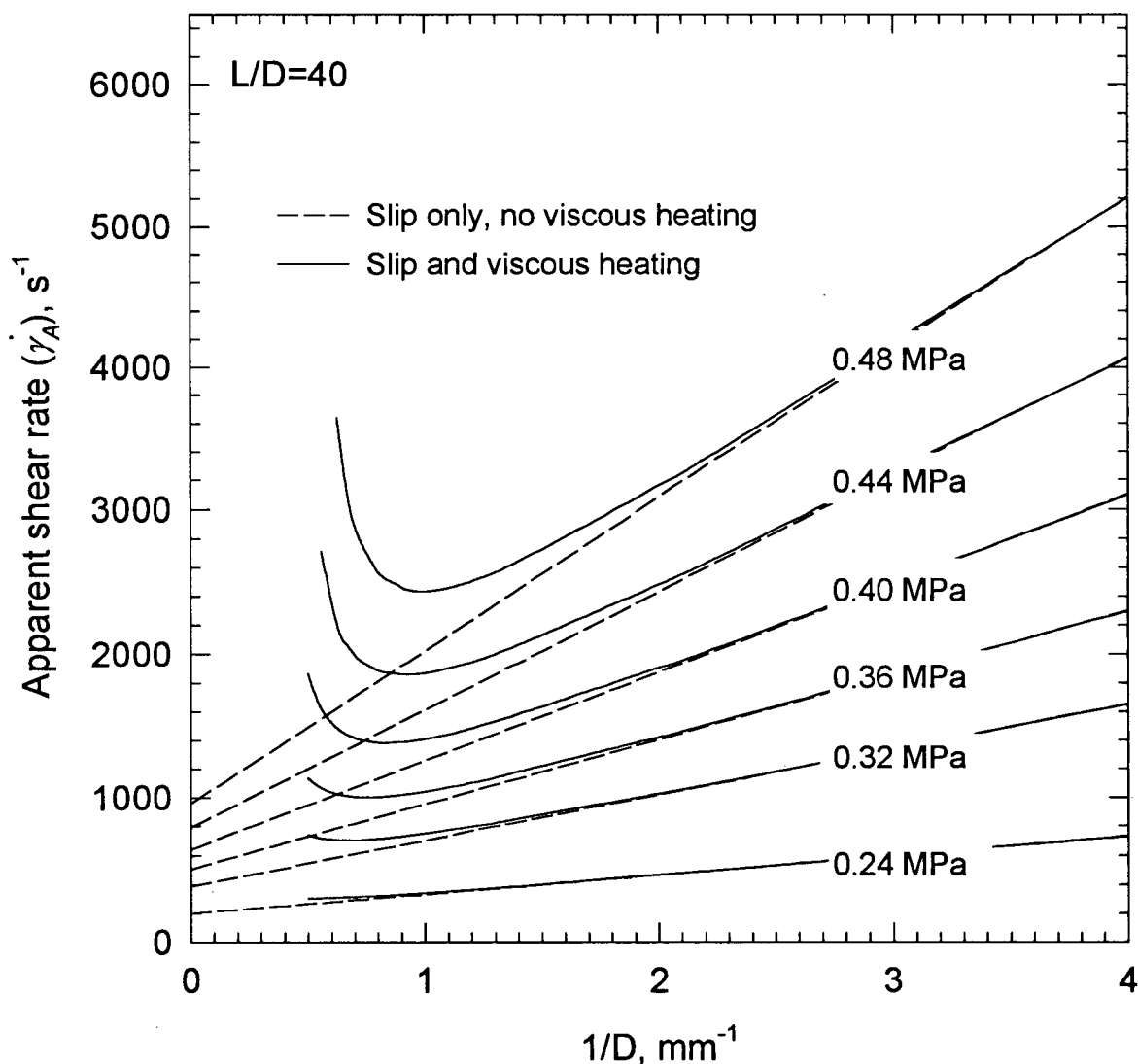
Figure 7-4. The effect of viscous heating on slip velocity measurements by means of
Mooney plot

(private communication) using an instrumented extruder and presented by Lupton and Regester (1965) (for example, see Figure 8 in their paper).

Shidara and Denn (1993) carried out experiments with a polystyrene resin using a slit rheometer with slits having gaps ranging from 34 to 765 μm. They provided an explanation for their results, which was found to be inconsistent with the Mooney technique. Their conclusion was that the observed effects were due to viscous heating. It should be pointed out that polystyrene, in general, has very high temperature and pressure dependence coefficients and therefore viscous heating effects may be dominant. Based on the present numerical results, it is reasonable to believe that the combined effects of viscous heating and wall slip resulted in such a gap dependence of their data. In fact, their Figure 4 indicates a gap dependence that is opposite to what one expects to obtain in the presence of slip.

It is clear from the above numerical results that, in cases where viscous heating is significant, data interpretation using only the Mooney technique is almost impossible or, if used, may lead to large errors in calculated slip velocities. One way to alleviate this is by using only data obtained with capillaries having small diameters. For such capillaries the effects of viscous heating are less significant. To see this more clearly, one may compare the slopes of the lines (=$8u_s$) in Figure 7-4 for the cases with and without viscous heating. The curves almost coincide for large values of $1/D$, that is for small diameters. Unfortunately, capillaries having sufficiently small diameters to make the thermal effect negligible, are not always available or their use does not provide adequate information to completely characterize the flow behavior of a polymer. In addition, to obtain experimental data from such small diameter capillaries is an extremely time-

consuming procedure and polymer degradation may become a factor due to the long pressure transients involved (Hatzikiriakos and Dealy, 1994).

Therefore, it would be desirable to have a mathematical method which, based on the experimental results, can calculate the true viscosity and slip velocity of the melts by accounting for viscous heating effects. Essentially, this method should be able to solve the inverse problem, that is, given the experimental results, estimate the slip velocity and rheological properties of the polymers (mainly viscosity) corrected for viscous heating effects. This is clearly an optimization problem. A procedure suitable for this purpose is described below.

7.5 Data Analysis Technique

To overcome the complications imposed by viscous heating effects, the following procedure is proposed for analyzing capillary rheometry data.

- Capillary rheometry experiments are carried out by using capillary dies having various diameters and L/D ratios (including orifice dies) and at different temperatures in order to assess the pressure, temperature, and end effects.

- Using the experimental data in the range of small apparent shear rates where the effects of wall slip and viscous heating are expected to be insignificant, the pressure dependence of viscosity can be determined.

- By applying the Rabinowitsch correction, the parameters of the power-law model, Equation (7-1), as well as the temperature dependence coefficient of viscosity can be calculated at small apparent shear rates.

- Using the entire set of experimental data, Equations (7-1)-(7-7) are solved in an iterative fashion to obtain the best fit of the calculated wall shear stress values to the experimental data. In the fitting process, the parameters of the slip velocity model are treated as adjustable. The average squared deviation between the predicted and measured values of the wall shear stress is used as the minimization criterion. The problem is subject to constraints on the parameters of the slip velocity model. Thus any constrained optimization procedure can be used for this purpose. Instead of Equation (7-7), any other appropriate form of the slip velocity model can be chosen, depending on the investigator's preferences.

- Using the optimal values of the slip model parameters, the slip velocity is calculated for a given value of the wall shear stress. If the slip velocity model used includes explicitly pressure and temperature effects, the local slip velocity can be calculated by solving Equation (7-1)-(7-7) and the average slip velocity is determined as the mean slip velocity along the die. For an approximate but fairly accurate estimate, the slip velocity can be calculated directly from the slip model for a given temperature and wall shear stress.

The method of optimization employed in this study is the Flexible Tolerance Method described in Himmelblau (1972). The method proved to be very reliable, though its execution time is fairly long. It provides only a local minimum, as do most local optimization methods. To determine a global minimum, several consecutive runs with different initial guesses should be carried out. The parameter estimates that provide the minimum value of the average squared deviation are considered to be the best fit parameters.

7.6 Interpretation of Experimental Data

The procedure described above was tested on various polymers, namely polypropylene (PP), high-density polyethylene (HDPE), linear low-density polyethylene (LLDPE), and Teflon® FEP. Below, the capillary flow of these resins is examined in order to assess the relative importance of slip and viscous heating effects.

7.6.1 Polypropylene

The first system examined within the context of the proposed procedure, was that studied by Kazatchkov *et al.* (1995). The polymer used in that study was polypropylene (PP) having a molecular weight M_w of 762,000. Experiments were carried out on an Instron constant-speed piston driven capillary rheometer using circular dies of various diameters and L/D ratios. Flow curves obtained for this resin using capillary dies of different diameters and constant $L/D=40$ are presented in Figure 7-5.

As it can be seen from Figure 7-5, these flow curves show no divergence, implying the absence of slip, at least in terms of the Mooney technique. However, in that study the authors concluded that slip is present, though its determination by the Mooney technique is impossible due to the fact that strong viscous heating effects mask the diameter dependence of the flow curves. This conclusion was drawn on the basis of the following observations. Polypropylene extrudates appear to be distorted for apparent shear rates beyond a certain value. These visual defects on the surface of extrudates are always accompanied by the presence of wall slip for other systems such as high density and linear low density polyethylenes (Ramamurthy, 1986; Kalika and Denn, 1987; Hatzikiriakos and Dealy, 1992a). Thus, the authors believed that this should also be the

case for polypropylene. Furthermore, application of the time-temperature superposition

principle to superpose viscosity data failed for apparent shear rates beyond a certain value

which was found to be the same as that which caused the appearance of surface defects.

In addition, viscosity data at higher temperatures were found to deviate more from a

power-law behavior, mainly due to the fact that slip velocity increases with temperature.

One may also deduce that the effect of viscous heating will be more significant for

PP than for HDPE and LLDPE by examining the flow activation energies, E^*, in the
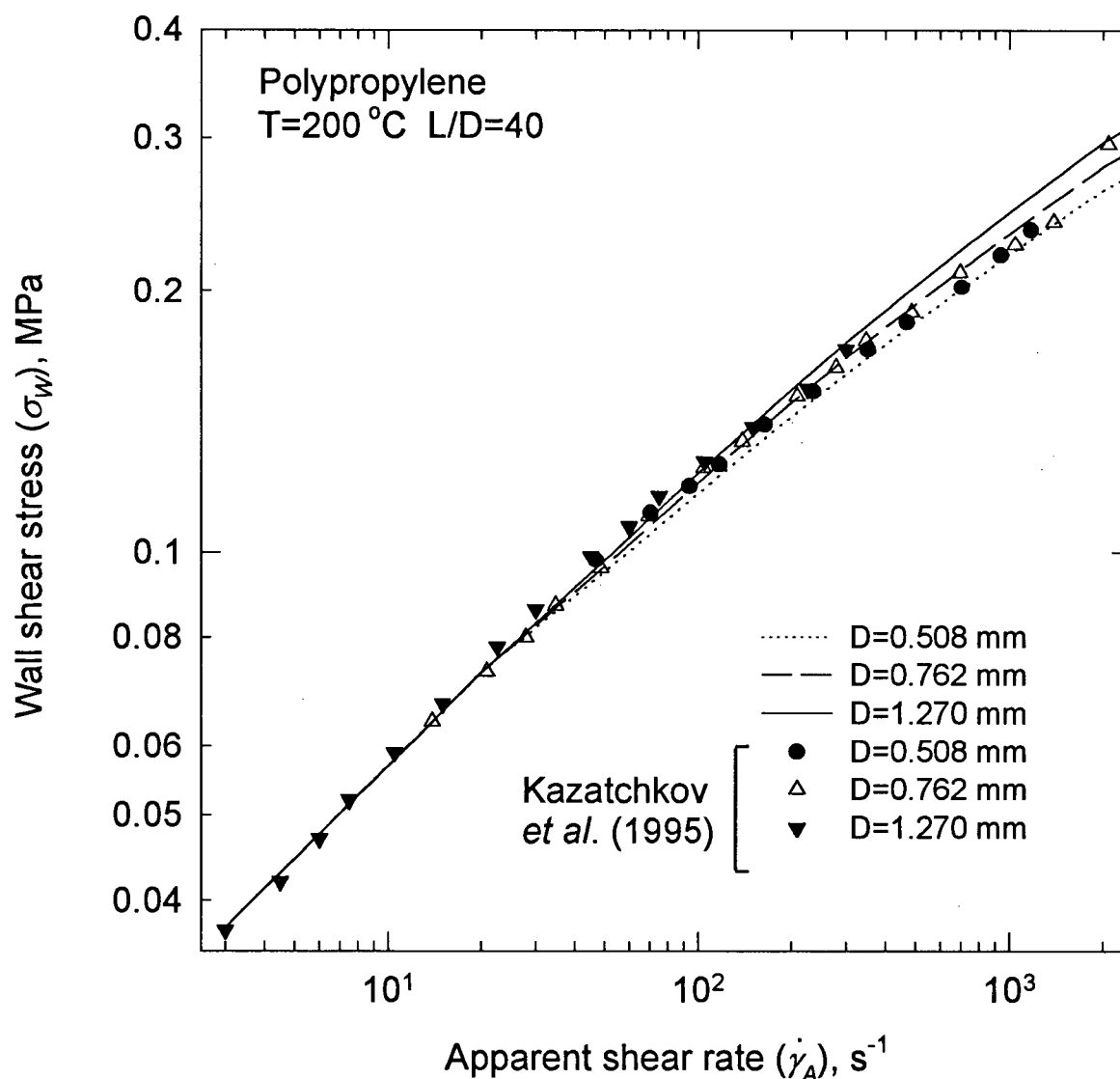
Figure 7-5. Experimental and calculated flow curves for a polypropylene resin for three capillary dies having the same L/D ratio of 40 and various diameters

Arrhenius type of equation used to model the temperature-dependence of viscosity $\eta=A\exp(E^*/RT)$ (Van Krevelen, 1991; Wang and Porter, 1995). For PP it is about 10 kcal/mole, for LLDPE about 6.3 kcal/mole, and for HDPE much less. On the other hand PS (the hypothetical material examined in Figures 7-1 through 7-4) has a very high value of E^*, close to 20 kcal/mole, which implies that viscous effects are even more dominant in the capillary flow of this resin.

Another way to conclude that viscous heating plays a significant role in the flow of PP is to calculate the Nahme number which compares the relative effect of temperature changes due to viscous heat generation to those due to heat conduction in the radial direction. This dimensionless number is defined as $\mathrm{Na} = A\bar{v}^2\bar{\eta}/\bar{k}$ (Winter, 1977), where A is the temperature dependence coefficient in Equation (7-1), $\bar{v}$ is the mean axial velocity, $\bar{k}$ is the mean thermal conductivity at the reference temperature, and $\bar{\eta}$ is the reference viscosity corresponding to a reference shear rate $\bar{\gamma} = \bar{v}/R$. For the apparent shear rate of 1000 s^{-1}, the mean velocity in the capillary of radius R=0.635 mm is 0.16 m/s, the thermal conductivity at 200 °C is 0.12 W/(m·K), $\bar{\gamma} = 250$ s^{-1}, and $\bar{\eta} \approx 500$ Pa·s. For these conditions of the flow of PP, the Nahme number is 1.07 which is greater than 0.1-0.5, thus indicating that the viscous dissipation leads to significant viscosity changes, i.e., changes that should be reflected in the temperature and velocity fields.

To check the validity of this conclusion, the proposed data analysis technique was used to calculate the slip velocity in the flow of molten polypropylene using the experimental data shown in Figures 7-5 and 7-6. Figure 7-5 plots the PP flow curves obtained using capillaries having a constant length-to-diameter ratio, L/D=40 and

different diameters, and Figure 7-6 plots the flow curves obtained using capillaries having a constant diameter and various length-to-diameter ratios, L/D.

The local slip velocity was modeled by using the modified power-law expression proposed by Hatzikiriakos and Dealy (1992a). This can be written as:

$$u_s = \frac{\xi_0 f_1(T)}{1 + (\sigma_c/\sigma_W)^{100}} \left(1 - c_1 \tanh \frac{E + c_2 \sigma_n/\sigma_W}{RT}\right) \left(\frac{\sigma_W}{\sigma_c I^{1/4}}\right)^m \qquad (7-15)$$

where ξ_0, c_1, c_2, and m are coefficients, $f_1(T)$ is a function of temperature (the WLF
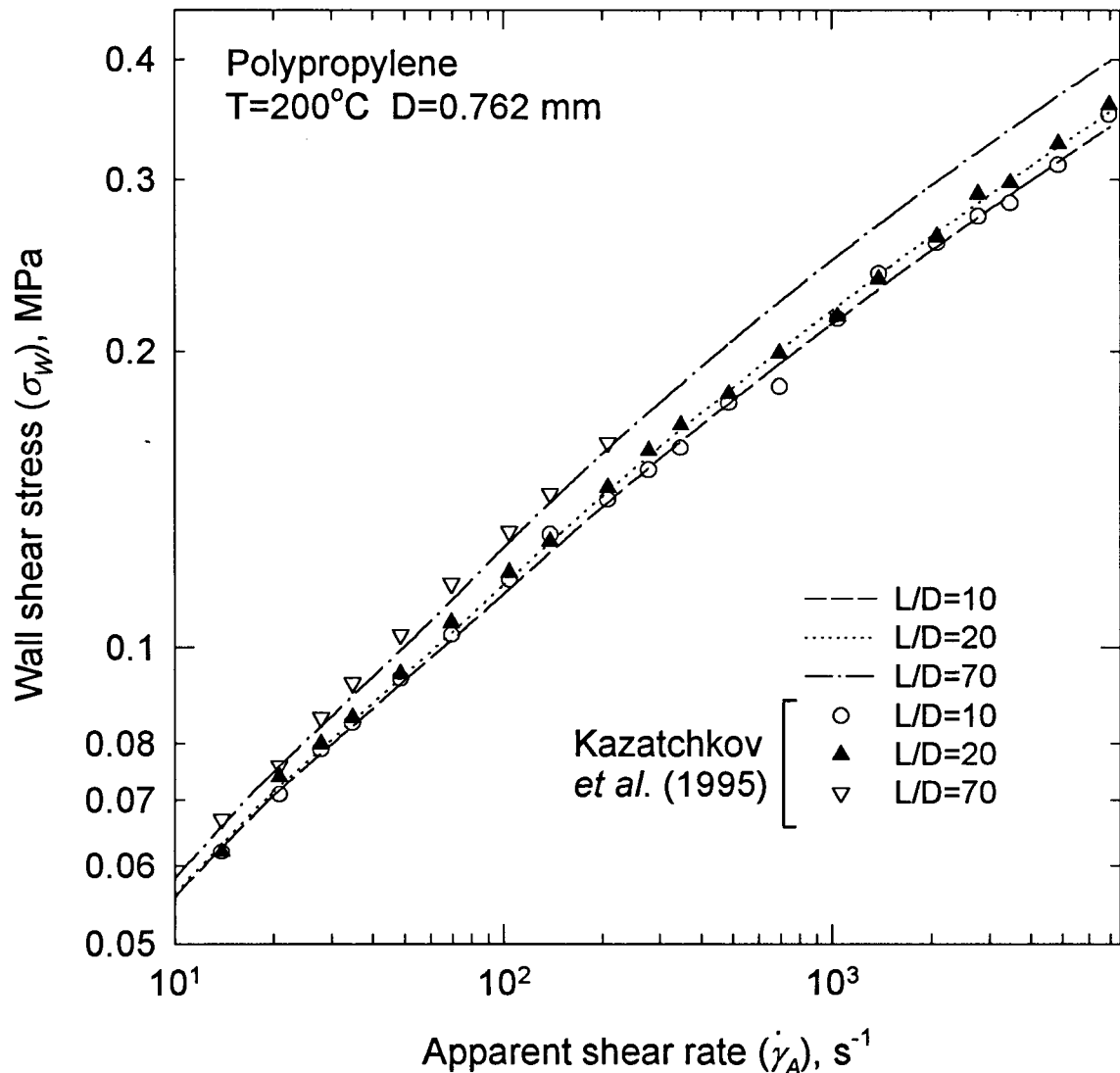
Figure 7-6. Experimental and calculated flow curves for a polypropylene resin for three capillary dies having the same diameter and various L/D ratios

equation is used, i.e., $f_1(T) = C_1(T\text{-}T_0)/[C_2+(T\text{-}T_0)]$ where C_1 and C_2 are constants) , E is an activation energy for adsorption/desorption, σ_w is the local wall shear stress, σ_n is the local normal stress at the wall, σ_c is the critical shear stress for the onset of slip, and I is the resin polydispersity. The denominator $1+(\sigma_c/\sigma_w)^{100}$ is included in order that the slip velocity is zero for wall shear stresses less than the critical value σ_c. The normal stress can be approximated by (Hatzikiriakos and Dealy, 1992a):

$$\sigma_n=P+50\sigma_W/12 \qquad\qquad (7\text{-}16)$$

Table 7-3. Constants for polypropylene

		PP
Polydispersity	I	1
Thermal conductivity of the wall	k_W, W/(m·K)	17.0
Equation (7-1)	A, K^{-1}	0.01
	K, Pa·s^n	21956
	T_{ref}, °C	200
	α, Pa	$5.9 \cdot 10^{-9}$
	n	0.34337
WLF equation	C_1	1.159
	C_2, K	109.43

Table 7-4. Calculated parameters of the slip velocity model, Equations (7-15) and (7-17) for PP

Parameter	Polypropylene	
	Equation (7-15)	Equation (7-17)
ξ_0, m/s	$0.8219 \cdot 10^{-2}$	$0.8219 \cdot 10^{-2}$
c_1	0.968	0.968
c_2, cal/mol	7.19	14.38
E, cal/mol	1422.6	1452.6
σ_c, Pa	$0.911 \cdot 10^5$	$0.911 \cdot 10^5$
m	4.897	4.897

Note that the slip model Equation (7-15) takes into account both the temperature and pressure dependence of the slip velocity. The values of the parameters for Equations (7-1) and (7-15) are tabulated in Table 7-3 along with other physical properties of polypropylene. The constant heat flux thermal boundary condition was used in the numerical simulations. The optimization program includes as constraints that (i) the adjustable parameters ξ_0, c_1, c_2, m, E, and σ_c be positive, and (ii) the slip velocity not exceed the average velocity obtained from the plug flow assumption. The number of experimental points was 43. The optimal values of the slip velocity model parameters are listed in Table 7-4. The calculations were repeated several times, each time starting with a different initial guess, and the program always converged to the same set of values. These values are believed to provide a unique solution to the problem and to be the global minimum as well. The average deviation from the experimental data was about 2.9%.

The calculated flow curves for the dies having diameters of 0.508 mm, 0.762 mm, and 1.27 mm and the same L/D ratio of 40 are presented in Figure 7-5, along with the experimental data points. One can see an excellent agreement between experimental and simulated data. In particular, the flow curves seem to almost coincide implying the absence of wall slip (no diameter dependence). However, the calculations have shown that slip does occur as discussed and presented below. Figure 7-6 shows fitted and experimental flow curves obtained for the capillaries of the same diameter and various L/D ratios which are again in very good agreement. Divergence between the flow curves indicates that the viscosity is a function of pressure.
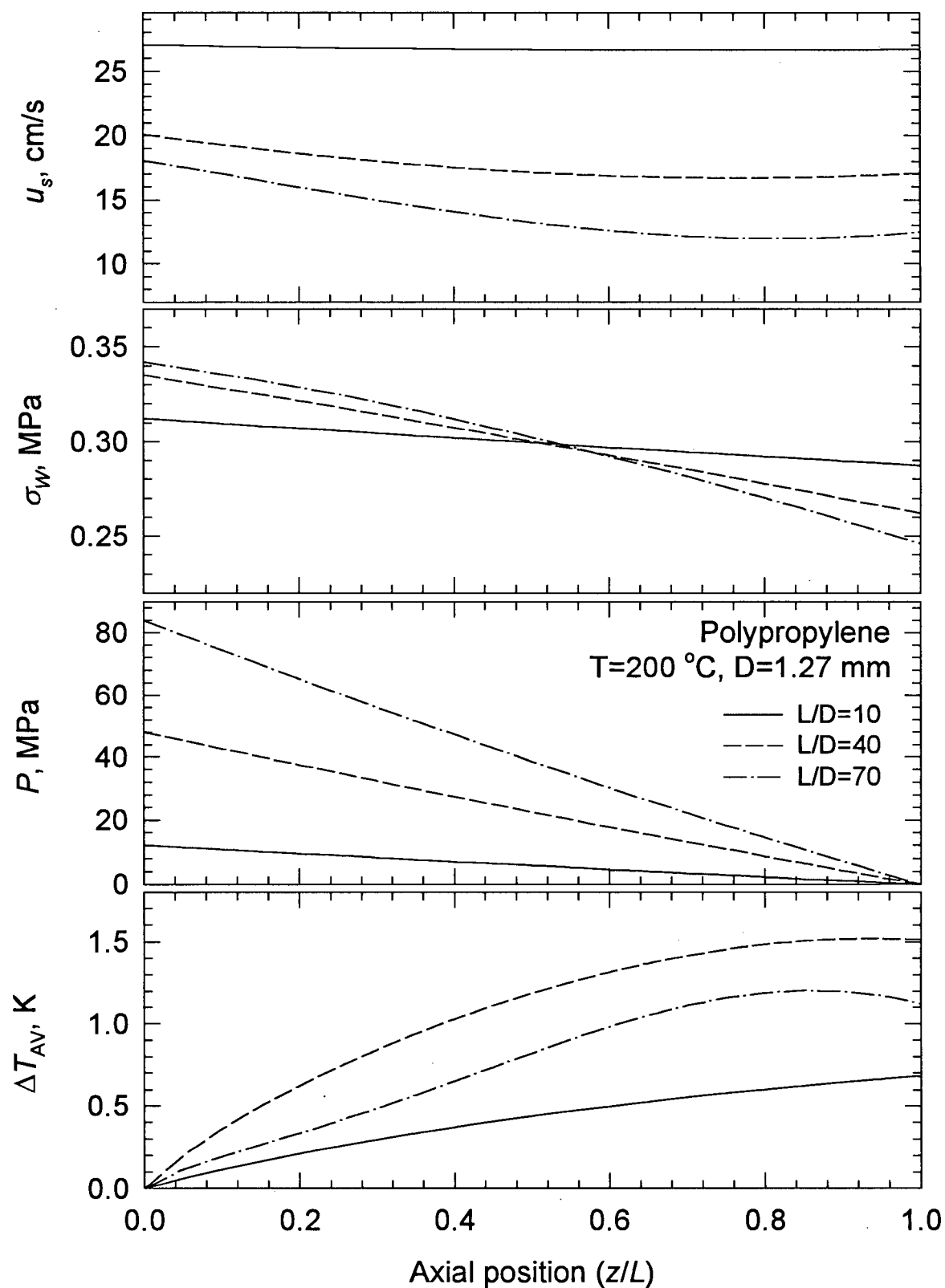
Figure 7-7. Calculated axial slip velocity, wall shear stress, pressure and average temperature rise in the capillary flow of a polypropylene resin for three dies having the same diameter and various L/D ratios

Figure 7-7 depicts predicted slip velocity, wall shear stress, pressure and temperature rise profiles (axial) for capillary dies having the same diameter and various L/D ratios. The average wall shear stress is 0.3 MPa for all dies. However, it can be seen that the actual wall shear stress profiles vary with the change of the L/D ratio. For a short capillary the shear stress is almost a linear function of the axial position decreasing gradually throughout the length of the capillary. However, in a long die the shape of the curve becomes slightly convex upward and the wall shear stress decreases significantly along the length of the die. The pressure drop is almost linear along the die. The slip velocity is strongly affected by the combination of these parameters, σ_W, T, and P. In short capillaries where the temperature rise is relatively small, it increases nearly linearly along the die. As the L/D ratio increases, the pressure becomes a factor and the average slip velocity decreases. However, since the effect of viscous heating is more pronounced for longer capillaries, the slip velocity is not constant throughout the die any more, thus decreasing with increase of temperature. The dip in the slip velocity profile becomes larger and deeper as the L/D ratio increases. At the die exit the reduction of pressure causes the slip velocity to increase, thus diminishing the effect of temperature.

Figure 7-8 presents predicted slip velocity, wall shear stress, pressure and temperature rise profiles (axial) for capillaries having L/D=40 and different diameters. The same trend can be observed in this case; that is, the slip velocity first decreases due to viscous heating, then passes through a minimum, and increases close to the die exit as a result of pressure reduction. The curvature of the slip velocity profile depends on the temperature rise which is greater for capillaries having a larger diameter.
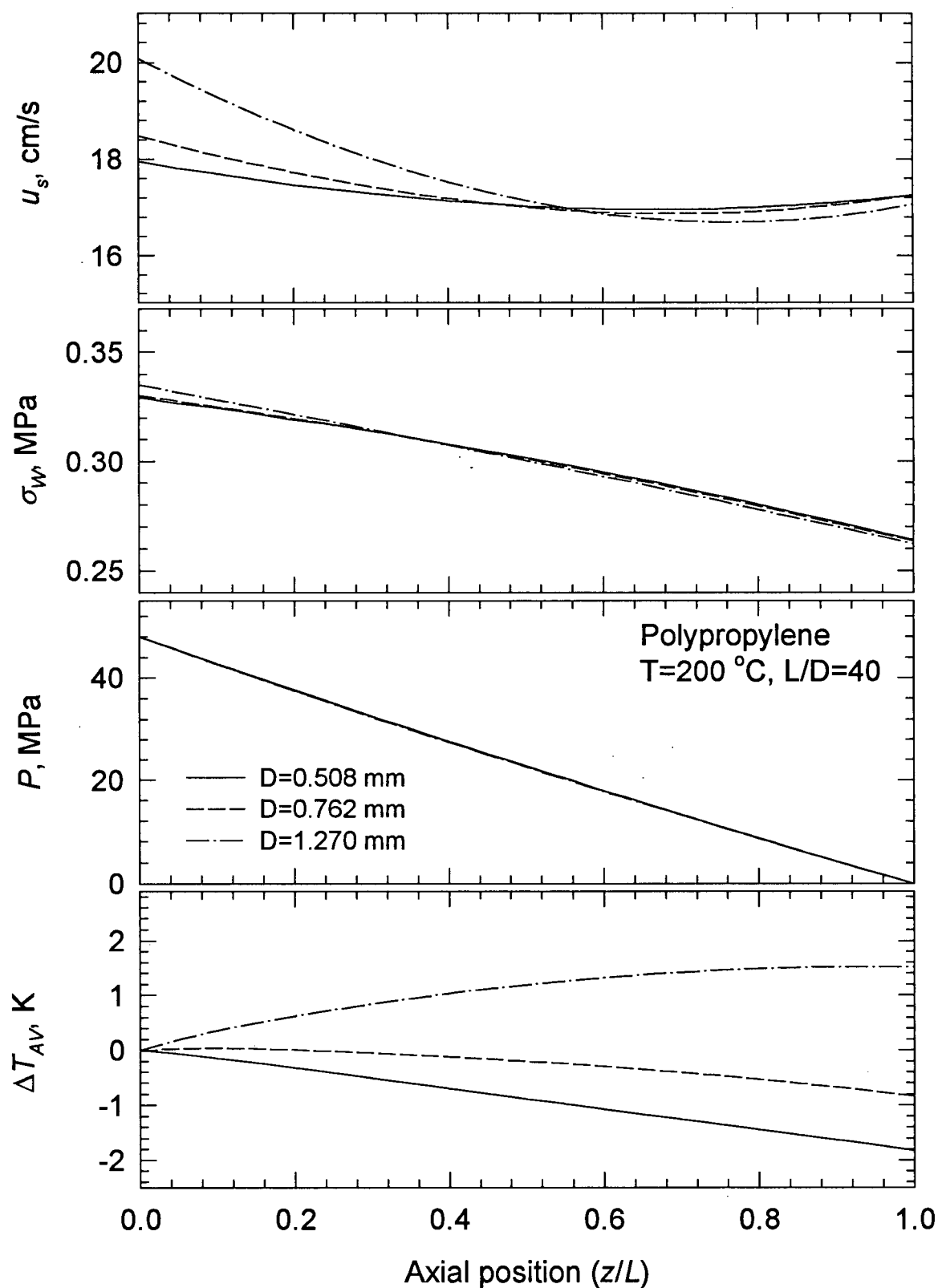
Figure 7-8. Calculated axial slip velocity, wall shear stress, pressure and average temperature rise in the capillary flow of a polypropylene resin for three dies having the same L/D ratio and various diameters
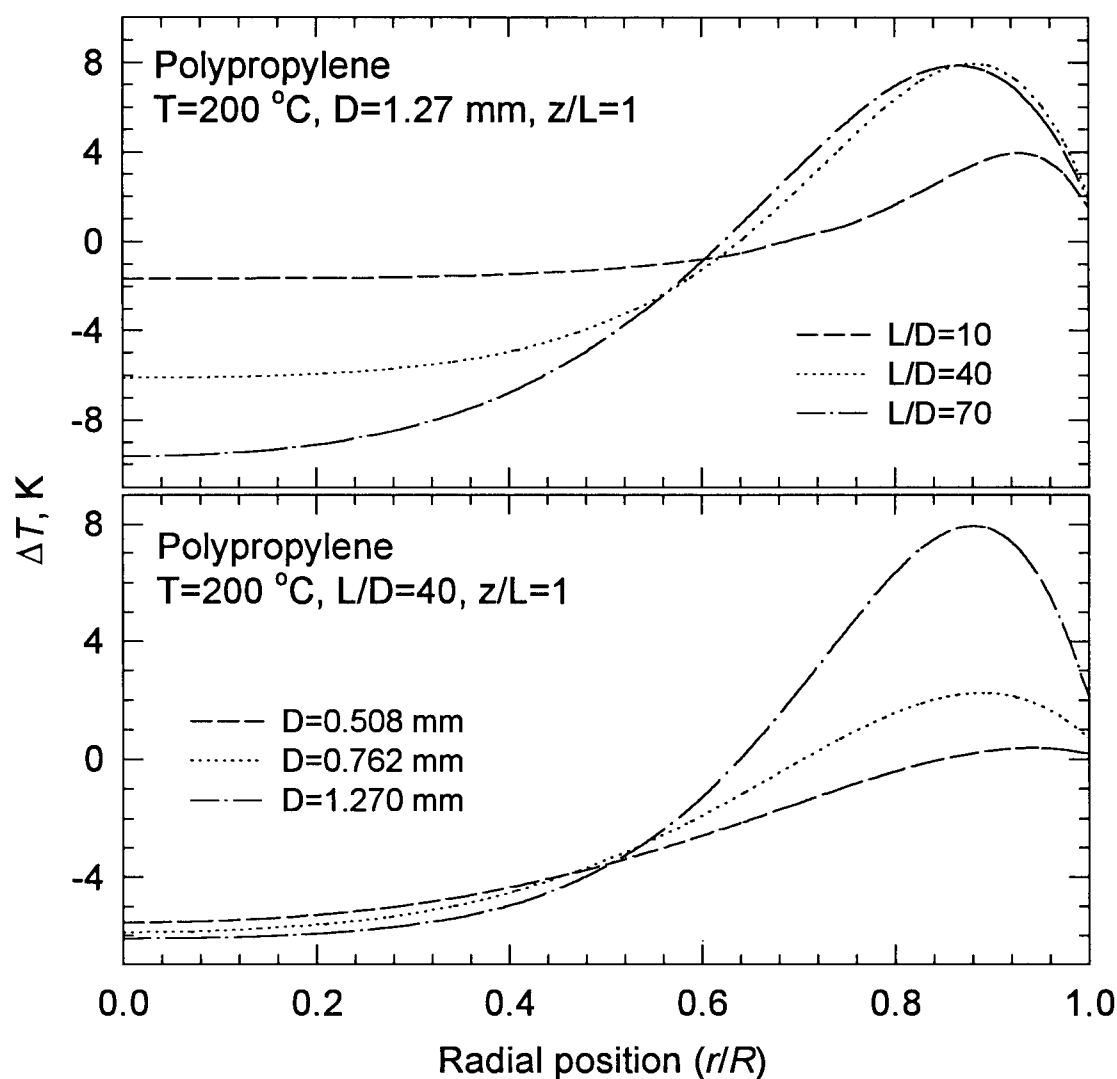
Figure 7-9. Calculated radial temperature profiles at the die outlet in the capillary flow of a polypropylene resin for dies having various *L/D* ratios and diameters

The average temperature rises plotted in Figures 7-7 and 7-8 are, in general, more pronounced for longer dies having the same diameter and for larger dies having a constant *L/D* ratio. In a long die the residence time of the melt is higher and thus the melt is subject to larger heat dissipation amounts. However, for long enough capillaries this trend may be reversed due to the fact that expansion cooling becomes significant. Indeed, as can be seen in Figure 7-7, the average temperature rise is higher in the capillary having

an L/D=40 than that in the capillary having an L/D=70. While energy dissipation is higher for the L/D=70 capillary, expansion cooling drops the temperature in the core region of the melt significantly and, as a result, the average temperature rise is kept small. In general, it can be seen in Figures 7-7 and 7-8 that the calculated average temperature rises are small and one would expect that viscous heating is not significant. However, the maximal temperature rise close to the wall may exceed the average value by several times, reaching quite significant values. It is this temperature rise which significantly influences the rheological measurements and always increases with L/D (D=const) and D (L/D=const). Figure 7-9 plots the radial temperature profiles at the die outlet for two cases described in Figures 7-7 and 7-8. It can be seen that the higher temperature rise occurs in the region close to the wall. This is the region of high shear and thus that of the largest temperature rise. At the same time this is the region where temperature has the strongest influence on the rheological measurements as well as the slip velocity. In the core region of the die, however, expansion cooling is dominant thus causing the temperature to drop significantly. Expansion cooling caused by the small but finite polymer compressibility is strongly affected by the pressure, hence it is more pronounced for the capillaries having larger L/D ratios.

From the slip velocity model used and the numerical results presented in Figures 7-7 and 7-8, it is obvious that the slip velocity is a function of the wall shear stress, wall normal stress and temperature, and thus it varies with the axial position along the die. However, it is often desirable to know the average slip velocity as a function of the average wall shear stress for capillaries having various length-to-diameter ratios. This can be obtained by first assuming that pressure changes linearly in a capillary (a good

approximation). Secondly, one can express the normal stress, σ_n, in terms of L/D, and

substitute the results into Equations (7-15)-(7-16) (for more details see Hatzikiriakos and

Dealy, 1992a). The following expression for the slip velocity can thereby be obtained:

$$u_s = \frac{\xi_0 f_1(T)}{1+(\sigma_c/\sigma_W)^{100}}\left(1-c_1\tanh\frac{E^*+c_2^*L/D}{RT}\right)\left(\frac{\sigma_W}{\sigma_c I^{1/4}}\right)^m \tag{7-17}$$

where $E^*=E+50c_2/12$, and $c_2^*=2c_2$. The significance of this equation is that the obtained

slip velocity values can now be compared directly with the experimentally determined

ones. Figure 7-10 plots the slip velocity of PP as a function of wall shear stress for

various capillary L/D ratios. The optimum values of the parameters in Equations (7-15)
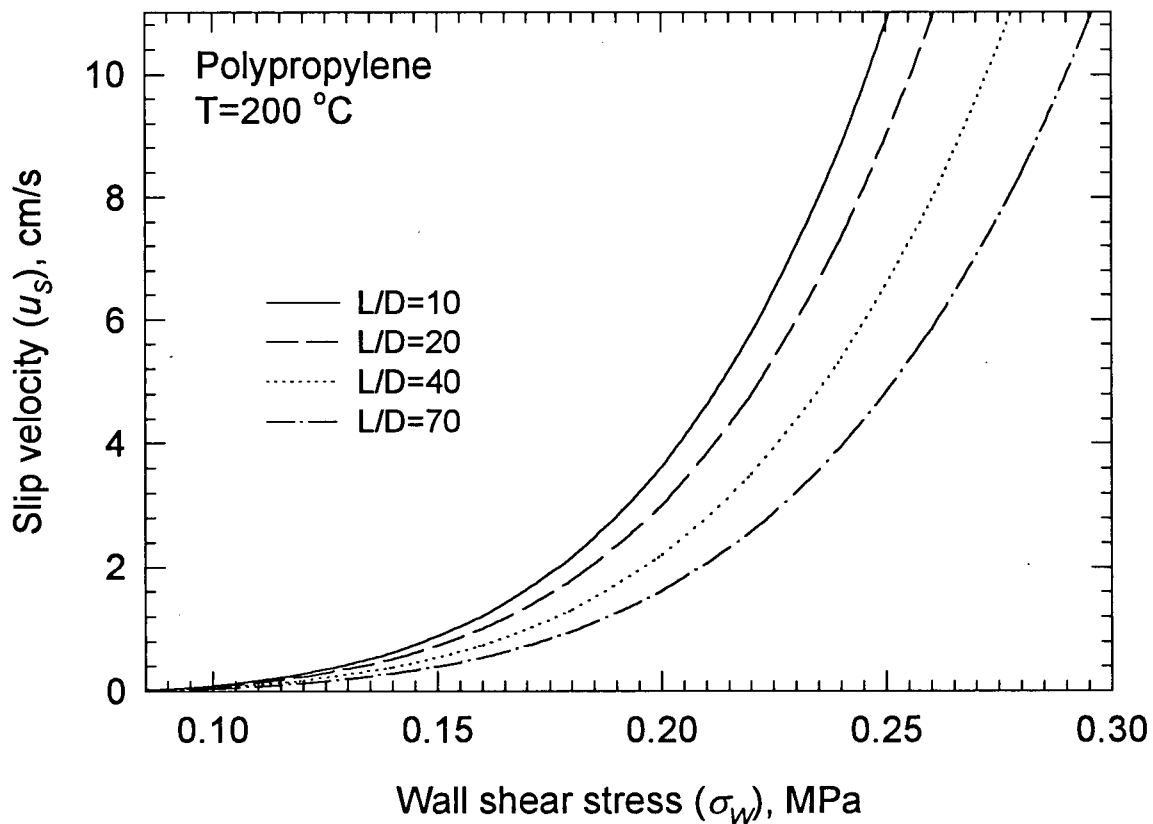
Figure 7-10. Calculated slip velocity of a polypropylene resin as a function of wall shear stress for capillary dies having various L/D ratios

and (7-17) calculated from the minimization algorithm are listed in Table 7-4. It can be

seen from Figure 7-10 that despite the apparent absence of slip from the experimental

data of Figure 7-5, the slip velocity of PP is considerable. At high enough shear stresses,

it exceeds that calculated for a HDPE (Hatzikiriakos and Dealy, 1992a). In addition, the

calculated slip velocities scale with the L/D ratio indicating the same trend as that

observed experimentally.
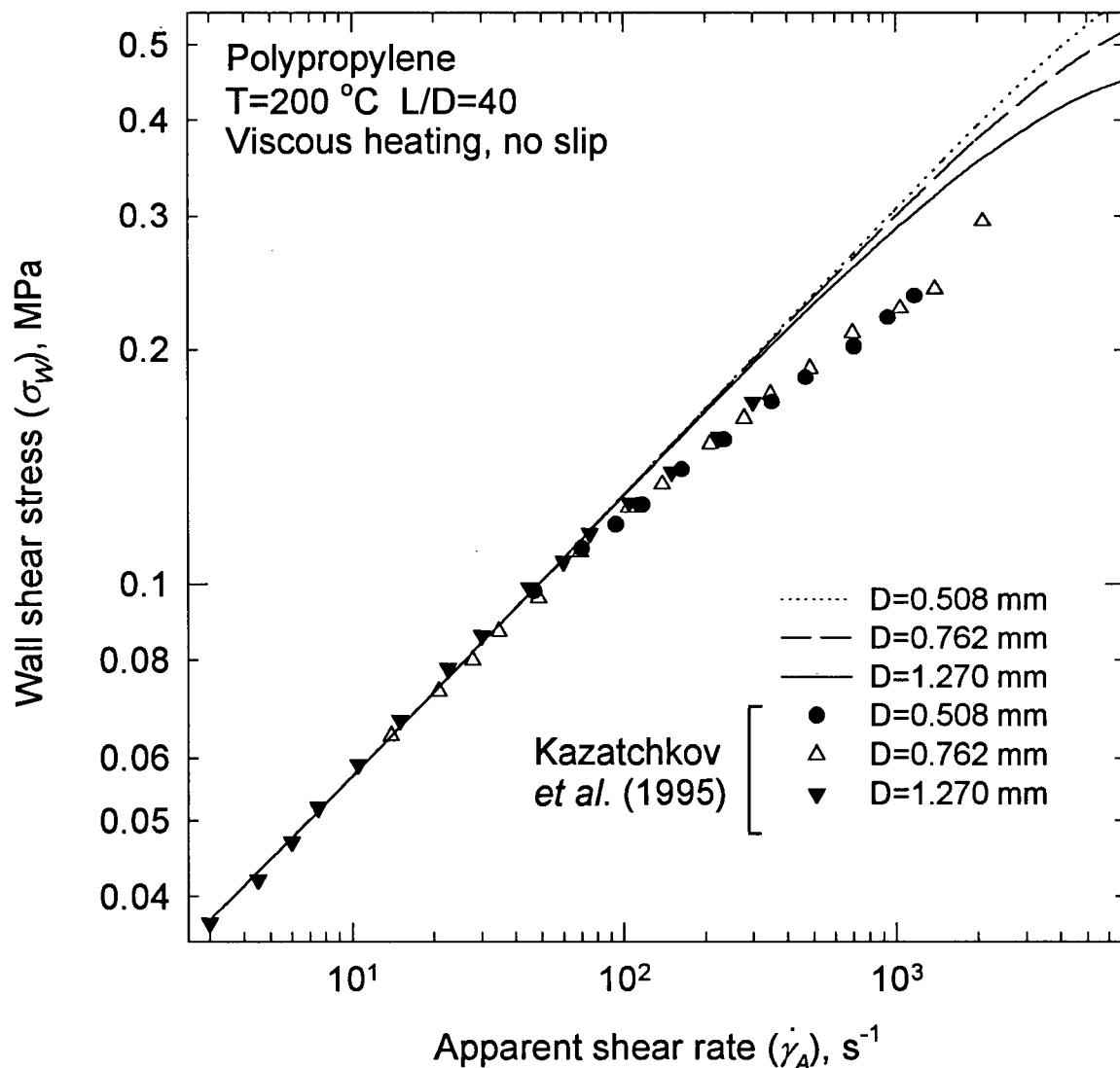
Figure 7-11. Experimental flow curves and those calculated in the absence of wall slip for
a polypropylene resin for three capillary dies having the same L/D ratio of 40
and various diameters

Figure 7-11 shows a comparison of the experimental results presented in Figure 7-5 with the model predictions in the absence of wall slip. It is clear that viscous heating is significant due to the presence of diameter dependence and the overall description of the data in the absence of wall slip becomes poor. Thus, the inclusion of wall slip is a necessary ingredient of the model in order for it to adequately describe the capillary flow of polypropylene at high shear rates where the effects of viscous heating and wall slip become significant.

7.6.2 Linear Low Density Polyethylene

The case of PP demonstrates how the slip velocity of a polymer can be calculated when the macroscopic experimental data imply the absence of slip (no diameter dependence of the flow curves). For such cases, the Mooney method is obviously not applicable. However, it would be interesting to examine a case where the capillary data were actually used to determine the slip velocity. In this example, by using the mathematical model, it should be possible to estimate the error that results from the curvature of the lines in the Mooney plot.

To answer this question, the experimental data for a linear low density polyethylene (LLDPE, Dowlex 2049) reported by Hatzikiriakos *et al.* (1995) were used to calculate the parameters of the slip velocity model for this polymer (Equation 7-15). The authors reported that the Mooney plots were severely curved and identified this as a viscous heating effect. In spite of this, straight lines were fitted to the data and thus the slip velocity was calculated as a function of the wall shear stress for a number of capillaries having various *L/D* ratios.

The values of the parameters used in Equations (7-1) and (7-15) are tabulated in Table 7-5. The number of experimental points was 46. The optimal parameter values of the slip velocity model calculated by the optimization technique are listed in Table 7-6. The average deviation from the experimental data was about 5.9%. Figure 7-12 shows the experimental and predicted flow curves for capillaries having the same L/D ratio and different diameters. As can be seen, the 5.9% deviation can be largely attributed to experimental error and comes primarily from the fitting of the data corresponding to the capillary die having the smallest diameter.

Table 7-5. Constants for LLDPE

		LLDPE
Polydispersity	I	3.9
Thermal conductivity of the wall	k_W, W/(m·K)	17.0
Equation (7-1)	A, K^{-1}	0.0075
	K, Pa·s^n	8100
	T_{ref}, °C	200
	α, Pa	$4 \cdot 10^{-9}$
	n	0.674
WLF equation	C_1	2.552
	C_2, K	83.61

Table 7-6. Calculated parameters of the slip velocity model, Equations (7-15) and (7-17) for LLDPE

Parameter	Polyethylene	
	Equation (7-15)	Equation (7-17)
ξ_0, m/s	$0.1227 \cdot 10^{-1}$	$0.1227 \cdot 10^{-1}$
c_1	0.988	0.988
c_2, cal/mol	15.27	30.54
E, cal/mol	1203.0	1266.6
σ_c, Pa	$0.807 \cdot 10^5$	$0.807 \cdot 10^5$
m	4.312	4.312
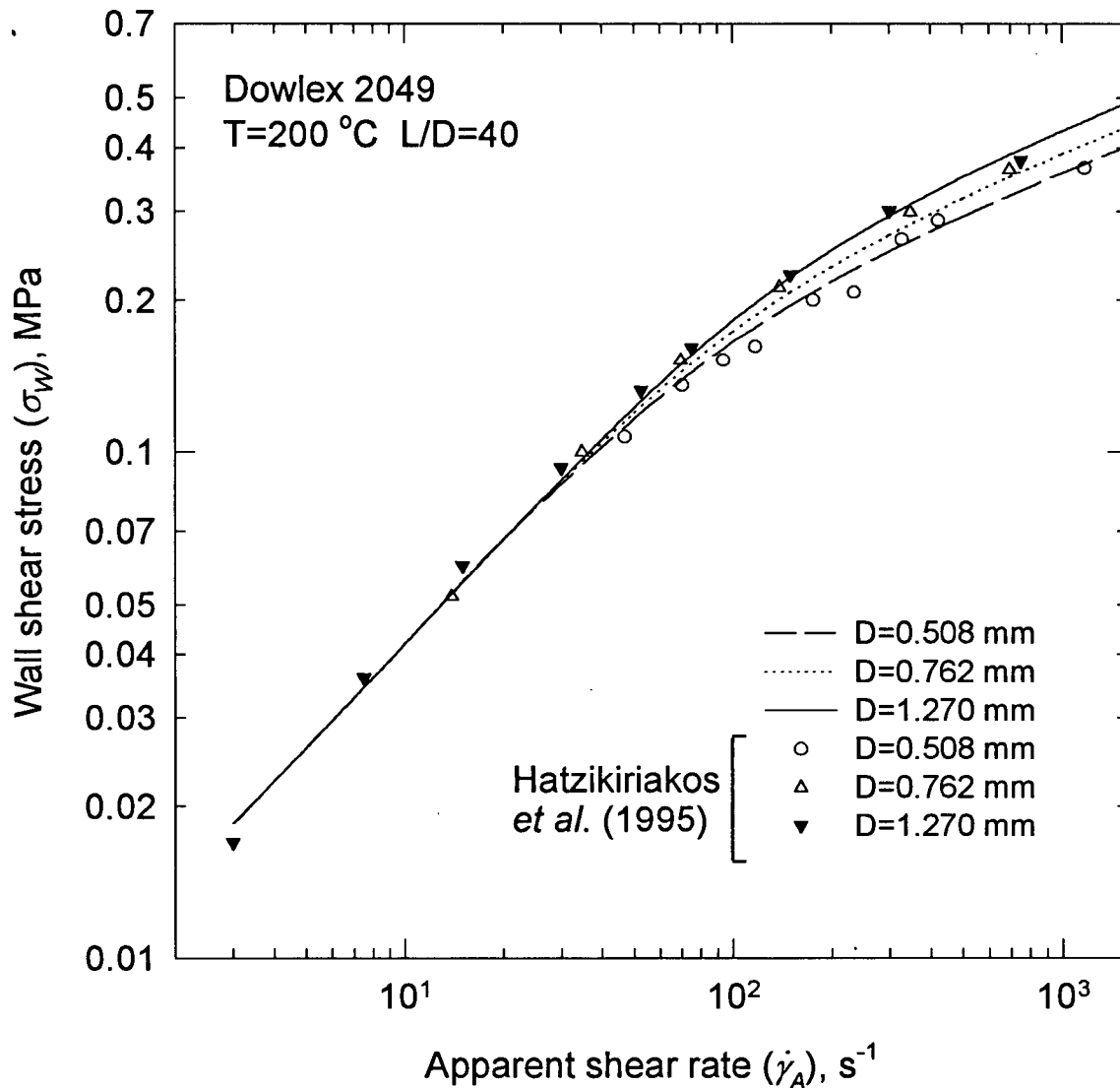
Figure 7-12. Experimental and calculated flow curves for a linear low density resin (Dowlex 2049) for three capillary dies having the same L/D ratio of 40 and various diameters

Figure 7-13 compares the slip velocities calculated by use of Equation (7-17) using the values of the parameters listed in Table 7-6 with those calculated directly from the macroscopic experimental data reported by Hatzikiriakos *et al.* (1995). One may identify quite significant differences between the slip velocity values predicted by the present procedure (continuous lines) and those calculated by using the graphical Mooney

technique (symbols). These differences become more significant at relatively high wall shear stress values (where viscous heating effects dominate). The agreement between the predicted values and the experimental data obtained for the special case of L/D=0 is remarkably good. These data correspond to the slip velocity obtained from a sliding plate rheometer operated at ambient pressure. This is due to the fact that viscous heating effects are negligible in a sliding-plate rheometer compared to those in a capillary
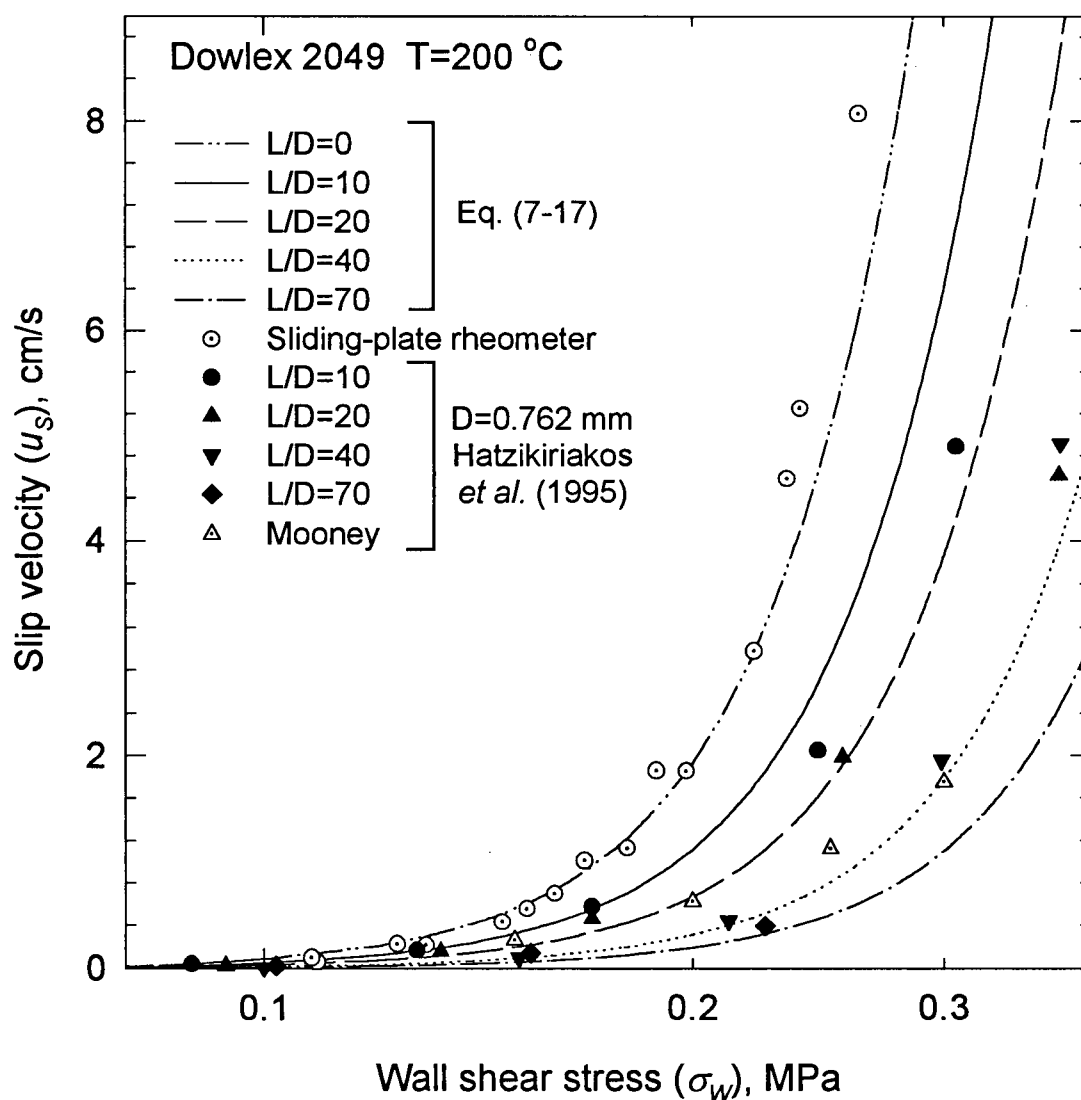
Figure 7-13. Experimental and calculated slip velocities of a linear low density resin (Dowlex 2049) as a function of wall shear stress for capillary dies having various L/D ratios

rheometer (Dealy, 1982). It should be noted that the sliding-plate rheometer data were not used in the fitting procedure. They were estimated by using the calculated values of the model parameters. In addition, it can be seen from Figure 7-13 that the disagreement between the slip velocity predictions and the capillary rheometer data increases with increasing L/D, that is with increasing significance of the viscous heating effects.

7.6.3 High Density Polyethylene

This example corresponds to a case where viscous heating is insignificant. In such cases, the Mooney technique results in fairly accurate estimates of the slip velocity. This is mainly due to the low degree of dependence of the material viscosity on temperature. The polymer under investigation is the high density polyethylene, Sclair 56B/3830, studied by Hatzikiriakos and Dealy (1992a). The values of the physical properties are listed in Table 7-7. Experiments were carried out on an Instron capillary rheometer using circular dies of various diameters and L/D ratios. The values of the slip velocity were obtained using a modified Mooney technique (Hatzikiriakos and Dealy, 1992a).

Table 7-7. Physical properties and constants in equations for Sclair 56B

Physical properties		Constants in Eq. (7-1)		Constants in Equation (7-15)	
Thermal conductivity k, W/(m·K)	0.255	A, K^{-1}	0.006	ξ_0, m/s	0.1078
Density at P=0 ρ_0, kg/m^3 (Eq.2)	807.5	K, Pa·s^n	22820	c_1	0.987
Compressibility β, Pa^{-1} (Eq.2)	1·10^{-9}	T_{ref}, °C	140	c_2, cal/(mol)	15.5
Heat capacity C_p, J/(kg·K)	2650	α, Pa	2·10^{-9}	E, cal/(mol)	1238
Polydispersity I	9.4	n	0.44	σ_c, Pa	0.9·10^5
				m	3.23

For this case, no data analysis technique was applied to calculate the slip velocity. The purpose of this section is to compare the results obtained by use of the model with

those in Hatzikiriakos and Dealy (1992a), where the effect of viscous heating was neglected. The difference between the two sets of results was expected to be small since the viscous heating effect was the least pronounced for this resin, amongst all the cases studied, since it has the lowest temperature dependence coefficient, A.

Figure 7-14 shows the results of a numerical simulation for the flow of Sclair 56B in a circular die of D=0.762 mm and L/D=100 at an apparent shear rate of $\dot{\gamma}_A$=549 s^{-1}. Agreement with Hatzikiriakos and Dealy (1992a) is remarkably good in spite of the fact
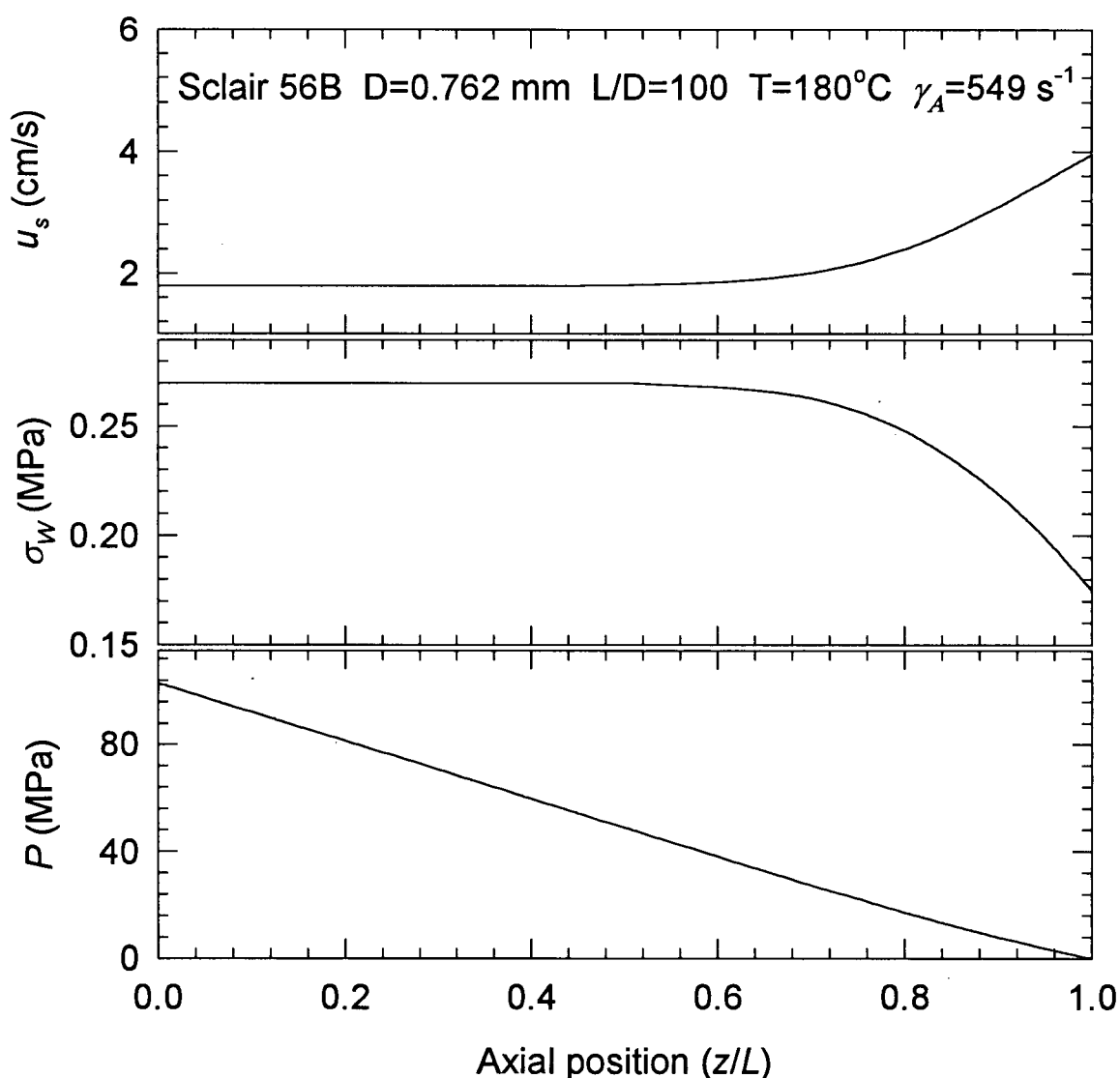
Figure 7-14. Slip velocity, wall shear stress, and pressure profiles along a capillary die

that, in their study, the effect of viscous heating was neglected. At these moderate

apparent shear rates, the effect of viscous heating is insignificant.

Figure 7-15 plots the calculated and experimental apparent flow curves for HDPE.

As a result of an overestimation of the slip velocity due to neglecting viscous heating in

Hatzikiriakos and Dealy (1992a), there is some disagreement between the calculated and

experimental apparent flow curves. This is due to the combined effect of wall slip and

viscous heating which shifts the calculated flow curves to higher values of the apparent
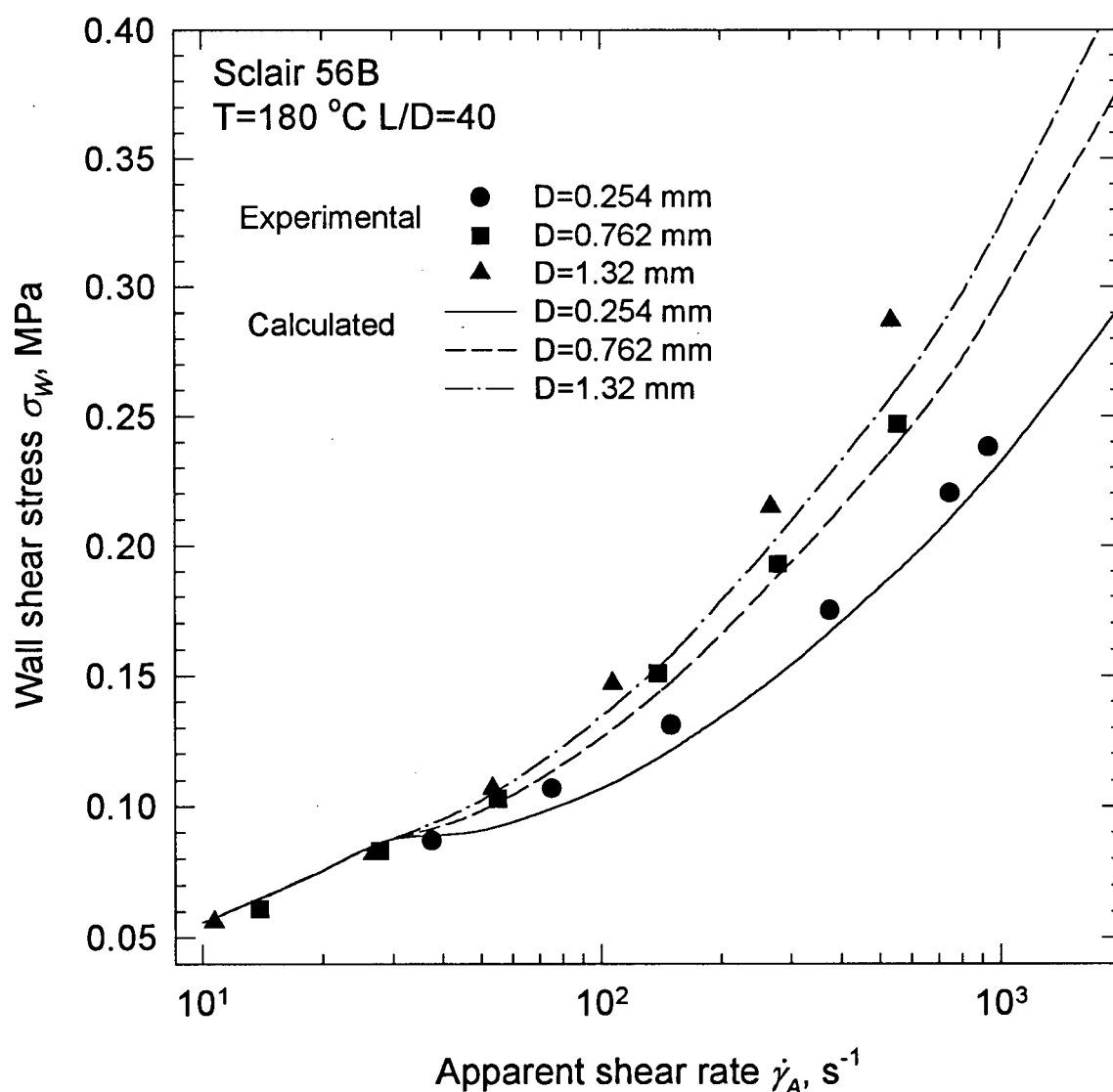
Figure 7-15. Apparent flow curves for Sclair 56B at 180 °C with capillaries of various diameters and L/D=40; experimental and calculated

shear rate. However, in general, this example demonstrates a case where the Mooney technique can be safely used to obtain in a fairy good estimate of the slip velocity.

7.6.4 Teflon® FEP

The final polymer that studied was Teflon® FEP 4100. The flow curves for this polymer are plotted in Figure 5-7. Looking at this figure, one can see that the slip model represented by Equation (7-15) is not applicable in this case, since it implies that the slip velocity is a monotonic function of the wall shear stress. However, there is a distinct maximum and minimum in the flow curve of Teflon® FEP 4100 (spurt flow). Modeling of this phenomenon requires a special slip model which results in a non-monotonic, S-shaped behavior of the slip velocity as a function of σ_W.

Such a model was recently presented by Leonov (1990) who developed a molecular model for the adhesive friction of elastomers. It can be presented in a non-dimensional form as:

$$\frac{\sigma_W}{\sigma_W^0} = f(u) = u\frac{1-(1+m+1/u)\exp(-m-1/u)}{1+km-\exp(-m-1/u)}$$
$$u = \frac{u_s}{u_s^0}$$

(7-18)

where σ_W^0 and u_s^0 are scaling factors for the shear stress, σ_W, and slip velocity, u_s, respectively, while m and k are parameters related to the molecular characteristics of the elastomer/wall interfce. These four parameters are considered to be adjustable. The plot of $f(u)$ is sketched in Figure 7-16. It exhibits a non-monotonic behavior with a maximum and minimum and thus can be used to simulate the spurt effect (oscillating melt fracture). Initially, the slip velocity increases with shear stress. This increase is due to the stretching
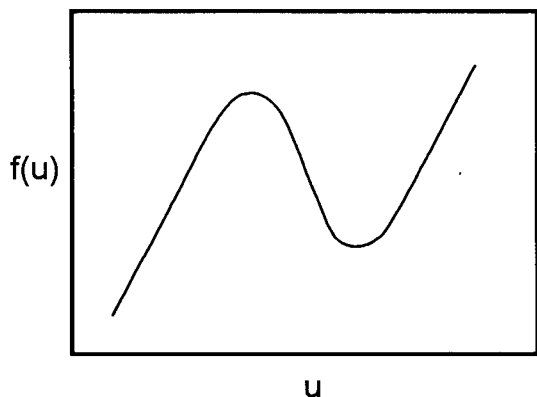
Figure 7-16. Sliding friction curve

of the bonds. On this branch, the slip velocity is microscopic. The second, decreasing branch is due to the rapidly decreasing average concentration of attached bonds that facilitates slip significantly. The third, upper increasing branch is due to a kinetic delay of bond detachment from the wall. Starting with the second branch, the increasing slip velocity is macroscopic. This would correspond to an almost plug flow.

The values of the parameters used in Equation (7-1) are tabulated in Table 7-8.

Table 7-8. Constants for Teflon® FEP 4100

		FEP 4100
Thermal conductivity of the wall *Equation* (7-1)	k_W, W/(m·K)	17.0
	A, K^{-1}	0.01
	K, Pa·s^n	3350
	T_{ref}, °C	350
	α, Pa	$1.2 \cdot 10^{-8}$
	n	0.827

The number of experimental points was 44. The optimal values of the parameters of the slip velocity model calculated from the optimization technique are listed in Table 7-9.

Table 7-9. Calculated parameters of the slip velocity model, Equation (7-18) for Teflon® FEP 4100

Parameter	Teflon FEP
	Equation (7-18)
σ_w^0, MPa	0.4698
u_s^0, m/s	$9.74 \cdot 10^{-4}$
k	3.082
m	0.01

Figure 7-17 shows experimental and predicted flow curves for capillaries having the same L/D ratio and different diameters. As can be seen, the fit is good for the first increasing and decreasing branches of the flow curve. However, for

the second increasing flow rate branch, the fit deteriorates with decrease in the diameter

of the die. It is believed that the problem is related to the slip velocity model used. The

model considers mainly adhesive failure as the causative mechanism of wall slip. While

this may be true for weak slip (the lower branch of the flow curve), the spurt effect

involves cohesive failure through the disentanglement of chains bonded at the interface

from the bulk flow rather than adhesive failure at the interface (Hatzikiriakos *et al.*,
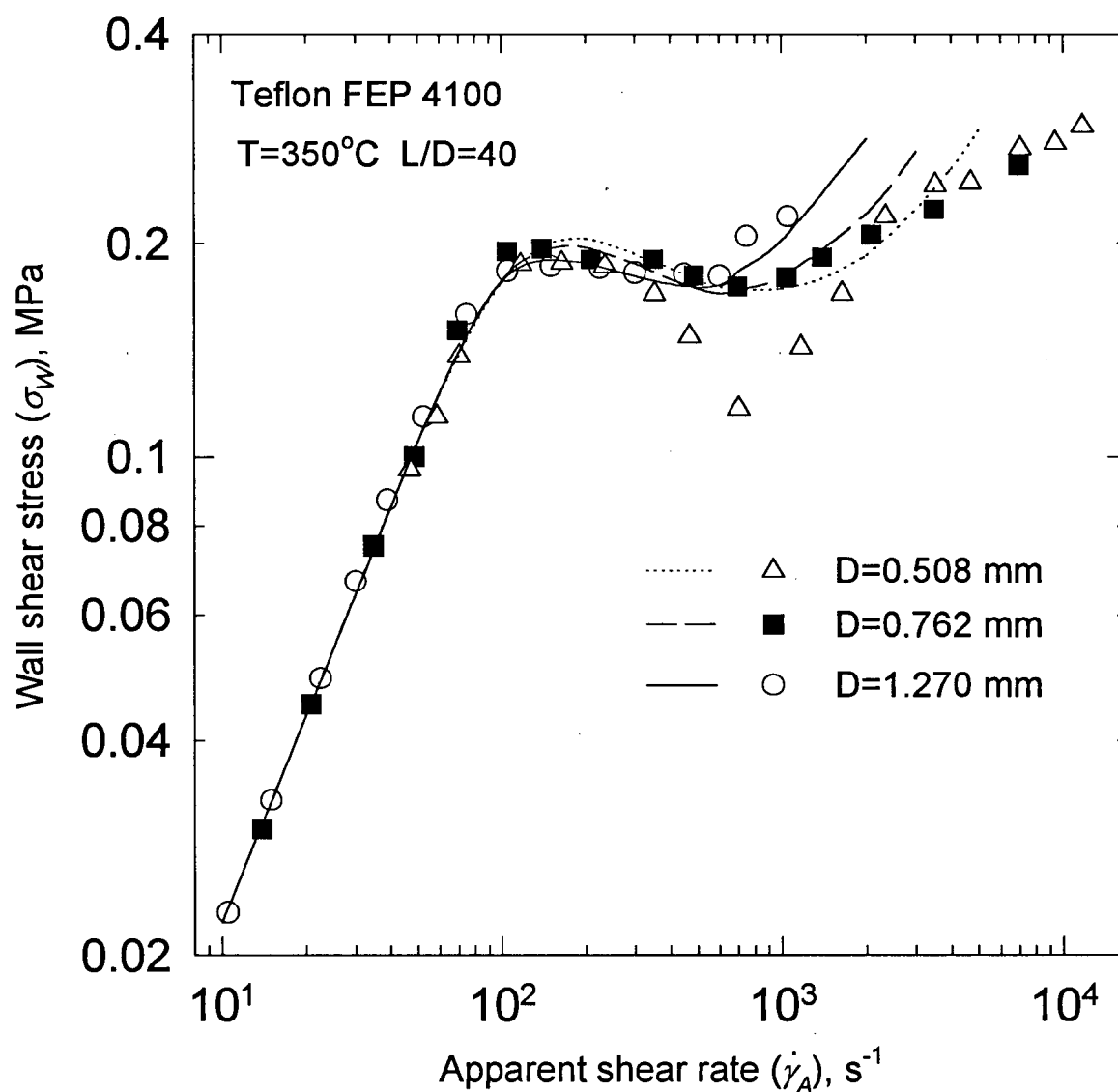
Figure 7-17. Experimental and calculated flow curves for Teflon® FEP 4100 for three
capillary dies having the same *L/D* ratio of 40 and various diameters

1997b; Wang *et al.*, 1996). As a result, the slip model (Equation (7-18)) underestimates the slip velocity for the upper branch of the flow curve, especially for capillaries having smaller diameters where the effect of wall slip is more pronounced. Thus, to describe the stable steady flow of a polymer at high flow rates, a more detailed slip model is required. However, Equation (7-18) is good in predicting the slip velocity up to moderate values of shear rates and suitable for a semi-quantitative description of the flow at high shear rates.

8 Extrusion of Molten Polymers with Processing Aids

he extrusion of fluoropolymers and polyolefins with various processing aids is studied and discussed in this chapter. First, it was found that polyethylene in small amounts of up to 0.1 wt. % works well as a processing aid in the extrusion of Teflon® FEP resins in the same way as fluoropolymers do in the extrusion of polyolefins. It dramatically reduces the pressure drop along the capillary die and eliminates extrudate distortion over the whole range of apparent shear rates up to the superextrusion region.

Second, the influence of a new processing additive (fine particles of boron nitride) on the processability of polyolefins and fluoropolymers in extrusion is studied. The equipment used includes both an Instron capillary rheometer with two types of dies, namely capillary dies and special annular dies (Nokia Maillefer wire coating crosshead) attached to the rheometer, and an extruder. A metallocene polyethylene and several Teflon® fluoropolymers were tested using these two pieces of equipment. The additive had no or very little effect on the extrudate appearance in the capillary geometry (both capillary and orifice dies with a different entrance angle were tested). The greatest influence of the additive occurs in crosshead dies and tips with a streamlined flow, where the additive particles seem to enhance melt slippage and relieve internal stresses. This action eliminates surface melt fracture and postpones the critical shear rate for the onset of gross melt fracture to significantly higher values depending on resin type, temperature, and additive content. To explain the possible mechanism for the effect of the additive on the processability of the resins, rheological measurements using both a parallel-plate and

sliding-plate rheometers were carried out. The rheology of the resins did not seem to change significantly with the addition of boron nitride except for the low-shear-rate (low-frequency) range where the behavior of the filled resin was found to be similar to that of a crosslinked polymer. Practical wire coating and tubing extrusion studies for these resins were also carried out. Finally, the combined effect of the boron nitride and Teflon® particles was found to result in even better processability of the metallocene polyethylene.

8.1 Introduction

It is well known that the rate of production of many polymer processing operations including fiber spinning, film blowing, extrusion, and various coating flows, is limited by the onset of flow instabilities (Petrie and Denn, 1976; Larson, 1992). In particular, as was discussed in Chapter 2, in extrusion processes where the throughput exceeds a critical value, small amplitude periodic distortions appear on the surface of extrudates (surface melt fracture or sharkskin) and at higher throughput rates these take a more severe form of larger irregular distortions (gross melt fracture) (Tordella, 1969). The surface melt fracture is believed to originate in the land of the die next to the die exit (Piau *et al.*, 1990), and gross melt fracture to be initiated at the die entry (Tordella, 1969; Vinogradov and Malkin, 1980).

To increase the rate of production by eliminating or postponing the melt fracture phenomena to higher shear rates, processing additives/aids must be used. These are mainly fluoropolymers that are widely used in the processing of polyolefins (HDPE, LLDPE) and other commodity polymers. They are added to the base polymer at low

concentrations (approximately 0.1%), and they essentially act as die lubricants, modifying the properties of the polymer-wall interface (increasing slip of the molten polymers). As a result of this lubrication effect, the onset of instabilities is postponed to much higher output rates and the power requirement for extrusion is significantly reduced. Note that these additives can eliminate only sharkskin and the so called stick-slip (oscillating or cyclic) melt fracture. To the best of author's knowledge, they do not appear to have an effect on the extrudate appearance in the gross melt fracture region.

One of the objectives of this chapter is to examine the use of polyethylene as a processing aid for Teflon® resins. It is interesting to note that Teflon® has been already been successfully used as a processing aid in polyethylene extrusion to eliminate sharkskin melt fracture (Hatzikiriakos *et al.*, 1994). Therefore, it would also be interesting to examine the opposite case, that is the possible use of polyethylene as a processing aid for Teflon® FEP resins.

Another objective of this chapter is to study the effect of boron nitride (BN) based compositions as a processing aid in the extrusion of a number of fluoropolymers and polyolefins. It is shown that compositions containing BN can be successfully used as processing aids to eliminate not only sharkskin melt fracture but also substantially postpone gross melt fracture to significantly higher shear rates well within the gross melt fracture region in the extrusion of polyolefins and fluoropolymers (Buckmaster *et al.*, 1997). The successful use of the boron nitride additives in two commercially important extrusion processes, namely tubing extrusion and wire coating, are also demonstrated. Finally, the combined effect of the boron nitride and Teflon® APA particles on the processability of polyolefins is examined.

8.2 Polyethylene as a Processing Aid in the Extrusion of Teflon® FEP

8.2.1 Experimental Evidence

FEP copolymers may act as processing aids in the extrusion of linear low density polyethylene, when added at amounts as little as 0.01 % weight. It has been observed that during extrusion, FEP particles that are finely dispersed in polyethylene come into contact with metal dies and displace the polyethylene from the surface. During extrusion, the fluoropolymer particles spread as a result of the shear stress and, as shown by ESCA analysis, eventually form a very thin layer that completely coats the die surface. Due to the poor adhesion characteristics between the polyethylene and the fluoropolymer, the polyethylene slips over the thin fluoropolymer coating. This enhanced slip significantly reduces the pressure required to extrude the polyethylene at a particular flow rate and eliminates sharkskin melt fracture (Figure 8-1). Optimum processing aid performance occurs when the melt viscosities of the polyethylene and the FEP additive are approximately equal. Moreover, to be more effective, the FEP must be dispersed into the polyethylene as very fine particles 0.2 μm in diameter or less.

Figure 8-1. Flow curve of linear polyethylene (PE) and that of polyethylene containing 250 ppm fluoropolymer (from Stewart *et al.*, 1993)

It is perhaps surprising to discover that polyethylene can be used in a similar manner as a processing aid in FEP resins to reduce extrusion pressure and eliminate sharkskin melt fracture. Figure 8-2 shows the apparent flow curves obtained at 350°C for pure FEP 4100 and that of a blend of FEP 4100 with 0.1% by weight of a finely dispersed linear low density polyethylene (GRSN/7047). The capillary die used had an L/D ratio of 40 and diameter of 0.762 mm. No Bagley correction was applied in this plot. It can be seen that the presence of the polyethylene dramatically decreases the shear stress
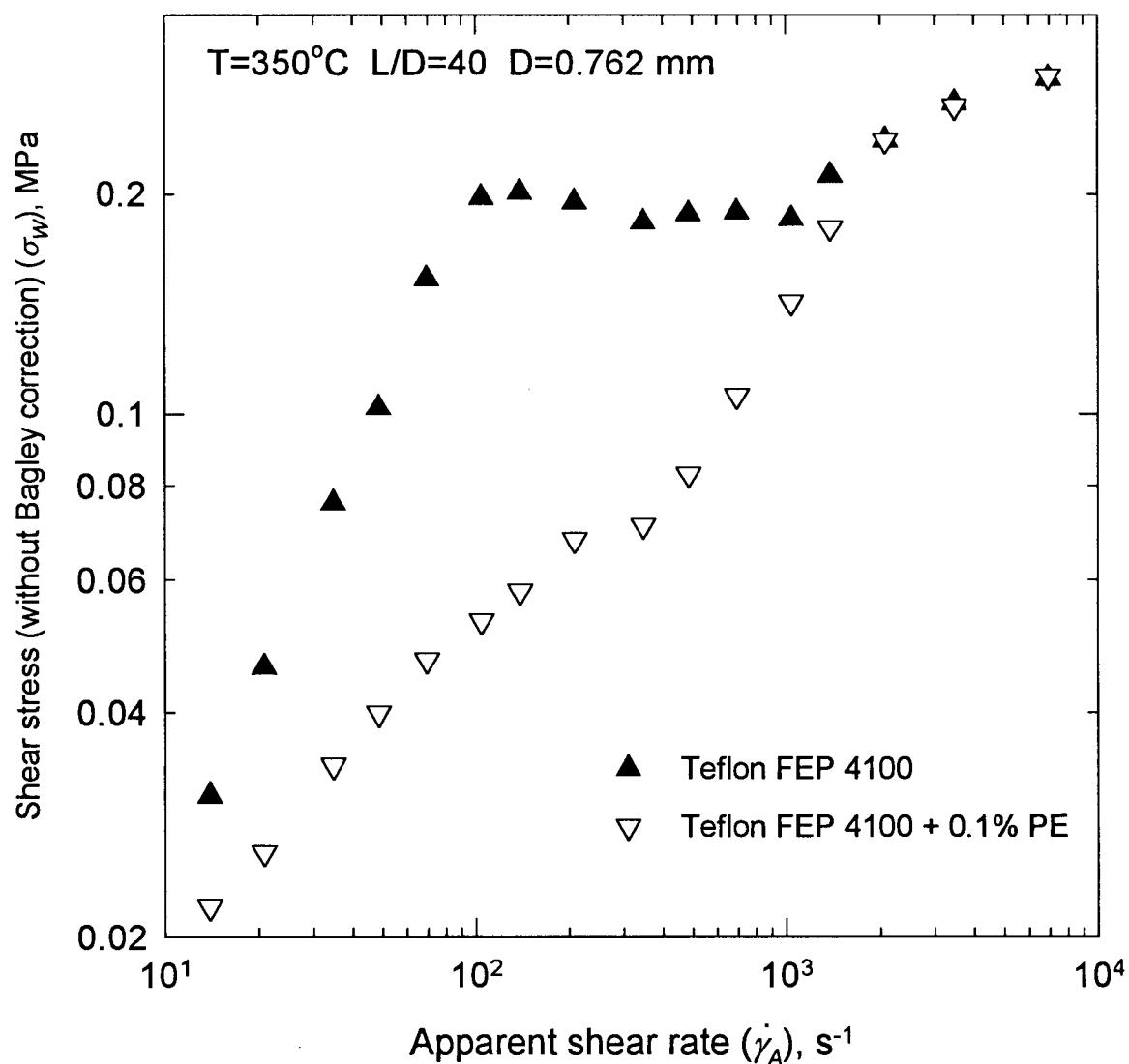
Figure 8-2. The effect of the addition of 0.1 % of polyethylene on the flow curve of resin FEP 4100 at 350 °C

practically over the whole range of apparent shear rates up to those in the superextrusion region (see Chapter 5). The polyethylene eliminates the sharkskin melt fracture, pressure oscillations and oscillating (stick-slip) melt fracture. Thus, the extrudates appear relatively smooth up to the shear rates of 1000 s^{-1}.

8.2.2 Mechanism

In the above experiment, polyethylene particles would tend to diffuse through the bulk of FEP towards the die wall due to its lower viscosity. However, it is the work of adhesion, i.e., the energy required to remove the polymer from the metal surface, that determines which component will eventually coat the die wall. Polyethylene has a greater affinity to metal surfaces than do FEP resins. Therefore, it is not surprising, in this experiment, that the metal die surface eventually becomes coated with a very thin layer of polyethylene. Since there is very little adhesion between FEP and polyethylene, at sufficiently high shear stress values it appears that FEP slips over the thin polyethylene layer on the die wall.

This then raises the question as to why a very small quantity of FEP resin, when finely dispersed in polyethylene, will completely coat the die wall during extrusion. The answer again lies in the relative values of the work of adhesion. Although the work of adhesion of FEP to base metal is less than the work of adhesion of polyethylene to metal, the work of adhesion of polyethylene to FEP is much less than either of these. Thus, if a very small FEP particle that is dispersed in polyethylene comes into contact with the metal die surface during extrusion, there will be very little force at the FEP/polyethylene interface acting to pull the particle off the surface. The polyethylene will slip over this

interface and will cause the particle to spread. On the other hand, the force acting to pull the polyethylene off the surface is the result of the wall shear stress during extrusion. The overall result is that the FEP particles accumulate, spread, and eventually form a very thin coating on the die over which the polyethylene can slip.

A similar behavior of other polymer blends was observed by Shih (1979). Examination of a broad range of fluorocarbon/hydrocarbon blends has led to the following general observations. To be effective, the minor component must be in a finely divided state, having particle diameter less than about 0.2 μm. It must also be at a very low concentration of less than about 1% by weight. For optimum performance, the viscosities of the two polymers should be approximately equal. The relative work of adhesion between the two polymers and the metal surface and between the polymers themselves determine the final performance. For example, fluoropolymers will displace nonpolar hydrocarbons with low work of adhesion, but will not displace polar polymers such as nylon, polyesters or poly(methyl methacrylate) from metal surfaces because of the very high value of the work of adhesion of these polymers with metals.

8.2.3 Transient Coating Experiments

The following transient experiments illustrate the process of wall coating by the polyethylene additive. In Figure 8-3a the apparent shear stress transient is plotted for the capillary extrusion of pure FEP 4100. The shear stress builds up rapidly until it assumes a steady-state value. When the blend of FEP 4100 + 0.1% PE is extruded through a clean die (Figure 8-3b), the shear stress passes through a maximum and as the polyethylene coats the interface, slip becomes a factor, and, as a result, the shear stress decreases. The

steady-state value is obtained after filling the reservoir several times (5 times). It should

be noted, however, that this response is not due to the degradation of polyethylene. Pure

polyethylene was extruded several times at these high temperatures for about one hour,

and in all cases the apparent shear stress remained practically constant.

The time required to obtain steady-state operation (steady shear stress) depends

on the apparent shear rate, the L/D ratio, and the diameter of the capillary die. The effects
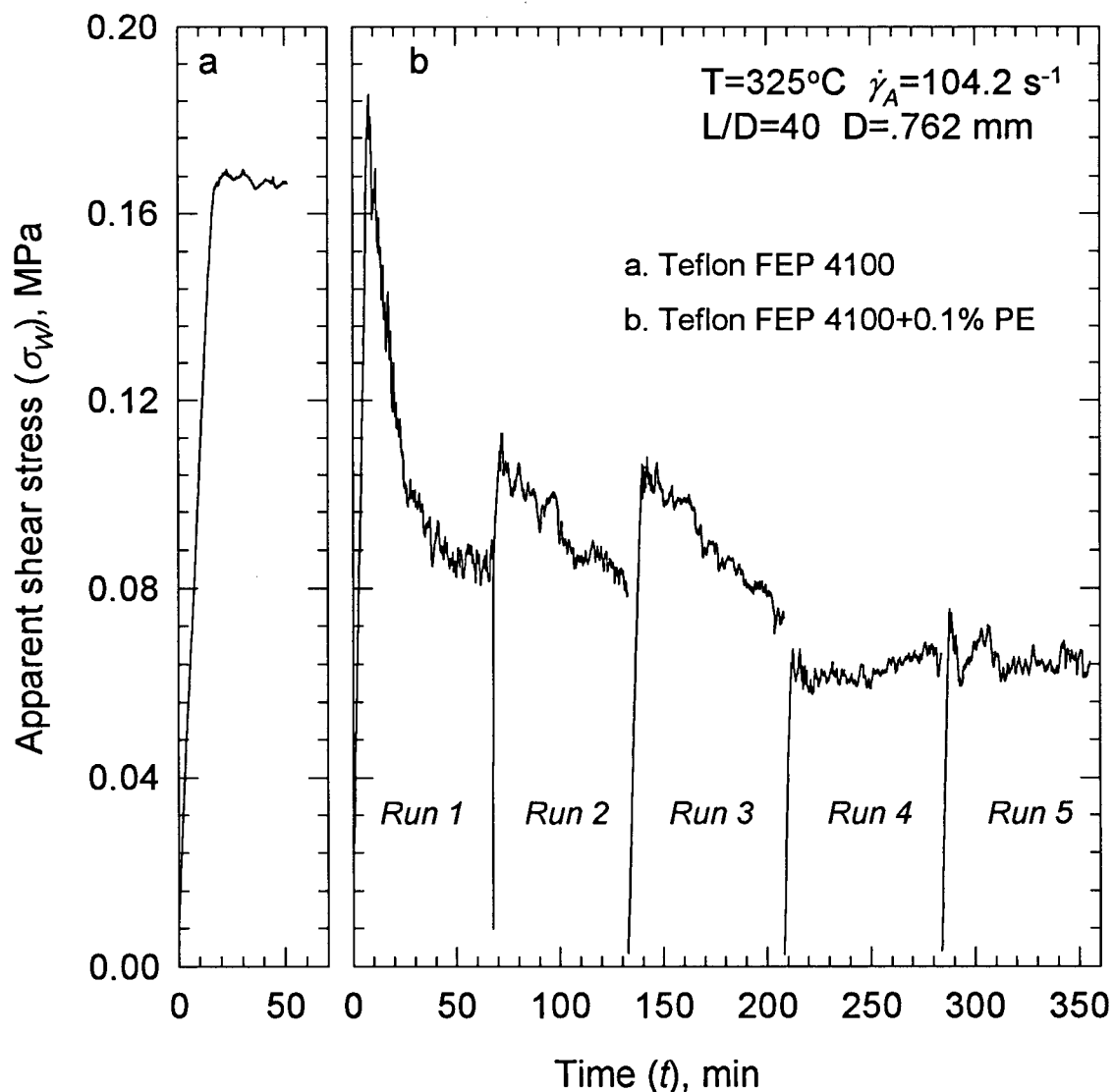
Figure 8-3. The effect of the addition of 0.1 % of polyethylene on the transient response in the capillary extrusion of FEP 4100 at 325 °C, $\dot{\gamma}_A$=104.2 s^{-1}, L/D=40 and D=0.762 mm.

of these parameters on the time required to obtain a steady-state response are illustrated

in Figures 8-4, 8-5, and 8-6, respectively. Specifically, Figures 8-4a, 8-5a, and 8-6a

illustrate the transient response in the absence of polyethylene, while Figures 8-4b, 8-5b,

and 8-6b illustrate the corresponding response with the addition of 0.1% polyethylene.

These figures should be compared with Figure 8-3 in order to observe the relative effect.

It can be seen that the time required to obtain steady state operation decreases with

increase in the apparent shear rate, and decreases with a decrease in the L/D ratio and

diameter of the capillary die. This should be expected if one interprets this time as the

time required to obtain a complete uniform coverage of the interface with polyethylene.

Thus, this time should be proportional to the area being coated. This means that decreas-
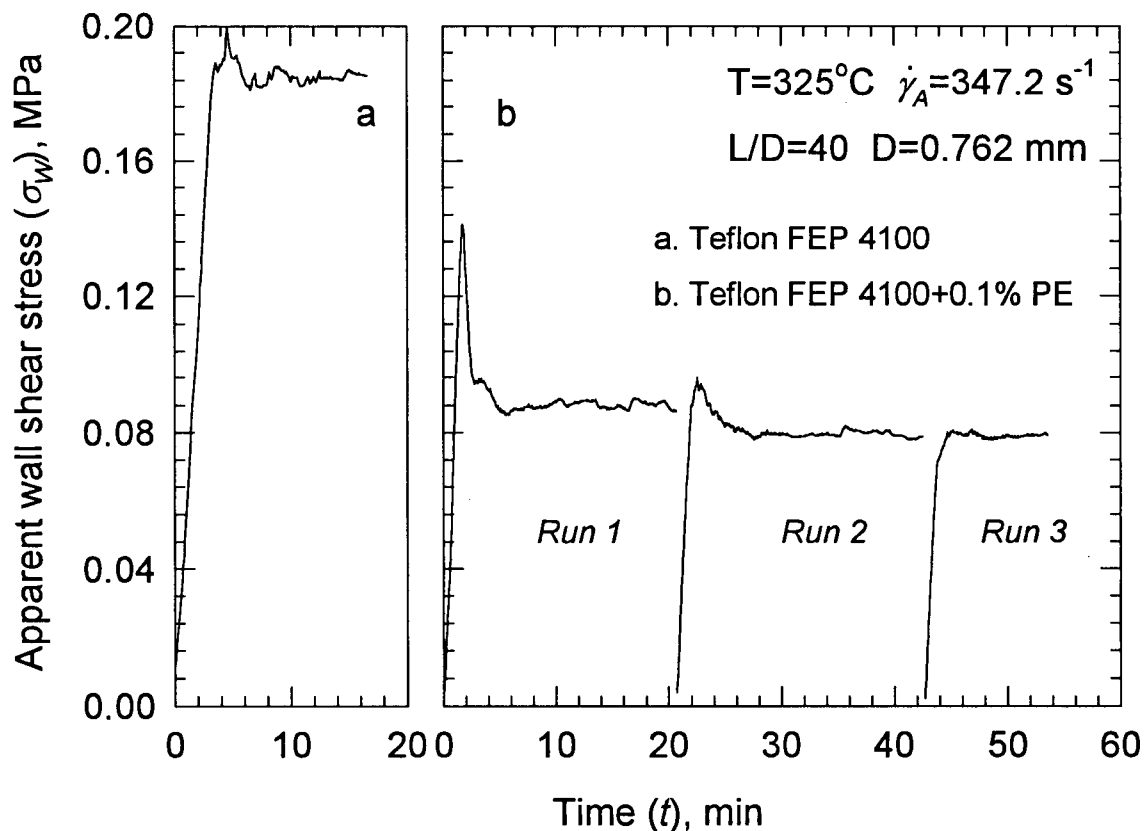
Figure 8-4. The effect of the apparent shear rate on the time required to obtain steady state operation in the capillary extrusion of FEP 4100 with the addition of 0.1 % of polyethylene (T=325 °C, $\dot{\gamma}_A$=347.2 s⁻¹, L/D=40 and D=0.762 mm). To see the effect compare with Figure 8-3
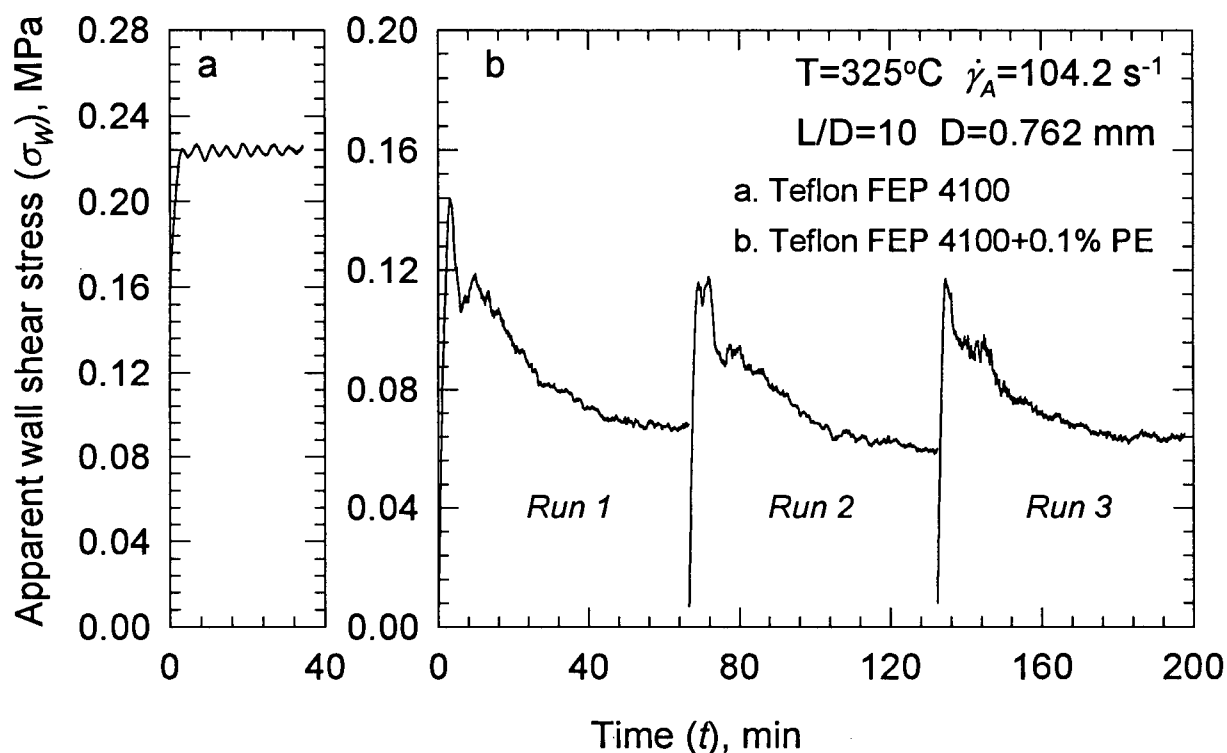
Figure 8-5. The effect of the L/D ratio of the capillary die on the time required to obtain steady state operation in the capillary extrusion of FEP 4100 with the addition of 0.1 % of polyethylene (T=325 °C, $\dot{\gamma}_A$=104.2 s^{-1}, L/D=10 and D=0.762 mm)
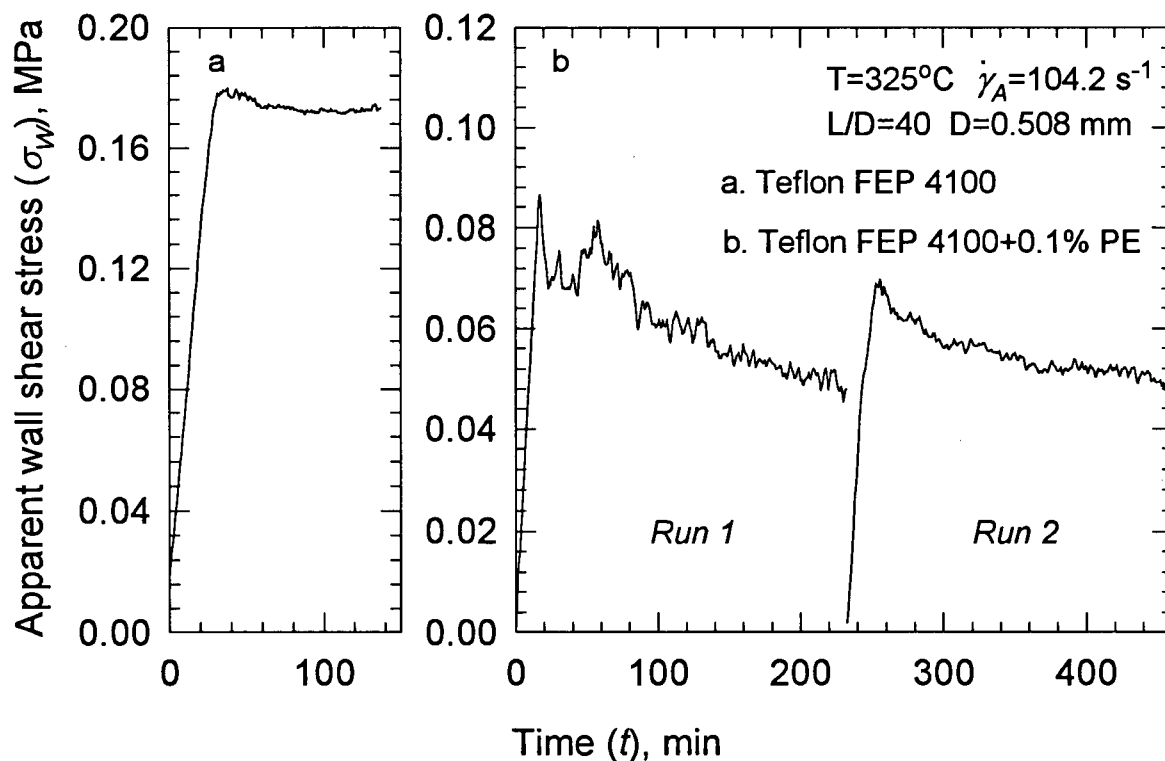
Figure 8-6. The effect of the diameter, D, of the capillary die on the time required to obtain steady-state operation in the capillary extrusion of FEP 4100 with the addition of 0.1 % of polyethylene (T=325 °C, $\dot{\gamma}_A$=104.2 s^{-1}, L/D=40 and D=0.508 mm)

ing the L/D ratio or diameter, D, and keeping all the other variables fixed decreases this area, and, therefore, the time required to obtain steady state operation decreases. On the other hand, increasing the apparent shear rate, the rate of the coating process increases, while the required time for steady-state operation decreases.

8.3 Extrusion of Fluoropolymers and Polyolefins with Boron Nitride as a Processing Aid

8.3.1 Experimental Evidence

The present section discusses the use of boron nitride as a processing aid for the extrusion of fluoropolymers and polyolefins (Buckmaster *et al.*, 1997). In polymer processing, it is used as a foam nucleating agent, and when added to the polymer melt acts as a very effective processing aid as will be seen in the present chapter.

Boron nitride is a solid lubricant whose structure resembles that of graphite (see Figure 8-7). In polymer processing, it is used as a

Key
● Boron
O Nitrogen

Figure 8-7. Structure of BN

foam nucleating agent in most commercial applications for fluoropolymer foams such as heat insulation, foamed tubing, etc. In the presence of a blowing agent added to the molten resin during extrusion, it nucleates the formation of voids in polymer extrudate. In this study, BN particles are used without a blowing agent, so that the extruded polymer is

unfoamed. The amount of boron nitride effective in providing improved extrusion performance can be as little as 0.001 wt %, preferably about 0.01wt %. It is used in combination with some other inorganic nucleating agents such as calcium tetraborate in amounts from 0.002 to 0.04 wt %.

During the extrusion of fluoropolymers or polyolefins with BN particles, the maximal shear rate at which the extrudate appears smooth is usually orders-of-magnitude higher than can ordinarily be achieved in the absence of this additive. More importantly, this maximal shear rate is usually much higher than that at which the virgin resin exhibits gross melt fracture. This means that BN, unlike fluoropolymers in the extrusion of polyethylene, can eliminate not only surface and stick-slip melt fracture but also significantly delay the onset of gross melt fracture to much higher shear rates. Specific examples of its use can be found below.

Another requirement of the process is that the extrusion experiments be carried out with a special crosshead die of the type used for wire coating. The significance of this statement is that similar experiments with BN repeated in a capillary rheometer do not result in a significant improvement of the processability of the resins. In other words, BN has little or no effect on melt fracture in a capillary die.

8.3.2 Extrusion Experiments

The two groups of polymers studied are polyolefins and fluoropolymers. The former includes two metallocene catalyzed polyethylenes, Exact® 3128 and Exceed® 116 (Exxon), and the latter involves the following DuPont Teflon® fluoro-copolymers of tetrafluoroethylene/hexafluoropropylene (Teflon® FEP) resins: type 100 (melt flow rate is

6.9), 3100 (17), 4100 (22), 5100 (20), and the following copolymers of tetrafluoro-ethylene/perfluoro-(propyl vinyl ether) (Teflon® PFA): type 340 (14.7), 345, and 350 (1.8).

Both rheometer and extrusion equipment were used to determine the shear rate at which smooth extrudates can be produced. The rheometer is the standard Instron piston-driven constant-speed capillary unit described previously. Two types of dies were used, namely circular dies having a 90° entrance angle, and a special annular crosshead die attached to the rheometer to simulate the wire coating process (see Figure 8-8). The crosshead was a Nokia Maillefer 4/6 that included dies and tips of various diameters ("tip" is the wire guide) with equal entry cone angles of 60° and the die land length of 7.62 mm. The molten polymer enters the die 2 via port 11 and is forced around the wire guide 16 towards the die orifice 8. The wire guide serves as a mandrel for the molten polymer, giving the extrudate 10 a tubular shape. The die passage 4 forms the exterior surface of the tubular shape, and the exterior surface of the cylindrical extension 24 forms
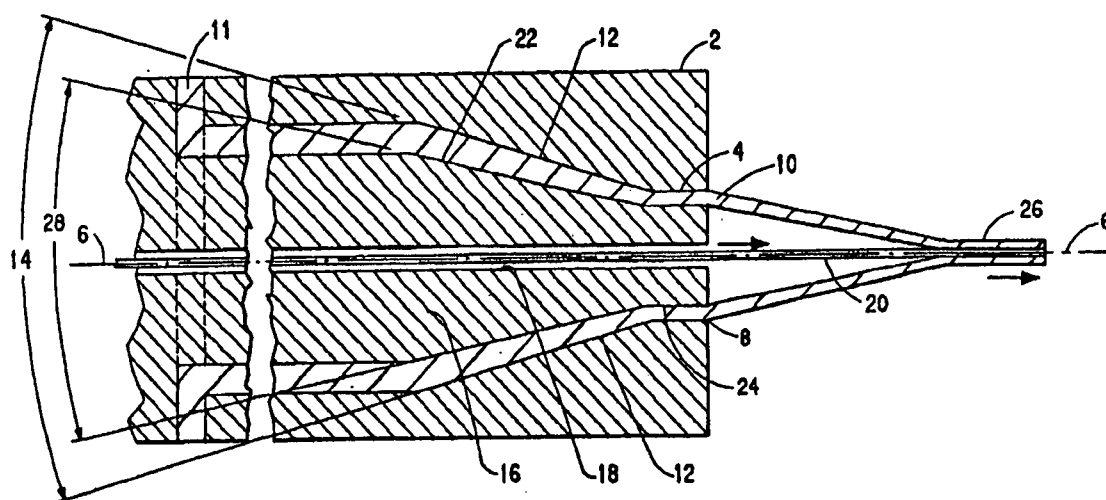
Figure 8-8. Crosshead die for wire coating (from Buckmaster *et al.*, 1997)

the interior surface of the tubular shape. The greater speed of the wire compared to the polymer extrusion rate causes the polymer coming into contact with the wire at a point remote from the orifice 8 to draw down to a thinner cross-section, forming a thin polymer coating 26 on the wire. This is a melt draw-down extrusion process with draw down ratio (DDR), which is the ratio of die orifice area to cross-sectional area of the polymer insulation, of at least 5:1. However, in the present study the pressure extrusion makes no use of wire and therefore DDR is irrelevant.

The extrusion equipment involved a 31.725 mm Entwistle extruder having a 31:1 length to diameter ratio and equipped with the same crosshead extrusion die. The Entwistle extruder with the Maillefer crosshead was also used for producing polyethylene tube, and a 45 mm extruder was used for a practical wire coating test with fluoropolymers. The working temperature was 163°C (325°F) and 204°C (400°F) in the case of polyethylene, 371°C (700°F) for FEP resins, and 385°C (725°F) for PFA resins. Composition resins with BN content varying from 0.01 to 2.5 mass %, along with virgin resins, were tested over a wide range of apparent shear rates from 10 to 7000 s^{-1}. All compositions were prepared by extrusion of the boron nitride/resin mixture in a 28 WP twin screw extruder.

8.3.3 Polyolefins

Figure 8-9 shows the flow curves of the virgin and filled Exact® 3128 (metallocene LLDPE) obtained using the capillary rheometer with a capillary die having D=0.762 mm and L/D=0 at T=163°C. The Bagley correction was determined by using an orifice die of

equal diameter and subsequently was applied to the raw data in order to get accurate

values for the wall shear stress. In the case of the virgin resin, sharkskin appears at about

35 s^{-1} followed by stick-slip and gross melt fracture at higher shear rates. The addition of

0.05% BN to the resin does not seem to noticeably change the rheology since the two

flow curves almost coincide. However, it has an effect on the extrudate appearance,

eliminating extrudate distortions in the range of shear rates corresponding to transition

from sharkskin to stick-slip melt fracture. This was the only case where a difference in
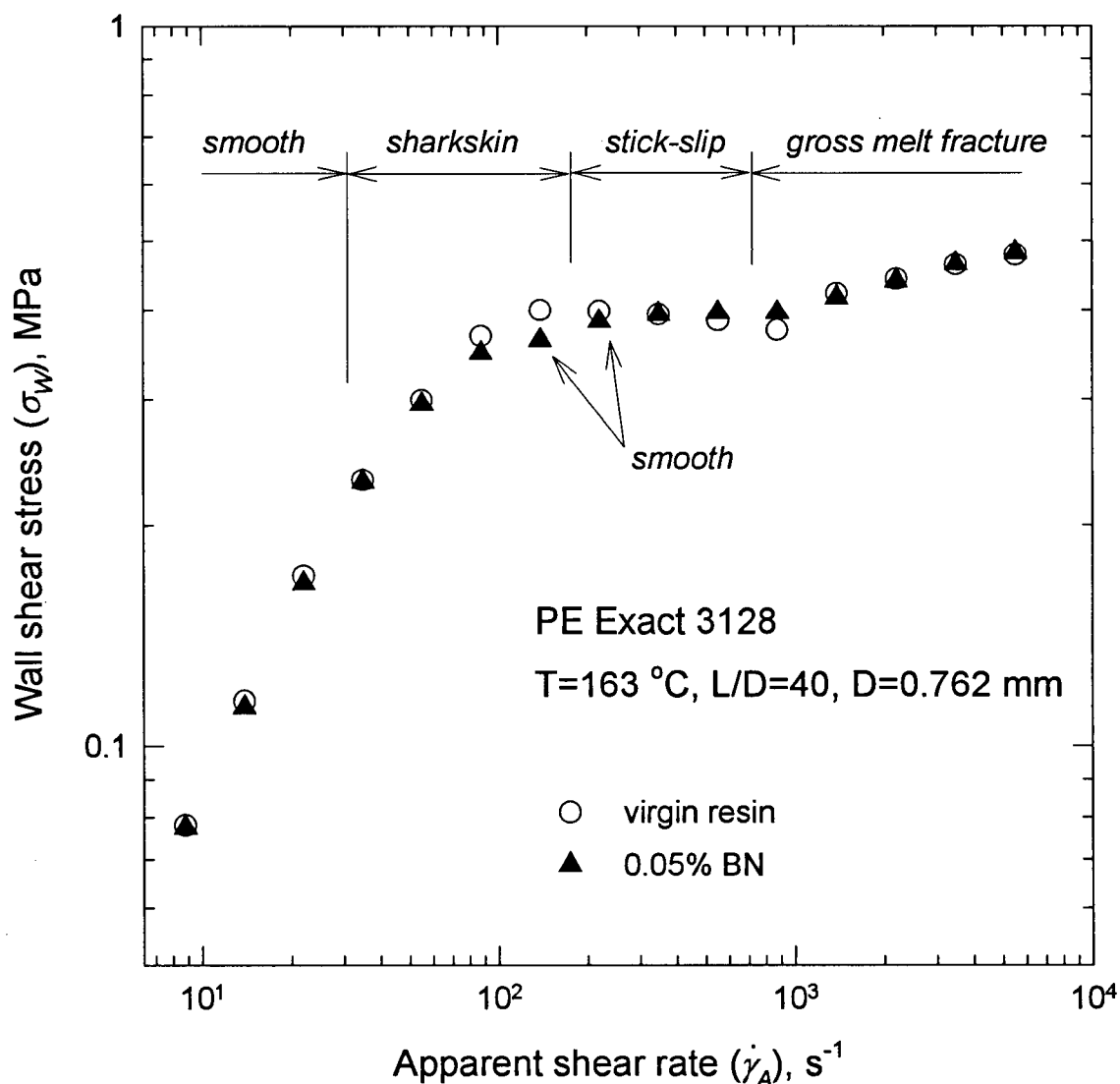
Figure 8-9. The flow curves for PE Exact 3128 without and with boron nitride obtained in a rheometer with a capillary die having L/D=40 and D=0.762 mm at 163 °C

performance between the virgin resin and the corresponding filled resin was found using a rheometer with a circular dies. All the other resins tested showed almost identical performance in traditional capillary rheometer tests for both the virgin and BN filled resins. A possible explanation for this will be discussed later.

However, when the same resins were run through the Maillefer crosshead die attached to the same rheometer at the same conditions, one can obtain completely different results. Figure 8-10 presents two flow curves obtained for the virgin resin and
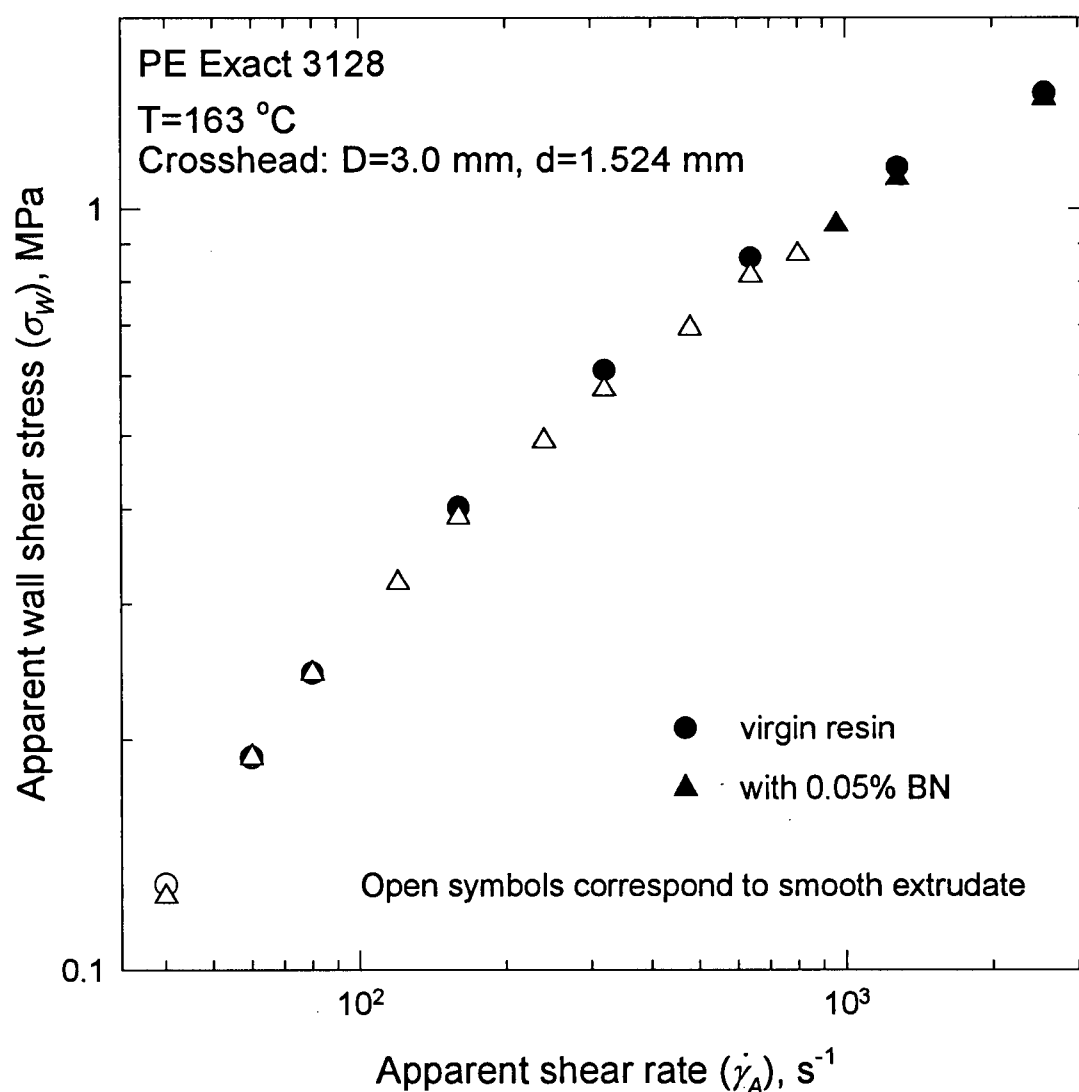
Figure 8-10. The apparent flow curves for PE Exact 3128 without and with boron nitride obtained in a rheometer with Nokia Maillefer crosshead having 3.00 mm die and 1.52 mm tip at 163 °C

that with 0.05% BN using a 1.524 mm tip and 3 mm die at $T=163°C$. The apparent shear rate was calculated by using the formula which applies to slit dies:

$$\dot{\gamma}_A = \frac{6Q}{0.25(D-d)^2\,0.5\pi(D+d)} \qquad (8\text{-}1)$$

where Q is the volumetric flow rate, d and D is the tip and die diameter, respectively. The apparent wall shear stress was estimated as the average of the stress at the inner and outer walls by using the following formula for a power-law fluid (Bird *et al.*, 1987):

$$\tau_{rz} = \frac{\Delta P D}{4L}\left(\frac{2r}{D} - \beta^2\,\frac{D}{2r}\right) \qquad (8\text{-}2)$$

where τ_{rz} is the shear stress at radius r, ΔP is the pressure drop, L is the length of the die land, and β is a parameter which depends on the geometry and the power law index (Bird *et al.*, 1987). The virgin resin starts exhibiting melt fracture at about 50 s^{-1}. The addition of BN virtually eliminates melt fracture in the broad range of apparent shear rates up to approximately 900 s^{-1}. This value corresponds to the region where gross melt fracture occurs. This is extremely important since BN seems to eliminate not only sharkskin and stick-slip melt fracture but also postpones gross melt fracture to higher rates. Such an effect has not been previously observed with other additives.

Experiments in the extruder showed that the maximal shear rate yielding a smooth extrudate is sensitive to the BN content. In Figure 8-11, one can see that optimal performance was obtained with the BN content of 0.01%; this composition resulted in a maximum shear rate for the onset of distortions of about 1000 s^{-1}. Increase in the BN concentration above 0.01% resulted in gradual decrease in the limiting shear rate for the onset of flow instabilities. Moreover, the highest concentration of BN (0.5%) did not completely eliminate sharkskin at low shear rates. This means that there exists a critical

concentration for optimal performance, which depends on the type of the resin and additive formulation.

To study the effect of temperature, the same compositions were tested at two different conditions, 163°C and 204°C. Figure 8-12 shows that increase in temperature shifted the apparent shear rate for the onset of melt fracture from 50 to 130 s^{-1} for the virgin resin. An addition of 0.01% BN had little effect; the onset of sharkskin was
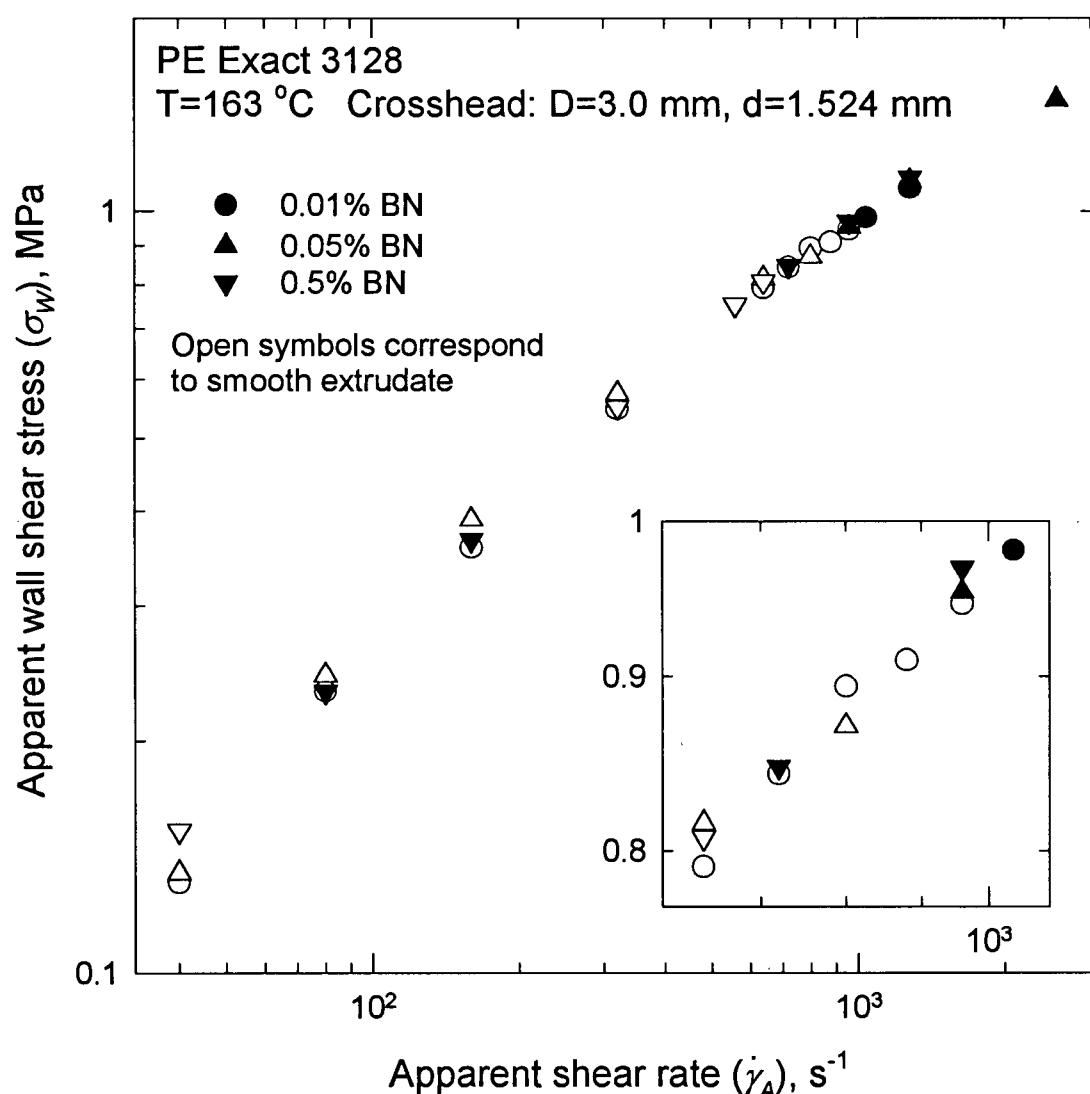
Figure 8-11. The effect of the boron nitride concentration on the processability of PE Exact 3128 in an Entwistle extruder with Nokia Maillefer crosshead having 3.00 mm die and 1.52 mm tip at 163 °C

delayed until 200 s^{-1}. With 0.05% BN, the polymer could be extruded at shear rates up to

1300 s^{-1} before the extrudate surface exhibited melt fracture. Further increases in the BN

content produced even greater improvements: at 0.1% BN the extrudate was smooth up to

1500 s^{-1}, and at 0.5% BN the limiting shear rate was 1600 s^{-1}, the maximum value

obtained. These results show that the optimal concentration of BN is significantly

influenced by the extrusion temperature.
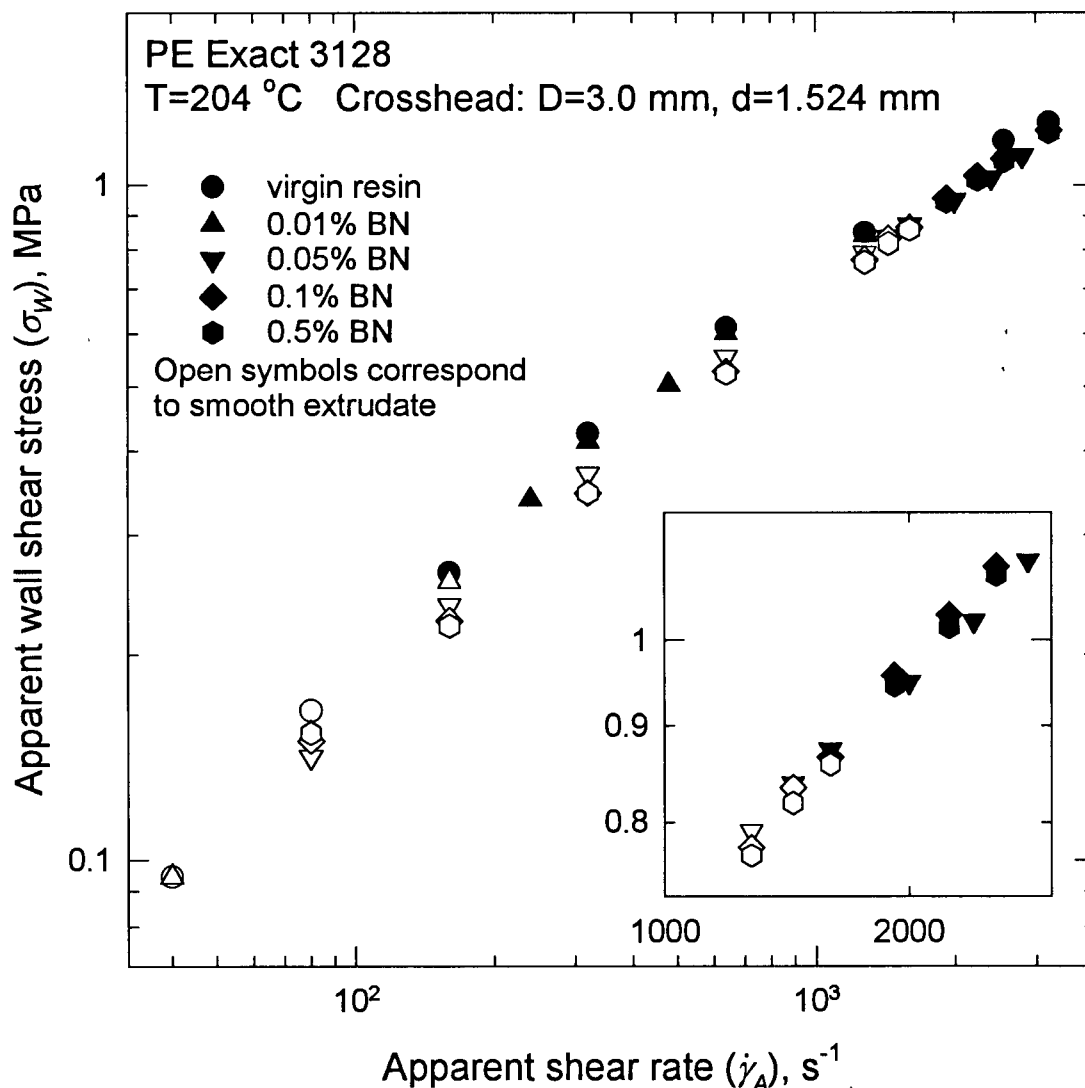
Figure 8-12. The effect of the boron nitride concentration on the processability of PE
Exact 3128 in an extruder with the crosshead having 3.00 mm die and 1.52
mm tip at 204 °C

Figure 8-13 shows photos of the extrudate samples obtained in the extrusion of PE Exact 3128 with and without BN. One can see that an addition of 0.01 wt.% BN results in smooth extrudate at shear rates where the extrudate would normally exhibit gross melt fracture.
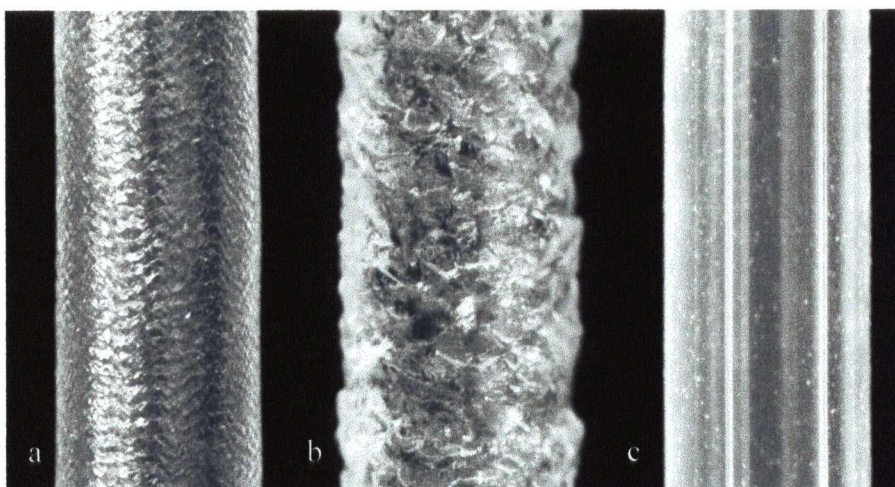
Figure 8-13. The extrudate samples of metallocene PE Exact 3128 at 163°C: a) sharkskin for pure PE at $\dot{\gamma}_A$=80 s^{-1}; b) gross melt fracture for pure PE at $\dot{\gamma}_A$=800 s^{-1}; c) smooth extrudate for PE with 0.01% BN at $\dot{\gamma}_A$=800 s^{-1}

Finally, a practical tubing test was carried out with Exact resin using the Maillefer crosshead at a melt temperature of 163 °C. The die and tip diameters are 3.1 mm and 1.53 mm. Smooth surfaced tubing was processed having a 2.13 mm outer diameter and 0.94 mm inner diameter at 600 s^{-1}. The loading of the BN was less than 0.05%.

8.3.4 Fluoropolymers

The rheological performance of FEP 100 resin was studied using the crosshead die mounted on the capillary rheometer. The maximum shear rate limit for achieving a smooth surface of extruded virgin FEP 100 resin was about 90 s^{-1}. The same resin with

the addition of 0.25% BN could be run without extrudate defects up to 140 s^{-1} and from

550 to approximately 1000 s^{-1}. The tests using the extruder with the same crosshead die

showed that in the presence of small amount of BN, smooth extrudate can be obtained for

the entire range of shear rates up to 4000 s^{-1}, which is well beyond the onset of gross melt

fracture for the extruded pure resin (Figure 8-14). It is believed that the difference in

performance between the rheometer and the extruder with the same crosshead die is due

to the much better mixing in the barrel of the latter. A decrease in the BN content to
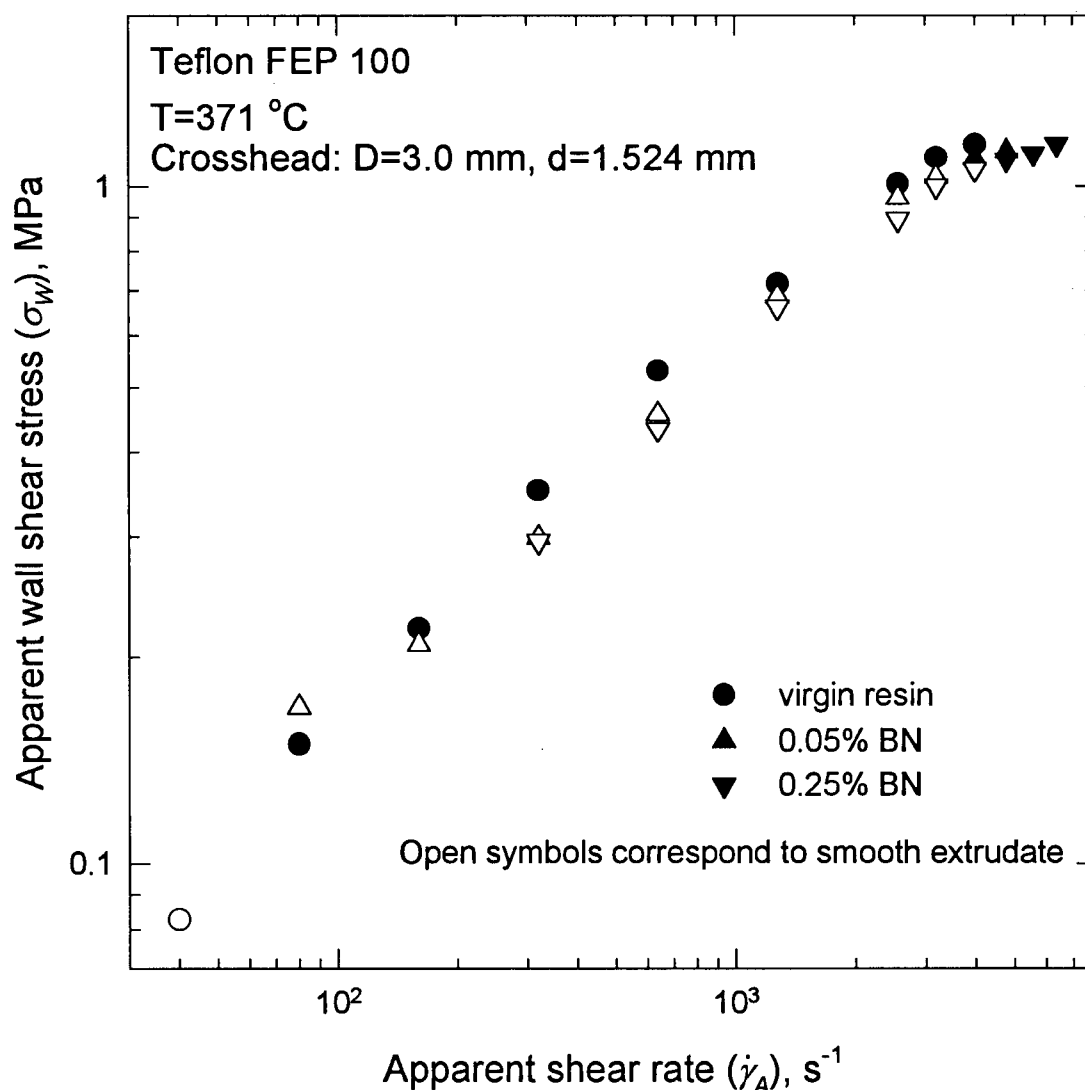
Figure 8-14. The effect of boron nitride on the processability of Teflon FEP 100 in an Entwistle extruder with the crosshead Nokia Maillefer having 3.00 mm die and 1.52 mm tip at 371 °C

0.05% resulted in a drop in the maximum shear rate for the onset of flow instabilities to about 3200 s^{-1}. Figure 8-15 shows photos of the extrudate samples of FEP 100 obtained in an extruder at 371°C.

The detailed rheological study of the FEP 4100 and 3100 resins using a capillary rheometer can be found in Chapter 5. In the superextrusion region, where the virgin extrudate is smooth, extrusion through the crosshead die does not produce as pronounced a supershear range as that through a circular die at 371°C. The extruder and Maillefer crosshead studies with the FEP 4100 filled with 0.17% of BN and dried overnight at 150°C yielded smooth extrudates at shear rates as high as 6000 s^{-1} (Figure 8-16). At 0.035% BN content, the maximum shear rate was 3200 s^{-1}. A similar performance was observed with FEP 3100 and FEP 5100.

The PFA fluoropolymers have higher melting points than FEP resins, so they were studied at the increased temperature of 385°C. Extrusion tests with the crosshead and the virgin PFA 340 resulted in melt fracture at a shear rate of about 100 s^{-1}, while the resin
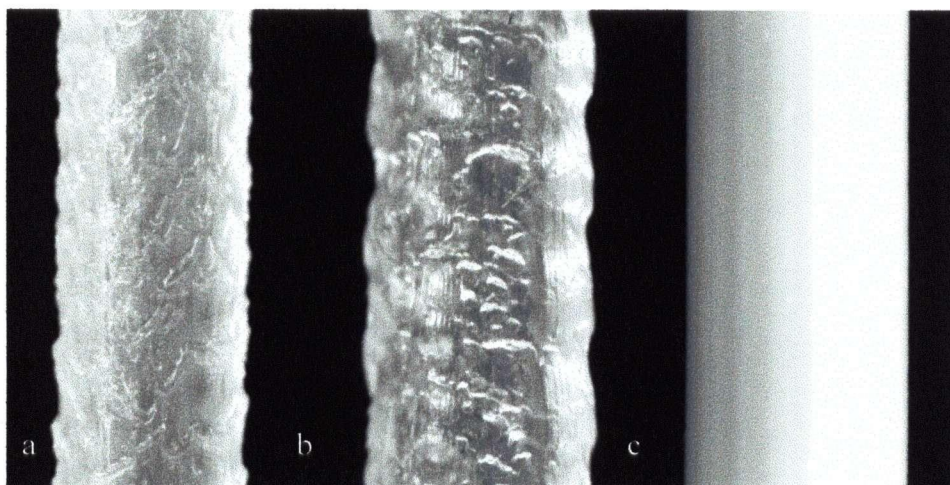
Figure 8-15. Extrudate samples of Teflon® FEP 100 at 371°C: a) sharkskin for pure PE at $\dot{\gamma}_A$=320 s^{-1}; b) gross melt fracture for pure PE at $\dot{\gamma}_A$=4000 s^{-1}; c) smooth extrudate for PE with 0.25% BN at $\dot{\gamma}_A$=4000 s^{-1}

with 0.25% BN could be processed without melt fracture up to 2000 s^{-1}. To summarize the results obtained for all the resins studied, the maximum shear rate at which the inner and outer surfaces of the tubing were smooth are shown in Table 8-1.

Finally, wire coating tests on FEP 4100 were carried out in the 45 mm Nokia Maillefer extruder with the crosshead having a 3.81 mm die and 1.905 mm tip. The screw speed was 11.6 rpm, and the melt temperature 388°C. The composition with 0.1% BN
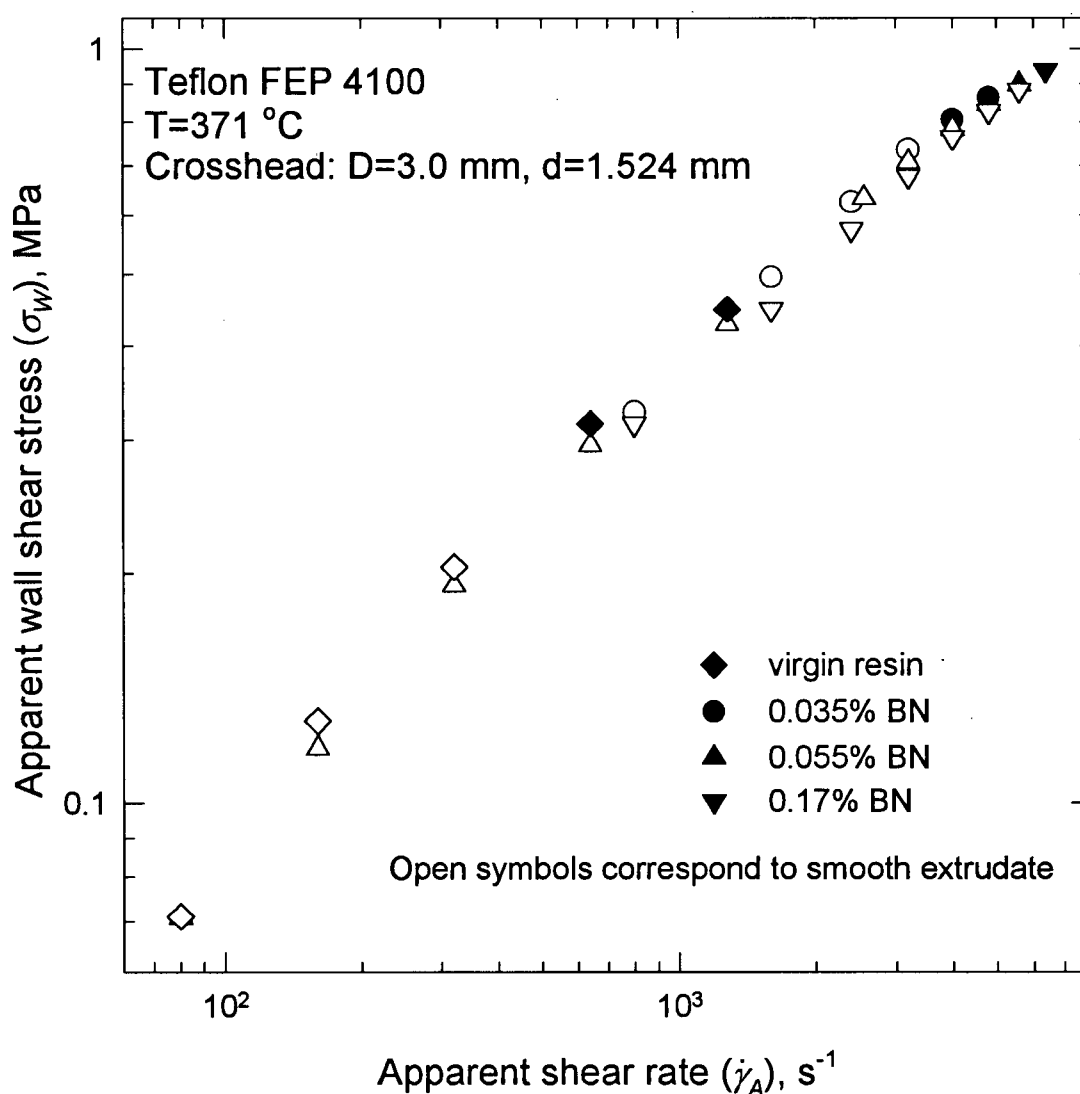
Figure 8-16. The effect of boron nitride on the processability of Teflon® FEP 4100 in an Entwistle extruder with the crosshead Nokia Maillefer having 3.00 mm die and 1.52 mm tip at 371 °C

was successfully run to obtain smooth inner and outer insulation surfaces at 100 m/min which corresponds to shear rates of approximately 800 s^{-1}. This shear rate was several times greater than that at which smooth interior surface insulation could be obtained for the virgin resin. Figure 8-17 compares the tightness of the insulation obtained with and without BN at the above conditions.

Table 8-1. Influence of boron nitride concentration upon tubular extrudate surface smoothness (extrusion tests in the Entwistle extruder with Nokia Maillefer crosshead 3.0 mm die and 1.52 mm tip)

T, °C	BN concentration, mass %	Maximum shear rate to yield smooth extrudate, s^{-1}
Polyethylene Exact® 3128		
163	0	50
	0.01	960
	0.05	800
	0.5	640
204	0	100
	0.01	200
	0.05	1280
	0.1	1440
	0.5	1600
FEP 100		
371	0	40
	0.05	3200
	0.25	4000
FEP 4100 (FEP 5100)		
371	0	350
	0.035	3200
	0.055	4000
	0.17	5600
FEP 3100		
371	0	250
	0.25	6000
PFA 340		
385	0	50
	0.25	2000
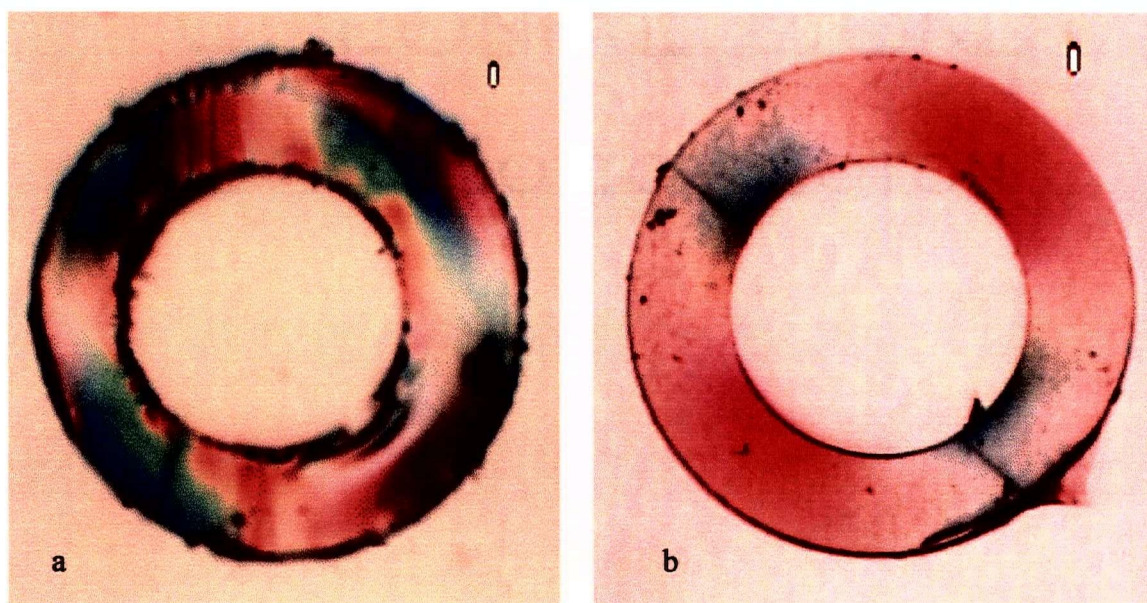
Figure 8-17. Teflon® FEP 4100 insulation samples obtained in 45 mm extruder with the crosshead having a 3.81 mm die and 1.905 mm tip: a) virgin resin; b) with the addition of 0.1% BN

8.3.5 Mechanism

To explain the effect of BN on the performance of fluoropolymers and polyolefins during the extrusion in a wire coating crosshead die, the following possible mechanisms will be discussed:

- Change in the rheology

- Effect of die geometry

- Wall slip

There may be some other explanations for this phenomenon; however, only these possible scenarios are considered below. In the following discussion, we concern ourselves only with metallocene PE. It is believed that the mechanism of the BN effect is

the same regardless of the nature of the polymer. It is noted that PE is a material that is much easier to work with compared to Teflon® FEP. This is mainly due to the lower operating temperature of the former.

8.3.5.1 Change in Rheology

To study possible effects of the BN addition to the resin on the rheology of a
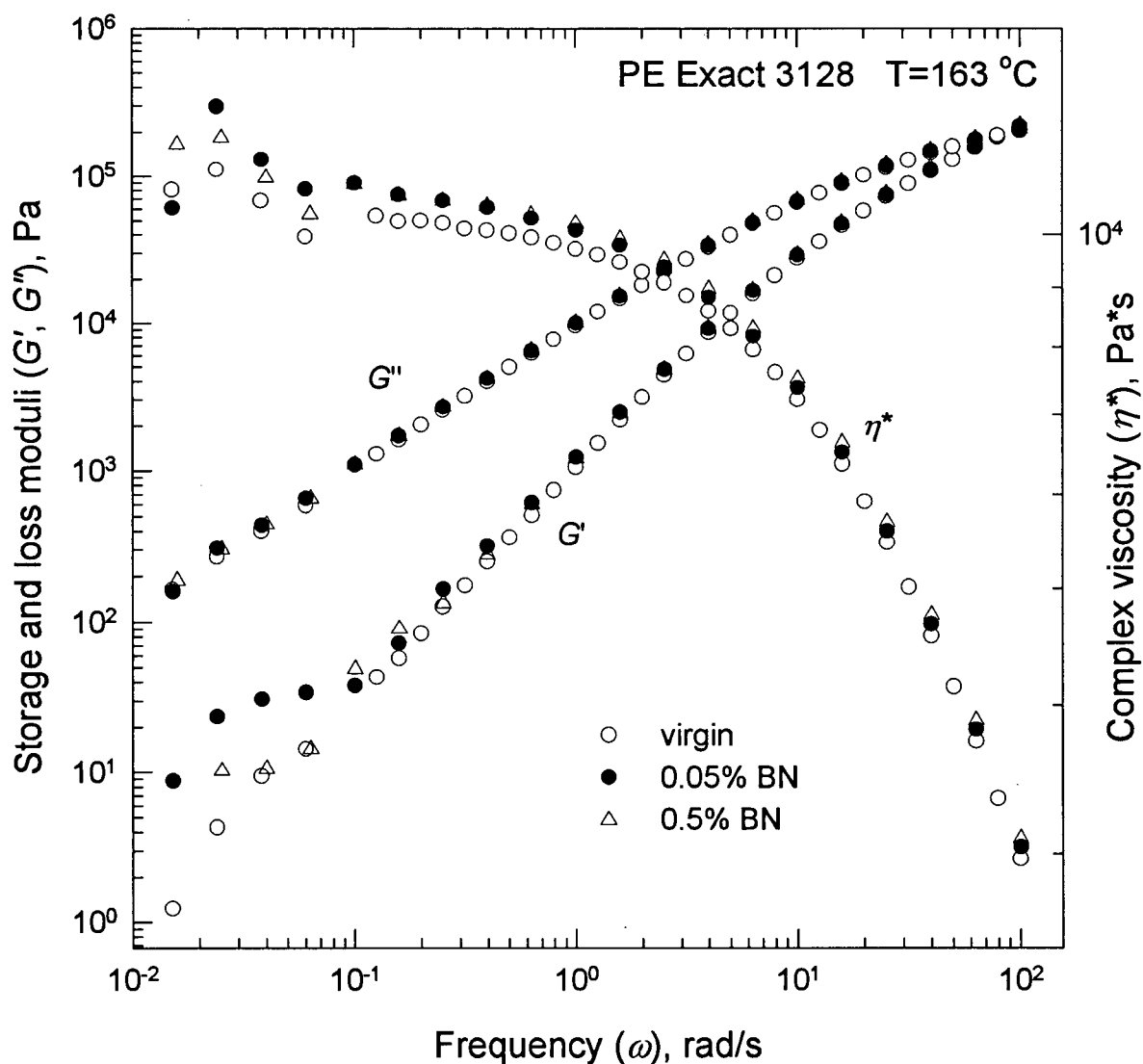
Figure 8-18. Dynamic moduli and complex viscosity of metallocene PE Exact 3128 (with and without BN) at 163 °C

polymer melt, linear oscillatory shear experiments were carried out for the metallocene PE Exact 3128 with and without BN in a Rheometrics System IV parallel-plate rheometer. The frequency sweeps were carried out at 163°C for the virgin resin as well as for resins containing 0.05 and 0.5 wt. % BN. Figure 8-18 depicts the dynamic moduli of the three resins along with their complex viscosities. In the case of the virgin resin there is no change in slope at low frequencies. However, for the filled resins and particularly at low frequencies, there is a characteristic shoulder similar to those observed for crosslinked and phase-separated polymers (Kapnistos *et al.*, 1996). This is because of form relaxation that occurs when the motion of polymer chains is slower than that of the BN particles at low frequencies. Thus longer relaxation times are seen in the latter case. Obviously, the viscosity of the filled resins is higher than that of the virgin one because of reinforcement. At higher frequencies above 1 rad/s, the curves coincide, since the motion of small portions of polymer chains dominates rheology (length scales involved are small at higher frequencies), and the BN has almost no effect. Although it is clear that the morphology of the resin is affected by the addition of BN, it is believed that this difference at low frequencies cannot explain the effect on the extrudate appearance, which one can see in the extrusion with a crosshead die.

Another series of experiments with this resin involved cessation of steady shear and relaxation carried out in an Interlaken sliding plate rheometer. Figure 8-19 shows the normalized shear stress decay coefficient for PE Exact 3128 with and without BN at different shear rates. The shear stress decay coefficient is defined as (Dealy and Wissbrun, 1990)

$$\eta^-(t,\dot{\gamma}) \equiv \tau^-(t,\dot{\gamma})/\dot{\gamma} \tag{8-3}$$

where $\tau^-(t,\dot{\gamma})$ is the shear stress decay function (stress as a function of time during relaxation) and $\dot{\gamma}$ is the shear rate prior to cessation.

One can see that there is difference in the relaxation process between the virgin and the filled resins at low shear rates. An addition of BN seems to slow down the relaxation. This is in agreement with the previous findings that the filled resin has some additional
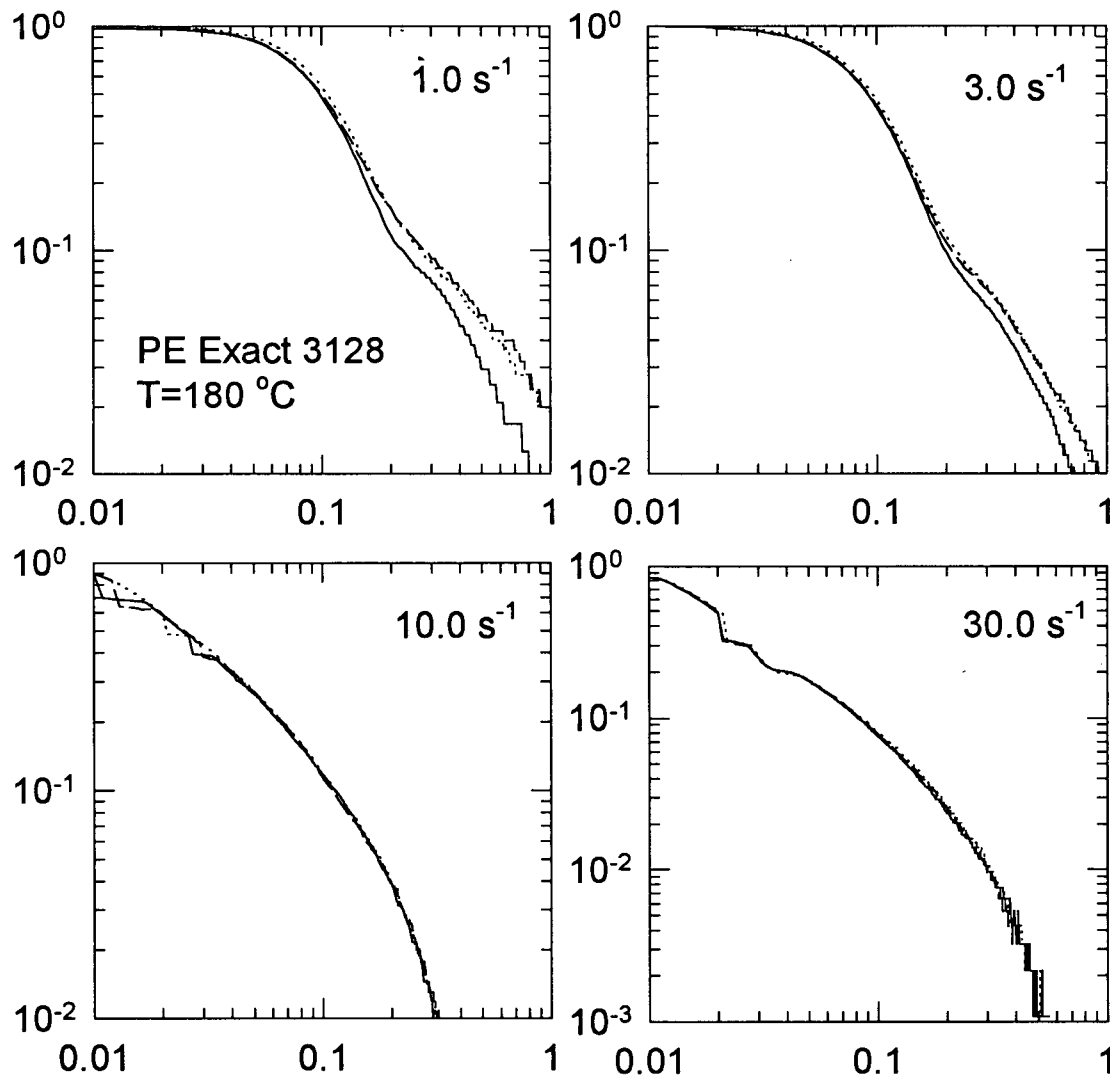
Figure 8-19. Shear stress decay coefficient, $\eta^-(t,\dot{\gamma})/\eta(\dot{\gamma})$, for metallocene PE Exact 3128 as a function of time (s) at 180°C and different shear rates. Solid lines correspond to the virgin resin, dashed lines to the resin with 0.05 wt. % BN, and dotted lines to 0.5 wt. % BN.

long relaxation modes (see Figure 8-18). However, at higher shear rates the curves are almost indistinguishable which means that the resin relaxes in the same way regardless of whether the BN is present or not.

At this point, one can say that BN at small concentrations has a very small effect on the rheology of the molten polymers. The almost identical shape of the flow curves of the pure and filled resins (see figures in the previous section) support this conclusion. It is believed that the insignificant hardening and somewhat more complex morphology at low shear rates cannot solely explain the dramatic effects that BN has on resin processability during extrusion in a crosshead die.

8.3.5.2 Effect of the Die Geometry

The fact that the effect of BN is more pronounced in a crosshead die rather than a capillary die implies that the die geometry is a factor in this phenomenon. Indeed, as can be seen in Figure 8-8, the crosshead die provides a very streamlined flow of the polymer. This is achieved by substantial conformation of the die inlet angle 14 and the included angle 28 of the conical surface 22 of the wire guide with the conical surfaces 12 and 22 being substantially parallel to one another. The annular gap between the conical surfaces is of uniform width along the pathway of the polymer. The result of this conformation of the conical surfaces is that the polymer entering the die through port 11 flows along the conically converging annular channel defined by surfaces 12 and 22 to enter the die inlet essentially without turbulence. It is known that the region of the die inlet is the site of the origin of gross melt fracture (see Section 2.5.2). That is why a streamlined flow at the die entrance is so important in this phenomenon.

An attempt to model such a streamlined flow was made by use of a capillary rheometer. For this purpose, a series of orifice dies (L/D=0) with a different entrance angle varying from 15 to 90° was used. The idea behind this experiment was to see how the entrance angle affects the extrudate appearance in the presence of BN.

Figure 8-20 plots the end pressure as a function of the apparent shear rate for four orifice dies having different entrance angles. As can be seen, in spite of a significant difference in the shape of the pressure drop curve for each die, the entrance angle has
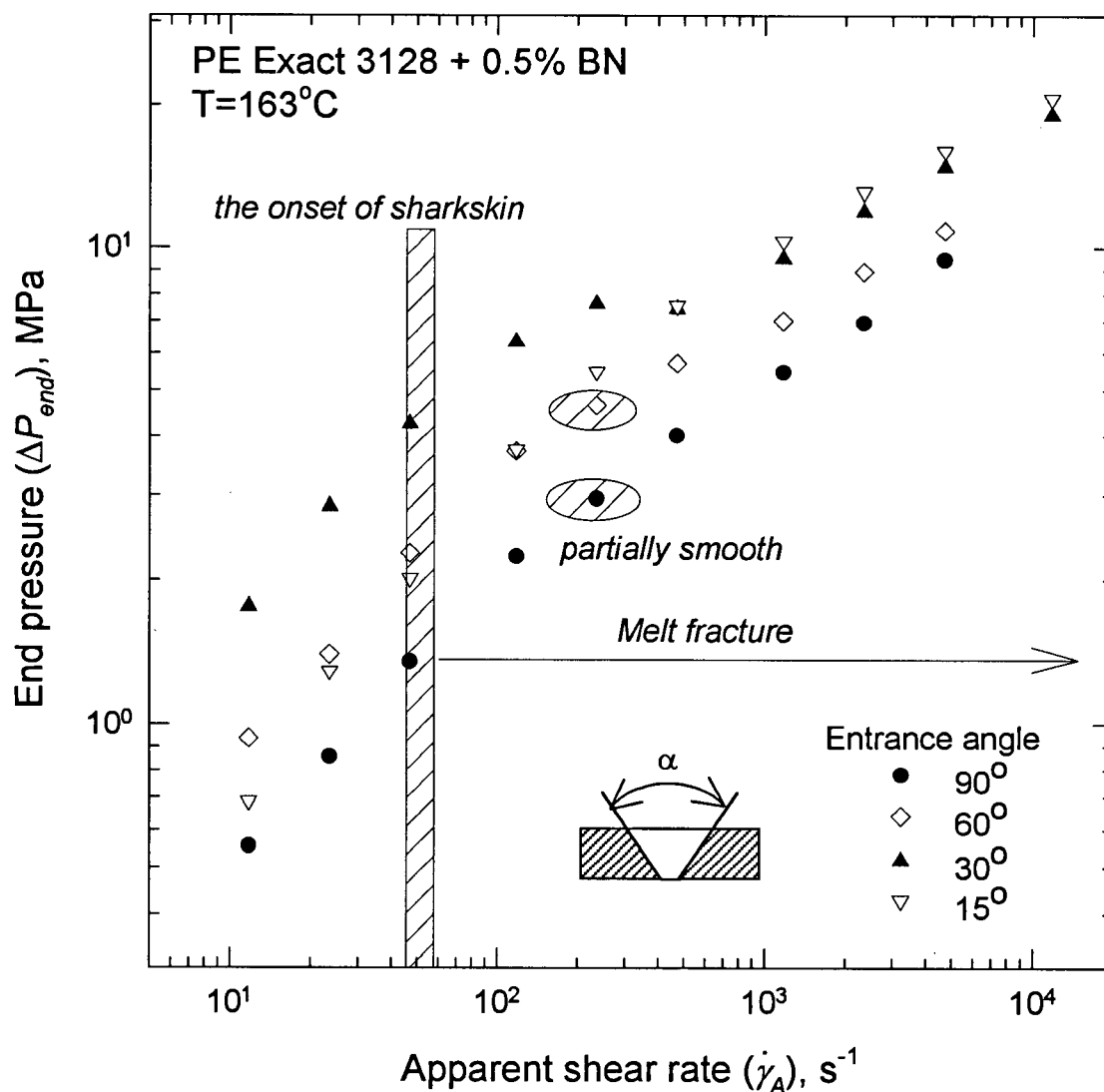
Figure 8-20. The effect of the die entrance angle on the extrudability of PE Exact 3128 in the presence of 0.5% BN

virtually no effect on the extrudate appearance. For all dies, sharkskin started at about 50 s⁻¹. This was expected because at this concentration BN does not completely eliminate sharkskin at low shear rates (see Figure 8-11). However, after the onset of melt fracture, the surface roughness persisted with increase in the apparent shear rate regardless of the die entrance. This means that a streamlined inlet region is a necessary but not a sufficient condition for the BN effect to be noticeable at this concentration. In fact, it is a combination of the slowly converging entrance and the annular geometry of the crosshead die that seem to provide the best conditions for the repression of melt fracture.

8.3.5.3 Wall Slip

As was mentioned before, wall slip is a primary cause of the enhanced processability of polyolefins in the presence of fluoropolymers. That is why it would be reasonable to assume that BN particles also enhance the slip behavior of molten polymers. However, it is unlikely that slip at the wall caused by the adhesion failure at the polymer-wall interface is a significant factor in this case. This wall interface slip is usually accompanied by a significant shift in the flow curve towards lower shear stress values (see Figure 8-1). However, such shifts are never observed with the BN-modified resins. In fact, while there is some deviation between the flow curves of virgin and filled resins, it is small compared to that caused by slip.

To prove this point, let us consider Figure 8-21. It shows the flow curves obtained for the metallocene polyethylene Exceed 116 at 204°C with a crosshead die attached to a rheometer. One can see that an addition of 0.2% BN has a very little effect on the flow curve compared to the virgin resin. On the other hand, an addition of 0.05% Viton®, a fluoropolymer widely used as a processing aid in the extrusion of polyolefins, causes the

flow curve to shift significantly towards lower shear stress values. Since the mechanism of the Viton® action is purely based on a lubrication effect, one can conclude that the mechanism of the BN effect is not associated with wall slip.

Thus, at this stage of investigation, the mechanism of the effect of BN on the processability of molten polymers is not well understood. A possible explanation could be the following. Different local concentrations of BN particles in the bulk flow could lead to the generation of zones with different viscosity. This may result into a fluid layer
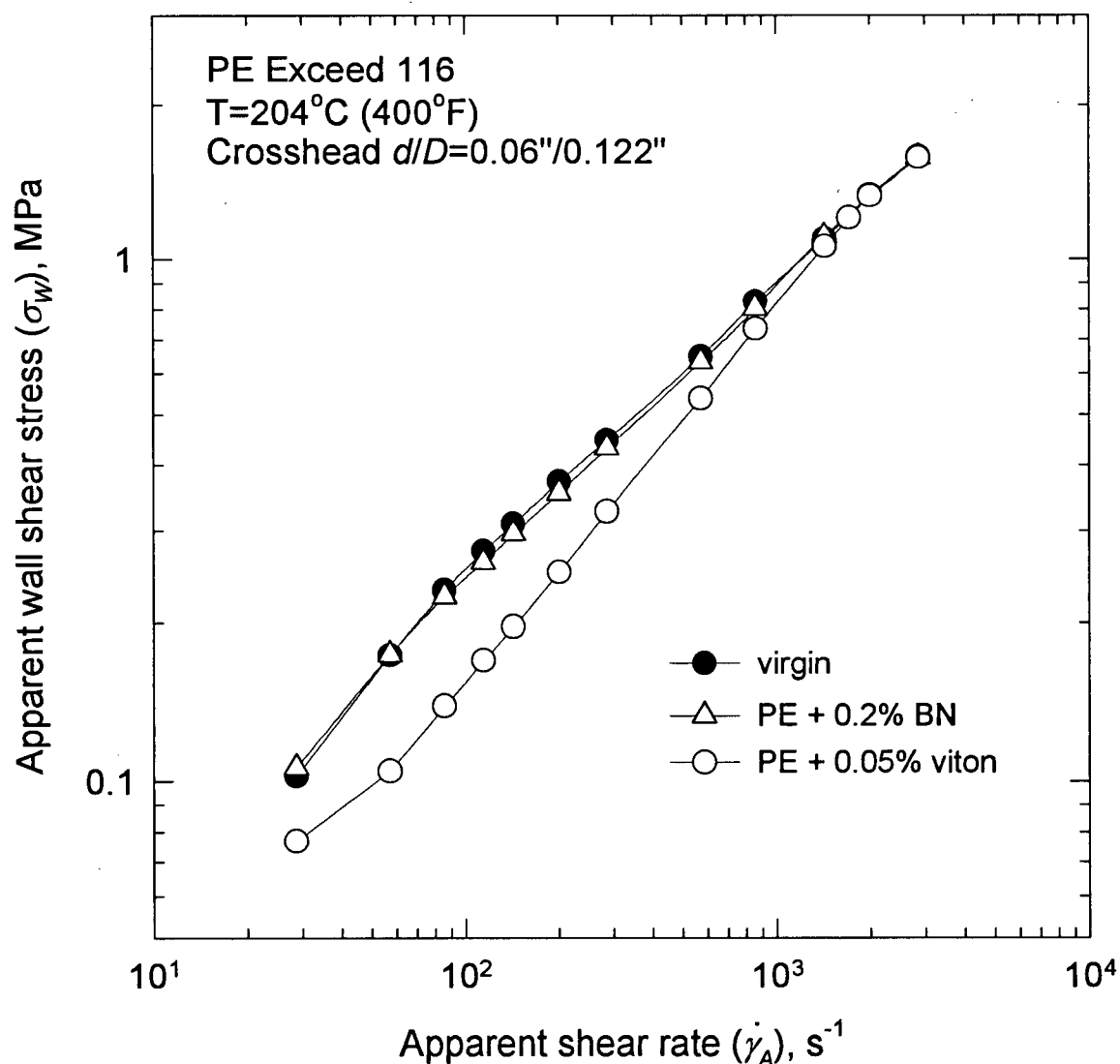
Figure 8-21. Comparison of the effect of BN and Viton® on the flow curves of the metallocene PE Exceed 116 obtained with a crosshead die at 204°C.

next to the die surface that has a much lower viscosity than the bulk. In a sense, this picture gives rise to an apparent slip and to deformations of the bulk of the molten resin that are smaller than any encountered by the virgin resin run at comparable throughputs. At the same time, the BN particles may act to nucleate tiny cracks in the bulk of the melt, thus releasing stress and leading to a much more homogeneous extrudate.

A final a possible explanation may lie in the shape of the die entrance. It seems that the annular entrance of the crosshead die provides much smoother streamlines than the plain capillary die. The fact that there is not much difference between the processing of virgin and filled resins in capillary extrusion is supportive of the last speculation. At any rate, the observed phenomenon requires additional studies such as visualization techniques in order to determine the specific mechanism of the effect of BN particles on the processability of various polymers.

8.4 The Combined Effect of BN and Teflon® on the Processability of Polyolefins

At this point, it is reasonable to assume that, since the mechanisms of the action of fluoropolymers as a processing aid and BN are essentially different, they might supplement each other if they were used together. Indeed, the fluoropolymer could work in the sharkskin and stick-slip fracture region, eliminating melt fracture and reducing the pressure drop. On the other hand, BN could work in the gross melt fracture region, where fluoropolymers have no effect, thus delaying the onset of melt fracture to even higher shear rates. The examples below demonstrate the possible use of such combined processing aids.

The first example involves the metallocene polyethylene Exact 3128. Figure 8-22 shows four flow curves obtained using a crosshead die attached to a capillary rheometer for the pure resin and for blends of PE with 0.05% by weight of a finely dispersed Teflon® APA-II, 0.05% BN, and 0.05% Teflon® APA-II and 0.05% BN. It can be seen that the presence of the BN particles has only a small effect on the flow curve. However, the onset of melt fracture with the addition of BN can be postponed from 60 to 1850 s^{-1}.
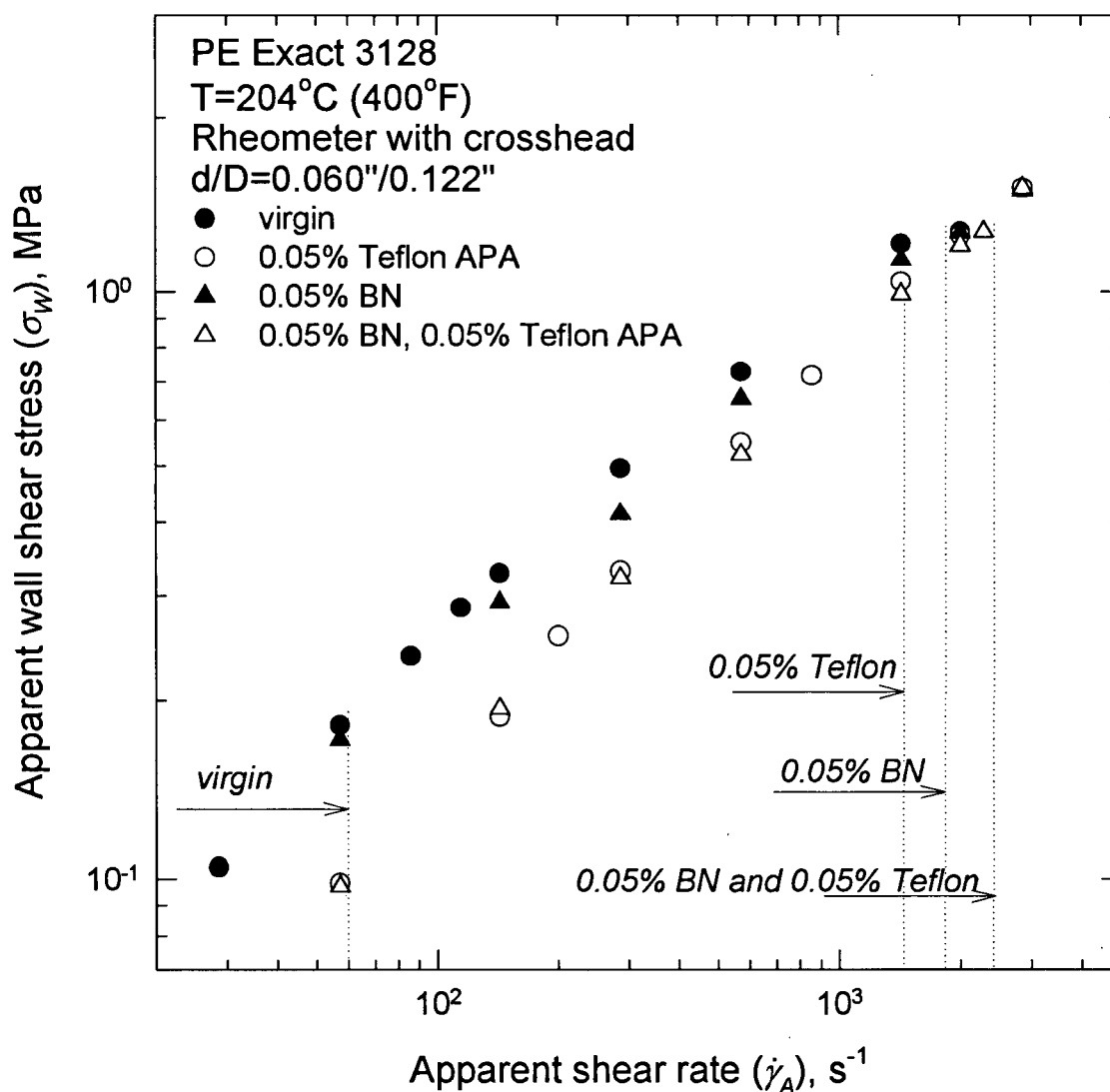
Figure 8-22. The effect of BN and Teflon APA additives on the processability of PE Exact 3128 obtained in a rheometer with Nokia Maillefer crosshead at 204°C

The addition of Teflon® particles decreases the shear stress practically over the whole range of apparent shear rates up to those in the gross melt fracture region regardless of the presence of BN. More important is the effect of the combination of the two processing aids (Teflon® and BN particles) on the onset of melt fracture. For this case, the critical shear rate is 2250 s^{-1}. Note that neither BN nor Teflon® added separately to this resin yielded such a high shear rate.
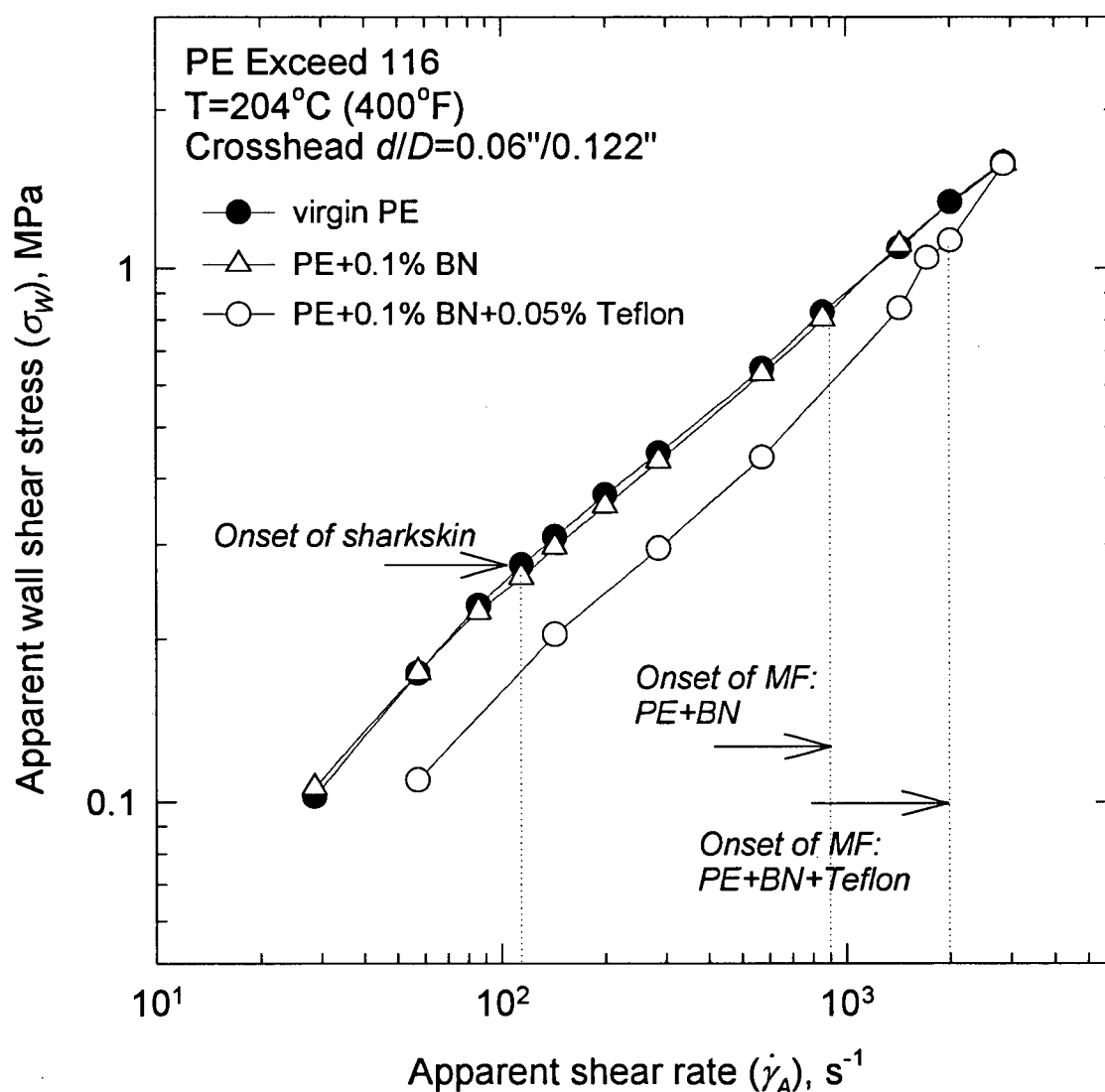
Figure 8-23. The effect of BN and Teflon APA additives on the processability of PE Exceed 116 obtained in a rheometer with a Nokia Maillefer crosshead at 204°C

The second example involves the metallocene polyethylene Exceed 116. Figure 8-23 shows the flow curves obtained for the pure resin and that with 0.1% BN and 0.1% BN+0.05% Teflon® APA-II. The addition of BN allows an increase in the maximal shear rate yielding a smooth extrudate from about 100 s^{-1} for the virgin resin to almost 1000 s^{-1}. The combined processing aid containing both BN and Teflon® results in the maximal shear rate of 2000 s^{-1} before melt fracture occurs.

In summarizing the combined effects of BN and Teflon® on the extrusion of polyolefins, it is necessary to emphasize that each of the two processing aids works in a different flow region. Teflon® eliminates sharkskin and stick-slip melt fracture while BN seems to postpone gross melt fracture to higher shear rates where Teflon® has no effect. Obviously, additional experiments are required to find the optimal concentration of each processing aid needed to obtain the best extrusion performance.

9 Conclusions and Contributions to Knowledge

9.1 Conclusions

Experiments were carried out in both parallel plate and capillary rheometers for a variety of tetrafluoroethylene/hexafluoropropylene (TFE/HFP) copolymers and TFE/HFP/perfluoro(alkyl vinyl ether) (TFE/HFP/PAVE) terpolymers, also known as Teflon® FEP polymers, having different molecular weights and compositions (i.e., HFP and PAVE contents). Dynamic linear viscoelastic data have shown that the critical molecular weight for the onset of entanglements, M_c, is about 100,000, a value much higher than those previously reported. The rheology of the high melting point resins (low content of HFP) was found to exhibit a strong dependence on thermal history during oscillatory-shear measurements because of residual crystallinity at temperatures well above their melting points. The processability of the wire coating Teflon® FEP resins was found to correlate with their composition, viscosity, ability to crystallize, and melt elasticity.

The capillary rheometer experiments revealed that surface melt fracture (sharkskin) appeared at critical shear stresses greater than about 0.18 MPa, practically independent of temperature in the range of 300 to 350 °C. At higher apparent shear rates, oscillating melt fracture was observed due to the presence of wall slip and compressibility of the melt. Furthermore, a superextrusion region was identified at apparent rates greater than those where oscillating melt fracture was obtained. In this region, the extrudate appears again smooth. This region was found to be wider at higher temperatures.

The rheological data obtained by means of both parallel-plate and capillary rheometers were used for a thorough rheological modeling of the behavior of these resins. The latter includes calculation of their linear relaxation time spectra and nonlinear parameters using a multi-mode Phan-Thien and Tanner (PTT) constitutive equation. The values of M_c recovered from the fitting procedure were close to the experimentally determined ones. The longest relaxation time was found to depend on the molecular weight in a similar way as the zero-shear viscosity does with a scaling factor of about 3.4. It was shown that the PTT model can represent rheological data for Teflon® FEP resins well and may be used in flow simulation of relevant processing, e.g. wire coating.

The problem of evaluating the slip velocity in the capillary flow of molten polymers based on experimental results (diameter dependence of flow curves) was studied in detail. It was found that in cases where viscous heating effects are significant, the traditional methods used to estimate the slip velocity (for example Mooney's technique) often fail to give accurate or even physically meaningful results. A new data analysis procedure based on a mathematical model for the nonisothermal capillary flow of polymer melts coupled with heat transfer is developed. The computer simulations can be used for two purposes: first, to provide detailed velocity, temperature, and pressure distributions, which can be useful in designing dies and, secondly, to recover the parameters of the employed slip velocity model corrected for the effect of viscous heating. The method was used to correct capillary experimental results obtained for various polymers, including PP, high and low density PE and Teflon® FEP. The results corrected for viscous heating effects were found to be consistent with the experimental data.

Finally, the effect of various processing aids on the processability of fluoropolymers and polyolefins in extrusion and wire coating was studied. First, it was found that polyethylene in amounts up to 0.1 wt. % works well as a processing aid in the extrusion of Teflon® FEP resins in the same way that fluoropolymers do in the extrusion of polyolefins. Second, the processing additive based on the boron nitride (BN) composition was found to eliminate sharkskin melt fracture and postpone gross melt fracture to significantly higher shear rates for a variety of polymers including a metallocene polyethylene, as well as several FEP and PFA resins. The degree of the effect was found to depend on the resin type, additive concentration and temperature. The combined addition of boron nitride and Teflon® particles resulted in an even better processability of the metallocene polyethylene.

9.2 Contributions to Knowledge

Several significant contributions to knowledge resulted from this research. These are as follows:

- For the first time, a thorough rheological characterization of well-defined TFE/HFP copolymers was performed. The critical molecular weight for the onset of entanglements determined for these polymers turned out to be much higher than previously reported values. Agreement was found between the values of the critical molecular weight obtained by means of relaxation time spectra and those found from direct experiments.

- The critical conditions for the onset of melt fracture as a function of temperature, molecular weight, and composition of Teflon® FEP resins were determined from capillary rheometer experiments.

- A new data analysis procedure based on a mathematical model for the nonisothermal capillary flow of polymer melts coupled with heat transfer is developed. The proposed technique can be used for two purposes. First, to provide detailed velocity, temperature, and pressure distributions which can be useful in designing dies and, secondly, to recover the parameters of the employed slip velocity model corrected for the effect of viscous heating. A reliable slip velocity model is crucial for numerical simulation and polymer process modeling.

- It is shown that polyethylene can be used as a processing aid in the extrusion of Teflon® in the same way that fluoropolymers are used as processing aids for polyolefins. A mechanism, based on the relative work of adhesion between the components of the polymer blend and the material of the die, is proposed to describe this phenomenon.

- Boron nitride was found to act as an effective processing aid in the extrusion of both fluoropolymers and polyolefins. For the first time, the processing aid was shown to not only eliminate sharkskin and stick-slip (oscillating) melt fracture, but also to postpone gross melt fracture to significantly higher shear rates. The critical conditions and the influence of operating parameters such as the temperature and BN concentration were determined.

9.3 Recommendations

Based on the experience gained during this study, the following recommendations for future work can be made.

- In Chapter 4, it was found that the critical molecular weight of low melting point TFE/HFP copolymers is close to 100,000, a value much higher than those previously reported for other polymers. However, for the group of the high melting point resins, there were insufficient experimental data to allow a similar conclusion to be drawn. It is desirable to carry out additional experiments with the low molecular weight FEP resins in order to see clearly the discontinuity in the relationship between zero-shear viscosity and molecular weight.

- In Chapter 7, a detailed technique to calculate the slip velocity from the capillary rheometer data is proposed that accounts for the thermal effects in viscoelastic flow. However, the thermal boundary condition at the wall did not include the thermal effect due to friction at the polymer-wall interface as a result of wall slip. This local temperature rise may be significant, and it should be taken into account at high slip velocity values.

- In Chapter 6, the PTT constitutive equation was used to model the rheological behavior of Teflon® FEP resins. It was found to describe well the rheological properties of these resins. In future, it may be used in numerical simulation of a capillary flow using the numerical procedure described in Chapter 7. Also a universal slip velocity model describing the polymer behavior in all flow regions should be developed.

- A numerical code suitable for modeling the wire coating process should be developed. It should include the equations of mass, motion, and energy for the shear and shear-free flows coupled with the PTT equation, the wall slip model, and other proper boundary conditions. The numerical simulation of the process under all operating conditions is needed for design purposes.

- Additional experiments should be carried out with boron nitride processing aid. These should include the extrusion of polymers at various concentrations of BN to find its optimal concentration as a function of the processing temperature and type of polymer. Experiments with dies of various geometry are also desirable to see how the die geometry affects the resin processability.

- A visualization study involving, e.g., the laser-speckle technique, is needed to identify the mechanism by which BN affects the extrusion of molten polymers. The visualization technique could also be used to independently measure the slip velocity, to allow comparisons with the results obtained by using the numerical technique developed in Chapter 7.

References

Adewale, K.P., Leonov, A.I., *Modeling spurt and stress oscillations in flows of molten polymers*. Rheol. Acta, 36, 110-127 (1997).

Astarita, G., Sarti G.C., *Thermomechanics of compressible materials with entropic elasticity*. Theoretical Rheology, Wiley, 123-137, NY, 1974.

Atwood, B.T., Schowalter, W.R., *Measurement of slip at the wall during flow of high density polyethylene through a rectangular conduit*. Rheol. Acta, 28, 134-146 (1989).

Bagley, E.B., *End corrections in the capillary flow of polyethylene*. J. Appl. Phys., 28, 624 (1957).

Bagley, E.B., Schreiber, H.P., *Effect of die entry geometry on polymer melt fracture and extrudate distortion*. Trans. Soc. Rheol., 5, 341 (1961).

Baumgaertel, M., Winter, H.H., *Determination of the discrete relaxation and retardation time spectra from dynamic mechanical data*. Rheol. Acta, 28, 511-519 (1989).

Baumgaertel, M., Schausberger, A., Winter. H.H., *The relaxation of polymers with linear flexible chains of uniform length*. Rheol Acta, 29, 400-408 (1990).

Baumgaertel, M., Winter, H.H., *Interrelation between continuous and discrete relaxation time spectra*. J. Non-Newtonian Fluid Mech., 44, 15-36 (1992).

Benbow, J.J., Lamb, P., *New aspects of melt fracture*. S.P.E. Trans., 3, 7 (1963).

Bergem, N., *Visualization studies of polymer melt flow anomalies in extrusion*. Proc. 8th Int. Congr. Rheol., Gothenberg, p. 50 (1976).

Binnington, R.J., Troup, G.J., Boger, D.V., *A low-cost laser-speckle photographic technique for velocity measurement in slow flows*. J. Non-Newtonian Fluid Mech., 12, 255-267 (1983).

Bird, R.B., Stewart, W.E., Lightfoot, E.N., *Transport phenomena*. 2nd ed., Wiley, N.Y., 1962.

Bird, R.B., Armstrong, R.C.; Hassager, O., *Dynamics of polymeric liquids, vol. 1: Fluid mechanics*. Wiley, NY, 1987.

Blyler, L.L., Hart, A.C., *Capillary flow instability of ethylene polymer melts*. Polym. Eng. Sci., 10, 193 (1970).

Boudreaux, E.,Jr., Cuculo, J.A., *Polymer flow instability: A review and analysis.* J. Macromol. Sci. - Rev. Macromol. Chem., C 16 (1), 39-77 (1977).

Brochard, F., de Gennes, P.-G., *Shear-dependent slippage at a polymer/solid interface.* Langmuir, 8, 3033-3037 (1992).

Buckmaster, M.D., Henry, D.L., Randa, S.K., *High speed extrusion.* U.S. Pat. No. 5,688,457 (1997).

Chu B., Wu C., Zuo J., *Light scattering characterization of PTFE.* Macromolecules, 20, 700-702 (1987).

Chu, B., Linliu, K., *Viscosity characterization of poly(tetrafluoroethylene) by centrifuge ball viscosimetry.* Macromolecules, 28, 2723-2727 (1995).

Cocci, A.A., Picot, J.J.C., *Rate of strain effect on the thermal conductivity of a polymer liquid.* Polym. Eng. Sci., 13, 337-341 (1973).

Cogswell, F.N., *Stretching flow instabilities at the exits of extrusion dies.* J. Non-Newtonian Fluid Mech., 2, 37-47 (1977).

Cogswell, F.N., *Converging flow and stretching flow: a compilation.* J. Non-Newtonian Fluid Mech., 4, 23 (1978).

Cox, H.W., Macosko, C.W., *Viscous dissipation in die flows.* AIChE J., 20 (4), 785-795 (1974).

Dealy, J.M., *Rheometers for molten plastics.* Reinhold, NY, 1982.

Dealy, J.M., Wissbrun, K.F., *Melt rheology and its role in plastics processing: theory and applications.* Reinhold, NY, 1990.

Denn, M.M., *Surface-induced effects in polymer melt flow.* Proc. XIth Int.Congr.on Rheology, Brussels, Belgium. In: Moldenaers P., Keunings R. (eds.) Theretical and applied rheology. Elsevier Science Publishers, 45-49, 1992.

Denn, M.M., *Issues in viscoelastic fluid mechanics.* Annu. Rev. Fluid Mech., 22, 13-34 (1990).

Denn. M.M., *Polymer flow instabilities: a picaresque tale.* Chem. Eng. Ed., 28, 162-166 (1994).

Dinh, S.M., Armstrong, R.C., *Non-isothermal channel flow of non-Newtonian fluids with viscous heating.* AIChE J., 28 (2), 294-301 (1982).

El Kissi, N., Piau, J.M., *The different capillary flow regimes of entangled polydimethylsiloxane polymers: macroscopic slip at the wall, hysteresis and cork flow*. J. Non-Newtonian Fluid Mech., 37, 55-94 (1990).

Elster, C., Honerkamp, J., *Modified maximum entropy method and its applications to creep data*. Macromolecules, 24, 310-314 (1991).

Feiring, A.E., Imbalzano, J.F., Kerbow, D.L., *Advances in fluoroplastics*. Trends in Polym. Sci., 2 (1), 26-30 (1994).

Ferry, J.D., *Viscoelastic properties of polymers*. Wiley, N.Y., 1980.

Galt, J., Maxwell, B., *Velocity profiles for polyethylene melts*. Modern Plastics, Dec., 115-132 (1964).

Giacomin A.J., Samurkas, T.; Dealy, J.M., *A novel sliding plate rheometer for molten plastics*. Polym. Eng. Sci., 29 (8) (1989).

Guskey, S.M. , Winter, H.H. , *Transient shear behavior of a thermotropic liquid crystalline polymer in the nematic state* . J. Rheol., 35, 1191-1207 (1991).

Hatzikiriakos, S.G., Dealy, J.M., *Wall slip of molten high density polyethylene. I. Sliding plate rheometer studies*. J. Rheol., 35 (4), 497-523 (1991a).

Hatzikiriakos, S.G., Dealy, J.M., *The effect of interface conditions on wall slip and melt fracture of high density polyethylene*. SPE ANTEC '91 Tech. Papers, 2311-2314 (1991b).

Hatzikiriakos, S.G., Dealy, J.M., *Wall slip of molten high density polyethylene. II. Capillary rheometer studies*. J. Rheol., 36 (4), 703-741 (1992a).

Hatzikiriakos, S.G., Dealy, J.M., *Role of slip and fracture in the oscillating flow of HDPE in a capillary*. J. Rheol., 36 (5), 845-884 (1992b).

Hatzikiriakos, S.G., Dealy, J.M., *Start-up pressure transients in a capillary rheometer*. SPE ANTEC '92 Tech. Papers, 1743-1746 (1992c).

Hatzikiriakos, S.G., *A slip model for linear polymers based on adhesive failure*. Intern. Polymer Processing, VIII 2, 135-142 (1993).

Hatzikiriakos, S.G., Dealy, J.M., *Start-up pressure transient in a capillary rheometer*. Polym. Eng. Sci., 34 (6), 493-499 (1994).

Hatzikiriakos, S.G., *The onset of wall slip and sharkskin melt fracture in capillary flow*. Polym. Eng. Sci., 34 (19), 1441-1449 (1994).

Hatzikiriakos, S.G., Kalogerakis, N., *A dynamic slip velocity model for molten polymers based on a network kinetic theory*. Rheol. Acta, 33, 38-47 (1994).

Hatzikiriakos, S.G., *A multimode interfacial constitutive equation for molten polymers*. J. Rheol., 39 (1), 61-71 (1995).

Hatzikiriakos, S.G., Hong, P.; Ho, W.; Stewart, C.W., *The effect of teflon coatings in polyethylene capillary extrusion*. J. Appl. Polym. Sci., 55, 595-603 (1995).

Hatzikiriakos, S.G., Heffner, G., Vlassopoulos, D., Christodoulou, K., *Rheological characterization of polyethylene terephthalate resins using a multimode Phan-Thien-Tanner constitutive relation*. Rheol. Acta, 36, 568-578 (1997a).

Hatzikiriakos, S.G., Kazatchkov, I.B., Vlassopoulos, D., *Interfacial phenomena in the capillary extrusion of metallocene polyethylenes*. J. Rheol., 41 (6), 1299-1316 (1997b).

Hill, D.A., Hasegawa, T, Denn, M.M., *On the apparent relation between adhesive failure and melt fracture*. J. Rheol., 34, 891-918 (1990).

Himmelblau, D.M., *Applied nonlinear programming*. McGraw-Hill, 498, NY, 1972.

Honerkamp, J., Weese, J., *Determination of the relaxation spectrum by a regularization method*. Macromolecules, 22, 4372-4377 (1989).

Howells, E.R., Benbow, J.J., *Flow defects in polymer melts*. Trans. Plast. Inst., 30, 240-253 (1962).

Jackson, J.K., De Rosa, M.E., Winter, H.H., *Molecular weight dependence of relaxation time spectra for the entanglement and flow behavior of monodisperse linear flexible polymers*. Macromolecules, 27, 2426-2431 (1994).

Kalika, D.S., Denn, M.M., *Wall slip and extrudate distortion in linear low-density polyethylene*. J. Rheol., 31 (8), 815-834 (1987).

Kapnistos, M., Vlassopoulos, D., Anastasiadis, S.H., *Determination of both the binodal and the spinodal curves in polymer blends by shear rheology*. Europhys. Lett., 34 (7), 513-518 (1996).

Kazatchkov, I.B., Hatzikiriakos, S.G.; Stewart, C.W., *Extrudate distortion in the capillary/slit extrusion of a molten polypropylene*. Polym. Eng. Sci., 35 (23), 1864-1871 (1995).

Kazatchkov, I.B., Rosenbaum, E.E., Hatzikiriakos, S.G.; Stewart, C.W., *The effect of molecular structure on the rheological behaviour of*

tetrafluoroethylene/hexafluropropylene copolymers. ANTEC'96 Tech. Papers, 42, 2120-2124, Indianapolis, May 5-9 (1996).

Ko, Y.S., Lodge, A.S., *Viscous heating correction for thermally developing flows in slit die viscometry*. Rheol. Acta, 30, 357-368 (1991).

Kraynik, A.M., Schowalter, W.R., *Slip at the wall and extrudate roughness with aqueous solutions of polyvinyl alcohol and sodium borate*. J. Rheol., 25, 95 (1981).

Kurtz, S.J., *The Dynamics of sharkskin melt fracture: effect of die geometry*. Proc. XIth Int.Congr.on Rheology, Brussels, Belgium. In: Moldenaers P., Keunings R. (eds.) Theretical and applied rheology. Elsevier Science Publishers, 377-379, 1992.

Kurtz, S.J., *Die geometry solutions to sharkskin melt fracture*. Advances in Rheology, ed. B. Mena, A. Garcia-Rejon and C. Rangel Nafaile, UNAM, Mexico City, Vol. 3, 399 (1984).

Lagasse, R.R., Maxwell, B., *An experimental study of the kinetics of polymer crystallization during shear flow*. Polym. Eng. Sci., 16, 189-199 (1976).

Larson, R.G., *Constitutive equations for polymer melts and solutions*. N.Y.:Butterworths, 364 pp., 1988.

Larson, R.G., *Instabilities in viscoelastic flows*. Rheol. Acta, 31, 213-263 (1992).

Laun, H.M., *Description of the non-linear shear behavior of a low density polyethylene melts of an experimentally determined strain dependent memory function*. Rheol. Acta, 17, 1 (1978).

Laun, H.M., *Polymer melt rheology with a slit die*. Rheol. Acta, 22, 171 (1983).

Leonov, A.I., *On the dependence of friction force on sliding velocity in the theory of adhesive friction of elastomers*. Wear, 141 (1), 137-145 (1990).

Lim, F.J., Schowalter, W.R., *Wall slip of narrow molecular weight distribution polybutadienes*. J. Rheol., 33 (8), 1359-1382 (1989).

Lin, Y.-H., *Explanation for slip-stick melt fracture in terms of molecular dynamics in polymer melts*. J. Rheol., 29 (6), 605-637 (1985).

Lupton, J.M., Regester, R.W., *Melt flow of polyethylene at high rates*. Polym. Eng. Sci., 5, 235 (1965).

Meissner, J, *Basic parameters, melt rheology, processing and end-use properties of three similar low density polyethylene samples*. Pure Appl. Chem., 42, 551-612 (1975).

Migler, K.B., Hervet, H.; Leger, L., *Slip transition of a polymer melt under shear stress.* Phys. Review Letters, 70 (3), 287-290 (1993).

Milthorpe, J.F., Tanner, R.I., *On the extrusion of visco-elastic fluids subject to viscous heating.* Intrn. J. Num. Methods in Engng., 24, 263-270 (1987).

Mooney, M., *Explicit formulas for slip and fluidity.* J. Rheol., 2, 210 (1931).

Moynihan, R.H., Baird, D.G.; Ramanathan, R., *Additional observations on the surface melt fracture behavior of LLDPE.* J. Non-Newtonian Fluid Mech., 36, 255 (1990).

Nason, H.K., *A high temperature - high pressure rheometer for plastics.* J. Appl. Phys., 16, 338 (1945).

Orbey, N., Dealy, J.M., *Determination of the relaxation spectrum from oscillatory shear data.* J. Rheol., 35 (6), 1035-1049 (1991).

Pearson, J.R.A, *Mechanics of polymer processing.* Chapman & Hall, London 1965.

Pearson, J.R.A., Shah, Y.T., *On the stability of non-isothermal flow in channels.* Rheol. Acta, 12, 240 (1973).

Pearson, J.R.A., Shah, Y.T., Vieira, E.S.A., *Stability of non-isothermal flow in channels I.* Chem. Eng. Sci., 28, 2079 (1973).

Penwell, R.C., Porter, R.S., Middleman, S., *Determination of the pressure coefficient and pressure effects in capillary flow.* J. Polym. Sci., A-2, 9(4), 731-745 (1971).

Petrie, C.J.S., Denn, M.M., *Instabilities in polymer processing.* AIChE J., 22 (2), 209-236 (1976).

Phan-Thien, N., Tanner, R.I., *A new constitutive equation derived from network theory.* J. Non-Newtonian Fluid Mech., 2, 353-365 (1977).

Piau, J.M., El Kissi, N., *The influence of interface and volume properties of polymer melts on their die flow stability.* Proc. XIth Int.Congr.on Rheology, Brussels, Belgium. In: Moldenaers P., Keunings R. (eds.) Theretical and applied rheology. Elsevier Science Publishers, 70-74, 1992.

Piau, J.M., El Kissi, N., Trenblay, B., *Low Reynolds number flow visualization of linear and branched silicones upstream of orifice dies.* J. Non-Newtonian Fluid Mech., 30, 197-232 (1988).

Piau, J.M., El Kissi, N., Trenblay, B., *Influence of upstream instabilities and wall slip on melt fracture and sharkskin phenomena during silicone extrusion through orifice dies*. J. Non-Newtonian Fluid Mech., 34, 145-180 (1990).

Porter, D., *Group interaction modelling of polymer properties*. Dekker, New York, 1995.

Pudjijanto, S., Denn, M.M., *A stable "island" in the slip-stick region of linear low-density polyethylene*. J. Rheol., 38 (6), 1735-1744 (1994).

Ramamurthy, A.V., *Wall slip in viscous fluids and influence of materials of construction*. J. Rheol., 30 (2), 337-357 (1986).

Rauwendaal, C., Fernandez, F., *Experimental study and analysis of a slit die viscometer*. Polym. Eng. Sci., 25, 765 (1985).

Reher, E.-O., Bothmer, D.; Schnabel, R., *Investigations into the wall slippage behaviour of polymer melts from the energy aspect*. Kunststoffe - German Plastics, 78 (11), 40-41 (1988).

Rosenbaum, E.E., Hatzikiriakos, S.G.; Stewart, C.W., *The melt fracture behaviour of Teflon resins in capillary extrusion*. SPE ANTEC '95 Tech. Papers, 41, 1111-1115 (1995).

Rosenbaum, E.E., Hatzikiriakos, S.G.; Stewart, C.W., *Flow implications in the processing of DuPont tetrafluoroethylene/hexafluoropropylene*. Intern. Polymer Processing, X (3), 204-212 (1995).

Rosenbaum, E.E., Hatzikiriakos, S.G., *The effect of viscous heating in capillary rheometry*. SPE ANTEC '96 Tech. Papers, 42, 1080-1084 (1996).

Rosenbaum, E.E., Hatzikiriakos, S.G., *Wall slip in the capillary Flow of molten polymers subject to viscous heating*. AIChE J., 43 (3), 598-608 (1997).

Rosenbaum, E.E., Randa, S.K., Hatzikiriakos, S.G., Stewart, C.W., Henry, D.L., Buckmaster, M.D., *A new processing additive eliminating surface and gross melt fracture in the extrusion of polyolefins and fluoropolymers*. SPE ANTEC '95 Tech. Papers, 44 (1998a).

Rosenbaum, E.E., Hatzikiriakos, S.G.; Stewart, C.W., *Rheological characterization of well-defined tetrafluoroethylene/hexafluoropropylene*. to be published in Rheol. Acta (1998b).

Rudin, A., Worm, A.T.; Blacklock, J.E., *Fluocarbon elastomer processing aid for LLDPE, HDPE and PP resins*. Processing and Property Enhancement Utilizing Modifiers and Additives in Polymers: First Intl. Conf., p.71-81 (1985).

Schowalter, W.R., *The behavior of complex fluids at solid boudaries.* J. Non-Newtonian Fluid Mech., 29, 25-36 (1988).

Shidara, H., Denn, M.M., *Polymer melt flow in very thin slits.* J. Non-Newtonian Fluid Mech., 48, 101-110 (1993).

Shih, C.-K., *Capillary extrusion and mold flow characteristics of an incompatible blend of two elastomers..* Science and Technology of Polymer Processing, MIT Press, Cambridge, 1979, 528-539.

Stewart, C.W., McMinn, R.S.; Stika, K.M., *A model for predicting slip velocity during extrusion with fluoropolymer processing additives.* J. Reinf. Plast. Composites, 12 (6), 633-641 (1993).

Stewart, C.W., *Wall slip in the extrusion of linear polyolefins.* J. Rheol., 37 (3), 499-513 (1993).

Stewart, C.W., . Private communication (1994).

Sukanek, P.C., Goldstein, C.A., Laurence, R.L., *The instability of plane Couette flow with viscous heating.* J. Fluid Mech., 57, 651 (1973).

Tanner, R.I., *Engineering rheology.* Oxford University Press, Oxford, 1985.

Tordella, J.P., *Unstable flow of molten polymers.* in Rheology, Vol. 5, F. R. Eirich, ed., Academic Press, NY, 57-92, 1969.

Tordella, J.P., *Fracture in the extrusion of amorphous polymers through capillaries.* J. Appl. Phys., 27, 454 (1956).

Tremblay, B., *Sharkskin defects of polymer melts: the role of cohesion and adhesion.* J. Rheol., 35 (6), 985-998 (1991).

Tschoegl, N.W., Emri, I., *Generating line spectra from experimental responses. II. Storage and loss functions.* Rheol. Acta, 32, 322-327 (1993).

Tuminello, W.H., *Molecular weight distributions of tetrafluoroethylene-hexafluoropropylene copolymers.* Polym Eng Sci., 29, 645-653 (1989).

Van Krevelen, D.W., *Properties of polymers: their correlation with chemical structure; their numerical estimation, and prediction from additive group contributions.* Elsevier, NY, 1991.

Vinogradov, G.V., Malkin, A.Ya., *Rheology of polymers.* Mir, Moscow, Springer, Berlin, 1980.

Vinogradov, G.V., Malkin, A.Ya., Yanovskii, Y.G., Borisenkova, E.K., Yarlykov, B.V., Berezhnaya, G.V, *Viscoelastic properties and flow of narrow polybutadienes and polyisoprenes*. J. Polym. Sci., A2 (10), 1061-1084 (1972a).

Vinogradov, G.V., Insarova, N.I., Boiko, B.B., Borisenkova, E.K., *Critical regimes of shear in linear polymers*. Polym. Eng. Sci., 12 (5), 323-334 (1972b).

Vinogradov, G.V., Ivanova, L.I., *Wall slippage and elastic turbulence of polymers in the rubbery state*. Rheol. Acta, 7, 243-254 (1968).

Vlassopoulos, D., Pakula, T., Fytas, G., Roovers, J., Karatasos, K., Hadjichristidis, N., *Ordering and viscoelastic relaxation in multiarm star polymer melts*. Europhys. Lett., 39(6), 617-622 (1997).

Waddon, A.J., Keller, A., *A temperature window of extrudability and reduced flow resistance in high-molecular weight polyethylene: Interpretation in terms of flow-induced mobile hexagonal phase*. J. Polym. Sci., B 28, 1063-1073 (1990).

Waddon, A.J., Keller, A., *The temperature window of minimum flow resistance in melt flow of polyethylene. Further studies on the effect of strain rate and branching*. J. Polym. Sci., B 30, 923-929 (1992).

Wang, J., Porter, R.S., *On the viscosity-temperature behavior of polymer melts*. Rheol. Acta, 34, 496-503 (1995).

Wang, S.Q., Drda, P.A., Inn, Y.W., *Exploring molecular origins of sharkskin, partial slip, and slope change in flow curves of linear low density polyethylene*. J. Rheol., 40 (5), 875-898 (1996).

Warren, R.C., *Viscous heating*. Rheological measurement, Elsevier, London, 1988, 119-149.

White, J.L., *Critique of flow patterns in polymer fluids at the entrance of a die and instabilities leading to extrudate distortion*. Appl. Polymer Symposium, 20, 155-174 (1973).

Winter, H.H., Baumgaertel, M., Soskey, P.R., *A parsimonious model for viscoelastic liquids and solids*. in Techniques in Rheological Measurement, Ed. Collyer, A.A., Chapman & Hall, London, 1993.

Winter, H.H., *Viscous dissipation in shear flows of molten polymers*. Advances in Heat Transfer, 13, 205-267 (1977).

Winter, H.H., *Analysis of dynamic mechanical data: inversion into a relaxation time spectrum and consistency check*. J. Non-Newtonian Fluid Mech., 68, 225-239 (1997).

Wu, S., *Dynamic rheology and molecular weight distribution of insoluble polymers: tetrafluoroethylene-hexafluoropropylene copolymers*. Macromolecules, 18, 2023-2030 (1985).

Ybarra, R.M., Eckert, R.E., *Viscous heat generation in slit flow*. AIChE J., 26 (5), 751-762 (1980).

Zhu, C., Byrd, R.H., Lu, P., Nocedal, J., *L-BFGS-B - FORTRAN subroutines for large-scale bound constrained optimization*. To appear in ACM Trans. Math. Software (1997).

Notation

A	temperature coefficient of viscosity, K^{-1}
a	parameter in the slip velocity equation (Eq. 7-7), $MPa^{-m} \cdot m/s$
a_T	shift factor
b	Rabinowitsch correction
C	Cauchy tensor
C_p	heat capacity, $J/(kg \cdot K)$
c_1, c_2	constants in the slip velocity model, Equation (7-15)
D	capillary diameter, m
D	tip diameter, m
E_a	activation energy for flow, J
E^*	constant in the slip velocity model, Equation (7-17)
e	Bagley end correction or energy in Equation (2-37)
G	shear modulus, Pa
G'	storage modulus, Pa
G''	loss modulus, Pa
G^*	complex modulus, Pa
G_d	amplitude ratio in oscillatory shear
G_N^0	plateau modulus, Pa
g_i	relaxation strength of the i-th Maxwell mode, Pa
g_N	constant in Equation (6-6)
$H(\lambda)$	relaxation time spectrum
H_g	glass transition constant in Equation (6-3)
h	gap between plates, m
I	melt polydispersity
K	power-law consistency index, $MPa \cdot s^n$

k	heat conductivity, W/(m · K)
k_W	wall thermal conductivity, W/(m · K)
L	capillary length or length of sample, m
L_0	initial length of sample, m
M	molecular mass of the interacting unit, g/mol
M_c	critical molecular weight for entanglement, kg/kmol
M_e	average molecular weight between entanglements, kg/kmol
M_n	number average molecular weight, kg/kmol
M_w	weight-average molecular weight, kg/kmol
m	parameter in the slip velocity equation (Eq. 7-7)
n	power-law exponent
n_e	slope of BSW spectrum in the entanglement zone
n_g	slope of BSW spectrum in the glass transition zone
P	absolute pressure, Pa
P_a	ambient pressure, Pa
P_d	driving pressure, Pa
P_{end}	Bagley correction, Pa
ΔP_{ex}	exit pressure drop, Pa
ΔP_{ent}	entrance pressure drop, Pa
Q	volumetric flow rate, m³/s
R	capillary radius, m or universal gas constant
SD	standard deviation
T	absolute temperature, K
t	time, s or wall thickness, m
T_g	glass transition temperature, K
T_{gel}	gel temperature, K
T_{ref}	reference temperature, K

T_W	temperature at the wall, K
u	melt velocity, m/s
u_s	slip velocity, m/s
$\mathbf{v}$	velocity vector
v_x, v_y, v_z	velocity components in x, y, and z direction, respectively, m/s
v_r	velocity component in radial direction, m/s
Δx	plate displacement, m
Z	parameter in the PTT model, Equation (6-10)

Greek Letters

α	pressure coefficient of viscosity, Pa^{-1}
β	constant in BSW spectrum, Equation (6-3)
δ	mechanical loss angle
ε	parameter of the Phan-Thien and Tanner model or coefficient of thermal expansion or Hencky strain
ξ	parameter of the Phan-Thien and Tanner model
ξ_0	coefficient in the slip velocity model, Equation (7-15)
$\dot{\varepsilon}$	Hencky strain rate
$\gamma(t)$	shear strain
$\dot{\gamma}_{ij}$	rate of deformation tensor, s^{-1}
$\dot{\gamma}$	shear rate, s^{-1}
$\dot{\gamma}_A$	apparent shear rate, s^{-1}
$\dot{\gamma}_{A,s}$	apparent shear rate, corrected for slip, s^{-1}
$\dot{\gamma}_w$	wall shear rate, s^{-1}
γ_0	strain amplitude in oscillatory shear
η	viscosity, Pa · s
η_0	zero-shear viscosity, Pa · s

η^0	viscosity at ambient pressure, Pa · s
η'	dynamic viscosity, Pa · s
η''	out-of-phase component of complex viscosity, Pa · s
η^*	complex viscosity, Pa · s
η_A	apparent viscosity, Pa · s
η_E	extensional viscosity, Pa · s
λ	relaxation time, s
λ_{max}	longest relaxation time, s
λ_c	critical relaxation time, s
π	internal pressure, bar, Equation (7-8)
ρ	density, kg/m³
σ_c	critical shear stress for the onset of melt fracture, Pa
σ_E	principal stretching stress, Pa
σ_n	normal stress, Pa
σ_w	wall shear stress, Pa
σ_0	stress amplitude in oscillatory shear, Pa
τ	stress tensor, Pa
τ_i	contribution of the i-th relaxation mode to the total stress
ω	frequency, rad/s or specific volume, cm³/g, Equation (7-8)